Flow processes forcing the development of the scour hole Beerenplaat in the Rhine-Meuse delta

by

K.P. (Karsten) van Duuren

in partial fulfillment of the requirements for the degree of

Master of Science in Civil Engineering

at the Delft University of Technology, to be defended publicly on Friday February 25, 2022 at 10:45

Student number: 4432940

Thesis committee: Dr. ir. A. Blom, Delft University of Technology, Chair

Dr. ir. B. Hofland, Delft University of Technology

Dr. ir. C. J. Sloff, Delft University of Technology, Deltares

Dr. L. M. Stancanelli, Delft University of Technology

An electronic version of this thesis is available on http://repository.tudelft.nl/.



Preface

In front of you is the final version of my master thesis on flow processes that force the scour hole Beerenplaat. It is the result of working over a year on this individual project and is the final product of my Master of Science in Hydraulic Engineering, with the specialization River Engineering. This thesis has been created in collaboration with the Delft University of Technology and Deltares.

Performing this research during the pandemic was challenging and presented many ups and downs. In the early phases of the project I troubled with finding my pace and focus. Working alone and from home throughout the different lockdowns was not helpful for this. Despite, the last few months were fruitful and with the right scope I made a good final sprint. During the thesis I improved my skills in programming, especially in Matlab, and experienced how to actually perform a scientific research. On top of that, I obtained respect for the difficulty that is paired with combining literature findings, field measurements and numerical modelling, to investigate a complex system. Looking back at the project, I am proud of what I achieved.

I would like to thank my daily supervisor Kees Sloff for his time and effort. Your recommendations during the many meetings and constructive feedback on my report, has steered me in the right direction. In addition, I would like to thank the other committee members, Astrid Blom, Bas Hofland and Laura Stancanelli for giving valuable input during the progress and individual meetings. I would like to thank Victor Chavarrias from Deltares, for sharing his knowledge on the Delft3D model and answering all my questions. A final thank you goes out to my girlfriend, family and friends for supporting and motivating me throughout this process.

K.P. (Karsten) van Duuren Delft, February 2022

Abstract

Since dikes are being tested on the risk of flow slides, much more attention is being given to scour holes in the Rhine-Meuse delta (Buschman et al., 2015). Huismans and van Duin (2016) and Koopmans (2017) were able to identify over 100 scour holes within the delta. Koopmans (2017) showed that these scour holes have very different growth rates, even if they are located within the same river branch. Most likely this is caused by either the heterogeneous subsoil, the presence of hydraulic structures, the geometry of the river or anthropogenic influences. Koopmans (2017) advises to individually study scour holes in the delta since the local variations in conditions cause different shapes, sizes and growth rates, making every scour hole unique. One of these is the scour hole Beerenplaat, which is located at the confluence/bifurcation of the Oude Maas and the Spui. It is a large scour hole which recently gained much more attention due to the construction of a pilot nourishment by Rijkswaterstaat.

By analyzing river bottom measurements taken with a Multibeam Echosounder, the morphological development of the scour hole Beerenplaat was investigated. It was found that the scour hole is highly dynamic, expanding in both upstream and downstream direction. This questions how the scouring process will continue in the future since it can pose great threat to the stability of both banks and dikes. Scour is dependent on the interaction between the hydraulic forcing and the resistance of the subsoil. No accurate geological maps or soil measurements are available, which can explain if the heterogeneous subsoil favours the dynamic development. Therefore it is opted to achieve a better understanding of the behavior of the scour hole Beerenplaat by investigating the hydraulic conditions. The hydraulic conditions are most likely characterized by two types of flow processes. It is however uncertain how the tide influences these flow processes and if they can explain the morphological development.

The first type of flow process is caused by the confluence/bifurcation Oude Maas and Spui. Sloff (2020) was the first to show that the scour hole is growing into the Spui, suggesting that the hydrodynamic forcing of the confluence/bifurcation plays an important role. It is however uncertain how the flow field at and around the scour hole Beerenplaat is shaped. Already known is that tide is of large influence since it can change the flow direction in the system. As a result, the system behaves as a confluence during ebb flow and a bifurcation during flood flow. These are each paired with different flow features such as flow accelerations, flow stagnation and additional turbulence.

With the help of Acoustic Doppler Current Profiler (ADCP) measurements and the output of a Delft3D model, the flow field at the confluence/bifurcation was investigated for four scenarios: peak ebb flow, flow changing from ebb \rightarrow flood, peak flood flow and flow changing from flood \rightarrow ebb. During peak ebb flow, the systems behaves as confluence and contains four of the six flow zones of an uni-directional confluence. These are the flow stagnation zone, flow deflection zone, maximum velocity zone and flow recovery zone. In addition, secondary flow patterns were found inside the scour hole, that can take the shape of three characteristic patterns. These all contain one vertical recirculation cell, which does not match with expectations based on literature. Most likely this is caused by the scour hole. During peak flood, flow the system behaves as a bifurcation splitting the flow over both the Oude Maas and Spui. The largest flow velocities occur just before the flow enters the scour hole, on the same location as during peak ebb flow. Secondary flow patterns were not observed during peak flood flow. If the flow is changing direction, either from ebb to flood or the other way around, no slack water conditions develop.

It is expected that the second type of flow processes at the scour hole Beerenplaat are the 3D flow processes. Bom (2017) and Stenfert (2017) have shown that 3D flow processes occur inside scour holes in heterogeneous subsoil. These processes are a (curved) recirculation zone, flow contraction and a horseshoe vortex. They are often paired with more turbulence and attack of the bed by the flow, promoting the scouring process locally. Due to the geometry of the scour hole, it is uncertain if they are also present in the field. On top of that, it is unknown how these 3D flow processes respond to the tide.

Therefore it was tried to investigate these 3D flow processes with again the ADCP measurements and the output of the Delft3D model. Unfortunately this was not possible, mainly due to the limitations of both the measurement and the model and the use of an incorrect geometry of the scour hole Beerenplaat. Based on the actual profile of the scour hole, it is expected that the (curved) recirculation zone develops at the steep slope of the scour hole Beerenplaat during ebb flow. If the other processes are present remains yet uncertain.

Nevertheless, it was investigated if the hydraulic forcing, caused by the confluence/bifurcation and the recirculation zone, can explain the morphological development of the scour hole Beerenplaat. With the help of computing bed shear stresses it was visualized where the confluence/bifurcation flow attacks the river bed the most, showing the areas vulnerable for scour. This could only be done for ebb flow, due to the incorrect geometry of the scour hole Beerenplaat in the Delft3D model. It was found that these areas vulnerable to scour were no match with the observed morphological development. Most probably, the attack of the bed during flood flow should be included to describe the expansion of the scour hole and growth towards the Spui. The expected presence of the recirculation zone can explain why the upstream slope of the scour hole Beerenplaat retains its shape during expansion and gives reasoning why the location with the largest scour depth has migrated upstream.

Overall, there can be concluded that the tide is of much influence on the identified flow processes and the morphological development of the scour hole Beerenplaat. The response of the flow processes during ebb flow intends to make the scour hole deeper and expands it in the downstream direction. During flood, it is expected that the scour hole has significant development in the upstream direction, and potentially into the Spui. Unfortunately it was not possible to confirm this. The heterogeneous subsoil could still affect the response of the scour hole Beerenplaat to the tide. For fully understanding the flow processes at the scour hole Beerenplaat, there is recommended to perform additional Delft3D model runs with an updated bathymetry and to develop a new model that is completely suitable to investigate the 3D flow processes inside the scour hole Beerenplaat. To properly understand and eventually predict the morphological development of the scour hole Beerenplaat, it is recommended to research and include the composition of the heterogeneous subsoil.

Pr	etace	9		ı	
Αŀ	ostra	ct		ii	
No	omenclature				
Li	st of	Figure	s	x	
Li	st of	Tables		xvi	
1	Intro	oductio	on	1	
	1.1	Backg	ground information	. 1	
	1.2	Proble	em description	. 3	
	1.3	Resea	arch objective	. 3	
	1.4	Appro	ach and outline of the report	. 4	
2	Con	ditions	s in the Rhine-Meuse delta and the site of the pilot nourishment	5	
	2.1	Syste	m review	. 5	
	2.2	Revie	w of relevant literature	. 7	
		2.2.1	Heterogeneous subsoil of the Rhine-Meuse delta	. 7	
		2.2.2	Scour holes in the Rhine-Meuse delta	. 8	
		2.2.3	Hydrodynamic processes inside scour hole	. 9	
		2.2.4	Development of scour holes	. 12	
		2.2.5	Confluence/bifurcation flow	. 15	
		2.2.6	Estuarine sand waves	. 18	
	2.3	Pilot n	nourishment	. 19	
		2.3.1	Location of nourishments	. 20	
		2.3.2	Monitoring measurements with a Multibeam Echosounder	. 21	
		233	Relevance for this research	22	

3	Mor	pholog	ical development	23
	3.1	Morph	ological development of scour hole Beerenplaat	23
		3.1.1	Scour depth	27
		3.1.2	Development stage	29
	3.2	Morph	ological development after the pilot nourishment	30
		3.2.1	Scour section 6	30
		3.2.2	Scour section 5	30
	3.3	Conclu	usion on sub research question 1	34
4	Flov	v proce	esses	35
	4.1	Metho	d	35
		4.1.1	Delft3D model	35
		4.1.2	ADCP measurements	37
	4.2	Flow fi	eld at confluence/bifurcation	37
		4.2.1	Base case: similar conditions	38
		4.2.2	Case 2: different conditions	49
		4.2.3	Secondary flow patterns during ebb flow	55
		4.2.4	Conclusion on sub research question 2	57
	4.3	3D flov	w processes	58
		4.3.1	Presence of 3D flow processes inside the scour hole Beerenplaat	59
		4.3.2	Conclusion on sub research question 3	65
5	Link	c betwe	en scour hole development and flow processes	66
	5.1	Recap	morphological development	66
	5.2	Conflu	ence/bifurcation flow	66
	5.3	3D flov	w processes inside the scour hole	70
	5.4	Conclu	usion on sub research question 4	70
6	Disc	cussior	1	72
	6.1		ological development	72
		6.1.1	MBES measurements	72
		6.1.2	Equilibrium scour depth	73

	6.2	Hydraulic conditions	73
		6.2.1 Comparison discharges model and ADCP measurements	73
		6.2.2 Flow field at confluence/bifurcation Oude Maas and Spui	74
		6.2.3 Secondary flow process	74
	6.3	Improvements and changes to the modelling approach	75
	6.4	Relevance for other scour holes in the Rhine-Meuse delta	⁷ 6
7	Con	nclusion	77
	7.1	Research objective	7
	7.2	Sub research questions	7
	7.3	Main research question	79
8	Rec	ommendations 8	31
	8.1	Recommendations based on this research	31
	8.2	Recommendations for the scour hole Beerenplaat	31
Re	efere	nces 8	36
	۸ ما ما	litional literature	37
A	Add A.1	Initiation of motion	
	Α. Ι	A.1.1 Adaptation Shields equation	
		A.1.2 Izbash	
	۸ 2	Sediment transport	
		Scour holes	
	Α.5	A.3.1 Types of scour	
		A.3.2 Empirical equation for equilibrium depth	
		A.3.3 Undermining of scour holes in heterogeneous subsoil	
		A.3.4 Effect of tide on scouring process	
	Α4	Flow and sediment transport in a river bend	
	A.5	Bed forms	
	7 1.0	A.5.1 Classification	
		A.5.2 Response of river dunes on changing river flow	
		A.5.3 Behaviour of marine sand waves	
		A.5.4 Tidal response of estuarine sand waves	
			_

В	Cha	racteristic time scour hole Beerenplaat	100
С	Estu	uarine sand waves	104
	C.1	Dimensions	.104
	C.2	Seasonal river flow and river dunes	.107
	C.3	Tidal conditions and response estuarine sand waves	.110
	C.4	Change in conditions since pilot nourishment	. 111
D	Cha	racteristics Delft3D model and field conditions	115
	D.1	Characteristics Delft3D model	.115
	D.2	Field conditions	.117
Ε	Con	nparison model results and ADCP measurements	119
F	Sec	ondary flow patterns	124
	F.1	Characteristic patterns	.124
	F.2	Conditions for development characteristic patterns	.130
	F.3	Summary	.134
	F.4	Velocities at four cross-sections for representative time steps	.135
	F.5	Secondary flow patterns in model results	.138
G	Ana	lysis horseshoe vortex ADCP measurements	141
	G.1	Identification of horseshoe vortex	.146
	G.2	Identification of wake	.147

Nomenclature

Abbreviations

Abbreviation	Definition
ADCP	Acoustic Doppler Current Profiler
DNS	Direct Numerical Simulation
FM	Flexible Mesh
MBES	Multibeam Echosounder
NAP	Normaal Amsterdams Peil
OM	Oude Maas
ppt	parts per thousand
Rkm	Rhine kilometer
	River kilometer
SP	Spui

Symbols

Symbol	Definition	Unit
C	Chézy coefficient	$[{\sf m}^{0.5}/{\sf s}]$
d	grain size	[m]
d	water depth	[m]
d_{50}	median gain size sediment	[m]
D*	sedimentological parameter	[-]
f_c	roughness function	[-]
g	gravitational acceleration	[m/s ²]
h	water depth	[m]
h_0	initial water depth	[m]
h_s	scour depth	[m]
H	height estuarine sand wave	[m]
L_{hole}	length scour hole	[m]
q_s	sediment transport per unit width	[m²/s]
Q	discharge	[m³/s]
r_0	relative turbulence intensity	[-]
S	salinity	[ppt]
t	time	[s]
t_1	characteristic time scale scour hole	[months]
Δt_{output}	interval at which model output is saved	[hr]
u	flow velocity	[m/s]
\overline{u}	depth averaged flow velocity	[m/s]

Symbol	Definition	Unit
\widetilde{u}	fluctuating flow velocity component	[m/s]
u_c	critical flow velocity at which grains start to move	[m/s]
\overline{u}_c	depth averaged critical flow velocity	[m/s]
u_{*c}	critical flow velocity	[m/s]
U_d	characteristic mean flow velocity	[m/s]
$U_{m,t}$	maximum flow velocity during tide	[m/s]
W_{hole}	width scour hole	[m]
x	coordinate in streamwise direction	[m]
x	RD coordinate	[m]
y	coordinate in cross-streamwise direction	[m]
y	RD coordinate	[m]
y_m	maximum scour depth	[m]
$y_{m,e}$	equilibrium scour depth	[m]
z	coordinate in vertical direction	[m]
z_b	bed level	[m]
α	angle upstream slope scour hole	[°]
α	derivative of flow velocity over time	[-]
α	coefficient for flow velocity and turbulence intensity	[-]
β	angle downstream slope scour hole	[°]
γ	coefficient in Breusers equation	[-]
Δ	relative density	[-]
η	water surface elevation	[m]
θ	temperature	$[^{\circ}C]$
ν	kinematic viscosity	$[m^2/s]$
ho	density	[kg/m ³]
$ ho_c$	density clay	[kg/m ³]
$ ho_s$	density sea water	[kg/m ³]
$ ho_s$	density sand	[kg/m ³]
$ ho_w$	density fresh water	[kg/m ³]
$ au_b$	bed shear stress	$[N/m^2]$
$ au_c$	critical shear stress	$[N/m^2]$
ψ_c	critical mobility parameter Shields	[-]

List of Figures

1.1	Overview of scour holes in the Rhine-Meuse delta (Huismans & van Duin, 2016)	1
1.2	Scour hole development in heterogeneous subsoil (Koopmans, 2017)	2
1.3	Location of the scour hole Beerenplaat	2
2.1	Overview of the Rhine-Meuse delta (Sloff et al., 2013)	5
2.2	Location of the scour hole Beerenplaat	6
2.3	Conditions and processes at the scour hole Beerenplaat	6
2.4	Hypothetical composition of the subsoil in the Rhine-Meuse delta (Huismans & van Duin, 2016)	7
2.5	Scour hole development in heterogeneous subsoil (Koopmans, 2017)	8
2.6	Scour hole growth in area and depth from 2009 until 2014 per section of the Rhine-Meuse delta (Koopmans, 2017)	9
2.7	2D flow processes at a scour hole, flow is from left to right. Obtained from Bom (2017), based on Hoffmans and Booij (1993).	10
2.8	Schematic presentation of flow lines inside a scour hole (Stenfert, 2017)	10
2.9	Flow contraction in a scour hole, based on Bom (2017)	11
2.10	Location of horseshoe vortex along the edge of a scour hole (Bom, 2017)	11
2.11	Four stages of scour hole development. Obtained from Bom (2017), based on Hoffmans and Verheij (1997)	13
2.12	Influence of live-bed and clear-water scour on scour depth (Hoffmans & Verheij, 1997).	13
2.13	Effect of tide on the profile of a scour hole, based on (Zuylen, 2015)	14
2.14	Six identifiable flow zones at a confluence. Obtained from Bilal et al. (2020), based on J. L. Best (1986)	15
2.15	Schematic illustration of hydrodynamic flow zones at a tidal confluence (Dai et al., 2020).	16
2.16	Flow field at a discordant confluence Bilal et al. (2020).	17
2.17	Secondary flow components in a confluent channel. Obtained from Shadeed et al. (2019), based on Weber et al. (2001)	18
2.18	Schematic presentation of flow over bedforms (Hulscher & Dohmen-Janssen, 2005)	19
2 10	River denth in m + NAP on June 2018 at the pilot site in the Oude Maas	10

List of Figures xi

2.20	and data from Laurens Baars (RWS-WNZ)	20
2.21	River depth at scour section 5 before and after the nourishment	20
2.22	River depth at scour section 6 before and after the pilot nourishment	21
2.23	Bathymetry measurement with a Multibeam Echosounder (Colbo et al., 2014)	22
3.1	Location of the river bottom at scour hole Beerenplaat	23
3.2	Location of α and β	25
3.3	Development of the river bottom in the axis of scour hole Beerenplaat	25
3.4	Contour lines of the edge of the scour hole Beerenplaat	26
3.5	Growth of the scour hole in the trench towards the Spui, based on Sloff (2020)	27
3.6	Scour depth development of the scour hole Beerenplaat.	27
3.7	First estimation of the scour depth development with the Breusers equation	29
3.8	Development of the river bottom in the axis of scour section 6	30
3.9	Development of the river bottom in the axis of scour section 5. Only the measurement of December 2017 has been taken before the pilot nourishment.	31
3.10	Presence of irregular bedforms before nourishment in June 2017 and systematic bedforms after nourishment in June 2019	32
3.11	Average height of the estuarine sand waves in scour section 5	32
3.12	River bottom measurements of scour section 5 in m + NAP. The red ellipse indicates the area where the nourishment is constructed in the spring of 2018	34
4.1	Comparison of measured discharges at Lobith	38
4.2	Comparison of water level at Spijkenisse (measured by Rijkswaterstaat)	39
4.3	Water levels at Spijkenisse measured by Rijkswaterstaat and computed in the model	40
4.4	Streamwise depth averaged velocities and river bottom at time step 359 (08:40) and ADCP measurement 2 (08:28)	41
4.5	Streamwise depth averaged velocities and river bottom at time step 363 (16:40) and ADCP measurement 6 (15:05)	41
4.6	Overview of the confluence/bifurcation Oude Maas and Spui	42
4.7	Secondary flow pattern during peak ebb flow (time step = 359). The velocity vectors show the cross-stream and vertical velocities	43
4.8	Depth averaged velocities during peak ebb flow (time step = 359)	44
4.9	Depth averaged velocities during flow changing from ebb to flood (time step = 362)	45
4.10	Depth averaged velocities during peak flood flow (time step = 363)	46

List of Figures xii

4.11	Cross-section at Rkm 995.63 during peak flood flow (time step = 363). The velocity vectors show the cross-stream and vertical velocities	46
4.12	Depth averaged velocities during flow changing from flood to ebb (time step = 358)	47
4.13	ADCP measurement 2 at Rkm 995.9 during ebb (08:28). The velocity vectors represent the cross stream and vertical velocities	48
4.14	ADCP measurements taken around cross-section Rkm 995.8 on 11 February 2021	49
4.15	Location of the ADCP measurements 2 and 6 taken during ebb and flood	49
4.16	Water levels at Spijkenisse measured by Rijkswaterstaat and computed in the model	50
4.17	Depth averaged velocities at peak ebb flow (time step = 1198)	51
4.18	Secondary flow pattern in cross-section at Rkm 995.75 (time step = 1198)	51
4.19	Depth averaged velocities at flow changing from ebb to flood (time step = 1200)	52
4.20	Depth averaged velocities at peak flood flow (time step = 1202)	53
4.21	Depth averaged velocities at flow changing from flood to ebb (time step = 1197)	54
4.22	Expected secondary flow process if no scour hole is present	55
4.23	Schematization of the development of recirculation cells for a flat river bottom and one with a scour hole. The numbers represent the order in which the recirculation cell develops.	56
4.24	Location of ADCP measurements	59
4.25	Velocities in both the model and the ADCP measurements, for identifying flow contraction.	61
4.26	Velocities in the model, for identifying the recirculation zone. Cross-sectional distance 0 m is located at the confluence/bifurcation.	62
4.27	Velocities in the model and ADCP measurements, for identifying the horseshoe vortex. The location of the cross-section (x/L_{hole}) is at half the length of the scour hole	64
5.1	Schematization of the scour hole Beerenplaat. The red arrows represent the direction in which the scour is expanding.	67
5.2	Bed shear stress at peak ebb flow during the base case (confluence, time step = 359)	69
5.3	Bed shear stress at peak flood flow during the base case (bifurcation, time step = 363).	69
5.4	Influence of the geometry of the scour hole on the flow near the river bed during flood. The black lines represent the situation of the model and red lines the field scenario	70
6.1	Density driven currents due to salinity differences.	74
6.2	Salinity at the scour hole Beerenplaat during peak ebb flow. Fresh water has a salinity of 0.5 ppt and sea water has a salinity of 35 ppt.	75
6.3	Illustration of tidal flow at a scour hole with a typical profile	76
A.1	Critical Shield parameter versus the sedimentological parameter (Hoffmans & Verheij, 1997)	88

List of Figures xiii

A.2	Sediment transport (Jansen et al., 1979)	89
A.3	Control volume for the derivation of the Exner equation, obtained from Bom (2017)	90
A.4	Control volume for clear-water and live-bed scour, based on Schiereck and Verhagen (2019)	91
A.5	Top view of the undermining process in a scour hole (Stenfert, 2017)	93
A.6	Illustration of flow in a river bend (van Balen, 2010)	94
A.7	Development of uniform flow (Wilkerson et al., 2019)	95
8.A	The transverse component in bend flow	95
A.9	Scour in a river bend (Hoffmans & Verheij, 1997)	96
A.10	GIS maps of the scour hole Beerenplaat and the Oude Maas (Rijkswaterstaat WNZ)	97
A.11	Bed form stability diagram according to multiple researchers (Kleinhans et al., 2017)	97
A.12	Illustration of different bed forms (van Rijn, 1993).	98
A.13	Superimposition of bed forms (Reesink et al., 2018)	98
A.14	Response of river dunes on a semi-diurnal tide, based on Kostaschuk and Best (2005).	99
B.1	Sieve data of 10 soil samples from the nourished sediments at the pilot site in the Oude Maas (Rijkswaterstaat WNZ)	103
C.1	Discharge at Lobith and estimated at the pilot site	108
C.2	Water surface elevation (η) at scour section 5	108
C.3	Monthly averaged low tide at Spijkenisse	111
C.4	Expected bedform height by the tide	111
C.5	River bottom measurements in m + NAP. The red arrows represent the distance along the channel where the estuarine sand waves are found	114
D.1	Location of the scour hole Beerenplaat	115
D.2	Bathymetry at partition 93 on 14 June 2018	117
D.3	Field conditions during the time frame of the model, investigated by V. Chavarrias (Deltares)	.118
E.1	Comparison of water levels at Spijkenisse (measured by Rijkswaterstaat)	119
E.2	Water levels at Spijkenisse measured in the field by Rijkswaterstaat and computed in	
	the model	120
E.3	Streamwise velocities and river bottom at time step 359 and ADCP measurement 2	120
E.4	Streamwise velocities and river bottom at time step 363 and ADCP measurement 9	122
F 5	Streamwise velocities and river bottom at time step 363 and ADCP measurement 6	122

List of Figures xiv

E.6	Velocities in both the ADCP measurement and model at Rkm 995.8	123
F.1	Four cross-sections at which the secondary flow patterns are analyzed	125
F.2	Cross sections showing the velocities at the scour hole Beerenplaat. Velocity vectors represent the cross-stream and vertical velocities.	125
F.3	Characteristic pattern 1 of the secondary flow downstream of the confluence Oude Maas and Spui.	126
F.4	Characteristic pattern 2 of the secondary flow downstream of the confluence Oude Maas and Spui.	127
F.5	Characteristic pattern 3 of the secondary flow downstream of the confluence Oude Maas and Spui.	128
F.6	Schematization of the development of recirculation cells for a flat river bottom and one with a scour hole. The numbers represent the order in which the recirculation cell develops	.130
F.7	Secondary flow patterns observed during ebb in 50 tidal cycles of the model. The tidal cycles are located between time step 599 - 915.	130
F.8	Comparison of cross-section three in model time step 657 and 658	132
F.9	Velocities at cross-section 3 on time step 358	132
F.10	Water levels at Spijkenisse according to the model and representative time steps at which the model output is analyzed for the three characteristic situations.	133
F.11	Velocities at cross-section 3 on time step 1334	133
F.12	Velocities at cross-section 4 on time step 1334	133
F.13	Depth averaged flow velocities at time step = 1198	134
F.14	Delft3D model output at time step 358 (= 13 Jul 2018 20:00)	135
F.15	Delft3D model output at time step 359 (= 13 Jul 2018 22:00)	136
F.16	Delft3D model output at time step 657 (= 7 Aug 2018 18:00)	136
F.17	Delft3D model output at time step 658 (= 7 Aug 2018 20:00)	137
F.18	Delft3D model output at time step 1198 (= 21 Sep 2018 20:00)	137
F.19	Delft3D model output at time step 1334 (= 6 Oct 2018 04:00)	138
F.20	Water levels for all analyzed time steps in table F.2.	138
G.1	Velocities measured at ADCP transect 2 (08:28)	141
G.2	Fluctuating turbulence component \widetilde{u} of ADCP transect 2 (08:28)	142
G.3	Location of turbulent fluctuation values of table G.1.	143
G.4	Locations where velocities are analyzed for identifying the horseshoe vortex	144
G.5	Velocities in the water column at the four locations of figure G.4	145

List of Figures	XV

G.6 Depth averaged turbulence \widetilde{u} values for identifying horseshoe vortex	146
G.7 Depth averaged turbulence \widetilde{u} values for identifying wake	147

List of Tables

2.1	The main characteristics of a non-tidal and a tidal confluence (Bilal et al., 2020) 16		
2.2	Monitoring measurements of the river bottom at the Rhine-Meuse delta	21	
3.1	Estimation of the edge expansion.	24	
3.2	Estimation of the slope angles	24	
3.3	Overview of parameters and values used to estimate the scour hole development	28	
3.4	Average height estuarine sand waves in scour section 5 (appendix C.1)	32	
4.1	Overview of model time steps and ADCP measurements for scenarios base case	39	
4.2	Overview of model time steps for scenarios case 2	50	
4.3	Comparison of discharges during peak ebb and peak flood flow at Rkm 995.9	50	
4.4	Features of the expected secondary flow patterns based on literature and the three characteristic shaped secondary flow patterns identified out of the Delft3D model	56	
4.5	Overview of 3D processes that can be present at scour hole Beerenplaat and the capability of the methods to show them	58	
4.6	Summary on the investigation of the 3D flow processes inside the scour hole Beerenplaat. A red cross means that the flow process was not observed.	65	
5.1	Summary of morphological development observed in the field and the morphological development suggested by the hydraulic forcing of the confluence/bifurcation and 3D flow processes during ebb.	71	
A.1	Critical velocity of clay (Ven Te Chow, 1959).	88	
C.1	Height of estuarine sand waves in February 2021	104	
C.2	Height of estuarine sand waves in June and December 2020	105	
C.3	Height of estuarine sand waves in June and December 2019	105	
C.4	Height of estuarine sand waves in June and December 2018	106	
C.5	Average water depth in scour section 5	107	
C.6	Change of flow velocities at scour section 5	109	

List of Tables xvii

C.7	Hydraulic changes and response of river dunes. The expected behavior of the river dunes has been obtained out of the literature described in appendix A.5	110
C.8	First estimation of equilibrium bedform height with empirical relation of Allen (1968)	111
C.9	Change in perturbations since the pilot nourishment	112
D.1	Main settings of the Delft3D model	116
E.1	Comparison of discharges in the model and the ADCP measurements during peak ebb flow.	121
E.2	Comparison of discharges in the model and the ADCP measurements during flood	121
F.1	Overview of the characteristic secondary flow pattern per representative time step	131
F.2	Secondary flow patterns present at two consecutive time steps of the ebb flow for 50 tidal cycles. The dash means that the velocities were very low and the system did not yet behave as a confluence with secondary flow patterns.	140
G.1	Averaged turbulence values in the streamwise direction. Bold values are 20 % larger than \widetilde{u}_{aver}	143

Introduction

1.1. Background information

Since dikes are being tested on the risk of flow slides, much more attention is given to scour holes in the Rhine-Meuse delta (Buschman et al., 2015). A flow slide is a failure mechanism of an underwater slope, that occurs when a substantial amount of sediment moves down slope (Alhaddad, 2021). These flow slides could lead to bank or dike failure, having significant consequences for the most densely populated regions of the Netherlands. Huismans and van Duin (2016) and Koopmans (2017) were able to identify over 100 scour holes in the delta, which can be seen in figure 1.1. Some of these scour holes are over 20 meters deep and are still growing yearly. As a result, they could create slopes that become unstable and potentially trigger a flow slide. Rijkswaterstaat wants to act on these scour holes to reduce the risk they pose on bank or dike failure.

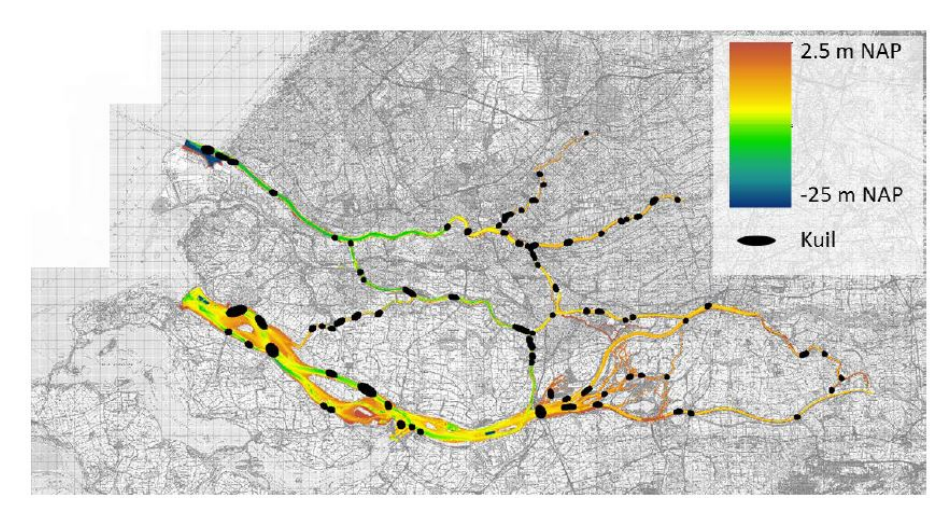


Figure 1.1: Overview of scour holes in the Rhine-Meuse delta (Huismans & van Duin, 2016).

Koopmans (2017) showed that the scour holes in the Rhine-Meuse delta have very different growth rates, even if they are located within the same river branch. The study identified that either the heterogeneous subsoil, the presence of hydraulic structures or the rivers geometry is responsible for this phenomena. Unique for the delta are the geological conditions. The subsoil consist out of poorly erodible clay and peat layers that have been deposited on top of highly erodible sand layers. The thickness and type of these layers differs at every location and can locally favour or limit the scouring process. This heterogeneous subsoil is also the cause that 40% of the scour holes are present in the delta (Koopmans, 2017). As illustrated in figure 1.2, events have occurred that locally removed the poorly erodible

top layers and exposed the highly erodible layers below. This has allowed for the development of these deep scour holes. Next to the geological conditions, the hydrodynamic conditions also vary locally in the delta. The Rhine-Meuse delta contains many confluences, bifurcation and bends which are paired with complex flow patterns. On top of that, hydraulic structures, such as bridge piers, are present that interfere with the flow. These varying geological and hydrodynamic conditions are responsible for the different growth rates of scour holes in the Rhine-Meuse delta. Koopmans (2017) advises to individually study scour holes in the delta since these local variations in conditions cause different shapes, sizes and growth rates, making every scour hole unique.

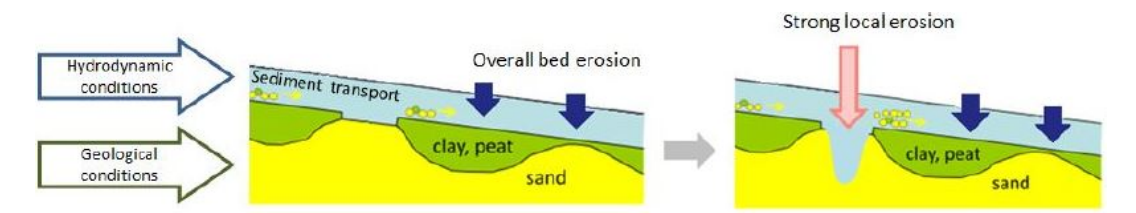


Figure 1.2: Scour hole development in heterogeneous subsoil (Koopmans, 2017).

In the need of understanding the formation and behaviour of the scour holes in the delta, research has been done in the last years. Sloff et al. (2013) researched the future development of the river bed and investigated possible management options with various numerical models. Commissioned by Rijkswaterstaat, Deltares executed the project "Advies beheer rivierbodem RMM" in which they laid focus on achieving insights regarding the dynamic bottom of the Rhine-Meuse delta. Additional, MSc graduation theses have been performed at Delft University of Technology in cooperation with Deltares. These theses focused on the origin of scour holes (Koopmans, 2017), small scale laboratory experiments simulating 2D scour hole development (Zuylen, 2015) and 3D scour hole development (Koopmans, 2017; Stenfert, 2017) and on creating a numerical model that simulates flow processes in small scale scour holes (Bom, 2017). This thesis will proceed forwards on the gained knowledge from these previous researches.

In 2018 Rijkswaterstaat performed pilot sand nourishments in scour holes at the Rhine-Meuse delta. The goal was to investigate if a nourishment is able to stabilize the deepening of the scour holes and reduce the risk they pose on stability of banks and dikes. The pilot site is located in the Oude Maas, which contains a very deep ellipsoidal scour hole called Beerenplaat. This scour hole is located closely to the confluence/bifurcation of the Oude Maas and Spui as can be seen on figure 1.3. It has gained the attention from Rijkswaterstaat for quite a while due to its dynamic behaviour and size. The scour hole is at its deepest -28 m + NAP.

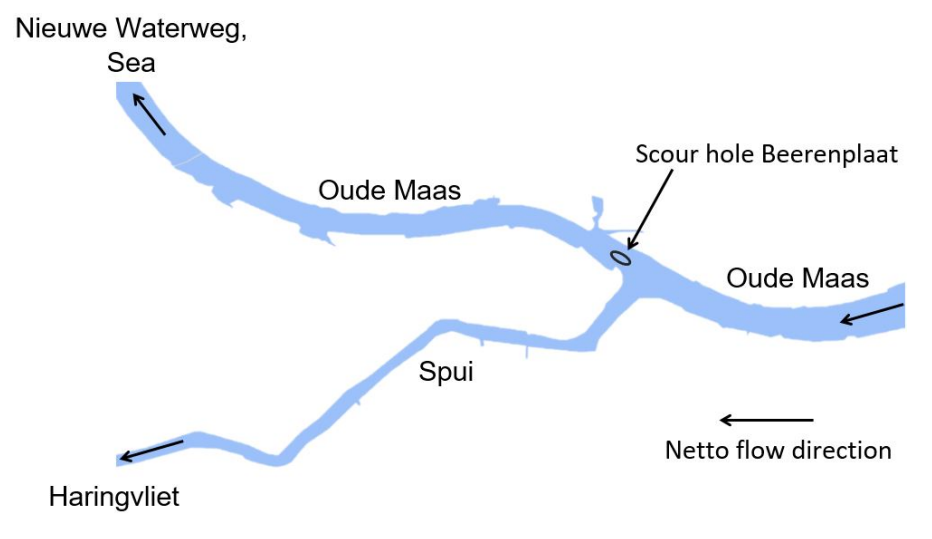


Figure 1.3: Location of the scour hole Beerenplaat.

1.2. Problem description

Understanding how scour holes in the delta behave and respond to local field conditions is important for Rijkswaterstaat to appropriate deal with them. This also applies for the scour hole Beerenplaat. The development of a scour hole depends on the interaction between the resistance (geological conditions) and the forcing (hydraulic conditions). Unfortunately, no accurate geological maps or bottom composition measurements are available, which can help in understanding the development of the scour hole Beerenplaat from the resistance perspective. However, measurements on the hydraulic conditions at the scour hole Beerenplaat are available due to the pilot nourishment. Based on these measurements and the previous researches on scour holes in heterogeneous subsoil, it is expected that the hydraulic conditions at the scour hole Beerenplaat are determined by two types of flow processes.

The first type of flow process is caused by the confluence/bifurcation Oude Maas and Spui. Koopmans (2017) listed the effect of the river geometry as contributor to the development of scour holes in the Rhine-Meuse delta. Sloff (2020) did a first analysis of the monitoring data from the pilot site and found that the scour hole Beerenplaat is growing in a shallow trench leading towards the Spui. This suggests that the hydrodynamic forcing of the confluence/bifurcation affects the development of the scour hole. An important aspect to this is the tide. At normal tidal conditions, without high river discharges, the tide causes flow reversal four times per day, which reshapes the flow field continuously. It is still uncertain how the flow field at this confluence/bifurcation Oude Maas and Spui is shaped during a tidal cycle and if this indeed plays a major role in the scouring process of the scour hole Beerenplaat.

The second type of flow processes is encountered inside the scour hole Beerenplaat. Bom (2017) and Stenfert (2017) found that 3D flow processes, such as a horseshoe vortex, curved flow recirculation zones and flow contraction, occur inside a scour hole in heterogeneous subsoil. These 3D processes could be important to describe the dynamic behavior of the scour hole Beerenplaat since they can locally accelerate the flow or induce additional turbulence. It is however uncertain if they are present since the geometry of the scour hole Beerenplaat is not exactly symmetrical and ellipsoidal. On top of that, the 3D flow processes were only investigated under uni-directional flow conditions. How the tide affects them is still an open question.

1.3. Research objective

The objective of this research is to better understand how the hydrodynamic flow processes, that force the scour hole Beerenplaat, are influenced by the tide and to establish a link between the behavior of scour hole and these hydrodynamic processes.

Main Research Question

How are the flow processes at the scour hole Beerenplaat influenced by the tide and in what way does this affect the morphological development of the scour hole?

Sub-Questions

- 1. What was the morphological development of the river bottom at the scour hole Beerenplaat and the location of the pilot nourishment in the Oude Maas?
- 2. How is the flow field at the confluence/bifurcation Oude Maas & Spui shaped during a tidal cycle?
- 3. Which of the 3D flow processes are present inside the scour hole Beerenplaat and what is the influence of the flow direction and intensity on them?
- 4. To what extend do the flow processes at the scour hole Beerenplaat and their tidal response give an explanation of the morphological development?

1.4. Approach and outline of the report

First, the conditions in the Rhine-Meuse delta and the site of the pilot nourishment will be reviewed in chapter 2. Chapter 3 focuses on describing the morphological development of both the scour hole Beerenplaat and the pilot site (*sub-question 1*). This will be done by using measurements of the river bottom taken with a Multibeam Echosounder by Rijkswaterstaat. In chapter 4, the flow processes and their tidal response are researched. This is first done for the flow caused by the confluence/bifurcation Oude Maas & Spui (*sub-question 2*) and after that for the 3D flow processes inside the scour hole (*sub-question 3*). This chapter will make use of the hydraulic measurements taken at the pilot site with an Acoustic Doppler Current Profiler. These measurements on its own are not enough to answer this question since they are only taken on one cross-section at the scour hole. Therefore a Delft3D model is used as well to give a broader picture of what is happening at the area of interest. In chapter 5, a link is established between the morphological development of the scour hole Beerenplaat and the flow processes (*sub-question 4*). The results on the previous research questions will be used for this. Chapter 6 provides a discussion on the performed research. Chapter 7 will present the conclusion and finally chapter 8 will give recommendations.

Conditions in the Rhine-Meuse delta and the site of the pilot nourishment

This chapter focuses on describing the current knowledge on this topic.

2.1. System review

Figure 2.1 gives an overview of the Rhine-Meuse delta. Seasonal river flow of the Rhine and the Meuse enters the system via the Lek, Waal and Bergsche Maas. The outflow into sea occurs via the Nieuw Waterweg and during high tide via the Haringvliet. This has been the case since the closure of the Haringvliet with a barrier and sluices in 1970. The closure of the Haringvliet also caused a redistribution of tidal flows. Nowadays, the tide is forced via the Nieuwe Waterweg, through the connecting branches Oude Maas, Spui and Dordtsche Kil to reach the Haringvliet and Hollandsch Diep. This has caused an increase of flow velocities, causing large scale erosion of these branches (Sloff et al., 2013). The scour hole Beerenplaat, located at the confluence/bifurcation Oude Maas and Spui, is located within these central branches (see figure 2.1 and figure 2.2).

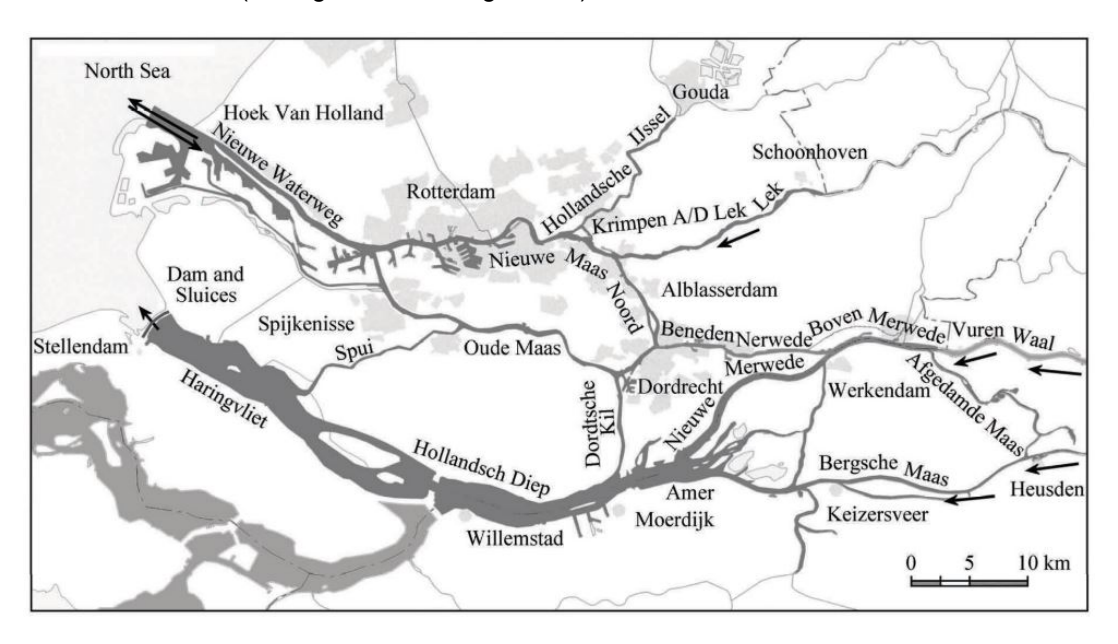


Figure 2.1: Overview of the Rhine-Meuse delta (Sloff et al., 2013).

2.1. System review 6

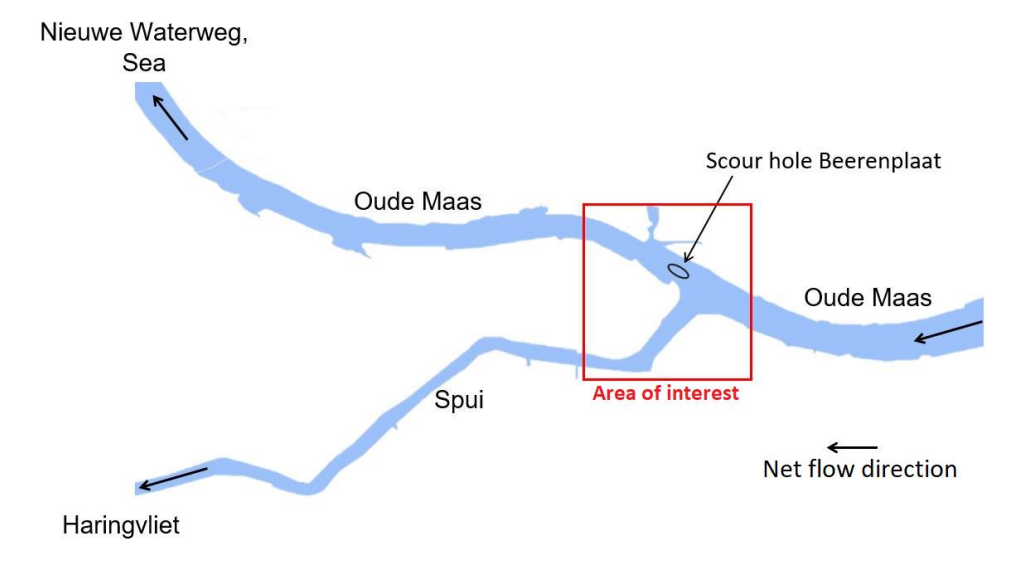


Figure 2.2: Location of the scour hole Beerenplaat.

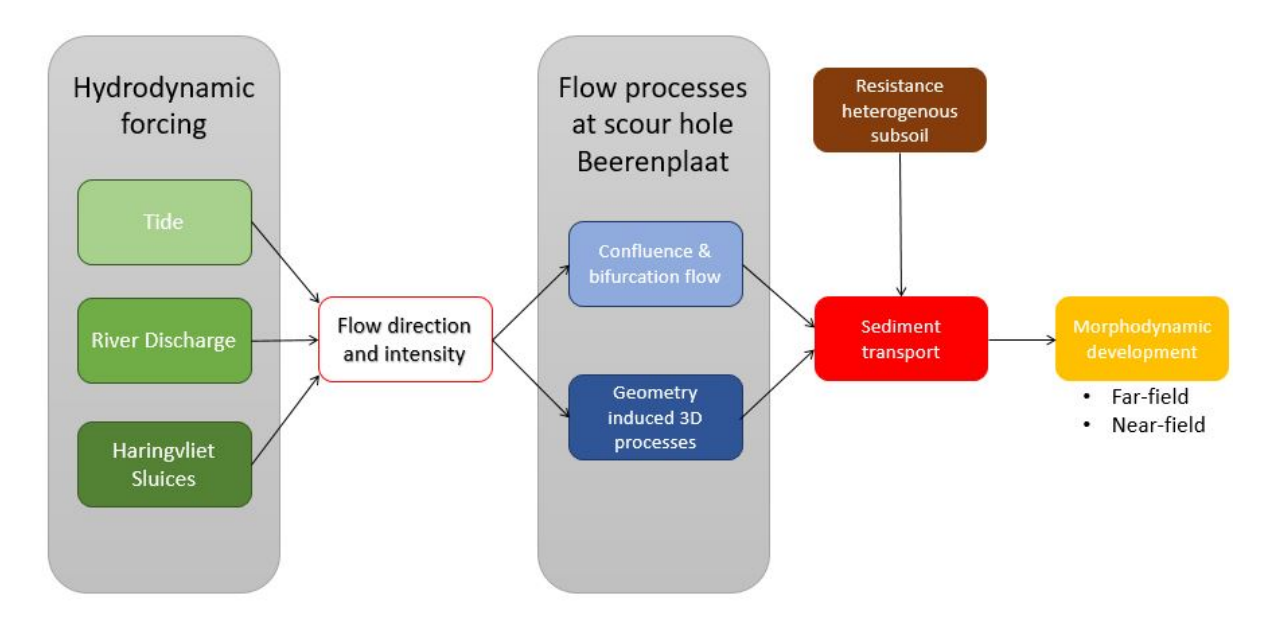


Figure 2.3: Conditions and processes at the scour hole Beerenplaat.

As can be seen in figure 2.2 the scour hole Beerenplaat is located in the Oude Maas close to the confluence/bifurcation with the Spui. The hydrodynamic forcing at this area of interest is determined by three factors: the river discharge, the tide and the operation of the Haringvliet sluices. The river discharge depends on the seasonal river flow in both the Rhine and the Meuse and varies significantly on a weekly to monthly basis. The second factor is the Haringvliet sluices. Since January 2019 the sluices of the dam are regularly left open, during the tidal flood period, to promote the ecology in the delta. How much they are opened is dependent on the river discharges in the Rhine and the Meuse and the salt intrusion into the delta. They can be opened much more during the high discharge season than during low discharge season. The dependence of the sluice operations on tides and river discharges causes water levels in the Haringvliet and Hollandsch Diep to vary in a complex way, which is difficult to quantify or predict. This has impact on the flows in the Oude Maas and Spui. The final factor is the tide which is able to penetrate into the area of interest via the Nieuwe Waterweg and the Oude Maas. The tide can completely change the flow direction in the branches of the river. It is able to significantly change the river flow, at the area of interest, on an hourly basis. The interaction of these

three factors determines the flow direction and intensity at the area of interest. Each of the factors force the hydrodynamics on a different time scale varying form hourly to monthly, making the system very diverse and dynamic.

Two types of flow processes are expected at the scour hole Beerenplaat, which characterize the flow field at the area of interest. These are the confluence/bifurcation flow and the geometry induced 3D flow processes. If these processes are present, how strongly they are and the shape in which they appear, is dependent on the flow direction and flow intensity of the system. The flow processes determine how the flow field is shaped, including regions of high velocities and turbulence. These regions are of main interest since they can result into sediment transport. However, the transport of sediment particles is also dependent on the resistance of soil particles. As already explained the Rhine-Meuse delta has a very heterogeneous subsoil containing poorly erodible layers such as clay and peat that are cohesive and highly erodible layers of sand. The configuration of these layers, at the area of interest, determines the resistance of the soil against sediment transport.

The morphological development at the area of interest can be sub-divided into far-field and near-field development. The near-field development refers to the location of the scour hole Beerenplaat. The far-field development refers to the river bottom further upstream or downstream of the scour hole. Sediment is transported out of the scour hole but can be deposited at locations with milder flow conditions. On top of that, Sloff (2020) has shown that bed load transport in the form of sand waves can occur at the area of interest, affecting the far-field morphological development.

What makes this system complex are the three hydrodynamic forcing factors behaving on different time scales, making the forcing side very dynamic and diverse. On top of that, no detailed mapping of the subsoil at the area of interest is available and therefore it is not possible to understand the resistance of the soil. As a result, it is impossible to give any indications of sediment transport at the scour hole. Nevertheless, a large scour hole has developed, meaning that much sediment transport has taken place. This thesis focuses on investigating the flow processes at the scour hole Beerenplaat and linking them to the near-field morphological development.

2.2. Review of relevant literature

2.2.1. Heterogeneous subsoil of the Rhine-Meuse delta

One of the key components for the development of scour holes in the Rhine-Meuse delta is the heterogeneous subsoil. The subsoil consist out of many different layers that are highly and poorly erodible. The four most significant deposits are the poorly erodible clay and peat layers, the highly erodible sand layer and channel belts. A hypothetical overview of the subsoil composition can be seen in figure 2.4.

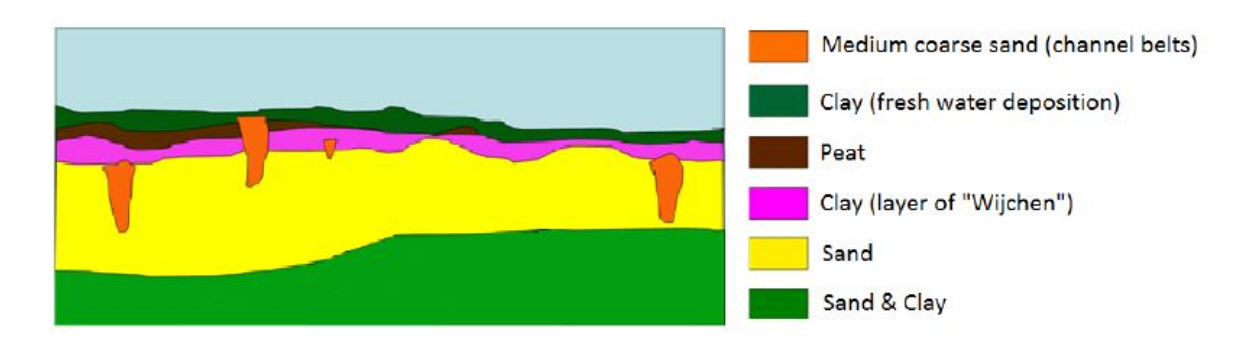


Figure 2.4: Hypothetical composition of the subsoil in the Rhine-Meuse delta (Huismans & van Duin, 2016).

The most important clay layer is called the layer of "Wijchen". It has been deposited during the Pleistocene and is the last layer protecting the highly erodible sand layer below (Huismans & van Duin,

2016). The layer of "Wijchen" is covered by a peat layer that has been formed during to the ending of the last glacial period. This caused a rapid sea level rise that turned the Rhine-Meuse delta into a sedimentation area (Koopmans, 2017). As a result, ground water levels rose and swamps were formed that over the years turned into a deposit of peat. Finally during the last centuries, flood events caused the deposits of "fresh" clay on top of this peat layer (Koopmans, 2017). The last major deposit is the channel belts as can be seen on figure 2.4. River avulsions formed channel belts of highly erodible sand that intersect the different layers.

2.2.2. Scour holes in the Rhine-Meuse delta

Origin

Previous studies (e.g. Koopmans (2017) and Sloff et al. (2013)) indicate that scour holes can form if sand pockets become exposed. This exposure is caused by either river bed erosion or dredging operations. Figure 2.5 shows an example of the formation of a scour hole in the delta if strong local erosion is present. Assessment of Koopmans (2017) showed that the closure of the Haringvliet, and the consequent bed erosion, was not responsible for the development of new scour holes in the delta. However, it may contribute to the growth of the already existing scour holes.

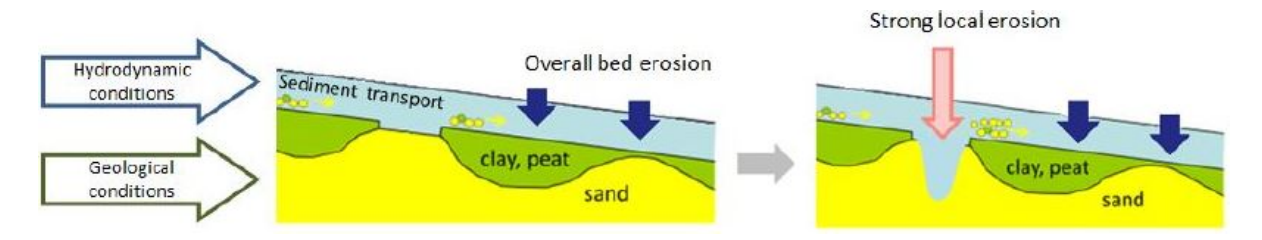


Figure 2.5: Scour hole development in heterogeneous subsoil (Koopmans, 2017).

Varying growth rates of the scour holes

Koopmans (2017) investigated the growth in depth and surface area of the scour holes in the Rhine-Meuse delta. The study made a distinction between the northern branches (Hollandse IJsel, Lek, Nieuwe Maas and Nieuwe Waterweg), the southern branches (Nieuwe, Beneden and Boven Merwede, Bergsche Maas and Hollandsch Diep) and the central connecting branches (Dordtsche Kil, Oude Maas, Spui and Noord). Figure 2.6 quantifies the growth of the scour holes in the delta. Koopmans (2017) concluded that the growth rates of individual scour holes vary significantly, even if they are located in the same river branch and are subjected to similar hydrodynamic conditions. Three causes were identified that could have contributed to the varying growth rates. The first cause is the presence of hydraulic structure (e.g. bridge piers, groynes, etc.). Secondly, the local river geometry can be of influence on the growth rates. A bend, bifurcation or confluence could cause significant local hydrodynamic changes and hence growth rates. Finally it could be a possibility that the closure of the Haringvliet led to different growth rates since this affected the flow through all branches. Unfortunately this could not be verified due to the lack of data before the closure in 1970. Due to these very different growth rates, Koopmans (2017) advises to study scour holes individually since every one is unique.

Analogy with other river deltas

The Rhine-Meuse delta is not the only delta that experiences deep scour holes. Beltaos et al. (2011) researched deep scour holes in the Mackenzie delta in Canada. Around 20 scour holes are present which are mostly located in river bends, constrictions or confluences. River geometry is the main cause of these deep scour holes but according to the study, the thaw-freeze processes could also have enhanced local soil erodibility. It concluded that there are still much knowledge gaps on the behaviour, stabilization and formation of the scour holes at this delta. Vermeulen, Hoitink, et al. (2014)

studied deep scour holes in bends of the Mahakam river in Indonesia. Scour holes are often located in river bends due to the occurring flow processes (see appendix A.4). However in the Mahakam river scour holes are present that are much deeper than normally found. According to Vermeulen, Hoitink, et al. (2014) one of the contributing aspects is presence of poorly erodible material. Together with the very sharp river bends this contributed to freezing the river plan form, resulting into the significantly deep erosion holes of the Mahakam river. On top of that, the mild river slope ($\approx 10^{-5}$) allows the tide to reach the scour holes that are located quite far upstream.

The two cases show that local deep scour holes are also formed in other rivers and deltas. The formation of these scour holes is influenced by many factors such as the soil, river geometry or tide just as in the Rhine-Meuse delta, making it a broader problem. These researches show that there is a need to better understand the behaviour and formation of local deep scour holes in rivers and deltas, to which this thesis contributes.

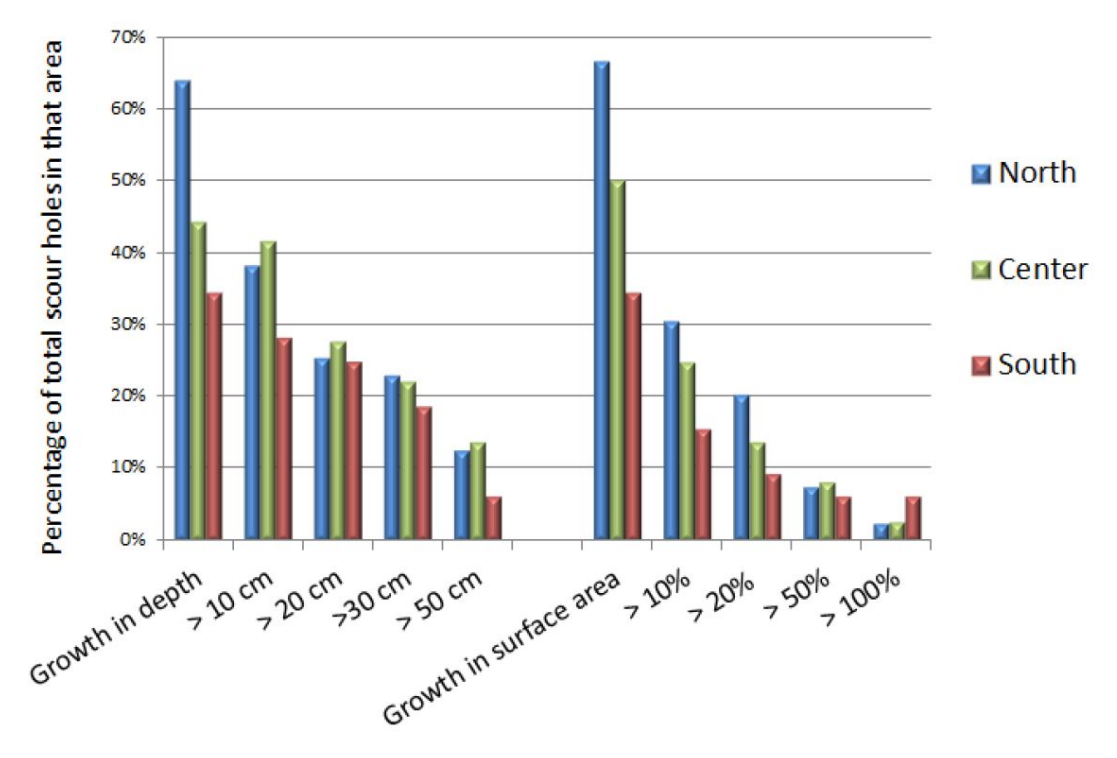


Figure 2.6: Scour hole growth in area and depth from 2009 until 2014 per section of the Rhine-Meuse delta (Koopmans, 2017).

2.2.3. Hydrodynamic processes inside scour hole

Bom (2017) and Stenfert (2017) both gave a clear expectation of the flow processes occurring inside scour holes. These studies divided the flow processes into 2D and 3D processes. Bom (2017) tried to simulate these flow processes in a numerical model and Stenfert (2017) focused on better understanding these processes with laboratory experiments. In this section there will be looked at these flow processes, the effect they have on sediments transport at a scour hole and at some findings regarding these processes by Bom (2017) and Stenfert (2017).

2D flow processes

The two important flow processes in a 2D scour hole are longitudinal recirculation and a mixing layer. Due to the sudden increase in depth the transient flow starts to slow down inside the scour hole. This causes a separation of flow and creates a mixing layer which is the transition between the recirculation zone and the transient flow. This mixing layer grows into the scour hole with a slope of 1:6 (\approx 10°).

until it "touches" the bottom of the scour hole at the reattachment point (Schiereck & Verhagen, 2019). At this reattachment point the flow is separated due to pressure difference. The area near and slightly downstream of the reattachment point appears to be the critical area of attack on the bed (Schiereck & Verhagen, 2019). According to Hoffmans (1992), this reattachment point is located around 6 times the scour depth downstream of the upstream edge. The recirculation zone is characterized with the dissipation of turbulent energy (Nakagawa & Nezu, 1987). Downstream of the reattachment point the flow start to develop a new wall-boundary layer that has its own system of turbulence and bed shear stress. Eventually this new wall-boundary layer will develop towards an equilibrium situation with uniform flow.

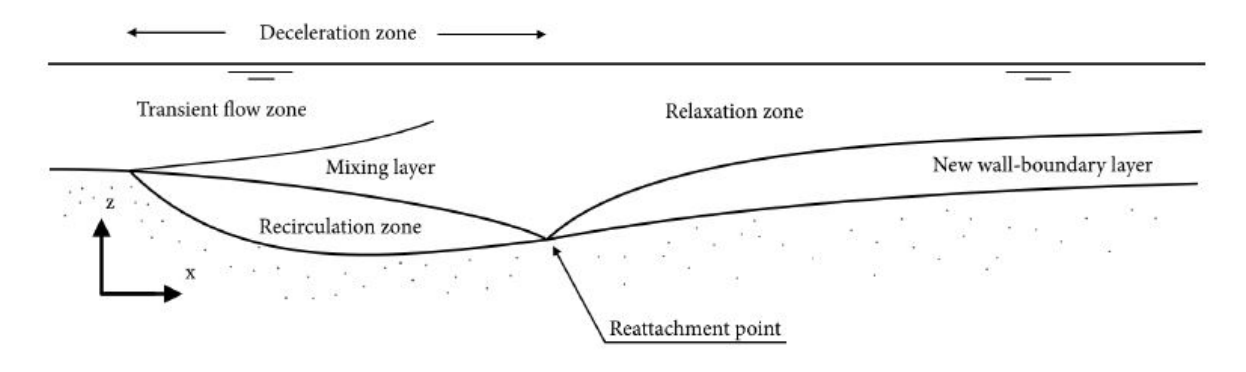


Figure 2.7: 2D flow processes at a scour hole, flow is from left to right. Obtained from Bom (2017), based on Hoffmans and Booij (1993).

3D flow processes

The 3D flow processes that are important in a scour hole are the curved recirculation zone, horseshoe vortex and flow contraction. Bom (2017) expects that these 3D flow processes are dominant with respect to the 2D processes since they caused deeper scour holes in laboratory experiments. In the 3D case, recirculation will also occur on the upstream edge. Due to the shape of the upstream edge of the scour hole the recirculation zone will be curved when seen from the top. Despite, the zone has the same characteristics as the longitudinal recirculation described in the 2D case (Bom, 2017).

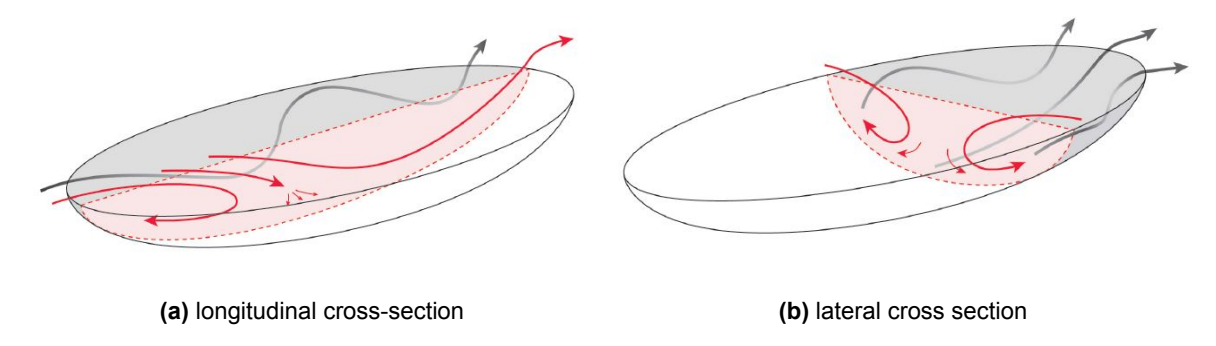


Figure 2.8: Schematic presentation of flow lines inside a scour hole (Stenfert, 2017).

According to Bom (2017) and Stenfert (2017) flow contraction is observed at a small scale symmetrical scour hole. Figure 2.9a shows a schematization of the flow lines in and around a scour hole. From this view there can be seen that the flow lines inside the scour hole contract, indicating that higher velocities are present. Bom (2017) reasons that this is caused by the redistribution of momentum due to the principle of continuity (Bom, 2017). The larger depth of the scour hole causes the discharge Q_2 to become lower than the discharges Q_1 and Q_3 on the sides. Therefore a redistribution occurs which forces the flow to contract into the scour hole as can be seen in figure 2.9c.

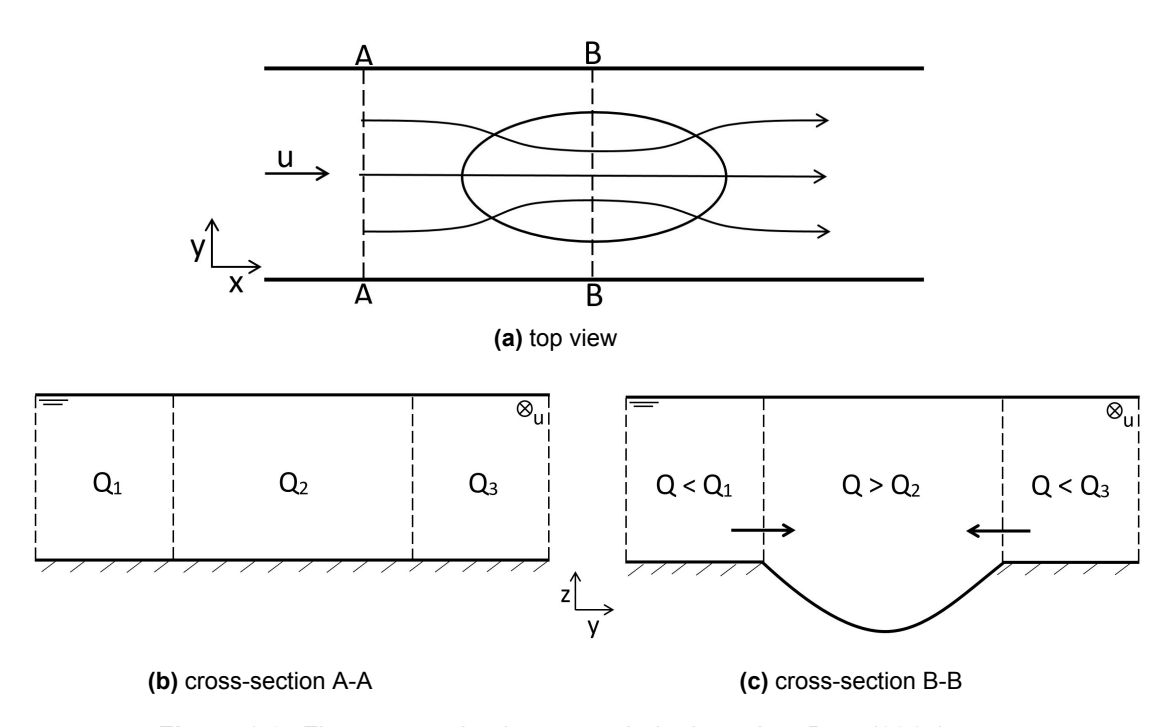


Figure 2.9: Flow contraction in a scour hole, based on Bom (2017).

During 3D experiments performed by Uijttewaal et al. (2016) the presence of the horseshoe vortex was first observed. Figure 2.10 shows that this horseshoe vortex is located at the upstream edge and follows the shape of the scour hole. Uijttewaal et al. (2016) assumes it develops due to local flow separation. This horseshoe vortex is characterized by lateral recirculation along the upstream slope as is schematised in figure 2.8b. It is only present until the reattachment point and then breaks into a less structured wake that leaves the scour hole (see figure 2.10). This wake has a higher turbulence intensity than the vortex and therefore the erosion rates at this wake are expected to be the highest. According to 3D experiments performed by Koopmans (2017) this wake develops at an angle of 1:8 which was also found by Uijttewaal et al. (2016). Bom (2017) hypothesised that there are three driving mechanisms required to form this the horseshoe vortex. These are a (curved) recirculation zone giving the flow a rotating character, flow contraction which adds momentum to the rotating motion and strengthens the vortex and a curved upstream edge which forces the vortex sideways.

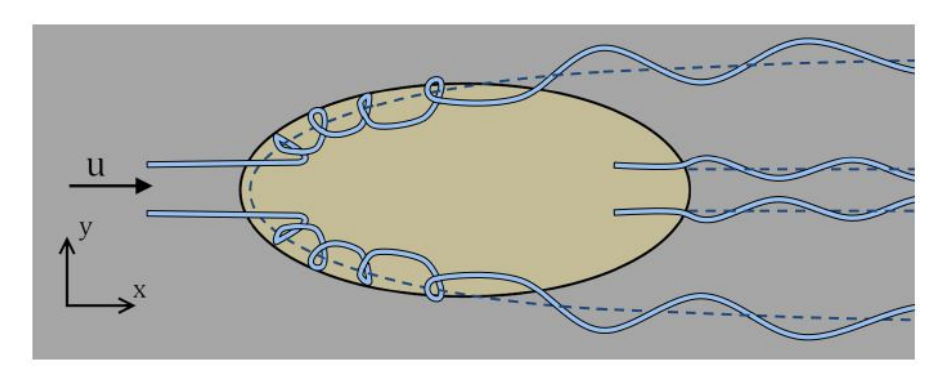


Figure 2.10: Location of horseshoe vortex along the edge of a scour hole (Bom, 2017).

Findings on 3D flow process by Bom (2017) and Stenfert (2017)

• Based on 3D experiments, Stenfert (2017) concluded that the reattachment point is located at 3.75 - 5 the maximum scour depth. The numerical model by Bom (2017) showed a reattachment point more downstream in the scour hole.

- The results of the 3D experiments by Stenfert (2017) showed actually no presence of flow contraction in the scour hole. However a slight divergence of flow was found downstream of the scour hole. The numerical model of Bom (2017) showed that converging of flow lines in the scour hole were present but only slightly. Stenfert (2017) expects that flow contraction is present in reality which questions the results of the 3D experiments. It could be possible that it happened very subtle and was therefore not be measured or observed in the small scale 3D experiments.
- Both in the 3D experiments and the numerical model, the presence of the horseshoe vortex was observed. Of this horseshoe vortex it is yet unknown if it occurs in the field since it is dependent on the geometry of the scour hole. In the 3D experiments and the numerical model an idealised and symmetrical scour hole was used which in reality won't be the case. Recommendations are in both researches to further investigate the presence of the horseshoe vortex and the influence of the scour hole geometry with field data.
- Out of the 3D experimental results Stenfert (2017) was able to conclude that 3D scour holes develop much faster than 2D scour holes. Therefore it can be concluded that either contraction of flow lines, the horseshoe vortex or the curved recirculation zone plays a important role in scour hole development.

Sediment transport due to 3D flow processes

Bom (2017) has also investigated how these 3D flow processes affect the morphodynamics of scour holes and concluded the following.

- If the recirculation zone is present, no more sediment transport will occur at the upstream slope. The recirculating flow never exceeds the critical value that is needed for structural sediment transport up hill. However, fluctuations in the recirculation flow might still be able to stir up sediments. The largest attack of the bed occurs at the reattachment point.
- Flow contraction is responsible for adding more momentum inside the scour hole. As a result more turbulence will be present in the downstream half of the scour hole and hence more erosion.
- The outwards directed horseshoe vortex at the side slopes of the scour hole can lead to undermining (for explanation undermining see appendix A.3.3). On top of that it also drags more momentum into the scour hole, resulting in more turbulence which in turn leads to more erosion.

2.2.4. Development of scour holes

Development stages

Zanke (1978) was able to derive four stages of scour hole development based on experiments simulating clear-water scour hole development behind a bed protection by Breusers (1966) and Dietz and Wittke (1969). The four phases are shown in figure 2.11. The first stage is the initiation phase. This phase is governed by the initiation of motion as described in appendix A.1. Due to flow conditions, sediment particles are moved or picked up and a depression in the bottom starts to develop. The second phase is the development phase. During this phase the depth of the scour hole increases significantly but the shape of the scour hole does not change (Hoffmans & Verheij, 1997). Due to the depression out of the first stage the flow is being separated and the flow processes, as described in section 2.2.3, develop. These cause an increase in turbulence that significantly increase the depth of the scour hole. The section upstream of the reattachment point is almost stable while the downstream section is still developing (Hoffmans, 1990). In the third phase the scour hole tends to stabilize. The larger depth of the scour hole slows down the flow which reduces the amount of scour taking place and thus the depth development of the scour hole. The scour hole mainly still develops in the longitudinal direction during this phase (Hoffmans & Verheij, 1997). In the final phase the scour holes reach an equilibrium. The deeper scour holes result in decreasing flow velocities that eventually become not critical enough to initiate motion of sediment grains. Combine this with a decreasing amount of turbulence due to smoothing of the slopes of the scour hole and the scour depth will be reach an equilibrium phase under

ideal conditions. Important to mentions is that this equilibrium phase is affected by the type of scour occurring at the scour hole. Looking at figure 2.12 there can be seen that in the case of clear-water scour the scour hole asymptotically reaches an equilibrium depth (Hoffmans & Verheij, 1997). In the case of live-bed scour the scour depth increases rapidly over time and then fluctuates around a lower equilibrium depth in response to bed features (Hoffmans & Verheij, 1997).

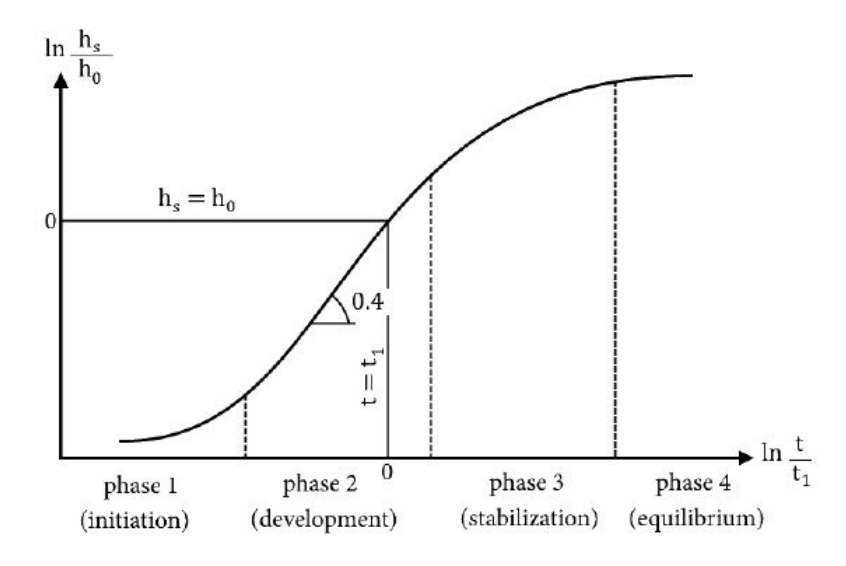


Figure 2.11: Four stages of scour hole development. Obtained from Bom (2017), based on Hoffmans and Verheij (1997).

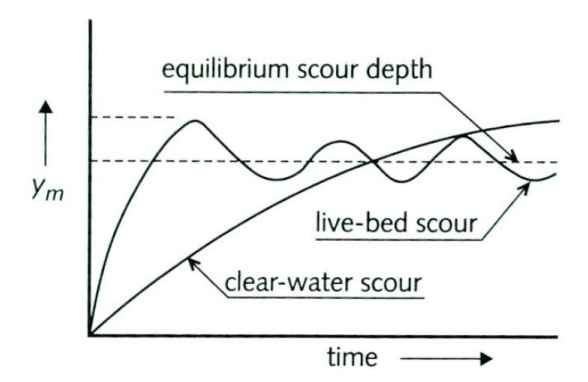


Figure 2.12: Influence of live-bed and clear-water scour on scour depth (Hoffmans & Verheij, 1997).

These four phases have been derived for unidirectional flow over a non-erodible bed protection. Results of 2D experiments performed by Breusers (1966) showed that a scour hole develops itself towards a shape as shown in figure 2.13a. A steep angle of the upstream slope was found, which probably is a result of balance in forces on that slope Bom (2017). Contrary the downstream slope is much more gentle. In the Rhine-Meuse delta the scour holes tend to show the similar kind of behaviour (Koopmans, 2017). However, conditions in the delta can differ a lot with respect to a scour hole behind a bed protection. This makes it uncertain if the scour holes at the delta even reach an equilibrium.

First of all geology plays an important role in the Rhine-Meuse delta. Some scour holes developed in former channel belts which can bound the dimensions, as was explained in section 2.2.1. Secondly, tidal effects play an important role in the Rhine-Meuse delta. The tide can change the flow direction in some of the branches. Experiments by McGovern et al. (2014) showed that the reversing flow directions will reshape the scour hole and make it more dynamic and symmetric. Furthermore a lower equilibrium depth was found. These conditions make scour holes in the Rhine-Meuse delta different with respect to scour holes behind non-erodible bed protection with unidirectional flow, to which extensive research

has been done. Therefore the applicability of the theory of scour hole development behind a non-erodible bed protection in the Rhine-Meuse delta has still some uncertain aspects. Despite, Hoffmans and Verheij (1997) suggest it can be used for the prediction of scour due to 3D flow, if it is combined with computational results or field measurements. Therefore it forms a basis of much of the recent research on scour holes in a heterogeneous subsoil (e.g. Koopmans (2017), Stenfert (2017), and Zuylen (2015)). On top of that, Huismans et al. (2021) thinks it is plausible that the scour holes at the Rhine-Meuse delta stabilize and reach an equilibrium depth, since the same physics apply. The deeper the scour hole becomes, the more energy it takes to transport sediment out of it, while generally the flow velocities within the scour hole decrease. Huismans et al. (2021) even lists the heterogeneous subsoil as a contributor. Poorly erodible layers and coarser Pleistocene sand layers are often located below the scour holes in the delta, slowing down the growth.

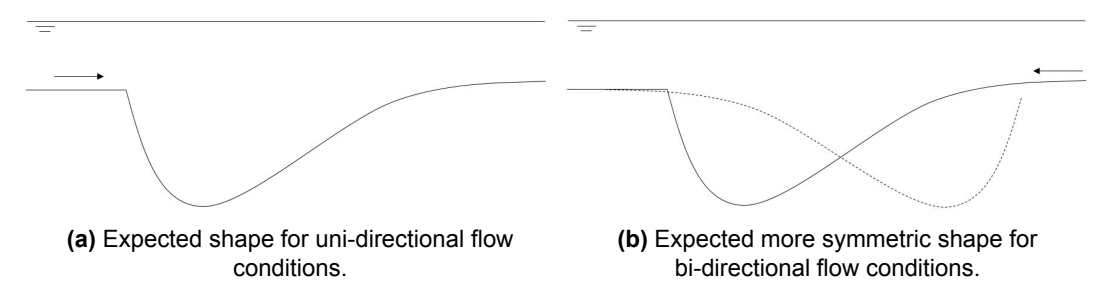


Figure 2.13: Effect of tide on the profile of a scour hole, based on (Zuylen, 2015).

Equilibrium scour depth

Much research has been done to the Breusers method which can describe development and equilibrium scour depth for scour holes behind non erodible bed protections. Hoffmans and Verheij (1997) claimed that the empirical equation of Breusers can be used in combination with computational results of horizontal models or with measurements, to predict local scour due to three-dimensional flow. A full explanation of the Breusers method can be found in appendix A.3.2. Koopmans (2017) and Stenfert (2017) investigated the applicability of the method for scour holes in heterogeneous subsoil.

Koopmans (2017) focused on computing the equilibrium depth of multiple scour holes in the Rhine-Meuse delta, by applying the Breusers method in combination with computational result of flow velocity simulations. The results were compared with observations in the field of scour holes that already stabilized. The study included the tidal effects at the delta by deriving a reduction factor for the flow velocities. Nevertheless, the results of the Breusers method over estimate the equilibrium depth seen in the field. Several reasons are given for this. In the delta the heterogeneous subsoil can limit the development of the scour. Furthermore, it is possible that the bottom of the scour holes in the field are located in a poorly erodible clay layer. Another reason for the overestimation could lie within the type of scour. The Breusers equation has been derived for clear-water scour conditions but in the field it can be expected that live-bed scour conditions can occur. Finally the study indicates that changes in local river geometry and hydraulic structures also influence the scour holes in the delta.

Stenfert (2017) performed small scale 3D laboratory experiment which focused on the flow patterns and the development of scour holes. The study fitted the characteristic time scale t_1 and the coefficient γ of the Breusers method to the measured data from these small scale experiments. There could be concluded that the fitted Breusers equation can be used as a first estimation but only for the early development stages. If the scour hole develops further the fitted Breusers equation fails to describe the development of the scour hole.

The results of the Koopmans (2017) and Stenfert (2017) partly contradict this claim of Hoffmans and Verheij (1997). Despite, the Breusers method is one of the only approaches to describe scour hole development due to three-dimensional flow, as is found at the scour hole Beerenplaat. Therefore it can be concluded that the method can be used as a first estimate of the scour depth development and the equilibrium depth.

2.2.5. Confluence/bifurcation flow

Much research has been done to the behaviour of flow at confluences. J. L. Best (1986) identified six different flow zones at a confluence under uni-directional flow conditions. These flow zones are a stagnation zone (1), a flow deflection zone (2), a separation or recirculation zone (3), shear layers (4), a maximum velocity zone (5) and a flow recovery zone (6). The most important zones for this research are the shear layers and maximum velocity zone, since they are paired with the largest shear stresses and probably also scour. The mixing of the tributary and main flow leads to the downstream shear layer (4) which enhances the turbulent mixing. At the shear layer there is a significant velocity gradient making the flow strongly turbulent, featuring high shear stresses and well-defined coherent flow structure such as Kevin-Helmholtz instabilities (Boyer et al., 2006). The maximum velocity zone (5) appears downstream of the junction next to the recirculation zone. Due to the constriction of the flow area and the presence of the flow recirculation zone zone, the flow accelerates leading to the largest velocities. It is important to identify the maximum velocity zone because maximum shear stresses, and therefore, scouring are expected to appear at this zone (Shakibania et al., 2010). The size of each of the zones is dependent on factors such as tributary flow ratio, confluence angle, bed discordance and upstream planform (Bilal et al., 2020). Important to mention is that there is still discussion on the presence of the horizontal flow recirculation zones in reality. Ashmore et al. (1992) states that natural confluences have partial or no zone of flow separation due to their banks changing direction more gradually than found in simplified flume experiments. However, the field study of Unde and Dhakal (2009) supported the existence of flow separations.

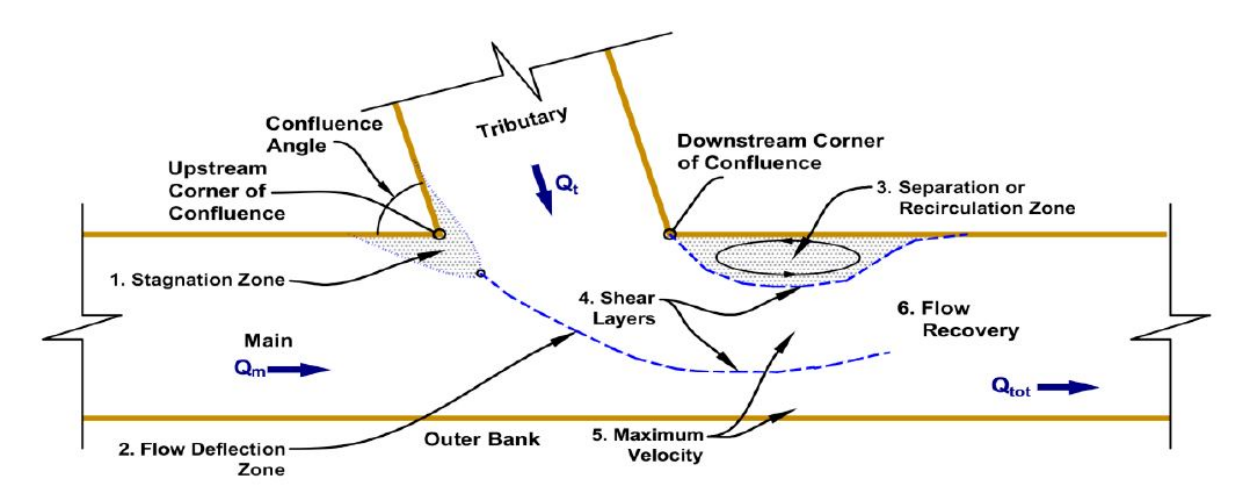


Figure 2.14: Six identifiable flow zones at a confluence. Obtained from Bilal et al. (2020), based on J. L. Best (1986).

Tidal conditions

Up to now, only confluences with uni-directional flow conditions were addressed. However, confluences can also be present in area's with tidal influence. Only recently some research has been done to bi-directional confluences. Bilal et al. (2020) reasons that this is caused by the complex behavior. In bi-directional conditions, the shift of the dominant processes between run-off and tides featuring periodical changes in both magnitude and direction makes the confluence behaviors more complex. Table 2.1 shows an overview of the main characteristics of a tidal and non-tidal confluence.

Despite the complex behavior some insight have been gained on tidal confluences. Dai et al. (2020) have investigated the near-surface flow patterns in a tidal cycle. A 3D numerical model (Delft3D) was used to simulate the flow patterns from the Sanjiangkou confluence in South-East China. The research was able to conclude that the flow is highly dynamic and that the near-surface flow patterns are always in transition. Based on the numerical computed flow field, the study gives a schematic illustration (figure 2.15) of the flow zones that are expected at a tidal confluence. This is done for four scenarios

which are during peak of flood flow (a), flow changing from flood to ebb (b), peak of ebb flow (c) and flow changing from ebb to flood (d). Out of these scenarios, the following suggestions are obtained for confluences with tidal conditions.

- At least one recirculation eddy is always present during a full tidal cycle.
- The size, location and rotation (clockwise or counterclockwise) of these eddies are dependent on the flow conditions.
- A slack water condition does not exist. There is always some ebb or flood flow in two of the three
 tributaries. This is caused by the different channel characteristics or the presence of a structure
 in each of the tributaries leading to different tributary flow regimes.
- The flow patterns repeat during a tidal cycle between the four cases highlighted in figure 2.15.
- Turbulence and secondary flow are enhanced with an increase of the confluence angle, a larger discharge ratio or the existence of bed discordance.

Items	Non-Tidal Confluence	Tide-Driven Confluence
Flow volume timescale	daily/seasonal	hours
Main sediment forcing	river run-off (fresh-water)	tides (salty-water)
Sediment concentration timescale	days-weeks	hours
Sediment transport direction	unidirectional	bidirectional
Morphodynamic adaption time scale	months-years	weeks-months/years

Table 2.1: The main characteristics of a non-tidal and a tidal confluence (Bilal et al., 2020).

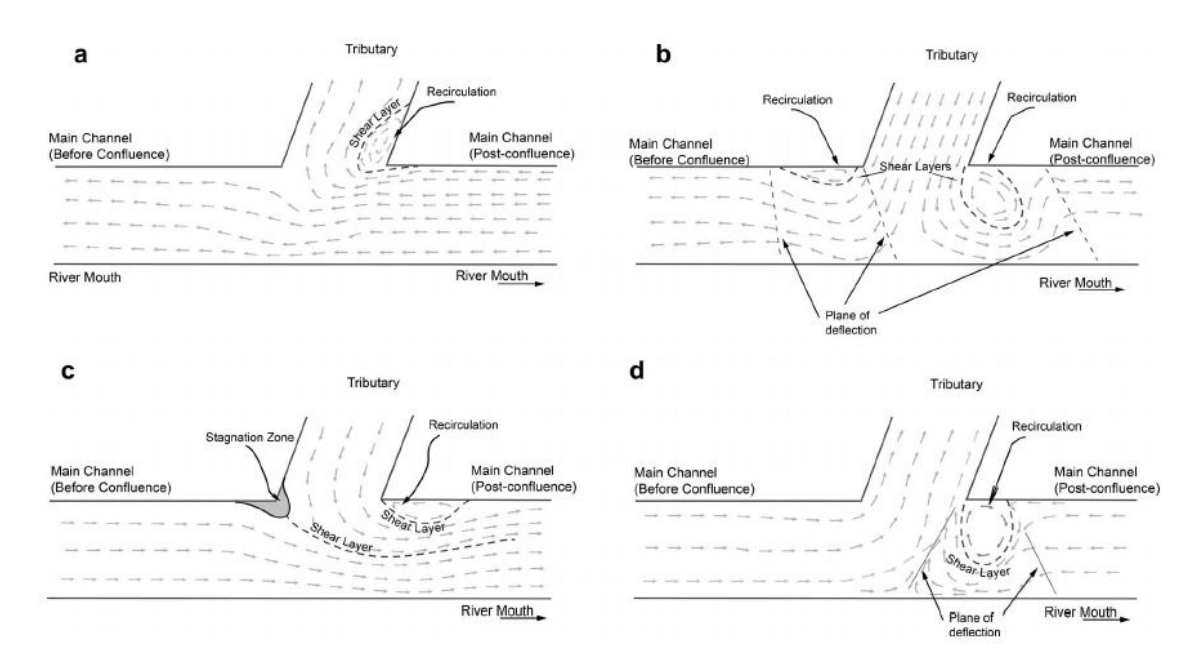


Figure 2.15: Schematic illustration of hydrodynamic flow zones at a tidal confluence (Dai et al., 2020).

Bilal et al. (2020) also looked at the morphological consequences of a confluence with bi-directional flow conditions by means of a field-study and numerical modelling with Delft3D. In the study area of this research 95 % of the sediment is suspended load. The sediment is transported by the tidal currents, especially during the spring tide. The flow and sediment changes are not always in phase, the sediment movement is significantly modified by the tides. Tidal currents are essential for stirring sediment, modifying the concentration of the suspended load and eventually transport. The study

also looked at the influence of the tide on the scour hole development near the confluence. At unidirectional confluences scour holes develop, as will be explained latter. This also occurs at bi-directional confluence. Bilal et al. (2020) could conclude that the erosion and deposition migrates in both directions, leading to growth of the scour hole in both directions. The flood tides govern the sediment transport and depositions while the ebb tides combined with the rivers run-off lead to erosion. For the scour hole development the flood tides plays a dominant role.

Discordant confluence

If two meeting tributaries at a confluence have their bed elevation at different levels, there is referred to a discordant confluence. Bed discordance has significant influence on the flow field at a confluence. Due to the discordance a second mixing layer develops between the two flows, paired with a recirculation zone at the bed level step as can be seen in figure 2.16. As a result faster mixing of the joining tributary flows occurs, resulting in minimal flow separation at the downstream corner of the confluence (Biron et al., 1993). Remarkably a bed discordance discourages the development of a scour hole at a confluence. With flume experiments on a 30° confluence, Biron et al. (1996) found no presence of helical cell generation or scour hole growth. Bilal et al. (2020) concluded that there is yet no clear relationship between scour holes and a discordant confluence. Despite, it can be said that a discordant confluence affects the flow regime, sediment transport and eventually the morphological development. Research on how discordance affects the previously identified flow zones at (tidal) confluence, is according to Bilal et al. (2020), not yet done.

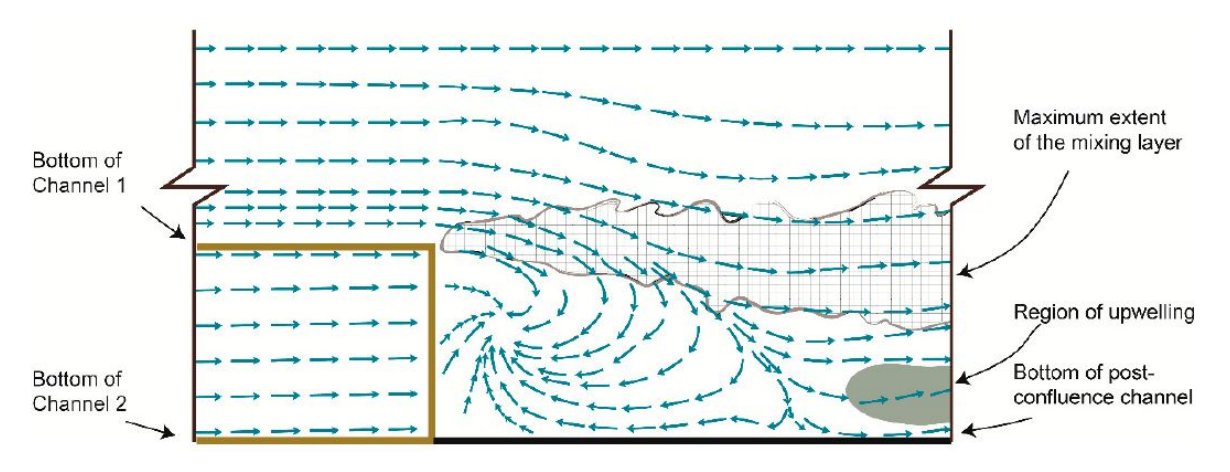


Figure 2.16: Flow field at a discordant confluence Bilal et al. (2020).

Secondary flow patterns at a confluence

Secondary flow patterns are present at a confluence. Figure 2.17 shows that secondary vortexes develop in both the branch and main flow. Song et al. (2012) explains that the development of these vertical recirculating cells starts by the branch flow (Q_b) . Due to the change in flow direction the centrifugal forces form a surface radial flow opposite to the deflection and a bottom inward current develops. This results into clockwise recirculation cells in the branch part of the flow, close to the inner bank. As a result the second vertical recirculating cell develops in the main part of the flow (Q_m) , which rotates in a counter clockwise direction close to the outer bank. This counter acting recirculation is responsible for the development of the shear layer. According to Song et al. (2012) this shear plane is skewed rather than vertical, due to the combined effects of the relative magnitudes of the merging flows and the non-uniform vertical velocity profile. The recirculating cells in both flows gradually fade and decrease in size in the downstream direction which is mainly caused by the viscosity of the flow (Song et al., 2012). Important to mention is that the secondary flow in the branch part of the flow can be more intense than in the main part of the flow, since the branch flow experiences much more curvature (Shadeed et al., 2019). According to this study, the intensity of the secondary flow patterns in both flows at a confluence is affected by the confluence angle, discharge ratio and bed discordance (Shadeed et al., 2021).

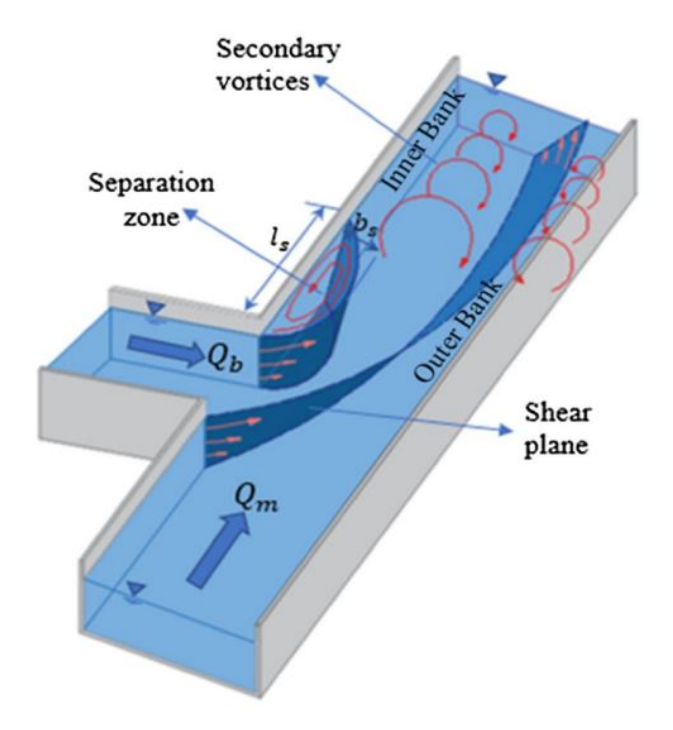


Figure 2.17: Secondary flow components in a confluent channel. Obtained from Shadeed et al. (2019), based on Weber et al. (2001).

Confluence scour

Scour holes are often observed downstream of a confluence with uni-directional flow. Parker (1983) was one of the first to gain insight in the behavior of scour holes downstream of confluences by using laboratory models. The study could conclude that the scour depth is mainly dependent on the average flow depth of the two upstream branches. On top of that, the study found that the confluence angle is of major influence on the scour depth. Biron et al. (1993) concluded that one of the factors leading to the absence and size reduction of scour holes downstream of a confluence is the bed discordance. Many hypothesis have been developed on what causes the formation of this scour hole. Yuan et al. (2018) found that helical motions by upwelling and downwelling flow, associated with high bed shear stresses, are responsible for sediment entertainment and generating the scour hole. As already mentioned, it is expected that the combination of large flow velocity and strong turbulence, as effect of the shear layer, are of significant influence on the development of the downstream scour hole. Until now, it is believed that an interaction of these hypothesis is responsible for the presence of these scour holes (Bilal et al., 2020). The scour holes also have an equilibrium scour depth, meaning they stabilize over time. Some empirical equations are available to estimate this (e.g. Breusers and Raudkivi (1991), Ghobadian and Shafai Bajestan (2007), and Khosravinia et al. (2020)), but only for uni-directional confluences.

2.2.6. Estuarine sand waves

Flow conditions in an estuary are characterized by a combination of seasonal river flow and tidal flow. This can causes the development of bedforms that contain characteristics formed by both flows types. One of these bedforms are the estuarine sand waves, which is a rather large rhythmic bedform (van der Sande et al., 2019). Not much research regarding the development and behaviour of this bedform is available. However, in literature (e.g. Hulscher and Dohmen-Janssen (2005) and van der Sande et al. (2019)), it is assumed that the behavior can be best described, by combining knowledge of both marine sand waves (formed in tidal zones) and river dunes (formed during seasonal river flow).

Marine sand waves are sinusoidal like bed features that are formed in coastal seas, where the tidal

motion is strong enough to generate shear stresses that can induce sediment transport. The generation mechanism for these marine sand waves in the M2-tide which results into symmetric bedforms. Additional tidal components could lead to a more asymmetric bed form. According to Hulscher and Dohmen-Janssen (2005), the temporal variations in migration rate and amplitude are much smaller than for river dunes. For example, the migration rate of marine sand waves is in the order of meters per year while that of river dunes is in the order of meters per day (Hulscher & Dohmen-Janssen, 2005). The larger river dunes are formed during seasonal bound flood events in rivers. The dunes are asymmetric. If the dune height is large enough, flow separation occurs behind them as is illustrated in figure 2.18b. This will result into additional turbulence. According to Julien et al. (2002) and Paarlberg et al. (2010) the dunes are heavily dependent on the river discharge. The researches investigated the response of dunes on flood waves and showed the existence of a hysteresis effect between the dune height and the discharge. This means that the maximum dune height occurs a couple of days to weeks after the highest discharge. After the flood event, the height of the river dunes decreases again, showing that the river dunes are only prominent part of the time (Hulscher & Dohmen-Janssen, 2005).

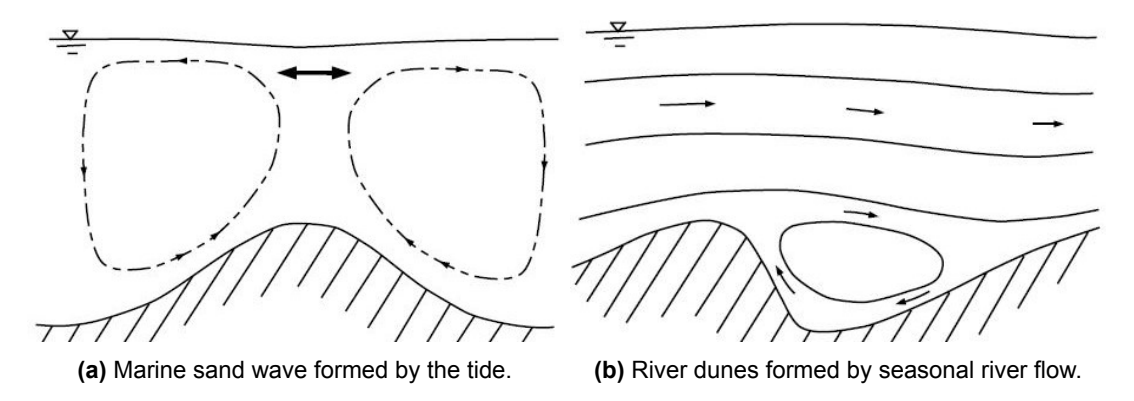


Figure 2.18: Schematic presentation of flow over bedforms (Hulscher & Dohmen-Janssen, 2005).

2.3. Pilot nourishment

As already touched upon, Rijkswaterstaat performed a pilot nourishment to investigate if nourishments can stabilize the river bed at the Rhine-Meuse delta. The nourishment has been constructed at the pilot site in the Oude Maas in the spring and summer of 2018. There has been nourished at two locations within this pilot site. These are scour section 5 (Rkm 999.5 - 1001) and scour section 6 (Rkm 996 - 997.5). Scour section 6 is a slightly deeper part of the river located close to the scour hole Beerenplaat, as can be seen on figure 2.19. Scour section 5 is located further downstream in a bend of the Oude Maas. There is referred to these locations as scour sections, since local erosion is occurring but not in the form of an ellipsoidal scour hole.

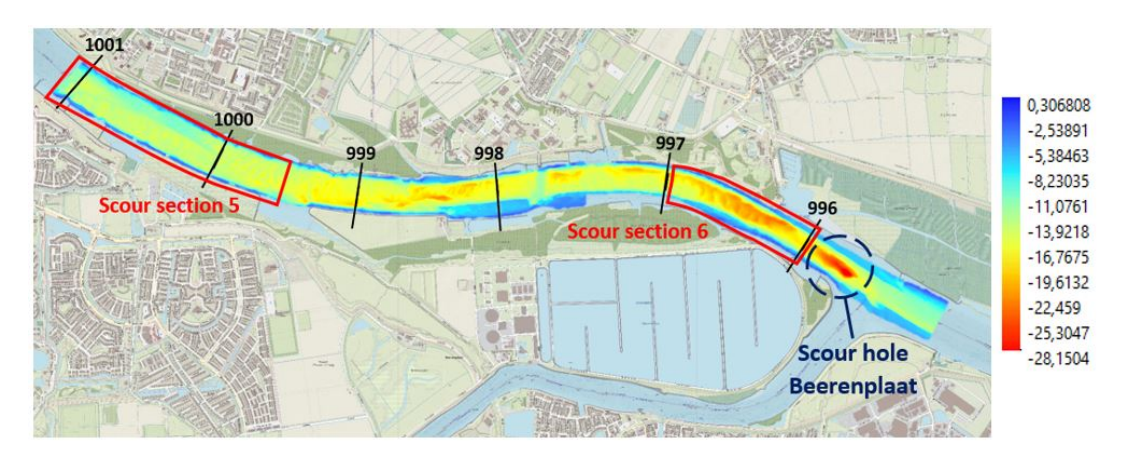


Figure 2.19: River depth in m + NAP on June 2018 at the pilot site in the Oude Maas.

2.3.1. Location of nourishments

Rijkswaterstaat constructed the nourishment in the first half year of 2018 with around 450,000 m³ of sediment dredged from the Nieuwe Waterweg. In figure 2.20 an overview of the river bottom before and after the nourishment can be found. It can be seen that the part of the nourishment at scour section 6 is located just downstream of the scour hole Beerenplaat.

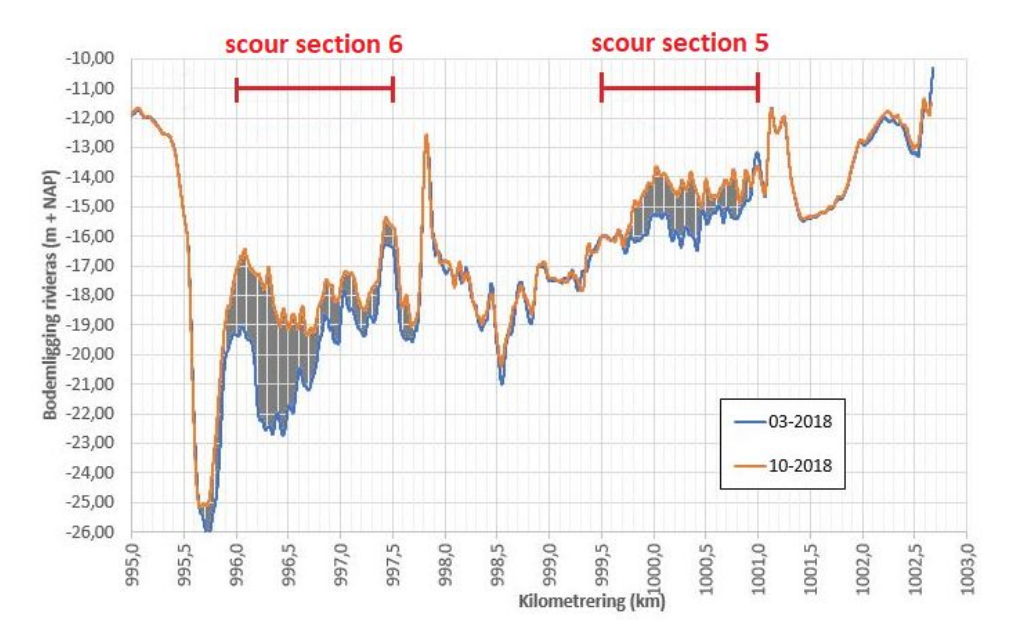


Figure 2.20: River bottom at the pilot site before and after the nourishment, based on (Sloff, 2020) and data from Laurens Baars (RWS-WNZ).

Scour section 5

At scour section 5 a shallow nourishment of \approx 140,000 m³ has been constructed. The nourishment is approximately one meter thick and follows the bottom profile as can be seen on figure 2.20. Figure 2.21 shows the height of the river bottom at scour section 5 before and after the nourishment. There can be seen that the nourishment was not constructed over the entire width of the scour section, but only on the deepest left side of the channel.

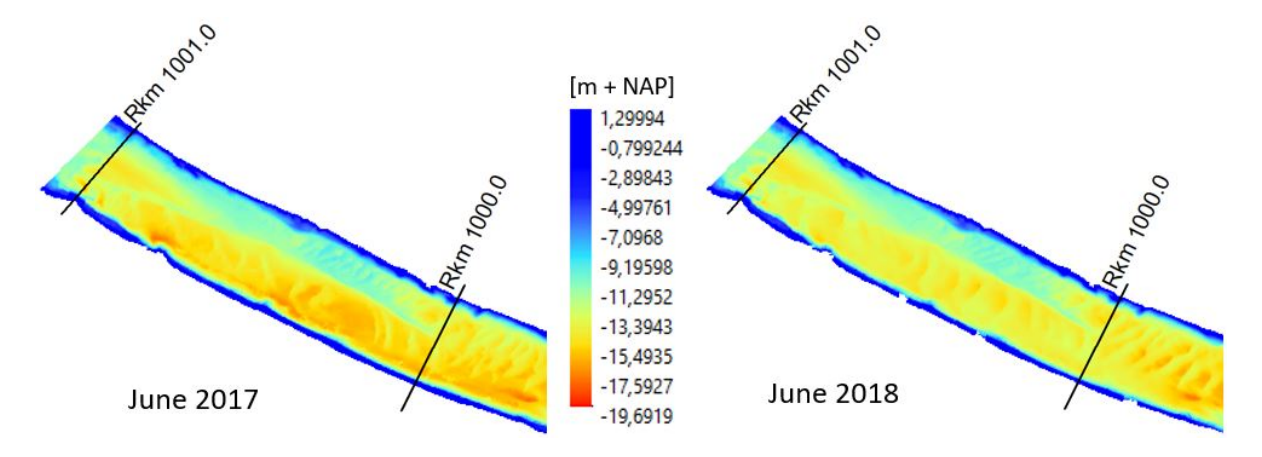


Figure 2.21: River depth at scour section 5 before and after the nourishment.

Scour section 6

Figure 2.22 shows the height of the river bottom before and after the nourishment. The nourishment at scour section 6, downstream of the scour hole Beerenplaat can be clearly observed. At this location a nourishment of \approx 300,000 m³ was constructed. The nourishment is located again in the deepest parts of the channel and locally enhances the river bottom with 1-3 meters of sediment.

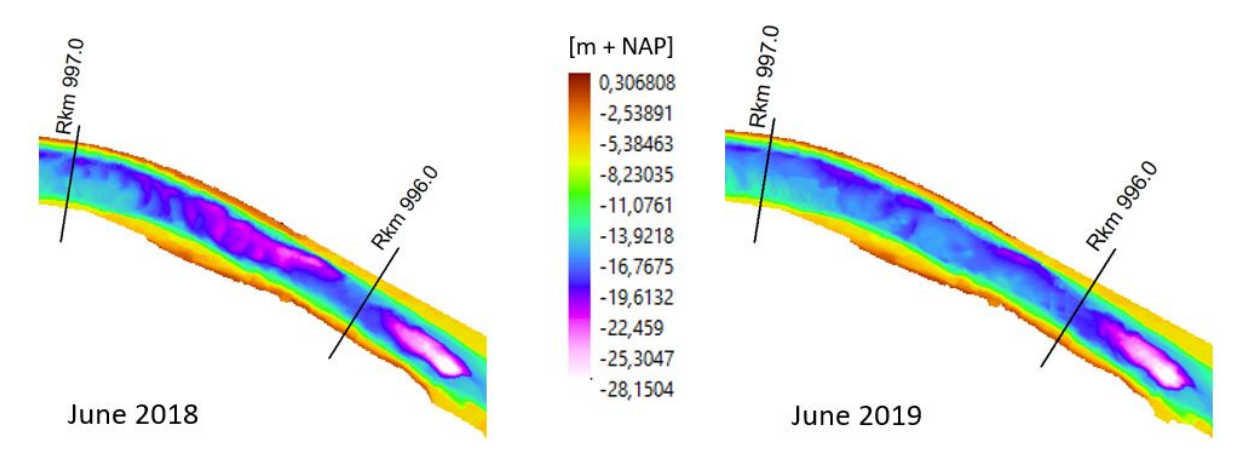


Figure 2.22: River depth at scour section 6 before and after the pilot nourishment.

2.3.2. Monitoring measurements with a Multibeam Echosounder

Measurements have been taken to monitor and understand the behavior of the river bottom and the pilot nourishment. Rijkswaterstaat measures the river bottom every 6 months with a Multibeam Echosounder bellow the hull of a survey vessel. These measurements have been taken for more than 20 years, allowing for a clear picture of both the river bottom development and behavior of the pilot nourishments.

The instrument uses acoustic sounds waves (echo) to measure the location of the river bottom. It sends out multiple beams in a fan shape towards the river bottom as can be seen on figure 2.23. By measuring the time a beam takes to travel back towards the instrument, the bathymetry can be constructed. Modern MBES provide measurements with extremely high vertical (typically <1% of water depth) and horizontal resolution (typically a small percentage of the water depth) (Colbo et al., 2014). The raw data has already been processed to x,y,z data points of the river bottom by Rijkswaterstaat. In table 2.2 an overview of the type of measurements and period can be found. Up to 2004 a Single-beam Echosounder was used, which is the precursor of the Multibeam Echosounder and only measures with a single beam. As a consequence, the density of data points and the accuracy is less.

type of data	measurement period
Single-beam Echosounder measurements (interpolated 5m x 5m)	2000 - 2004
Multibeam Echosounder measurements (5m x 5m)	2005 - 2011
Multibeam Echosounder measurements (1m x 1m)	2011 - 2021

Table 2.2: Monitoring measurements of the river bottom at the Rhine-Meuse delta.

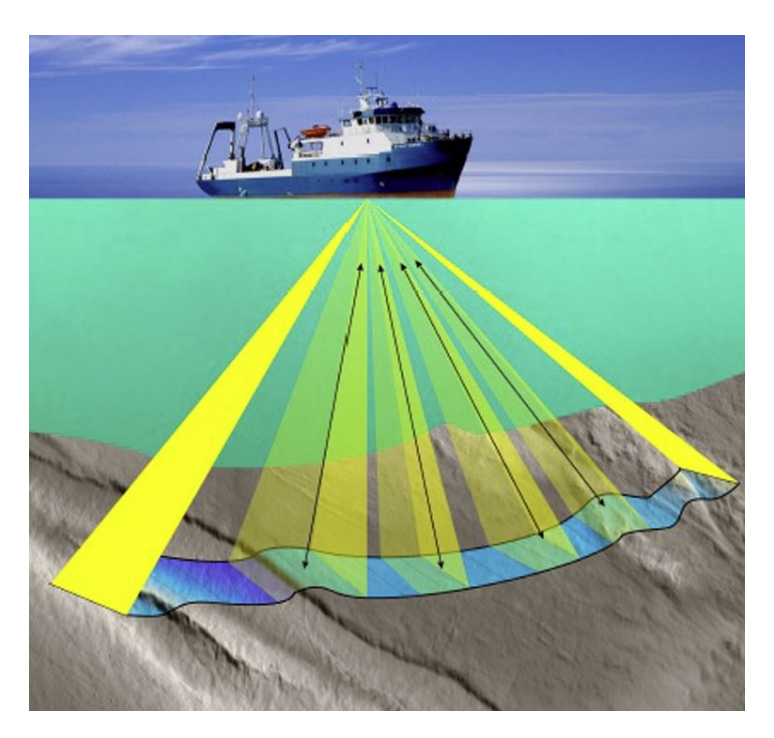


Figure 2.23: Bathymetry measurement with a Multibeam Echosounder (Colbo et al., 2014).

Review of pilot nourishment

Sloff (2020) did a first review of the MBES measurements taken after the pilot nourishment. It could conclude that the pilot nourishment moves gently downstream in the form of a sand wave. The sand wave has a yearly propagation of around 100 meters in the seawards direction. Around 45,000 to 50,000 m³ of the nourishment is yearly eroded. The study predicts that the nourishment is completely removed by 2026, assuming a linear trend. These erosion values match with those present at the pilot site before the nourishments. The pilot nourishment was not able to change that. For now it appears that nourishments are able to temporarily stabilize the scour sections in the Rhine-Meuse delta. They can become a suitable management strategy to deal with the scour holes in the Rhine-Meuse delta. Especially since Rijkswaterstaat intends to make 350,000 m³ of dredged sediment yearly available for dealing with these scour holes (Rijkswaterstaat, 2019).

2.3.3. Relevance for this research

Due to the pilot nourishment much more attention has been paid to the scour hole Beerenplaat. For understanding and monitoring the pilot nourishment, measurements have been taken. Investigation of these measurement has already lead to some questions regarding the behavior of the scour hole Beerenplaat (see section 1.2), which have contributed in establishing the objective of this research. On top of that, the MBES measurements can be used for analyzing the morphological development of the scour hole Beerenplaat and the scour sections, in the first sub research question. Furthermore, Rijkswaterstaat performed velocity measurements to understand the hydraulic conditions at the pilot site, as will be further explained in section 4.1. These will be used for to investigate the flow processes at the scour hole Beerenplaat.

Morphological development

This chapter focuses on answering the sub-research question: "What was the morphological development of the river bottom at the scour hole Beerenplaat and the location of the pilot nourishment in the Oude Maas?". For answering this question will be made use of the MBES measurements taken by Rijkswaterstaat. First the morphological development of the ellipsoidal scour hole Beerenplaat is discussed. This will be done for the period March 2004 until February 2021. The scour hole was not present in measurements taken before and in March 2004. The most recent available measurement has been taken in February 2021. Within this period the river bottom changed from being relatively flat to this deep dynamic scour hole. After investigating the morphological development of the scour hole Beerenplaat, there will be looked at the river bottom at the location of the pilot nourishment. This will be done with MBES measurements taken just before the nourishments until February 2021, the most recent available measurement.

3.1. Morphological development of scour hole Beerenplaat

The morphological development of scour hole Beerenplaat is first investigated by analyzing a longitudinal cross-section in the center of the scour hole. Figure 3.1 shows the development of the river bottom at this cross-section. The measurement of 2004 had still a quite flat river bottom while in March 2005 already a six meter deep hole has developed. In the following measurements the scour hole grows in both upstream and downstream direction.

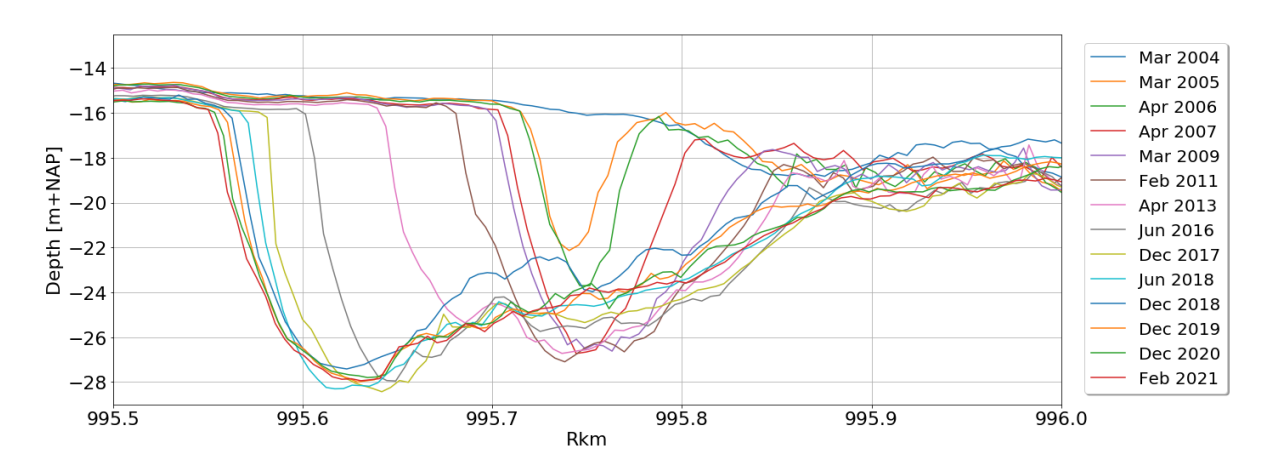


Figure 3.1: Location of the river bottom at scour hole Beerenplaat.

The development of the scour hole up to February 2021 can be sub dived into three phases, which can be seen in figure 3.3. During the first phase the scour hole expands itself in both the upstream and downstream direction. The development in the downstream direction is larger than in the upstream direction. Table 3.1 shows an estimation of the edge expansion which confirms this. What also stands out in the first phase, is the flattening of the downstream slope. It starts quite steep but overtime more erosion occurs close to the edge than inside the hole, leading to the flattening of the downstream slope. Table 3.2 contains an estimation of the slope angle of both the upstream (α) and downstream slope (β). The flattening can clearly be seen by the reduction of the slope angle β . For the upstream slope there can be observed that it becomes slightly steeper during the first phase.

In the second phase the scour hole behaves quite differently. The expansion of the upstream slope is much larger than that of the downstream slope. Despite, the flattening of the downstream slope is not stopped. As can be seen in table 3.1, the angle of the upstream slope is fluctuating around $21-25^{\circ}$ except for the measurement of December 2017, which is significantly more steep. Two potential causes are identified. It can be possible that the heterogeneous subsoil is responsible for this. A poorly erodible layer could be locally present which has larger resistance against scour. The other possibility is that this is a measurement error. One other observation can be done during development phase two. The deepest location of the scour hole is moving along with the upstream expansion of the scour hole.

The third phase has been chosen based on the pilot nourishment constructed in the summer of 2018. In figure 3.3c it can be observed that the downstream slope is raised between June 2018 and December 2018, most likely a result of the pilot nourishment. This phase gives the indication that the growth of the scour hole slows down. However, this is caused by the denser measurement interval. Table 3.1 shows that the expansion of the edge per month, of both the upstream and downstream slope, is even slightly larger than in the second phase. During this phase the scour hole Beerenplaat has the typical shape of scour hole under uni-directional conditions. As can be seen in table 3.2 the flattening out of the downstream slope has stopped and the angle of the upstream slope is quite constant. Most likely the scour hole will keep on expanding but the shape it currently has, will probably persist. Remarkable is that the pilot nourishment has eroded again quite quickly and the river bottom went back to its original shape, which it retained for the following years. This indicates that there are some poorly erodible layers present, since the non-cohesive sediments of the nourishment can be eroded but the river bottom not. The subsoil most likely bound the scour hole to its currents shape at this location.

	expansion edge			
	[m /	[m / month]		
	upstream down			
phase 1	0.49	1.56		
phase 2	1.23	0.34		
phase 3	1.35	0.58		

Table 3.1: Estimation of the edge expansion.

		slope angle	
		α	β
	Mar 2005	16.7°	11.8°
Phase 1	Apr 2006	15.0°	15.8°
r nase i	Apr 2007	17.2°	10.9°
	Mar 2009	18.9°	7.4 °
	Feb 2011	21.8°	6.0°
	Apr 2013	23.4°	4.3°
Phase 2	Jun 2016	23.0°	4.4°
	Dec 2017	38.7°	3.2°
	Jun 2018	25.3°	2.8°
	Dec 2018	23.2°	1.6°
Phase 3	Dec 2019	24.8°	1.3°
FIIASE 3	Dec 2020	24.0°	1.5°
	Feb 2021	20.1°	1.3°

Table 3.2: Estimation of the slope angles.

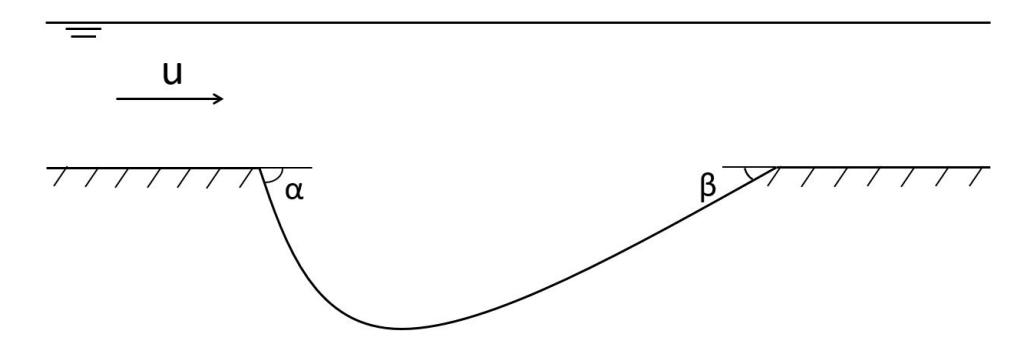


Figure 3.2: Location of α and β .

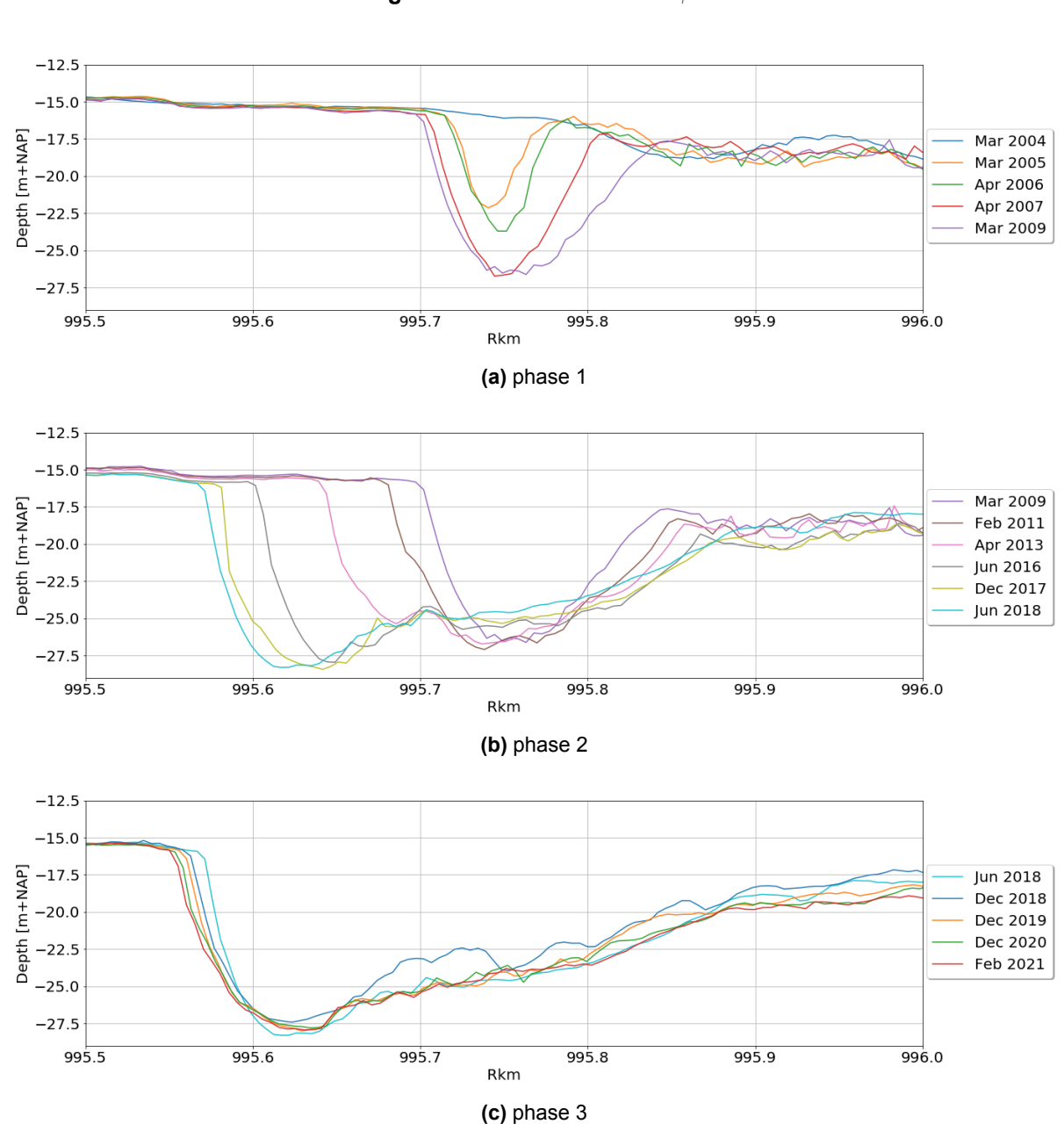


Figure 3.3: Development of the river bottom in the axis of scour hole Beerenplaat.

Besides understanding the shape and size scour hole with respect to the depth, it is also important to understand the development in the other dimensions. Figure 3.4 shows the contour lines of the edge of the scour hole Beerenplaat. Again here, it can clearly be observed that from March 2005 - March 2009 (phase 1) the scour hole developed more downstream than upstream. The scour hole formed mainly on the left side of the river and expanded towards the middle of the river during this first phase. After that, the scour hole developed significantly more upstream until April 2013, followed by both upstream and downstream expansion until June 2018 (phase 2). It can be seen that the scour hole is still located in the center of the river during almost the entire development, with not much changes in third phase. During the last two phases the width of the scour hole Beerenplaat did not change much.

Why the scour hole is growing in different directions during each phase, is not yet understood. A few hypothesis are given that could explain this behavior.

- Locally the resistance of the soil is increased/decreased. This refers to the alternating poorly and highly erodible layers of the Rhine-Meuse delta. The poorly erodible layers take much longer to erode which can result into this grow pattern. Unfortunately no soil samples or accurate geological maps are available to either confirm or reject this hypothesis.
- Alternatively, the flow conditions responsible for forcing the scour have changed in between the
 measurements leading to periodically more or less scour. It is however expected that this is
 not the case. As already explained in section 2.1 the hydrodynamic forcing at the scour hole
 Beerenplaat varies from an hourly to monthly time scale. The interval between different phases
 is in years and therefore it is not expected to be the cause.
- It can be possible that some large vessels are responsible for the development pattern of the scour
 hole Beerenplaat. The propeller wash of these vessels can significantly increase the forcing of
 scour. Despite being present for only a short time, they could remove the poorly erodible layers
 and expose the highly erodible layers below. Koopmans (2017) also listed this as one of the
 causes for the development of the many scour holes in the Rhine-Meuse delta. At this moment
 no vessel data is available to either confirm of reject this hypothesis.

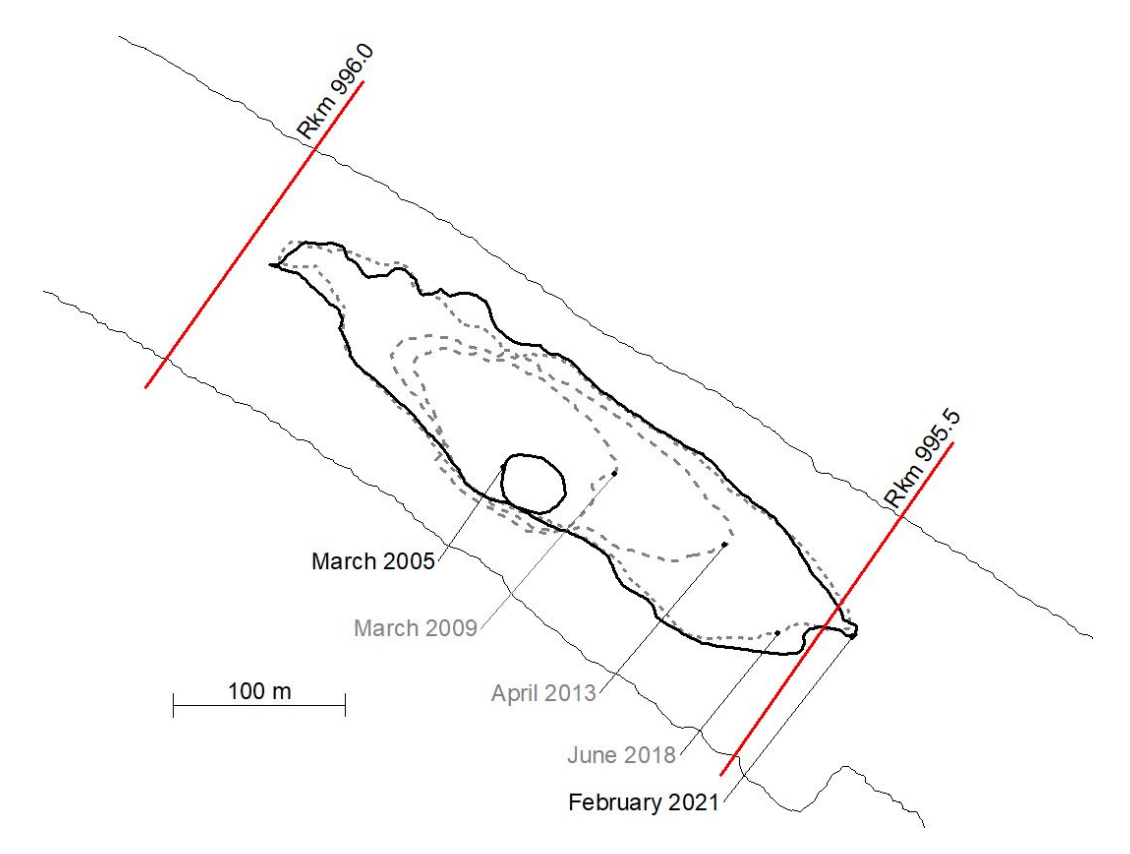


Figure 3.4: Contour lines of the edge of the scour hole Beerenplaat.

What could not yet been observed out of this figure, but was identified by Sloff (2020), is the development of the scour hole in a trench towards the Spui. According to the study, the confluence/bifurcation flow plays an important role within the development since the scour hole Beerenplaat is being pulled into the Spui. Figure 3.5 shows how the scour hole expanded between September 2012 and February 2021. There can be seen that the scour hole has grown upstream, towards the confluence/bifurcation, and in the direction of the Spui. The bulge of the scour hole is clearly bending towards and into the trench, suggesting that further development will follow this trend.

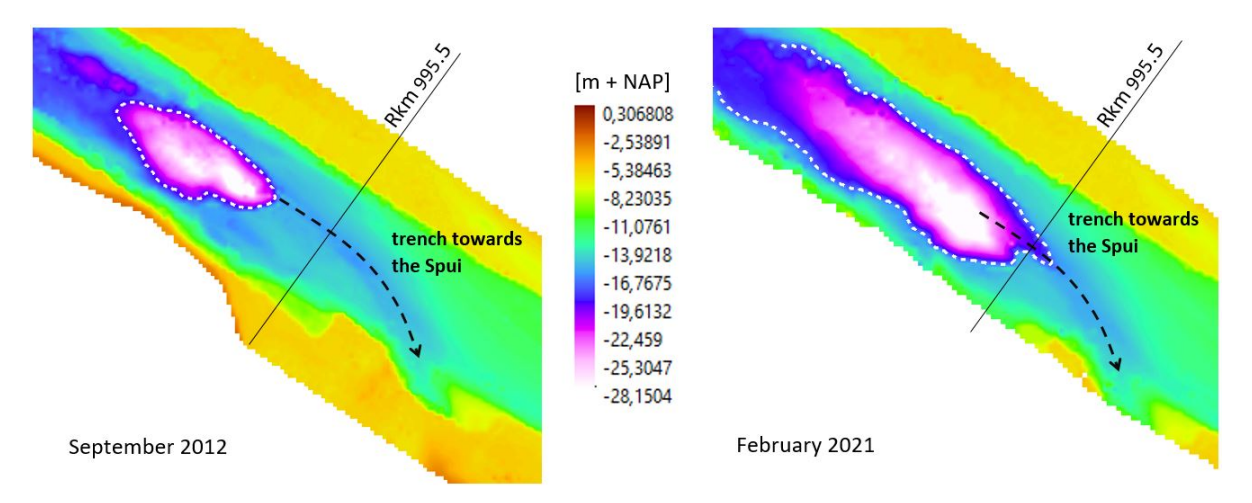


Figure 3.5: Growth of the scour hole in the trench towards the Spui, based on Sloff (2020).

3.1.1. Scour depth

Up until now, a clear description of the profile and dimensions of the scour hole, including field estimations and reasoning for the behavior, has been given. The third development phase has suggested that the scour hole will not become much deeper. As explained in section 2.2.4, scour holes move through different development stages to eventually reach an equilibrium depth and profile. The analysis of the MBES data in the previous section has shown that the profile of the scour hole is still quite dynamically expanding but that the scour depth is stabilizing. This section will focus on the development of the scour depth. This will help in understanding the behavior of the scour hole and in the decision making for future interventions. Figure 3.6 shows the scour depth of the scour hole Beerenplaat over time, as was measured with the MBES.

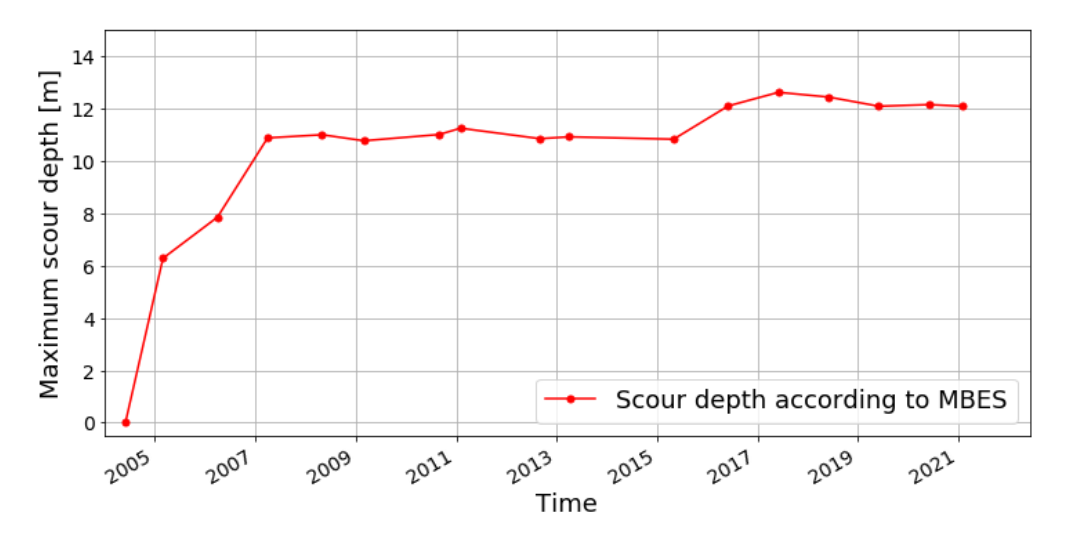


Figure 3.6: Scour depth development of the scour hole Beerenplaat.

What can be seen is that the scour depth grows very fast until 2007 and then tends to stabilize. It appears as if the scour hole Beerenplaat is reaching an equilibrium depth. This was plausible but not known upfront due to the heterogeneity of the subsoil and the tidal conditions (Huismans et al., 2021). Therefore it can be questioned what the equilibrium depth of the scour hole Beerenplaat is and if this has already been reached. Out of figure 3.6 an initial guess of an equilibrium depth of 12-13 meters for the scour hole Beerenplaat can be done. A slightly more detailed approach is to determine the equilibrium scour depth with the Breusers method. As was explained in section 2.2.4, the equation of Breusers is still the best approach to describe scour depth development due to 3-dimensional flow. However, it should be seen as a first estimate and the results should be interpreted with some caution. Especially since using this equation requires some assumptions and fitting of parameters. Important to mention is that the scour depth is smaller than the initial water depth h_0 upstream of the confluence. The initial water depth is the location of the river bottom plus the average water surface elevation. According to the MBES measurements the river bottom is located at approximately -15.85 m + NAP. The average water surface elevation at the Rijkswaterstaat measurement station in Spijkenisse is around 0.226 m + NAP. As a result, the initial water depth $h_0 = 16.08$ m, which is much larger than the scour depth seen in figure 3.6. Therefore the adapted Breusers equation (3.1) by Van Velzen et al. (2015) is used to describe the scour depth development of the scour hole Beerenplaat. There is referred to appendix A.3.2 for an explanation of the variables, units and other governing equations.

In literature it is common to fit the equilibrium depth $y_{m,e}$ and the coefficient γ based on experimental data or field measurements since these parameters are dependent on the type of scour hole and flow conditions (e.g. Koopmans (2017) and Stenfert (2017)). The only remaining unknown parameter is the characteristic time scale t_1 . As explained in appendix A.3.2, this time scale in a tidal environment can be computed with equation (3.2). The equation requires sediment characteristics of the river bottom which are unfortunately not known. Section 2.2.1 has shown that the bottom mainly exists out of alternating sand and clay layers. Therefore it is chosen to work with two cases, a scour hole developing in a pure sand layer and one in a pure clay layer. It is expected that the field behavior of the scour hole Beerenplaat is somewhere in between these scenarios. An important remark to make, is that using the Breusers equation for cohesive soils such as clay, is out of the applicability range. Despite, it is still used to obtain a better understanding of how non cohesive soils could affect the scour depth. In appendix B the values for the parameters of equation (3.2) are explained and the characteristic time scale t_1 is computed for both cases. In table 3.3 an overview of this can be found, paired with the fitted values for the coefficient γ and the equilibrium scour depth $y_{m,e}$. The fitting has been done with non-linear least squares.

$$\frac{y_m}{y_{m,e}} = 1 - e^{-\left(\frac{t}{t_1}\right)^{\gamma}} \tag{3.1}$$

Where: t [s] time $y_{m,e}$ [m] equilibrium scour depth y_m [m] maximum scour depth at t γ [-] coefficient t_1 [s] characteristic time (equation (B.1))

$$t_1 = \frac{K \cdot h_0^2 \cdot \Delta^{1.7}}{\left(\alpha \cdot U_d - u_c\right)^{4.3}}$$
 (3.2)

		Sand	Clay
t_1	[months]	5.51	77.86
γ	[-]	0.36	0.28
$y_{m,e}$	[m]	12.0	17.17

Table 3.3: Overview of parameters and values used to estimate the scour hole development.

With these parameters, the field measured scour depth can be estimated and an indication of the future development can be obtained. Figure 3.7 shows this for each of the cases. It can be seen that the clay case shows the best fit with the MBES measurements. The case with the homogeneous sand subsoil overestimates the initial growth of the scour hole (2005 - 2007) and flattens out quite quickly, while the scour depth in the field appears to become larger. The case with pure clay layer is increasing more graduate, which could be expected since the equilibrium scour depth of the sand subsoil is 12 m and that of the clay subsoil 17.17 m. Also observed is that the measured scour depth is oscillating around both cases, which can be explained by live bed scouring conditions. As discussed in section 2.2.4, this is caused by bed features that enter the scour hole from upstream. As a result, it is difficult to conclude which of the cases is most appropriate. The scour depth could for example reduce after 2021 and keep oscillating around the equilibrium depth of the sand case (12 m). However, the third development phase, explained in section 3.1, has given strong suggestion that the scour hole has reached non-cohesive layers which stabilizes the scour holes profile. Nevertheless, following the indication of the Breusers equation for the clay scenario, shows that the scour hole will most likely become deeper. Only the scouring processes is significantly slowed down due to the large characteristic time scale of the cohesive layers, hence stabilization is observed. Despite, it is known that the heterogeneous subsoil consist out of alternating layers of both sand and clay. Therefore it is expected that the scour hole Beerenplaat behaves somewhere in between the two extremes. Following the indication of the Breusers equation, the scour hole Beerenplaat will eventually reach an equilibrium scour depth somewhere between 12 - 17.17 m. Therefore it is expected that the scour hole will become deeper in the next years and potentially create steeper and less stable slopes.

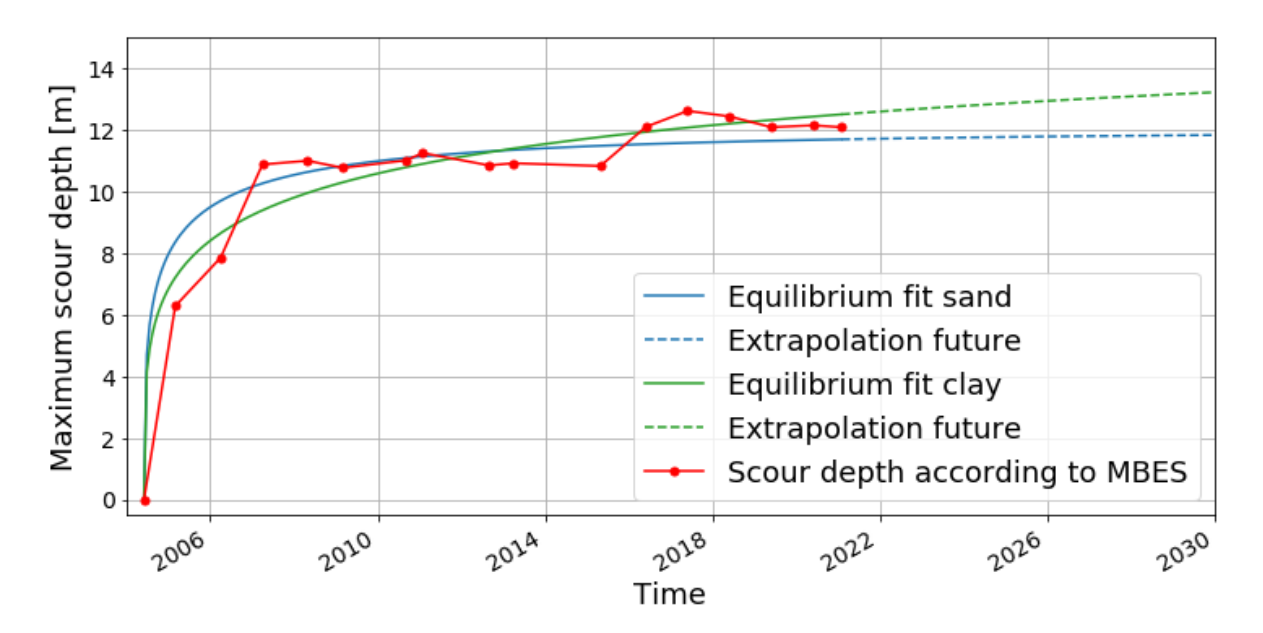


Figure 3.7: First estimation of the scour depth development with the Breusers equation.

3.1.2. Development stage

The previous sections have shown that the scour hole Beerenplaat has not yet reached an equilibrium stage. Looking at the upstream and downstream expansion of the scour hole, relatively large growing rates were observed in both directions. However, the width of the scour hole seems to be bound to its current shape. The same applies for the current profile of the scour hole Beerenplaat. The analysis of the scour depth has indicated that the scour hole will most likely become deeper and has not yet reached its equilibrium depth. How much deeper is mainly dependent on the subsoil. Overall it can be concluded that the scour hole Beerenplaat has not yet reached the equilibrium stage, but is close to, or in, the stabilization stage. Therefore some growth in most dimension is expected. As a result, the threat it poses to the stability of dikes and banks will most likely increase and additional intervention measures, such as the pilot nourishment, can be desired.

3.2. Morphological development after the pilot nourishment

The pilot nourishment is performed at two locations in the Oude Maas, as was discussed in section 2.3.1. The first location was scour section 6, which is located slightly downstream of the scour hole Beerenplaat. The other location is scour section 5. Important to mention is that the nourishments have not been constructed simultaneously. The nourishment at scour section 5 has been constructed in the spring of 2018 and the nourishment at section 6 in the summer of 2018.

3.2.1. Scour section 6

Figure 3.8 shows the development of the river bottom in the axis of scour section 6. There can be seen that the constructed nourishment has significantly raised the river bottom. The nourishment appears to still be present, but has locally eroded 10 - 25 %. What can be seen as well, is that the river bottom contained some bedforms before the pilot nourishment in June 2018. These bedforms had a height of around one to two meters. It appears that after the pilot nourishment, similar bedforms did not develop. Overall it can be said that the pilot nourishment successfully stabilized the river bottom at scour section 6 during the period June 2018 until February 2021. It has prevented the river bottom from becoming much deeper, but only temporarily since the nourishment is eroding.

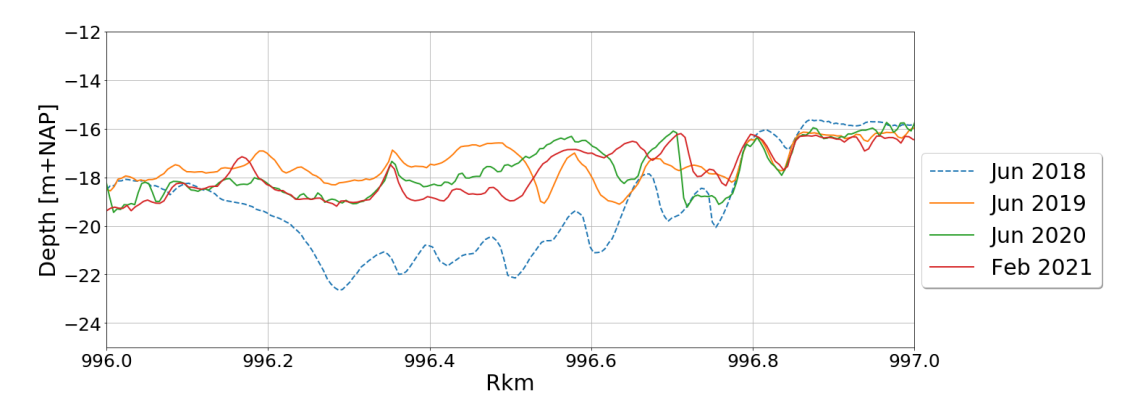


Figure 3.8: Development of the river bottom in the axis of scour section 6.

3.2.2. Scour section 5

In figure 3.9 the development of the river bottom after the nourishment in the axis of scour section 5 can be seen. It shows that erosion of the river bottom is occurring but that the nourishment is still present in February 2021. The nourishment was initially quite flat and contained some small irregular asymmetric bedforms. However, since the nourishment the bedform height has increased with a systematic pattern, almost like a sinusoidal wave. Hulscher and Dohmen-Janssen (2005) and van der Sande et al. (2019) classify this type of bedform as estuarine sand waves, due to their rather large height, asymmetric form, systematic pattern and slow migration speed. These estuarine sand waves are influenced by both the seasonal river flow and the tide. Figure 3.10 shows that such estuarine sand waves were not present before the nourishment at scour section 5. In June 2017 there were some irregular bedforms with an average height of approximately one meter. As can be seen in figure 3.9, the bedforms became larger and more systematic in the years after the pilot nourishment. It really characterizes the river bottom at scour section 5. These bedforms have developed at the same location where the nourishment was constructed. This questions if the nourishment has caused the development of this bedform. Especially a shallow nourishment that follows the river bottom, as was constructed here. Possibly, Rijkswaterstaat wants to perform more of these nourishments in the future. At shallower parts of the delta, this large bedform height can pose a danger to the navigability of vessels.

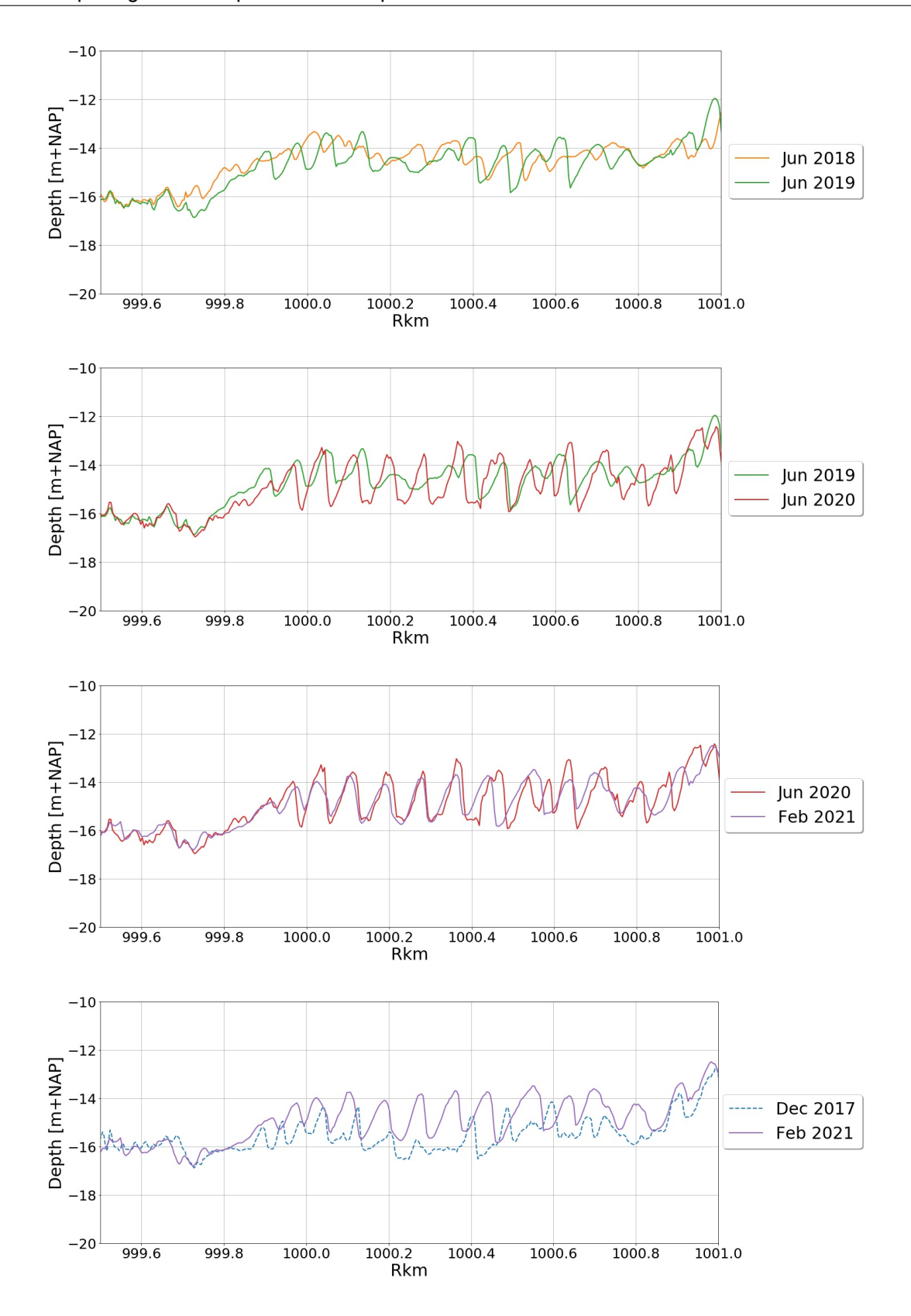


Figure 3.9: Development of the river bottom in the axis of scour section 5. Only the measurement of December 2017 has been taken before the pilot nourishment.

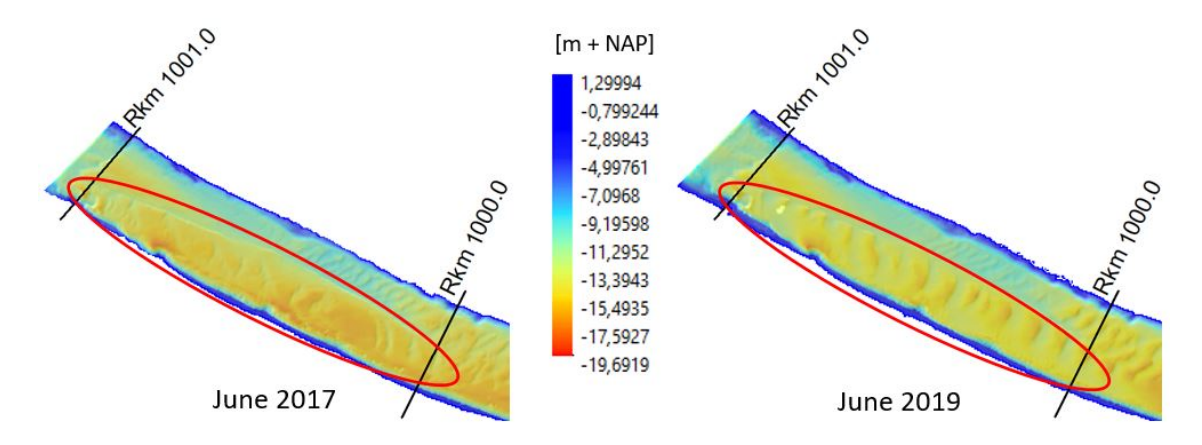


Figure 3.10: Presence of irregular bedforms before nourishment in June 2017 and systematic bedforms after nourishment in June 2019.

Bedform growth

MBES measurements taken after the pilot nourishment have been used to quantify the average height of the estuarine sand waves in table 3.4. Noticeable is that in the course of two years the average height of the sand waves increased with with more than 1.3 meters from June 2018 until June 2020. After that, the bedform height reduces again. In appendix C.1 an overview of the amount of dunes and height of each dune can be found.

Month	Year	Average height
June	2018	0.69 m
December	2018	0.87 m
June	2019	1.24 m
December	2019	1.25 m
June	2020	1.95 m
December	2020	1.91 m
February	2021	1.40 m

Table 3.4: Average height estuarine sand waves in scour section 5 (appendix C.1).

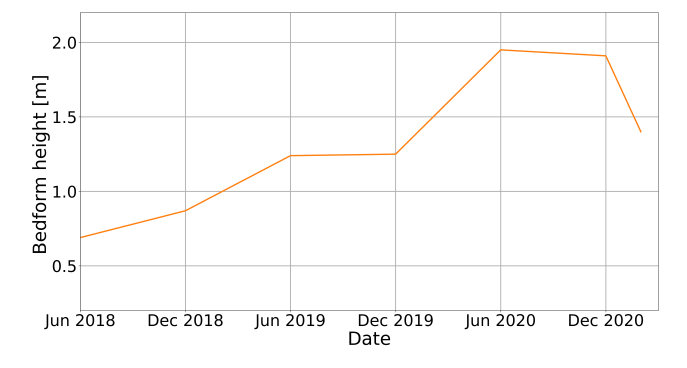


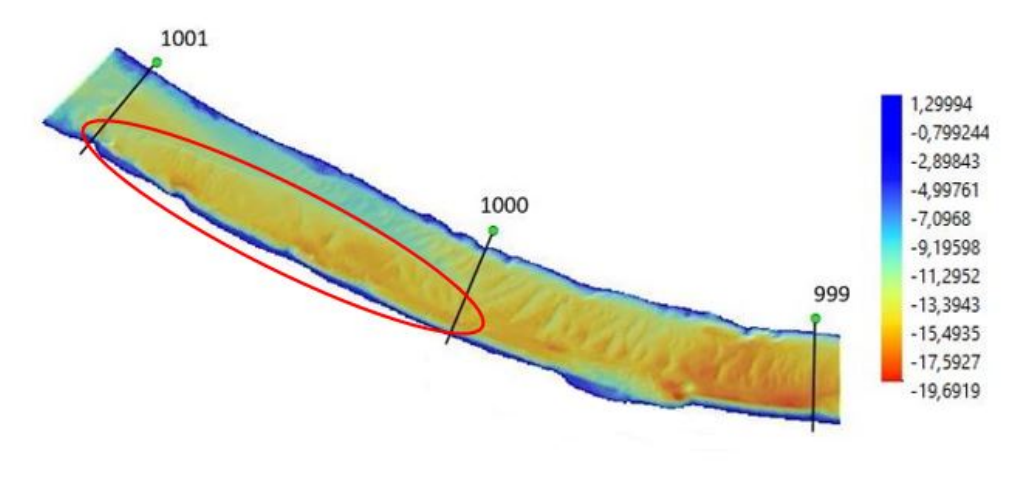
Figure 3.11: Average height of the estuarine sand waves in scour section 5.

As described in section 2.2.6 the height of the estuarine sand waves is dependent on the hydraulic conditions that force them. The best course of action was to look separately at the influence of seasonal river flow (forming the river dunes) and the tide. Therefore a short analysis of the hydraulic conditions is done, to get a better understanding why the estuarine sand waves have grown. This entire analysis can be found in appendix C. Below a summary of the approach and findings is given.

The presence of river dunes is heavily dependent on the flow velocities, which are responsible for bed load transport, and water levels. The water levels form the upper limit of the dune height. However due to the sea, the daily averaged water levels are almost fixed at scour section 5. Therefore it is tried to tackle this with flow velocities and literature findings. Unfortunately no flow velocity measurement station is located at scour section 5. Therefore an alternative approach is taken which computes the change in flow velocity over time and neglects tidal effects. It uses estimates of the discharges at the pilot site and water levels measured at an upstream and downstream measurement station. This change of flow velocity is represent by the factor α . If $\alpha>1.0$ the change in flow velocities is positive indicating that they have increased over time. Contrary, $\alpha<1.0$ indicates a negative change meaning a decrease in flow velocities over time. In appendix C.2 the factor α has been computed monthly from

June 2018 until February 2021. This change in flow velocity is in turn used to describe the theoretical response of river dunes, as was explained in appendix A.5.2, and is compared to the actual development of the estuarine sand waves. What could be concluded was that the seasonal river flow partly explains the growth of the estuarine sand waves. The response of the river dunes was not always similar as the behavior of the estuarine sand waves. On top of that, the river dunes are, according to literature, only prominent part of the time while the bedforms seen in the MBES measurement are quite systematic and continuously present. This suggest that another mechanism should be included. This other mechanism is the tide. The tidal conditions at the pilot site and the contribution to the growth of the estuarine sand waves are investigated in appendix C.3. The tide has caused the continuous presence of the bedforms at scour section 5. It has supported in the growing phase of the estuarine sand waves and most likely plays an important factor in reaching an equilibrium height. A first estimation with an empirical relation has indicated that the estuarine sand waves are close to their equilibrium height.

The tidal forcing and the river discharge together can qualitatively explain the growth of the estuarine sand waves at scour section 5. Unfortunately it is with the current data and literature not possible to give any quantitative contributions of either forcing mechanism. Still unanswered is why the estuarine sand waves have only developed after the pilot nourishment. In appendix C.4, a list of individual hypothesis is given on which conditions could have changed and triggered the formation of the estuarine sand waves. These hypothesis include the type of sediment at the river bottom, the grain size of the sediments, the amount of perturbations and migration from upstream. It seems very unlikely that the estuarine sand waves have entirely migrated into scour section 5 from upstream. Figure 3.12 shows that the upstream sand waves are almost bound to their current location and do not enter scour section 5 during a period of almost 5 years. Only a few irregular migrating bedforms were encountered during this period, but these were not similar as the estuarine sand waves seen in figure 3.10. Most plausible is that the pilot nourishment has introduced sufficient non-cohesive sediments, allowing the hydraulic conditions to form these bedforms. The simultaneous growth of the bedforms in the entire nourishment seems to agree with this (see figure 3.9). However, any influence of upstream bedforms is not yet ruled out. The estuarine sand waves show a skewed profile suggesting that there is net migration towards sea in scour section 5. Hence there could still be some influences from upstream. Further investigation of the formation of estuarine sand waves is recommended to conclude if this is a one time occurrence or that these bedforms should be linked to shallow nourishments in the Rhine-Meuse delta.



(a) September 2012

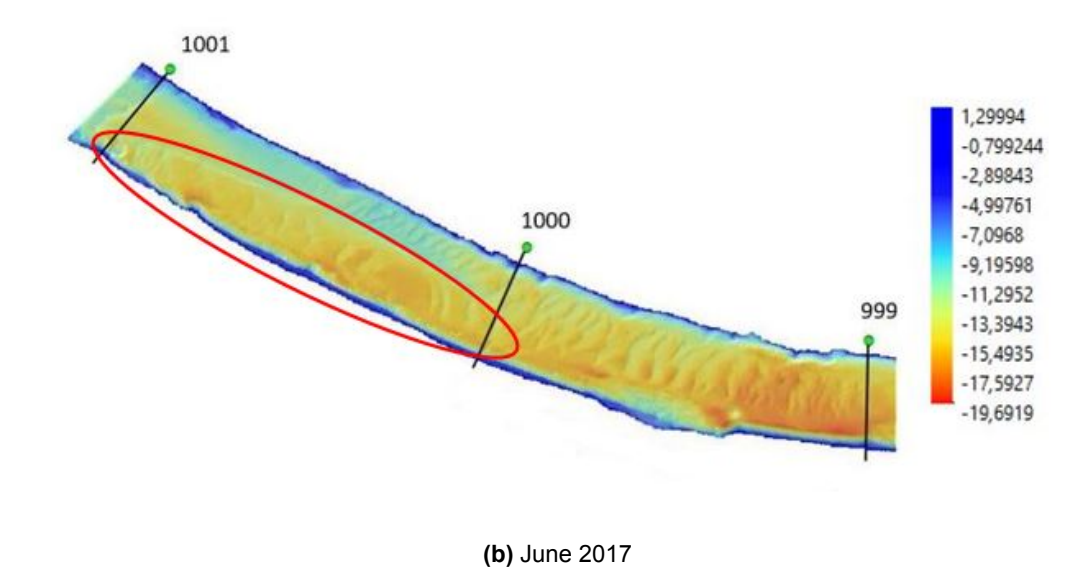


Figure 3.12: River bottom measurements of scour section 5 in m + NAP. The red ellipse indicates the area where the nourishment is constructed in the spring of 2018.

3.3. Conclusion on sub research question 1

This chapter has focused on answering the question "What was the morphological development of the river bottom at the scour hole Beerenplaat and the location of the pilot nourishment in the Oude Maas?". The most important findings that answer this question are listed below.

- The scour hole Beerenplaat is a very dynamic and deep hole that grows in both upstream and downstream direction. It has developed in different phases with different growth rates in either direction. Most likely this is caused by either the heterogeneous subsoil, varying hydraulic conditions or anthropogenic influences such as the propeller wash of vessels. The scour hole is growing in the upstream direction into the Spui, suggesting that the hydraulic forcing of the confluence/bifurcation Oude Maas and Spui plays an important role. During the upstream growth, the slope angle remained constant and the deepest point of the scour hole migrated along. The upstream and downstream growth rates of the scour hole show no indication that the scour hole Beerenplaat has reached an equilibrium stage. This is supported by the scour depth development and the first approximations of the equilibrium depth with the Breusers equation. Probably the scour hole is close to, or in, the stabilization stage. However, there are no indications that the scour hole Beerenplaat will yet stop growing. Therefore interventions to protect the stability of dikes and banks, such as the pilot nourishment, can be required in the future.
- The part of the pilot nourishment at scour section 6 has stabilized the river bed. Approximately 10 - 25 % of the nourished sediments has eroded during the period June 2019 - February 2021.
 No significant bedforms have developed after the pilot nourishment.
- The smaller and shallower part of the pilot nourishment at scour section 5 is also still present in February 2021. After the nourishment, large and systematical estuarine sand waves developed. These are forced by both the seasonal river flow and the tide and were not observed prior to the pilot. It is hypothesised, that due to the nourishment more suitable sediment (noncohesive) became available that allowed the hydraulic conditions to form these estuarine sand waves. Unfortunately no additional field measurements of the subsoil are available to confirm this hypothesis.

4

Flow processes

This chapter focuses on answering the sub research questions two and three, which are "How is the flow field at the confluence/bifurcation Oude Maas & Spui shaped during a tidal cycle?" and "Which of the 3D flow processes are present at the scour hole Beerenplaat and what is the influence of the flow direction and intensity on them?". First, an explanation will be given of the methods used to answer these sub research questions. After that, section 4.2 answers the second sub research question and finally section 4.3 answers the third sub research question.

4.1. Method

These sub research questions will be answered by using the output of a Delft3D model and field measurements. As part of the pilot nourishment, Acoustic Doppler Current Profiler (ADCP) measurements have been taken at the pilot site in the Oude Maas. These measurements consist out of a few transects at the scour hole Beerenplaat, taken only during peak ebb and flood flow and for one specific river discharge. This does not give a clear and representative image of what happens at the entire scour hole and the confluence/bifurcation during a tidal cycle. Therefore the system is further investigated with the help of results from a Delft3D model.

4.1.1. Delft3D model

The Delft3D model output that will be analyzed in this research has been created with the Delft3D Flexible Mesh suite (Delft3D FM). The model is 3D and simulates the entire Rhine-Meuse delta in the Netherlands. Both the suite and the model have been created by Deltares. This researches only uses the output of the Delft3D model and does develop or improve it. Out of this suite, the module D-Flow Flexible Mesh (D-Flow FM) is used for the hydrodynamic simulations of the Rhine-Meuse delta. The program can carry out simulations on hydrodynamic flow, waves, water quality and ecology.

Mathematical formulation D-Flow FM

As mentioned, the hydrodynamic situation of the model has been simulated with D-Flow FM. This is a multi-dimensional (1D, 2D and 3D) hydrodynamic simulation program which calculates non-steady flow and transport phenomena that result from tidal and meteorological forcing on structured, unstructured and boundary fitted grids (Deltares, 2021). Flexible Mesh indicates that the (unstructured) grid consists out of flexible combinations of triangles, quadrangles, pentagons and hexagons. For this model the 3D functionality of D-Flow FM has been used. It solves the Navier-Stokes equation for an incompressible fluid, under the shallow water and Boussinesq assumptions. These assumptions imply the following.

4.1. Method 36

• Incompressible fluid means that the fluids density remains constant in the entire flow. It does not change when the pressure changes.

- The Boussinesq approximation implies that the effect of variable density is only taken into account in the pressure term.
- Under the shallow water equations, vertical accelerations are assumed to be small compared
 to gravitational acceleration and therefore neglected. This reduces the the vertical momentum
 equation to a hydrostatic pressure equation. It makes the model very suitable to model flow
 phenomena of which the horizontal length and time scales are significantly larger than the vertical
 scales (Deltares, 2021).

For an elaborate and full explanation of the governing equations there is referred to Lesser et al. (2004). The equations in the model are capable of resolving the turbulent scales (large eddy simulation), but are most of the time not able to resolve the turbulent fluctuations since the hydrodynamic grids are too coarse (Deltares, 2021). Therefore the Navier stokes equation is Reynolds-averaged, introducing horizontal Reynolds stresses that account for the turbulent fluctuations. These are determined by the model with the eddy viscosity concept (for details see Rodi (1984)).

Motivation model choice

As shown above, the D-Flow FM contains some assumptions to ensure that the model can solve the equations efficiently. These assumptions make the model not suitable for all flows, but give it a range of applications. This section motivates why it is chosen to analyze the output of a Delft3D model for answering sub research question two and three and why specifically this model of the entire Rhine-Meuse delta has been used.

In the second sub research question the flow field at the confluence/bifurcation Oude Maas and Spui will be analyzed during a tidal cycle. This is well within the range of areas of applications of the model, since it can simulate both tidal and river flow cases (Deltares, 2021). On top of that, the horizontal scales at the confluence/bifurcation (kilometers) are much larger than the vertical scales (\approx 30 meters) creating no conflict with the shallow water equations. It is expected that the flow patterns associated with a confluence/bifurcation, such as horizontal recirculation zones, shear layers and secondary flow with recirculating cells, are captured within the model results. An important remark, is that the representation of these patterns could be influenced by the eddy viscosity's and hence the turbulence model.

The third sub research question focuses on investigating the behavior of the 3D flow processes inside the scour hole, as were explained in section 2.2.3. Most of these 3D flow processes are paired with turbulence, which are often the smaller scale turbulent fluctuations. Therefore the Delft3D model is not able to simulate all these 3D flow processes. This is especially the case for the lateral recirculations within the horseshoe vortex and probably also for the (curved) recirculation zone. Probably since it is still possible that the hydrodynamic grid in the streamwise direction is not too coarse. The model should be capable for investigating the flow contraction. Overall, it makes the model not the best choice for investigating these 3D flow processes.

Despite, it is still chosen to work with the output of a Delft3D model. It is most likely suitable for investigating the second sub research question regarding the confluence/bifurcation flow. On top of that, it should be able to use the Delft3D model for investigating the flow contraction. It is accepted that the model can not be used for investigation of the horseshoe vortex and probably the recirculation zone. Potentially the field measurements can give some insights on these parts. Alternatively, literature findings can be used in combination with the identified geometry of the scour hole Beerenplaat, to construct hypothesis on the field presence of these 3D flow processes.

The 3D Delft3D model of the entire Rhine-Meuse delta has been in development at Deltares for quite a while. Due to the increasing capabilities of numerical models, the model has been updated with every version of Delft3D. As a result, a lot of improvement have been made. As a result, the model is able to simulate discharges and water levels with a good accuracy in the entire delta. On top of that, the model can simulate the larger scale horizontal flow processes and is 3D. Therefore it is chosen to work with

the output of this specific model. The focus within this research lies on the confluence/bifurcation Oude Maas and Spui, including the scour hole Beerenplaat. Since the model simulates the entire Rhine-Meuse delta, only a partition of the model results is used. A full explanation of the characteristics of the model is given in appendix D.1.

4.1.2. ADCP measurements

Flow velocity measurements have been taken with an Acoustic Doppler Current Profiler. The instrument makes use of the Doppler shift principle. It transmits sound waves through the water column that are reflected by suspended particles and the river bottom. Some of these reflected sound waves are directed backwards to the instrument which is able to measure the reflected frequency. With the transmitted and reflected frequencies the change in frequency can be computed (i.e. the Doppler shift) which can quantify the flow velocity (Kostaschuk et al., 2005). The instrument emits 4 beams of acoustics waves simultaneously in different directions to measure all velocity components. The water column is hereby dived into multiple bins at which a flow velocity value is determined. In conventional data processing it is assumed that flow in between the beams is homogeneous to derive an averaged velocity (Vermeulen, Sassi, et al., 2014). As a result it can filter out turbulent structures within the flow. Another limitation of the ADCP device is that it can not measure the velocities in the entire water column. Close to the river bottom there is acoustic deflection of the side lobe, causing interference and making it not possible to measure the velocities. Close to the water surface the velocities are not measured since the instrument needs to be submerged into the water and requires a blanking distance (Simpson, 2002).

As part of the pilot nourishment, Rijkswaterstaat identified three normative situations during which ADCP measurements should be taken. These measurements are taken during an entire tidal cycle with different conditions that are listed below.

- Normal discharge (2000-2400 m³/s at Lobith) and normal tide
- High discharge (6000-8000 m³/s at Lobith) and normal tide
- Normal discharge (2000-2400 m³/s at Lobith) and spring tide

For this research, the ADCP measurements taken during a tidal cycle on 11 February 2021 are available. At this date there were high discharges at Lobith of around 6000-6300 m³/s. The measurements have been taken on four different transects at the pilot site. Only one of these four transects is located at the scour hole Beerenplaat, on which is focused during this research. At this transect the velocities are measured at a grid with Δx = 0.1 m, Δy = 0.4 m and Δz = 0.5 m.

4.2. Flow field at confluence/bifurcation

The goal of this section is to answer the second sub research question "How is the flow field at the confluence/bifurcation Oude Maas & Spui shaped during a tidal cycle?". This will be done mainly by using the output of the Delft3D model described in the previous section. In contribution there will be made use of the ADCP measurements and literature findings. To answer the research question, two different cases will be investigated.

- 1. The first case is referred to as the base case. During this case a tidal cycle in the Delft3D model will be analyzed, which has similar conditions as the tidal cycle during which the ADCP measurements have been taken. In this way the observations done in the model results can be compared with the ADCP measurements, such that the accuracy of the model can be reviewed.
- 2. During the second case, a tidal cycle of the Delft3D model with completely different conditions (discharge and water levels) will be analyzed. In this way, there can be investigated how the conditions are of influence on shaping the flow field. These results can not be compared with any measurements, but help in better understanding the systems behavior.

In both of these cases, four different scenarios are investigated during this tidal cycle. The semi-diurnal tide and the seasonal varying river discharge ensure that the flow field is continuously changing. As a result, no long term situation is representative for the flow field at the confluence/bifurcation Oude Maas and Spui. Therefore the flow field is analyzed at four different scenarios, encountered during each tidal cycle. These scenarios are peak ebb flow (1), flow changing from ebb to flood (2), peak flood flow (3) and flow changing from flood to ebb (4). The two peak scenarios are of importance since they show the most extreme situations. The two scenarios where the flow is changing are included to show how the river discharge collides with the tide, forcing the flow direction to change at the confluence/bifurcation.

4.2.1. Base case: similar conditions

In the following sections of this research there is often referred to time steps. These are not the numerical time steps at which the model runs, but the time steps at which output is generated (Δt_{output}).

A limitation of the base case is that the time frame of the model does not span the moment the ADCP measurements have been taken. The model simulates the field conditions from 14 June 2018 until 17 November 2018, while the ADCP measurements have been taken on 11 February 2021. As a result, there is searched for a new period, within the time span of the model, that has similar field conditions as found on 11 February 2021.

Selection new period

As was shown in section 2.1, three factors determine the flow direction and intensity at the confluence/bifurcation Oude Maas and Spui. These are the tide, the river discharge and the operating of the Haringvliet sluices. The operating of the sluices did not yet happen in 2018 and is therefore not included within the model and hence the decision on a new period. The tidal conditions can be investigated by looking at the water level at Spijkenisse, located slightly downstream of the confluence/bifurcation Oude Maas and Spui. At this location, Rijkswaterstaat measures the water levels. Unfortunately no discharge measurement stations are located nearby, which can be used for the selection of the new period. Therefore they will be compared at Lobith, which is often used as representation of the discharge intensity in the Dutch river network. After a new period is selected, the discharges in the model will be computed and compared with the ADCP measurements.

Figure 4.1a shows the discharges at Lobith during the ADCP measurements. What can be observed is that there are relatively high discharges between the 6300 - 6000 m³/s. In figure 4.1b can be seen, that the discharges during the time frame of the model, June 2018 until half November 2018, are much lower. No period with similar high discharge characteristics as during the ADCP measurements is found. As a result no new period can be selected based on this criteria. It can only be based on the water levels.

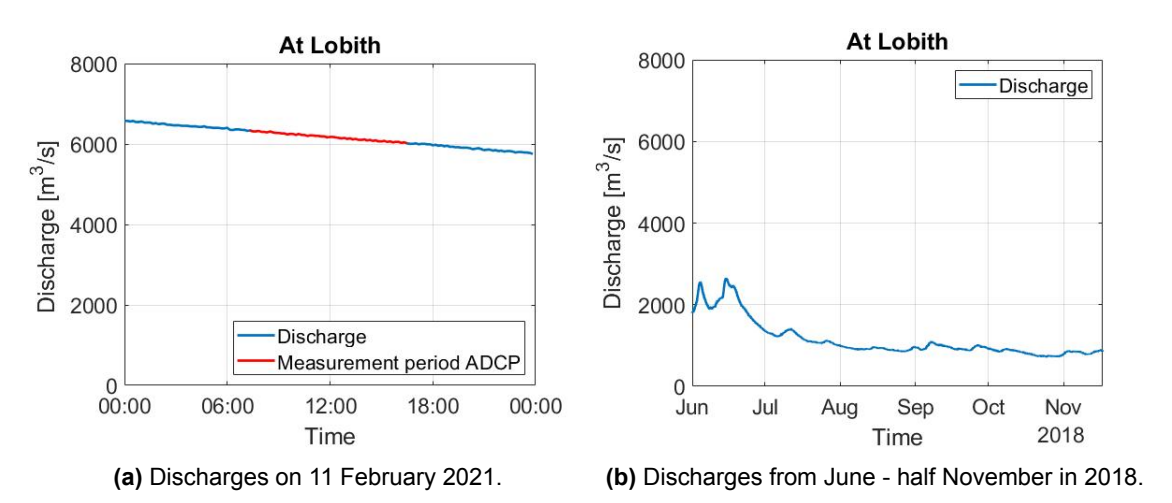


Figure 4.1: Comparison of measured discharges at Lobith.

During the investigation of the tidal cycles within the time frame of the model, one period was found that has very similar water levels as on 11 February 2021. The interval, consisting out of almost 2 tidal periods, is from 13 July 2018 12:30 until 14 July 2018 12:30. In figure 4.2 the measured water levels at Spijkenisse can be seen for both periods together with the moments the ADCP measurements have been taken. The water levels during this period in 2018 are the closest match the field conditions found in 11 February 2021.

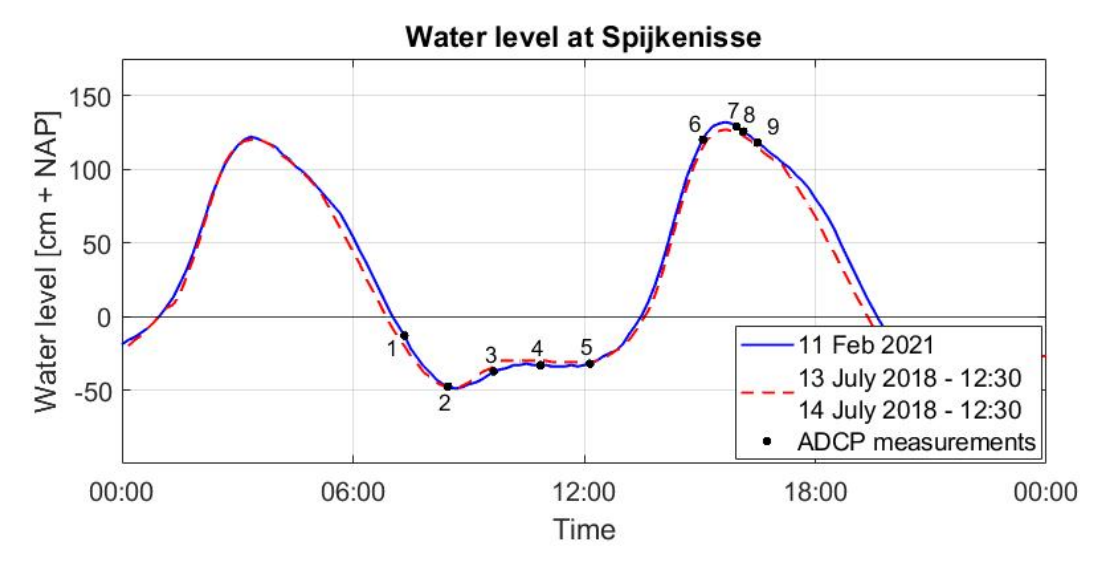


Figure 4.2: Comparison of water level at Spijkenisse (measured by Rijkswaterstaat).

Model output time steps

The model results should be investigated at the four scenario (peak ebb flow, ebb \rightarrow flood, peak flood flow, flood \rightarrow ebb). However, the model only stores the computed result every two hours. Therefore it should be checked if the time steps at which the model output is generated during the new period, match with the four scenarios. Figure 4.3 shows the time steps and water levels at which output is generated during this new period. The green numbers represent the output time step of the model, which are a quite good with the four scenarios. The model results are computed at both the ebb and peak flows (e.g. points 359, 360, 363) and during the switching of flow direction (e.g. 358 and 362). This makes the new period suitable to analyze the flow field during the four scenarios. On top of that, it allows for a good comparison with the ADCP measurements during both peak ebb and peak flood flow. Table 4.1 shows for each of the four scenarios which time step of the model output is analyzed and which ADCP measurement is used for comparison. Unfortunately, no ADCP measurements were taken when the flow is changing from ebb to flood or the other way around.

	Scenarios	Time step model	ADCP measurement
1.	peak ebb flow	359 (t = 08:40)	2 (t = 08:28)
2.	$ebb \to flood$	362 (t = 14:40)	_
3.	peak flood flow	363 (t = 16:40)	9 ($t = 16:30$)
4.	$flood \to ebb$	358 ($t = 06:40$)	_

Table 4.1: Overview of model time steps and ADCP measurements for scenarios base case.

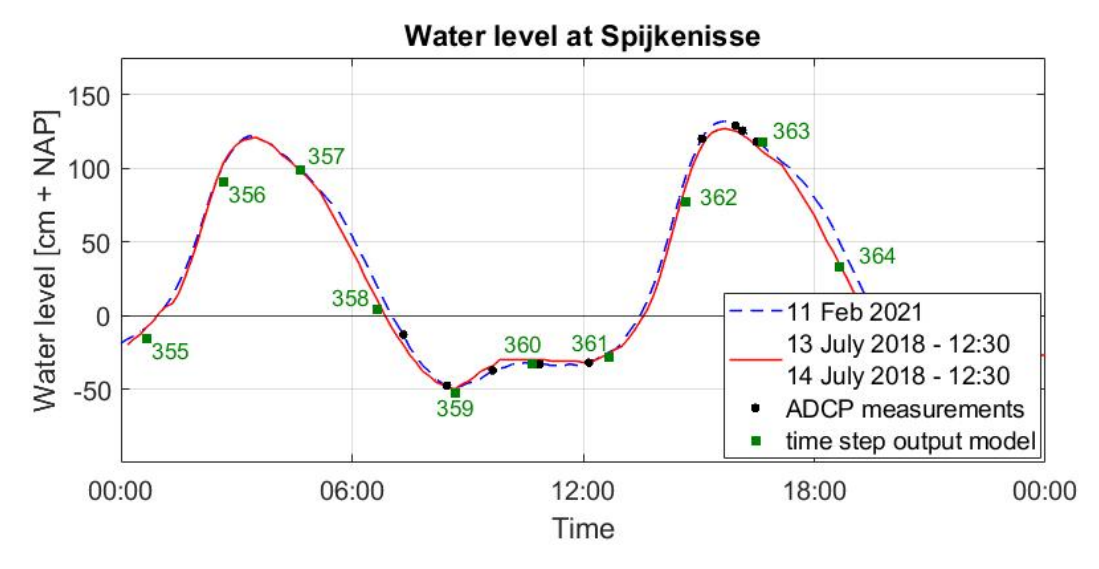


Figure 4.3: Water levels at Spijkenisse measured by Rijkswaterstaat and computed in the model.

Match between flow velocities in the model and ADCP measurements

The new period was chosen based on the water levels at Spijkenisse. However, not yet addressed is how accurate this period in the model can describe the discharges and velocities on 11 February 2021. Therefore the ADCP measurements are compared to the model results at roughly the same location. The full comparison has been made in appendix E for both peak ebb and peak flood flow. Below a brief summary of this is given.

It was found that during peak ebb flow, the flow velocities in model show similar characteristics as in the ADCP measurements. The average velocity of the model cross-section slightly underestimates the average velocity the ADCP transect, with around 10 %. As can be seen on figure 4.4, this mainly occurs on the location with the largest velocities. Nevertheless, the flow characteristics such as direction and order of magnitude are similar.

During peak flood flow the model was less accurate. The average velocity in the models cross-section overestimates the average velocities of the ADCP transect with 30 %, if there is accounted for a time delay of 1 hour and 35 minutes. Figure 4.5 shows that the largest overestimation occurs on the left side of the cross-section, where the Spui is located. The time delay is included since the peak flood flow comes much earlier than is reproduced by the model. This suggests that the model struggles with simulating the moment the flow velocities change direction in the system. Nevertheless, the model showed again similar flow characteristics as the ADCP measurements if this time delay is included. Therefore the results of the base case during peak flood flow will not be compared with ADCP measurement 9 (taken at 16:30), as was suggested in table 4.1, but with ADCP measurement 6 (taken at 15:05).

It can be possible that the robustness of the model in both time and space plays a role in the under- and overestimation of the average velocities. The model has a time step of $\Delta t_{output}=2$ hours, while the ADCP measurement show that the discharge can change with 300 m³/s in only 11 minutes (between ADCP measurement 7 & 8, see appendix E). On top of that, the grid of the model is $\Delta x, y \approx$ 25 m and Δz = 1 m, while the ADCP device measures at a grid with Δx = 0.1 m, Δy = 0.4 m and Δz = 0.5 m. This makes the model robust with respect to the ADCP measurements in both time and space. As a result, it can not capture the flow as detailed and specific as the ADCP measurements.

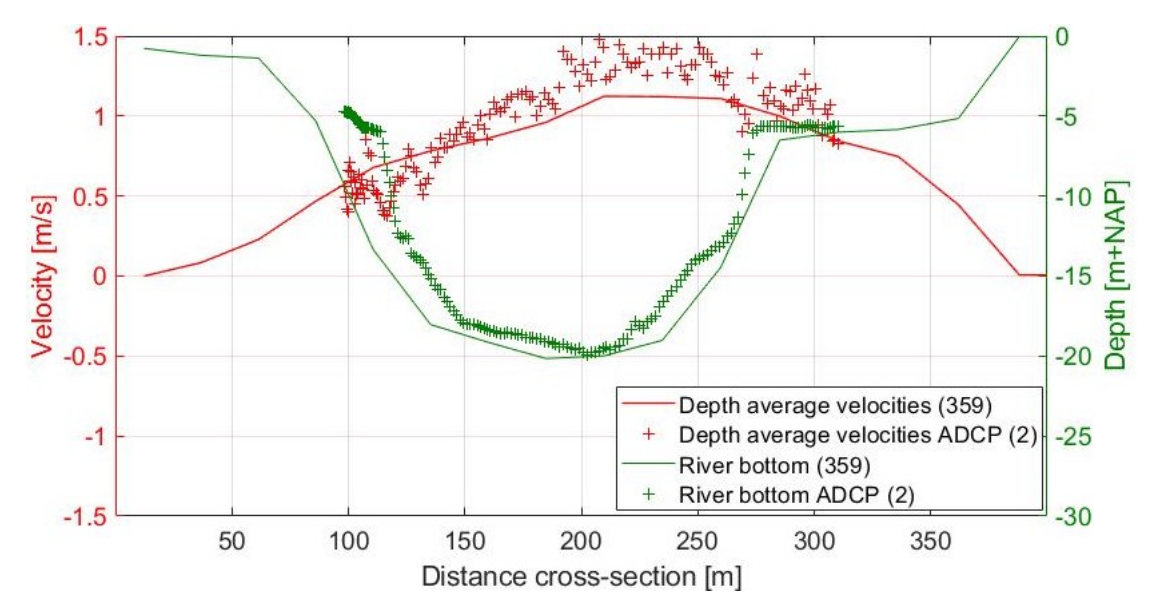


Figure 4.4: Streamwise depth averaged velocities and river bottom at time step 359 (08:40) and ADCP measurement 2 (08:28).

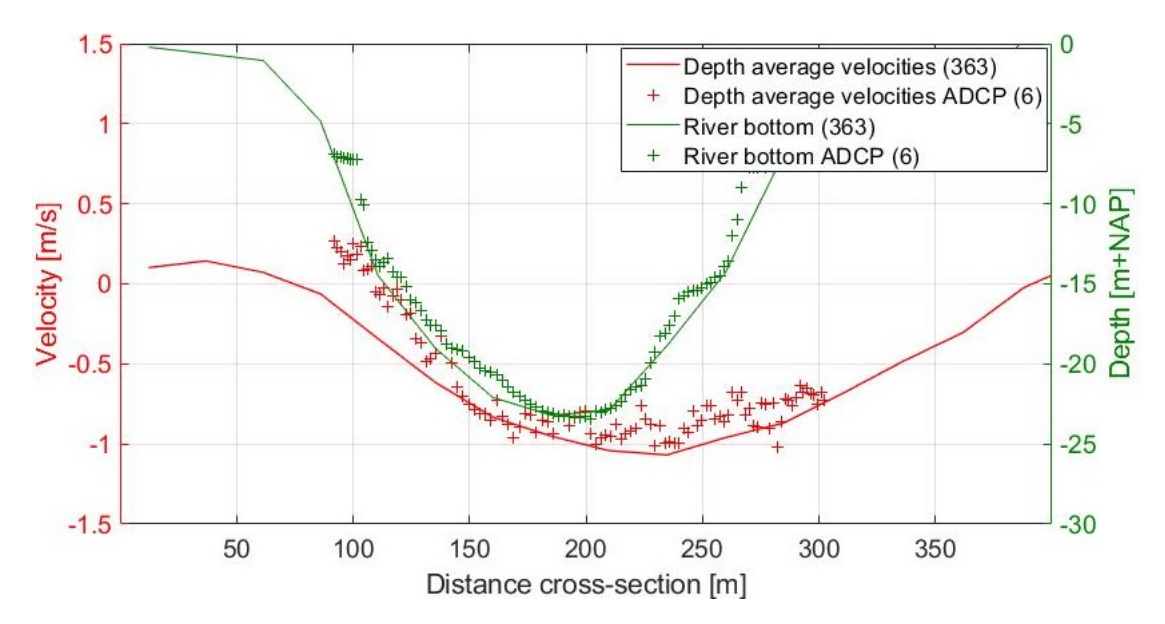


Figure 4.5: Streamwise depth averaged velocities and river bottom at time step 363 (16:40) and ADCP measurement 6 (15:05).

The goal of using the Delft3D model in this chapter is to get a better understanding the velocity field at the entire confluence/bifurcation, since the ADCP measurements have only been taken on a few transects. As listed above, there are some slight differences between the model results of this new period and the ADCP measurements. However, the flow directions and the order of the velocity magnitudes behave similarly during both peak ebb and peak flood flow. Therefore the limitation that the time frame of the model and the ADCP measurements do not match is accepted for these two scenarios. The Delft3D model results during this new period can be used in combination with the ADCP measurements, for answering this sub-research question. Unfortunately no comparison could be done for the two scenarios with changing flow direction due to the lack of ADCP measurements. Despite, the results of the model for these scenarios will still be analyzed to get better insights on how the system could behave.

Model results base case

An overview of the confluence/bifurcation Oude Maas and Spui and some reference points can be seen in figure 4.6. The four scenarios of the base case will be investigated in the order: peak ebb flow (1), flow changing from ebb to flood (2), peak flood flow (3) and flow changing from flood to ebb (4). The flow field will be interpreted with the help of literature findings that were described in section 2.2.5. If possible, the findings will be verified by help of the ADCP measurements.

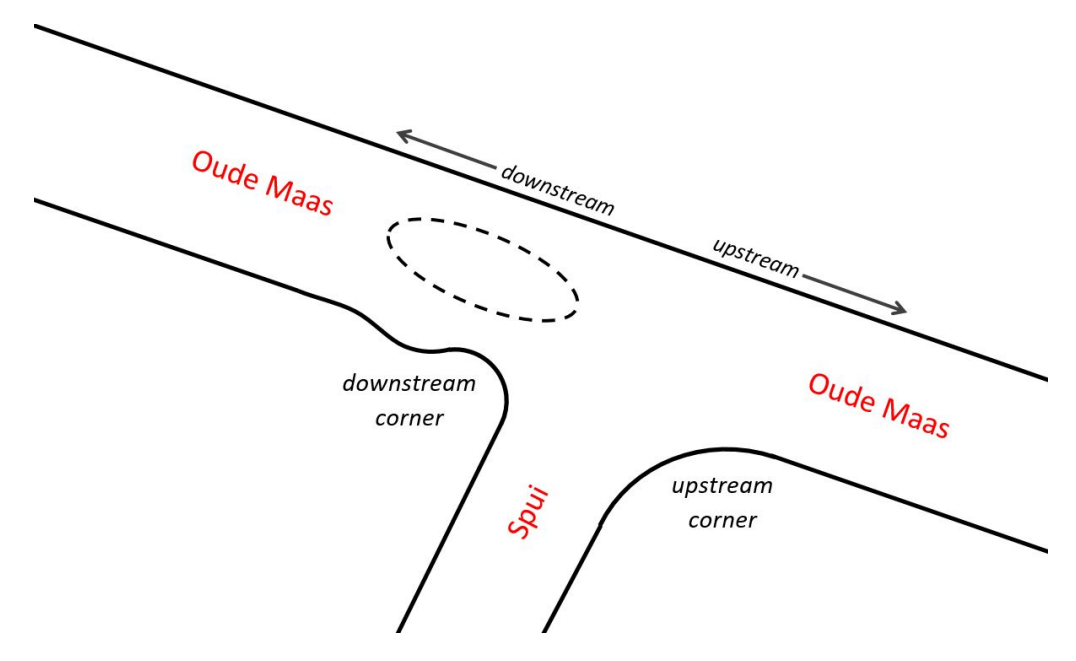


Figure 4.6: Overview of the confluence/bifurcation Oude Maas and Spui.

Scenario 1, peak ebb flow

The peak ebb flow conditions are found at time step 359 of the model. In figure 4.8 an overview of the depth averaged velocities at the confluence/bifurcation Oude Maas & Spui can be seen. What can be observed is that the system behaves as a confluence during ebb. Flow is coming from both the Spui and the Oude Maas, joining above the scour hole. The depth averaged flow velocities inside the scour hole are less than either upstream or downstream of it. This makes sense since a larger depth means and increased flow area and hence a local reduction of the flow intensity. The largest flow velocities are found downstream of the scour hole, where the flow of the both the Oude Maas and the Spui have completely joined. As explained in section 2.2.5, six different flow zones can be distinguished at a confluence under uni-directional flow conditions. This question if these six zones are also encountered during ebb flow at the confluence/bifurcation Oude Maas and Spui.

- A flow stagnation zone (1 in figure 2.14) can be observed on the upstream corner of the confluence. The flow velocities are almost zero here. A point bar has not developed, most likely due to the tidal conditions. It is also possible that the discordance of the river bed hinders the formation of such a point bar.
- The flow deflection zone (2) can be seen in the area between the flow stagnation zone and the scour hole. At this location the flow of both tributaries collide forcing both into a new direction. The most deflection is seen at the flow coming out of the Spui since this is the most out of line with the post-confluence channel.
- A horizontal flow recirculation zone (3) is not observed in figure 4.8. It would be expected that this zone is present just after the downstream corner of the confluence (x = 88800 m, y = 428100 m). As was discussed in section 2.2.5, the presence of a flow recirculation zone in the field is still an

uncertainty since river banks can change more gradually than flumes. Probably this is the case for the confluence/bifurcation Oude Maas and Spui. At the downstream corner of the confluence the river bank has a notch, suggesting that the river bank has adapted here over time. The flow can follow this notch preventing the avoiding the formation of a recirculation zone during ebb flow.

- The shear layer (4) seems to be present at the confluence. There can be observed that the flow velocities are not similar over the width of the scour hole, while upstream of the confluence the flow in the center is quite uniform. This shows that two flows with different velocities are running parallel to each other. According to Bilal et al. (2020) this indicates the existence of a shear layer. At this shear layer, mixing of the two different flows would occur with the goal of creating even flow velocities in both streams. However, the presence of the shear layer is also dependent on the two counter acting recirculating cells that occur downstream of the confluence (see section 2.2.5). Looking at the cross-section in figure 4.7, this can not be observed. Only one recirculation cell is present. This questions what is happening here and therefore the secondary flow will be further investigated in section 4.2.3. Therefore it is not yet possible to comment on the presence of the shear layer downstream of the confluence. Nevertheless, some shear is expected at the confluence since two flows with different velocities are running alongside each other.
- As already mentioned the largest velocity zone (5) is found just downstream of the scour hole. It would be expected that this zone is located closer towards the confluence. Probably, this is caused by the presence of the scour hole and the absence of the flow recirculation zone. The depth of the scour hole leads to a flow expansion and hence lower velocities. On top of that, the flow is not constricted by the flow recirculation zone. As a result the largest velocity zone is not found at this location but seen when the flow leaves the scour hole. The flow is forced upwards and constricted to the a smaller cross-section, leading to these maximum flow velocities.
- Flow recovery zone (6) is not present within the frame of figure 4.8. The flow velocities downstream of the scour hole are still varying over the center of the river meaning that the two flows have not merged completely. Despite, it is expected that the flow recovery zone is present further downstream in the Oude Maas, leading eventually to equal velocities in the center of the river.

The points above have shown that the bi-directional confluence Oude Maas and Spui behaves quite similar during peak ebb flow as a confluence under uni-directional flow conditions. The main differences are found at the shear layer and horizontal flow recirculation zone. The presence of the shear layer is uncertain since only one vertical flow recirculation cell was found in a cross-section. The horizontal flow recirculation zone is absent in the model results. However, for both applies that this is most likely caused by the river geometry (notch in bank and scour hole) and not the bi-directional flow conditions. Less likely but still possible is that the turbulence settings of the Delft3D model are responsible for this.

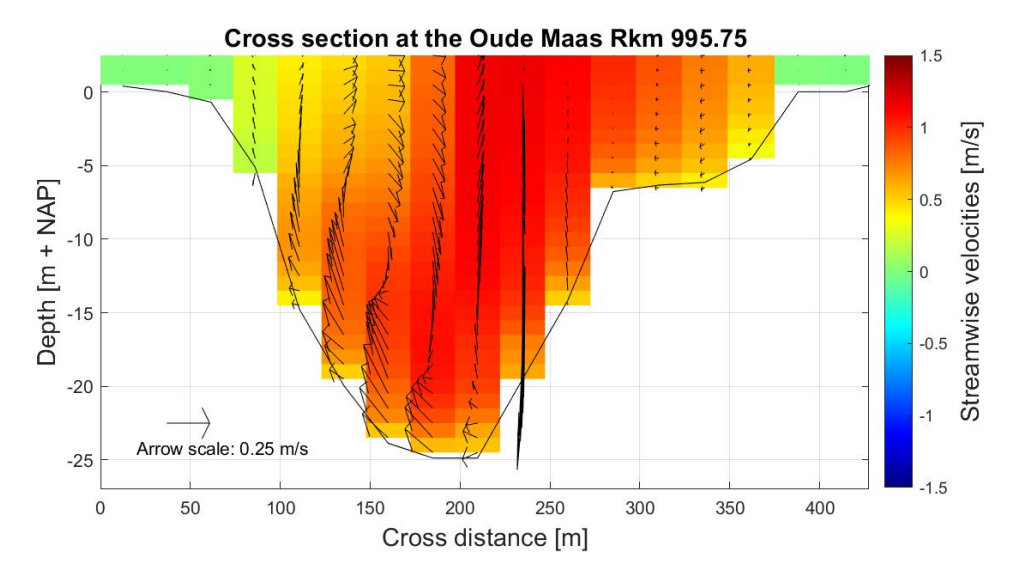


Figure 4.7: Secondary flow pattern during peak ebb flow (time step = 359). The velocity vectors show the cross-stream and vertical velocities.

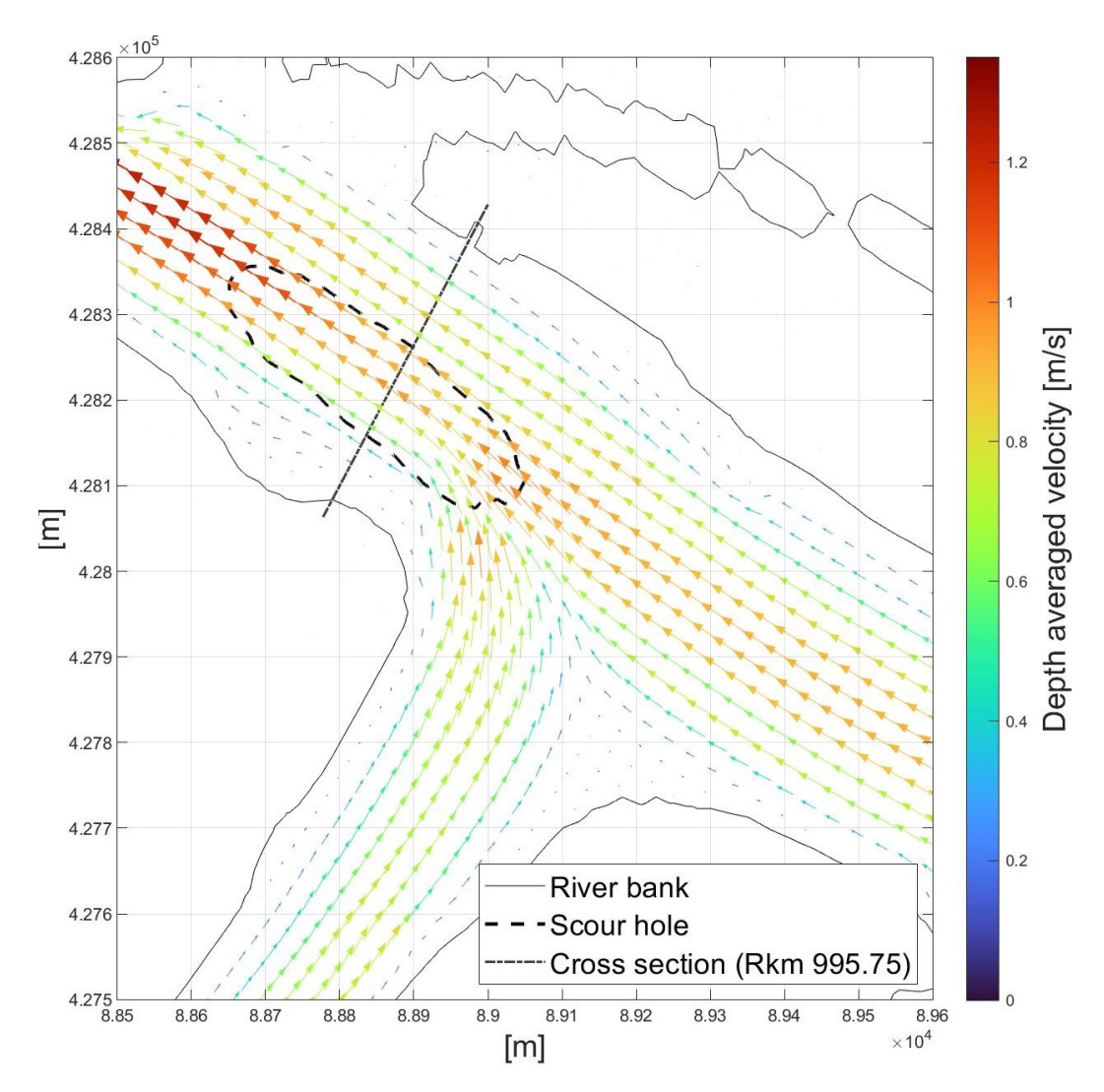


Figure 4.8: Depth averaged velocities during peak ebb flow (time step = 359).

Scenario 2, flow changing from ebb to flood

Figure 4.9 shows the depth averaged velocities at the moment the flow is changing from ebb to flood. Since the velocities are much smaller than in the peak ebb flow scenario, the velocities are plotted with a different scale for better visualization. What can observed is that the flow in the center of the Oude Maas and above the scour hole is still seaward directed, while on the sides the flow is land inwards directed. This shows that no slack conditions exist at this confluence which is eventually caused by the rivers geometry. Due to the different shaped banks and the presence of the scour hole, the flow is not uniform over the entire Oude Maas. As shown in the first scenario, the flow is much larger in the center than on the sides leading to a slower change of the flow direction here. As a result, the flow is able to change much more earlier in the entire Spui than in the Oude Maas. According to literature, horizontal reciruclation zones would be expected at the Spui. However, none of these features can be observed in the figure below.

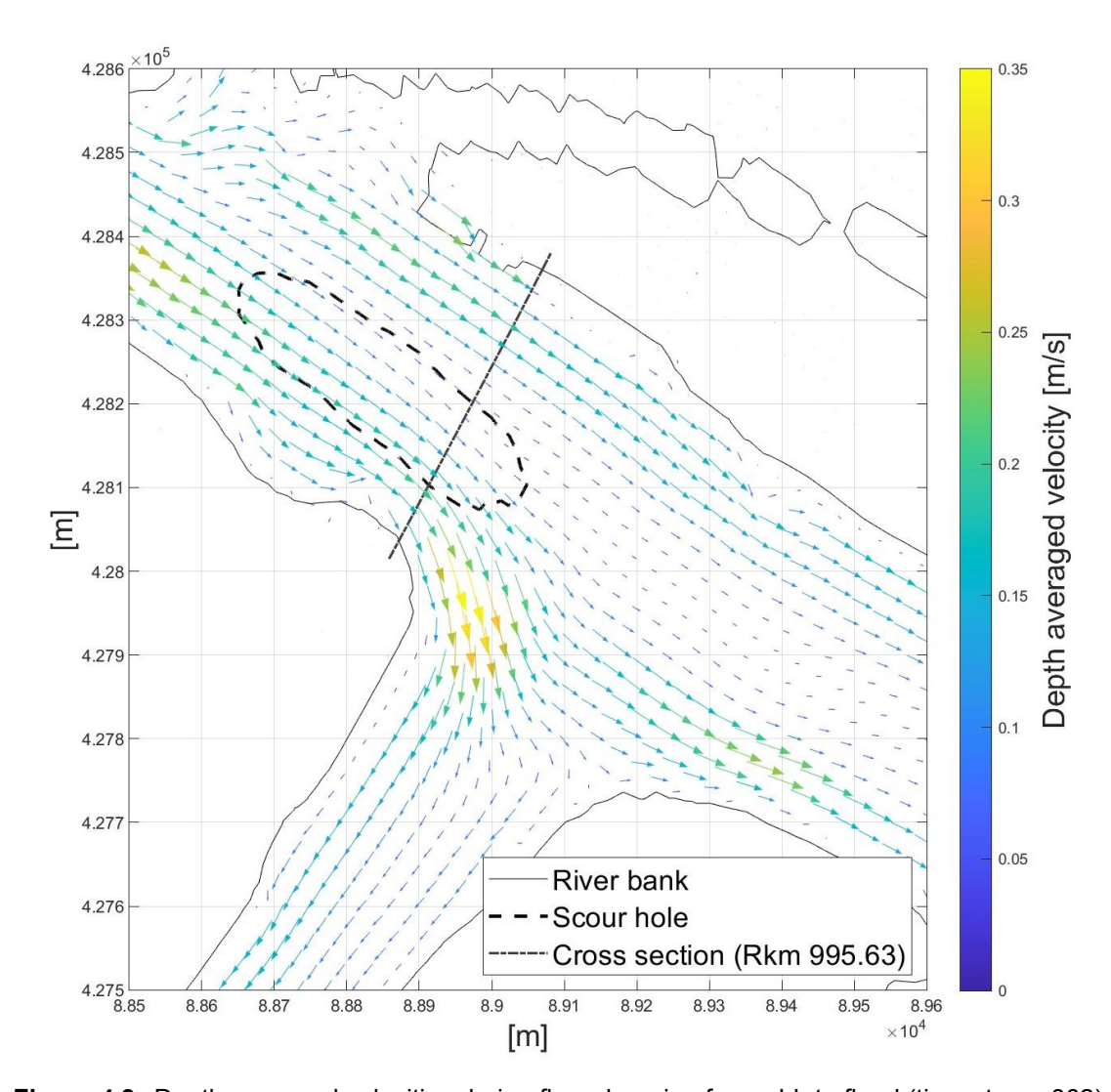


Figure 4.9: Depth averaged velocities during flow changing from ebb to flood (time step = 362).

Scenario 3, peak flood flow

What can be observed in figure 4.10 is that during peak flood flow the system behaves as a bifurcation. The flow is being split over the tributaries Oude Maas and Spui with the largest part of the flow staying in the Oude Maas. The largest flow velocities are found on the same location as during peak ebb flow, but now the flow enters the scour hole here. The largest velocities are not necessarily found when the flow enters or leaves the scour hole but are dependent on the flow area and hence the confluence/bifurcation. If the flow leaves the scour hole, the largest flow velocities are found in the direction of the Oude Maas, not in the trench towards the Spui.

What also can be observed is that the flow velocities inside the scour hole are again not evenly distributed over the width of the hole. This suggests that the flow is divided into two different streams. Looking at figure 4.11, it can indeed be seen that the cross-stream flow components are directed towards the Spui dividing the flow into the two tributaries. According to literature, a horizontal recirculation zone would be expected inside the Spui. However such feature can not be seen there in figure 4.10. A very small flow recirculation zone is observed at the downstream corner of the confluence/bifurcation, which is not expected here. Most likely this is caused by the geometry of the river. The flow is already being pulled into the direction of the Spui, but ends up in the notch of the river bank forming this recirculation zone.

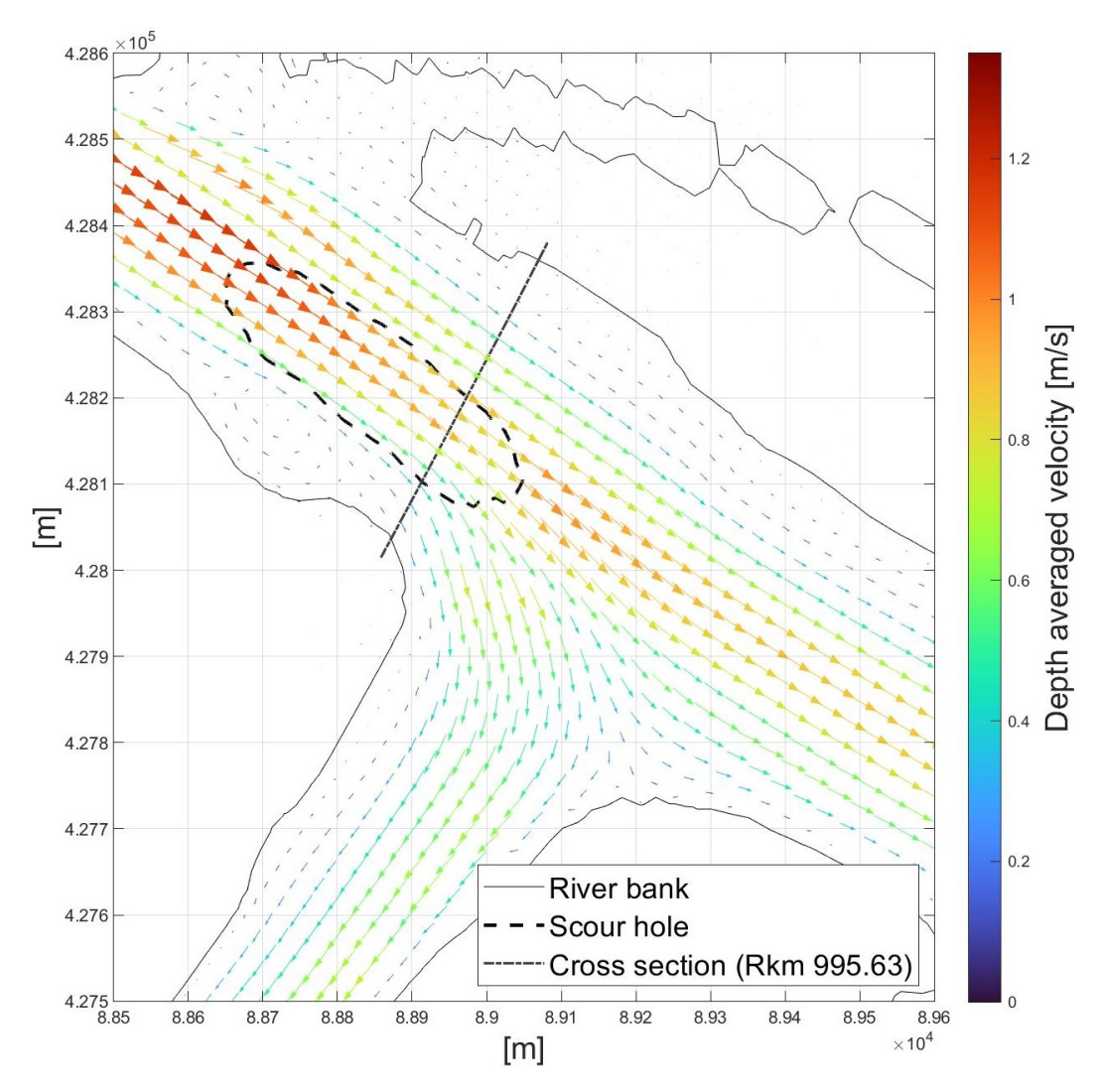


Figure 4.10: Depth averaged velocities during peak flood flow (time step = 363).

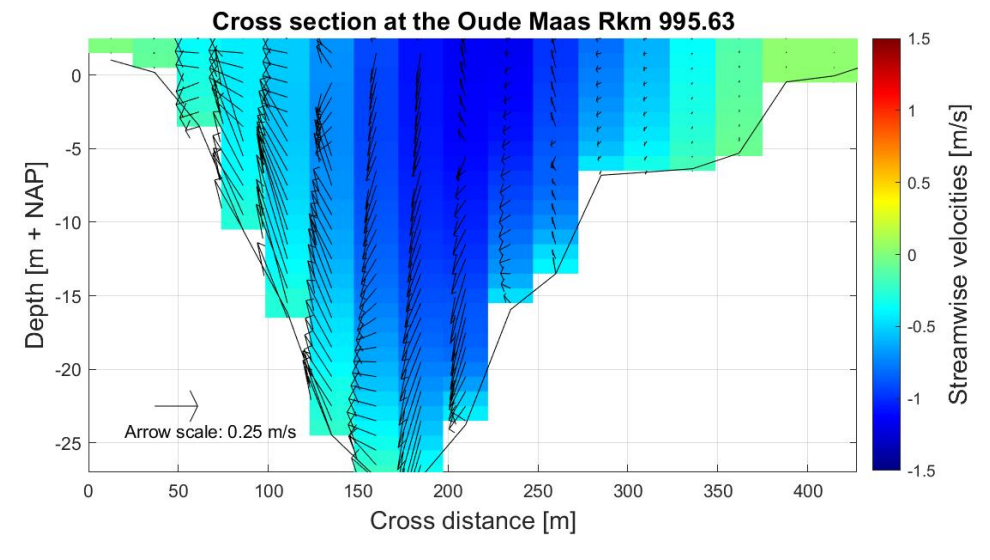


Figure 4.11: Cross-section at Rkm 995.63 during peak flood flow (time step = 363). The velocity vectors show the cross-stream and vertical velocities.

Scenario 4, flow changing from flood to ebb

figure 4.12 shows the depth averaged velocities if the flow is changing from flood to ebb. Again, the scale on which the depth averaged velocities are shown, is much smaller than during peak flood and ebb flow. The flow behaves similar as the flow changing from ebb to flood (scenario 2) but in the opposite direction. Similarly, the largest flow velocities are found on the sides of the Oude Maas and the smallest in the center. The flow in the Spui already changed direction and mixes with the flow of the Oude Maas, on the left side of the scour hole. Again no horizontal vortexes or recirculation zones are observed. Good to mention is that the system is moving towards the ebb scenario, meaning it will eventually behave as a confluence with the six identified flow zones. The flow stagnation zone and recirculation zones have not yet developed here. The flow is still in major transition towards the confluence case observed at peak ebb flow.

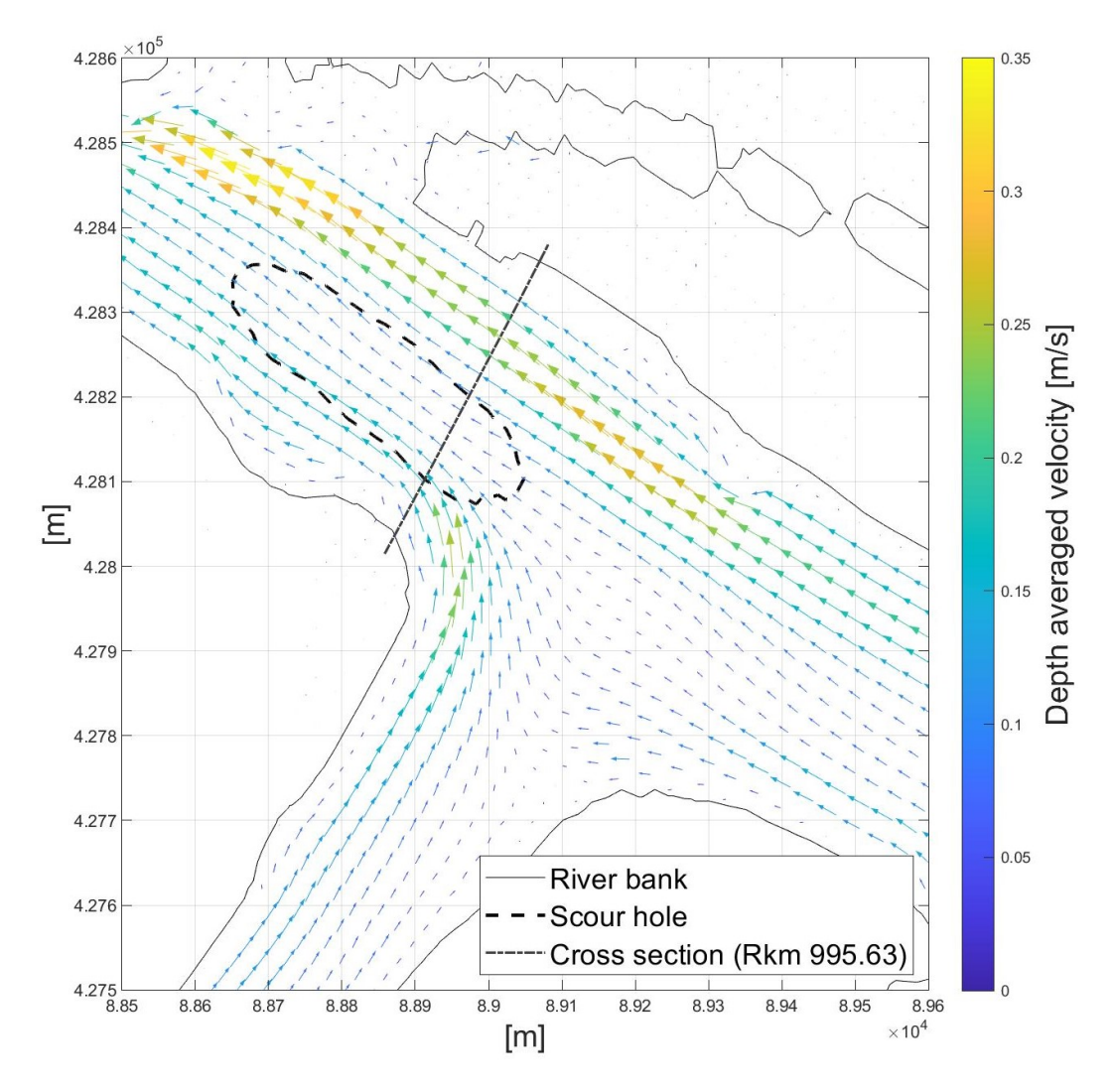


Figure 4.12: Depth averaged velocities during flow changing from flood to ebb (time step = 358).

Verification with ADCP measurements

Not all findings within the two peak scenarios can be verified since the ADCP measurements are taken on only at a few transect at the Oude Maas. For example, it does not show the velocities in the Spui. As a result, no confirmation can be given on, for example, the system behaving as either a confluence during ebb or a bifurcation by flood. Also the confirmation of the presence of different flow zones is not possible. What can be done is looking at the shear layer and the distribution of the flow velocities over the scour hole.

Figure 4.13 shows the velocities at peak ebb flow measured by the ADCP device in cross-section 2 (see figure 4.15). The results of the Delft3D model have shown the system behaves as a confluence during peak ebb flow, containing a shear layer characterized by recirculation cells. Such characteristics are not observed in the ADCP measurement. As described in section 2.3.2, processing of the ADCP measurements assumes that flow between the beams is homogeneous. This could have filtered out these characteristics. Nevertheless, the ADCP measurement do not show a slight hint of such a recirculation cell. Making it a question if these recirculation cells are present in the field. The model has also shown that the distribution of flow velocities over the width of the scour hole is uneven. The largest flow velocities are found on the right side of the scour and the smallest of the left. This is seen for both the peak ebb and flood velocities and is caused by the splitting and joining of the flow in the Oude Maas and the Spui. The ADCP measurements in figure 4.14 confirm this. There is indeed seen that the velocities are unequal distributed over the width of the channel and that the largest velocities are found on the right side in both the ebb and flood scenario. The ADCP flood measurement in figure 4.14b shows that the velocities on the left side of the scour hole are still positive during flood flow, something that was not observed in the model results.

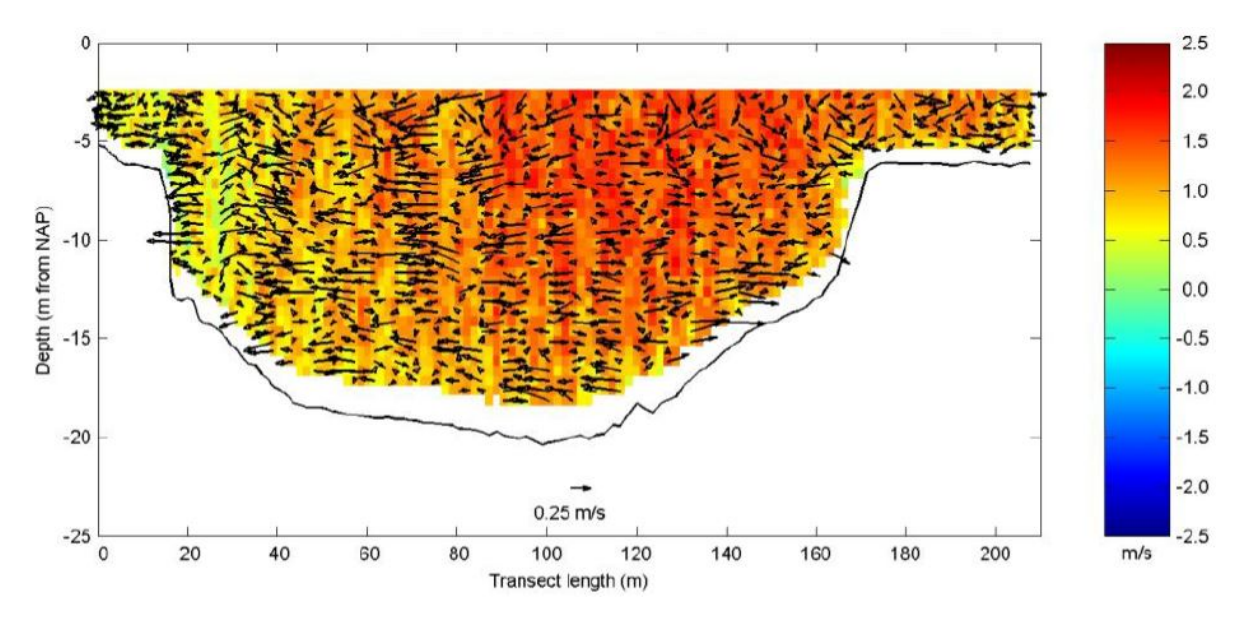
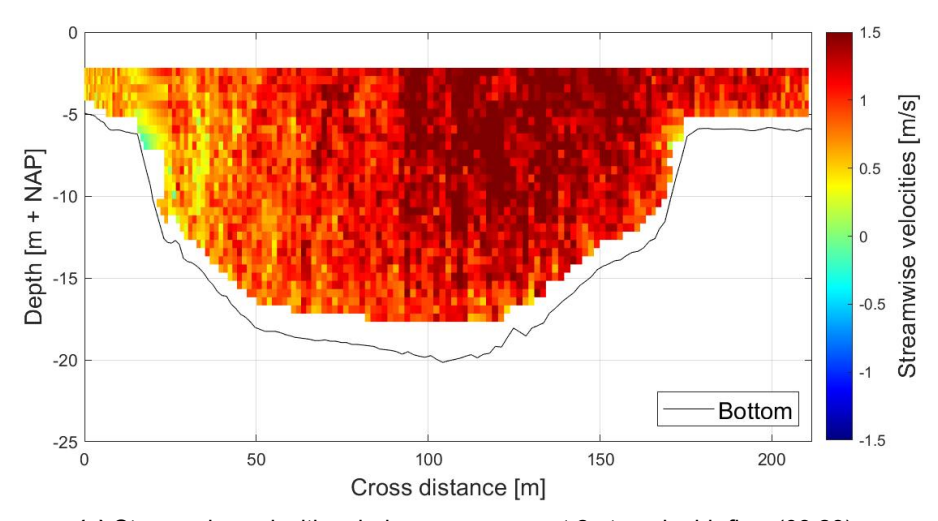
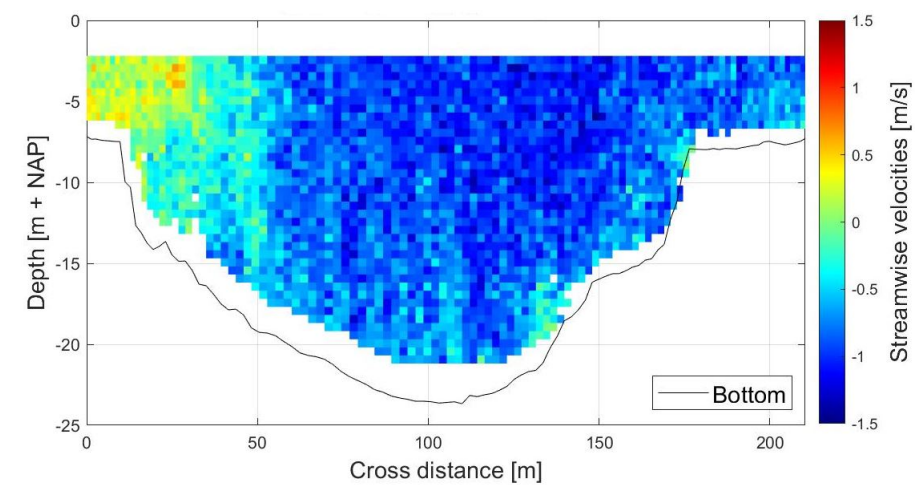


Figure 4.13: ADCP measurement 2 at Rkm 995.9 during ebb (08:28). The velocity vectors represent the cross stream and vertical velocities.



(a) Streamwise velocities during measurement 2 at peak ebb flow (08:28).



(b) Streamwise velocities during measurement 6 at peak flood flow (15:05).

Figure 4.14: ADCP measurements taken around cross-section Rkm 995.8 on 11 February 2021.

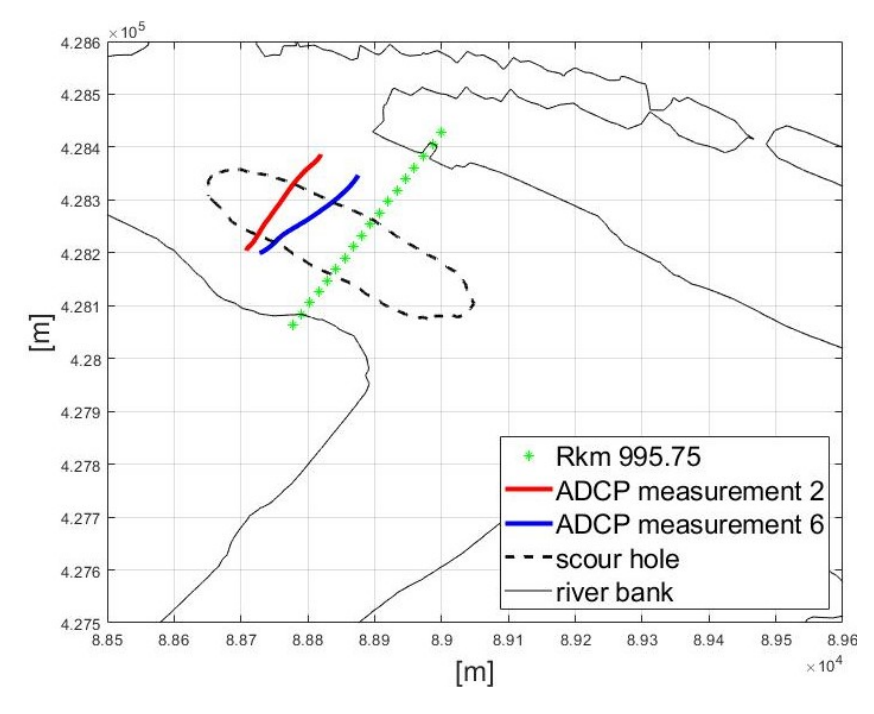


Figure 4.15: Location of the ADCP measurements 2 and 6 taken during ebb and flood.

4.2.2. Case 2: different conditions

In this section the model results for the four scenarios with different water levels and discharges will be analyzed, to see how this affects the shaping of the flow field during a tidal cycle.

Model time steps and conditions

A different period within the time frame of the model is selected, which has different surface elevations and hence discharges. The new period is from 21 September 2018 11:00 until 22 September 11:00. In figure 4.16 can be seen how the water levels during case 2 differ with the base case and the field conditions on 11 February 2021, when the ADCP measurement were taken. Table 4.2 shows which time steps of this new period will be used for each scenario and what their matching dates are. Table 4.3

compares the discharges of case 2 with the base case. It shows that there are lower discharges during ebb flow and larger discharges land inwards during flood flow.

	Scenarios	Time step model	Date	Time
1.	ebb	1198	21 September 2018	20:00
2.	$ebb \to flood$	1200	22 September 2018	00:00
3.	flood	1202	22 September 2018	04:00
4.	$flood \to ebb$	1197	21 September 2018	18:00

Table 4.2: Overview of model time steps for scenarios case 2.

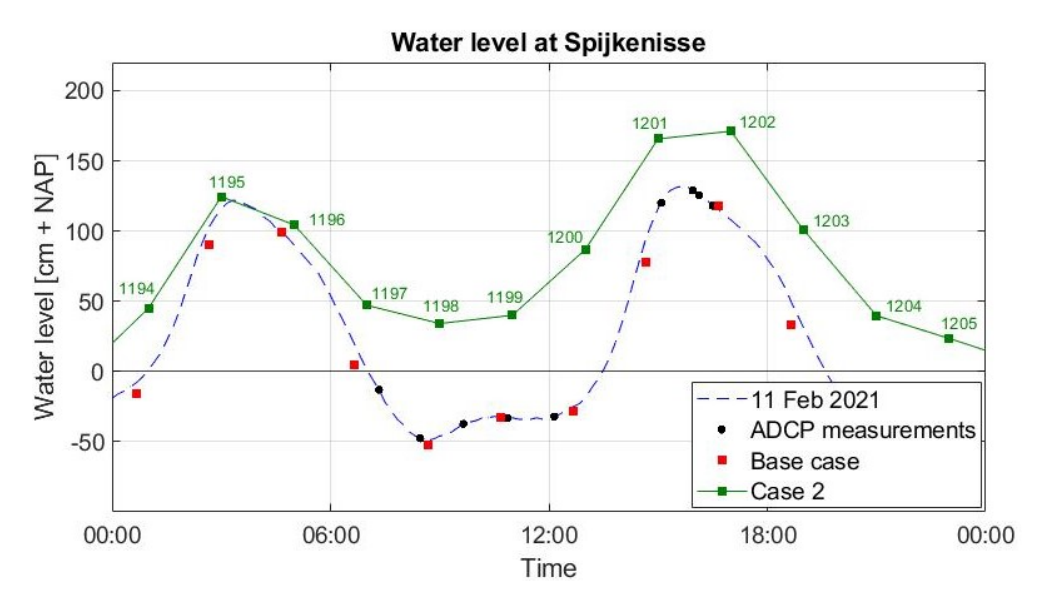


Figure 4.16: Water levels at Spijkenisse measured by Rijkswaterstaat and computed in the model.

	Time step	Discharge	Time step	Discharge
	base case	base case	case 2	case 2
ebb	359	4047.0 m ³ /s	1198	2443.3 m ³ /s
flood	363	$-3740.7 \text{ m}^3/\text{s}$	1202	$-4318.9 \text{ m}^3/\text{s}$

Table 4.3: Comparison of discharges during peak ebb and peak flood flow at Rkm 995.9.

Results

Scenario 1, peak ebb flow

As shown in table 4.3, the discharges during peak ebb flow are much lower in the second case. This results into lower velocities as can be seen in figure 4.17. The depth averaged velocities are much more uniform than in the base case. No larger velocity zone in the center of the Oude Maas can be observed. Despite, the flow still behaves as a confluence. This questions again if the six flow zones are present. A flow stagnation zone at the upstream corner of the confluence is seen. The flow of the Spui deflects and joins the Oude Maas, confirming the presence of the deflection zone. Again here no horizontal flow recirculation is observed. Figure 4.18 shows the presence of secondary flow patterns. Similarly as in the base case, one recirculation cell can be observed downstream of the confluence. Remarkable for this case is the counter-clockwise rotation of the vertical recirculation cell on the left side of the channel.

Normally a clockwise recirculation would be expected at the left side of the channel, as was seen in the base case. This observation will be included during the investigation of the secondary flow patterns in the next section. Despite, the model results indicate no presence of a shear layer downstream of the confluence. A large velocity zone could also not be identified. Overall it can be concluded that the flow field during peak ebb flow has the similar characteristics as the base case. It only has lower velocities, causing less developed and distinguishable flow zones during the peak ebb flow scenario.

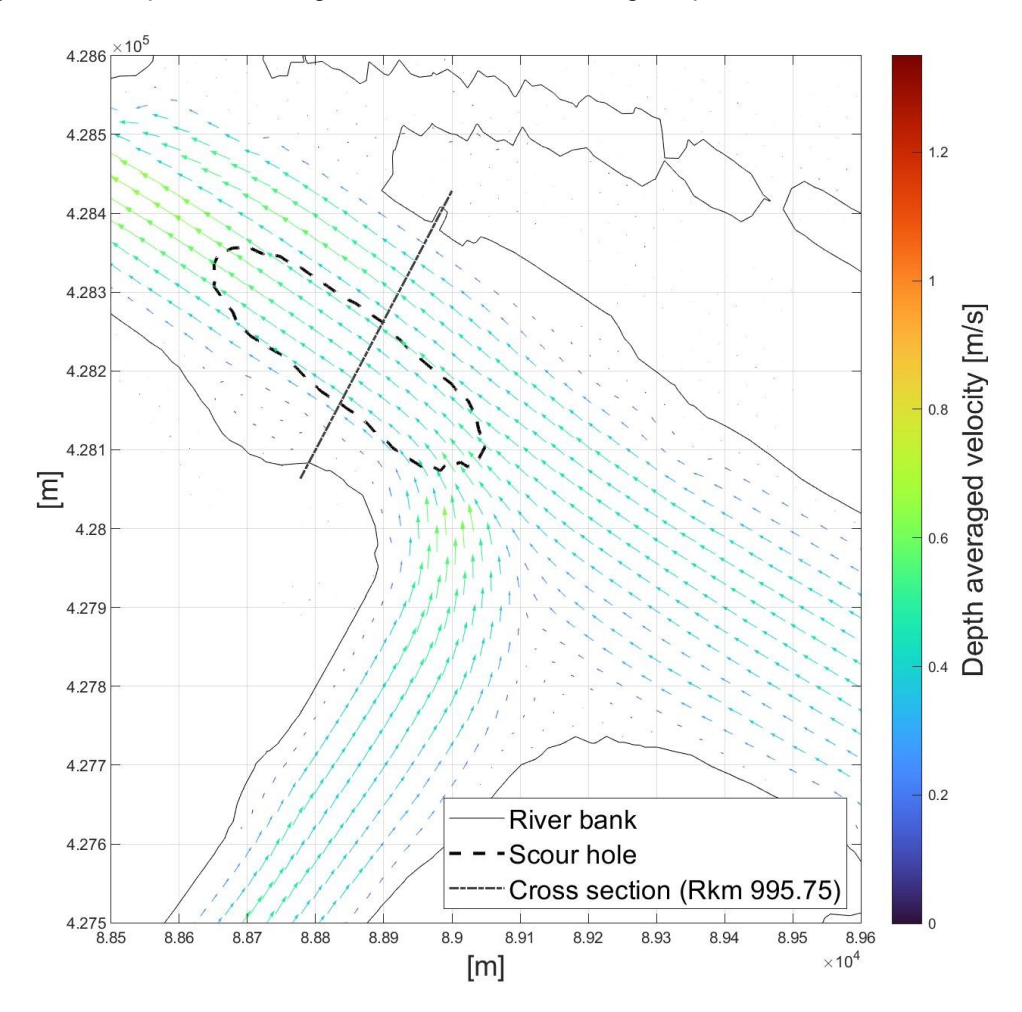


Figure 4.17: Depth averaged velocities at peak ebb flow (time step = 1198).

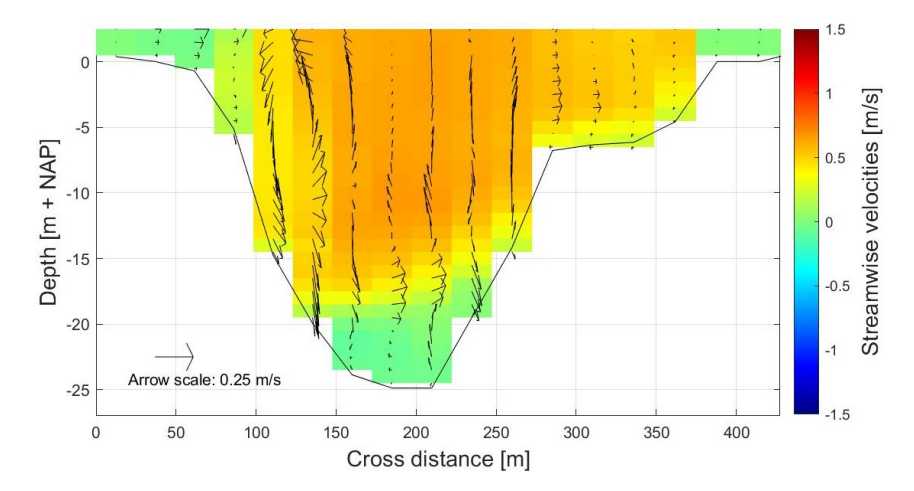


Figure 4.18: Secondary flow pattern in cross-section at Rkm 995.75 (time step = 1198).

Scenario 2, flow changing from ebb to flood

Again here a smaller scale is used to visualize the flow velocities at the moment it changes direction. Figure 4.19 shows the depth averaged velocities at this scenario. Some horizontal recirculation zones can be observed at both the upstream corner of the confluence/bifurcation and the notch in the river bank on the downstream corner, which were not present during the base case. The flow in the center of the Oude Maas is still moving sea wards while the tide is already forcing the flow above the scour hole and in the Spui in the other direction. These different directed flows in combination with the geometry of the river, are responsible for the formation of these horizontal recirculation zones. Furthermore, it appears that the flow is in a much earlier stage of transition than the flow field found in the same scenario of the base case. At the base case it was found that the center velocities in the Oude Maas were close to zero and the velocities on the sides of the channel had already changed direction land inwards. In this second case none of the flow has completely changed its direction. It still has the same seawards direction as during ebb flow or the velocities are close to zero. This explains why characteristics observed here, were not all seen in the base case.

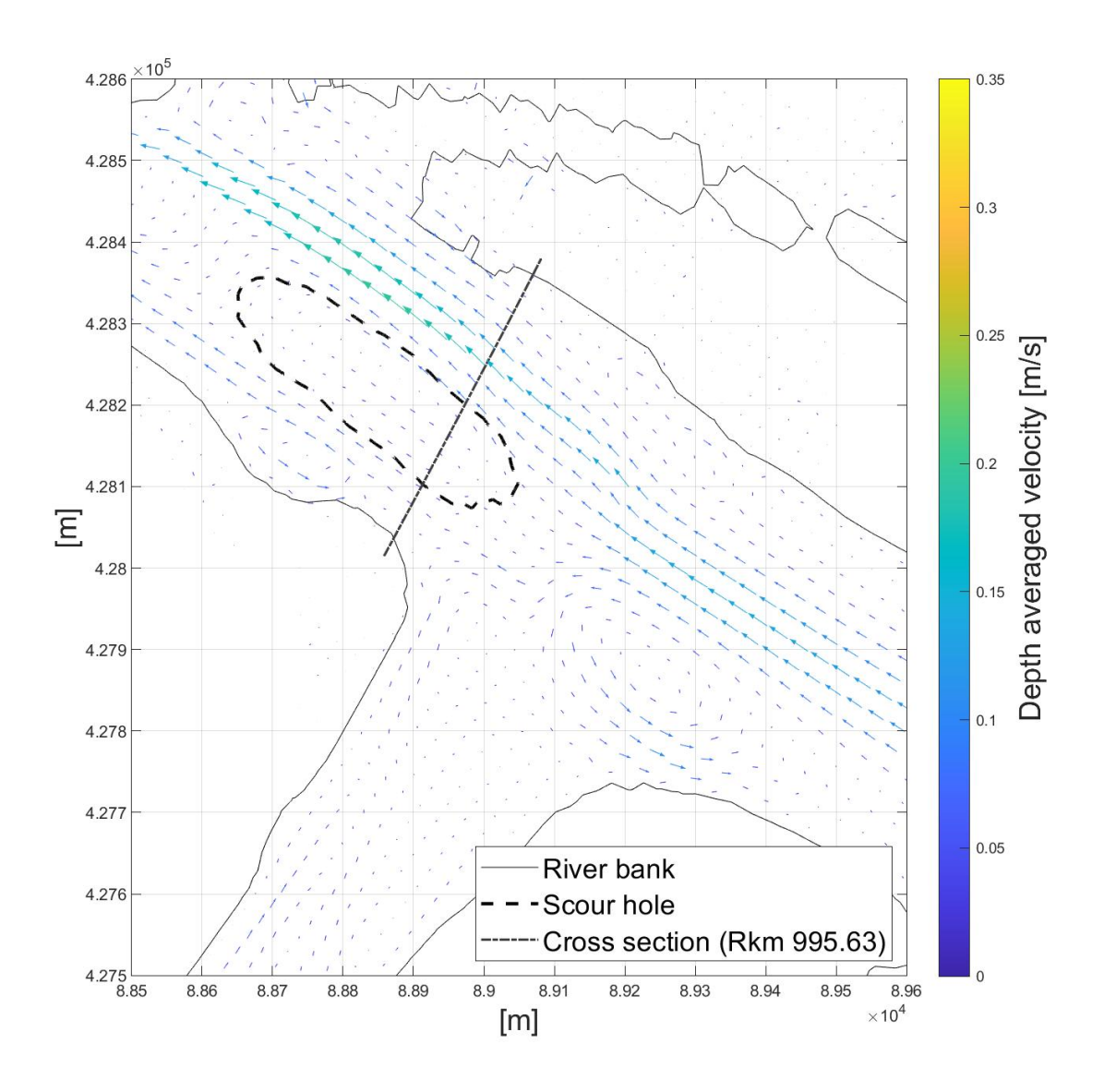


Figure 4.19: Depth averaged velocities at flow changing from ebb to flood (time step = 1200).

Scenario 3, peak flood flow

During flood flow larger discharges are present leading to larger depth averaged flow velocities in case two than in the base case, as can be seen in figure 4.20. Nevertheless, the system still behaves as a bifurcation with again the largest amount of the flow staying in the Oude Maas. What can be seen better, is the presence of an acceleration zone when the flow enters the Spui. Similarly as during the base case, the flow velocities are unequally distributed over the width of the scour hole. The largest flow velocities are still found on the same spot as during peak ebb flow, before the flow enters the scour hole. Not seen is the horizontal flow recirculation zone in the notch of the river bank.

Due to the larger velocities directed into the Spui during the second case, the flow seems to attack the upstream corner of the confluence. During the base case the flow follows the geometry of the river bank better and does not directly attack it. This case shows however an attack of the river bank here. Erosive patterns at this junction can thus be explained by these larger velocities, occurring not during every tidal cycle.

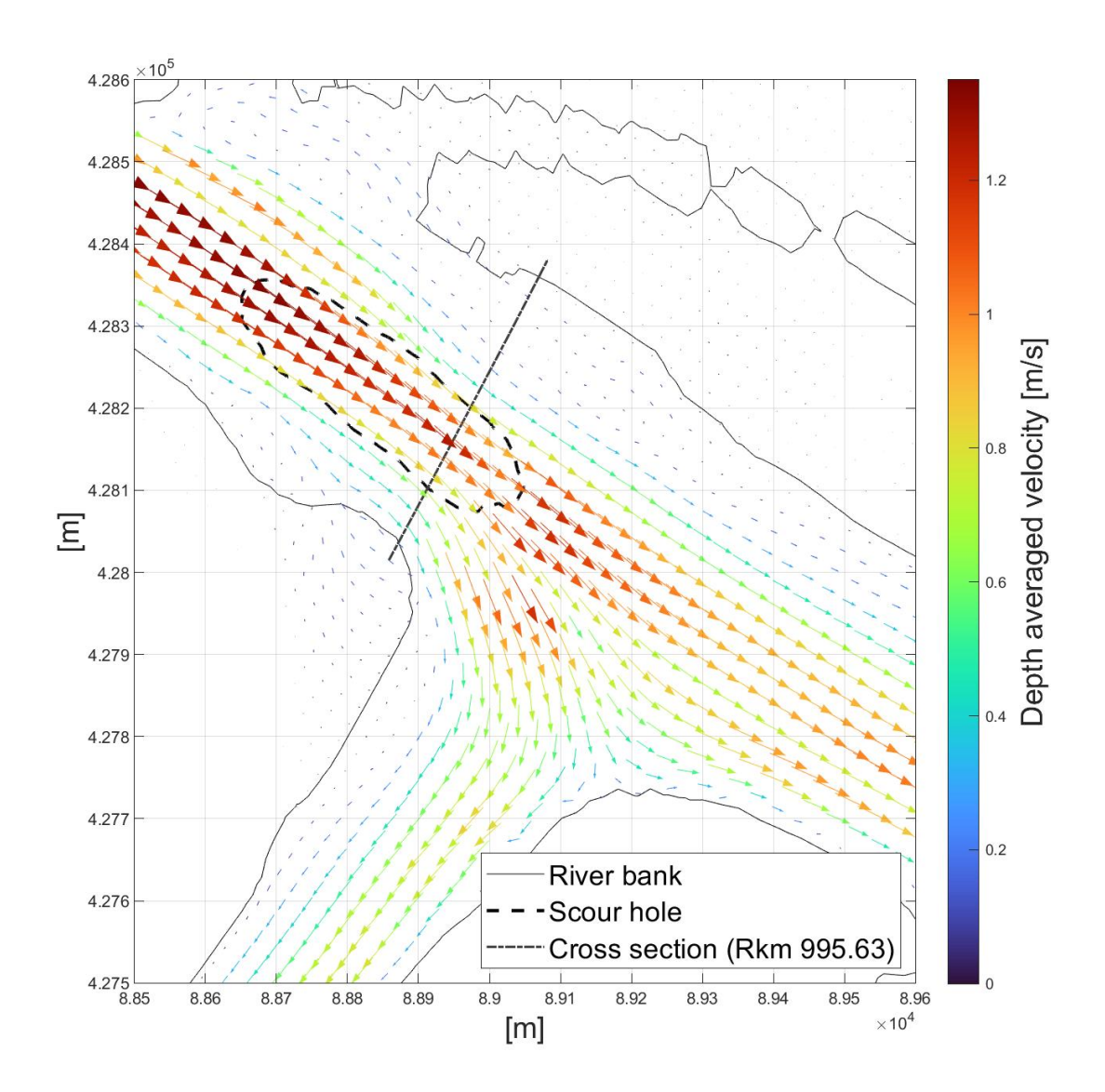


Figure 4.20: Depth averaged velocities at peak flood flow (time step = 1202).

Scenario 4, flow changing from flood to ebb

Figure 4.21 shows the depth averaged velocities when the flow is changing the flood to ebb. These again contain a smaller scale to better visualize them. Just as in scenario 2 of the second case, the flow is a much earlier phase of transition than the same scenario of the base case. The tidal influence is becoming less and the river discharge gets a better handle on forcing the flow direction. This leads to different flows with different intensity and direction resulting eventually in the formation of the large horizontal recirculation cell at the entrance of the Spui. This characteristics was not observed in the base case.

This scenario confirms that no slack conditions exist at bi-directional confluences. Due to the different streams with varying flow intensity and direction, no moment exists at which slack water is found at the entire confluence/bifurcation. This was similar for both this case and the base case.

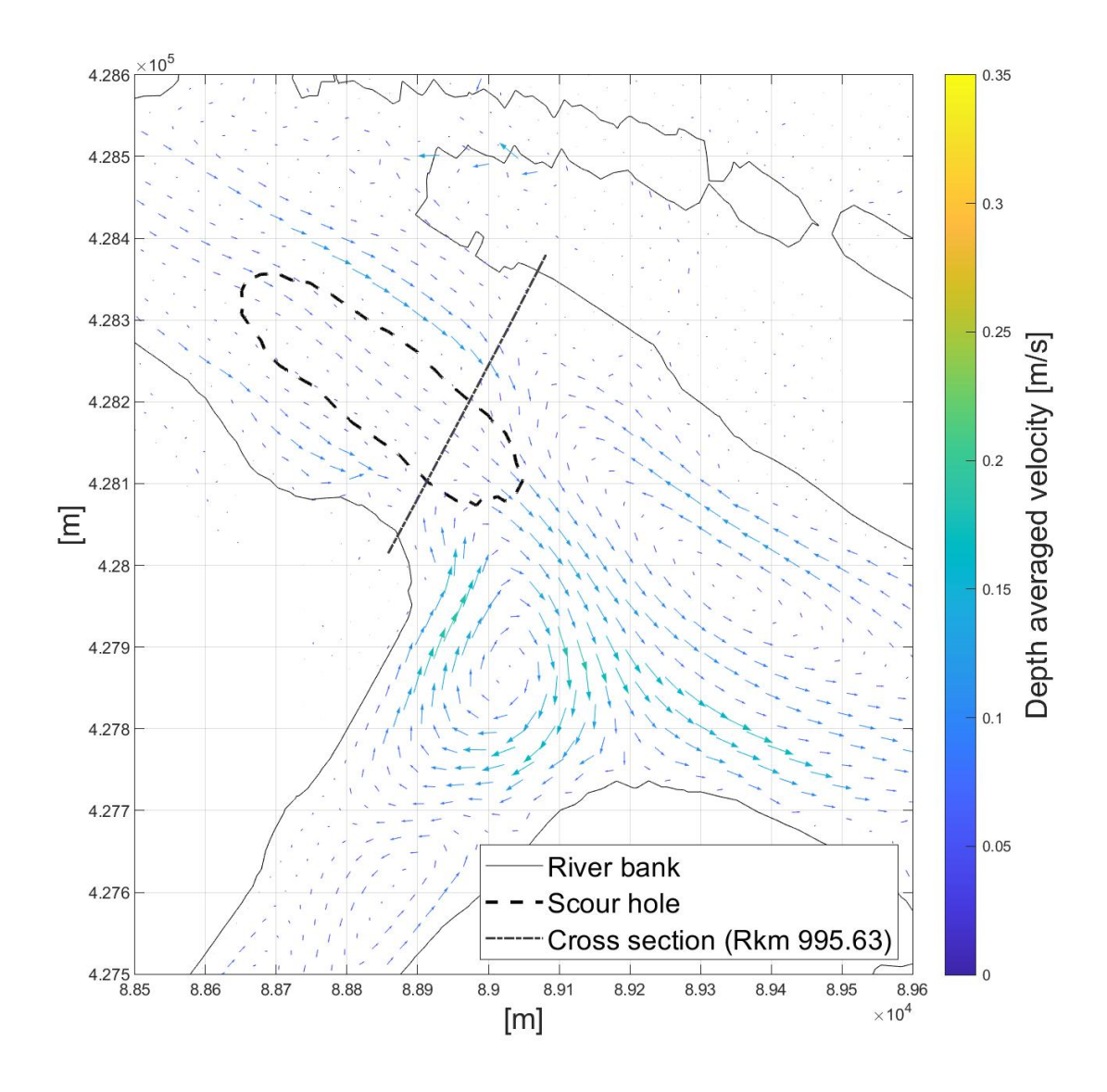


Figure 4.21: Depth averaged velocities at flow changing from flood to ebb (time step = 1197).

4.2.3. Secondary flow patterns during ebb flow

Secondary flow patterns were encountered during the peak ebb flows in both cases, when the system behaved as a confluence. However, the rotation direction of the secondary flow patterns was different, which questions what is happening here. A thorough analysis of the secondary flow patterns is performed in appendix F. It was found that the secondary flow can be shaped in three characteristic patterns inside of the scour hole Beerenplaat. Before these are explained an expectation is given, of how the secondary flow should be shaped if the system behaves as a confluence. This expectation is based on the literature findings described in section 2.2.5. Unfortunately, no literature could be found on secondary flow at confluences that contain a scour hole. Therefore this expectations is given, while neglecting the presence of the scour hole Beerenplaat. Figure 4.22 shows the expected secondary flow patterns at the confluence Oude Maas and Spui. Two vertical recirculation cells would develop, each in one part of the joining flows. The recirculation cell in the flow of the Spui is the largest and rotates in the clockwise direction. The other cell is smaller, located in the flow of the Oude Maas and rotates in counter-clockwise direction. Both cells should shrink in size in the streamwise direction.

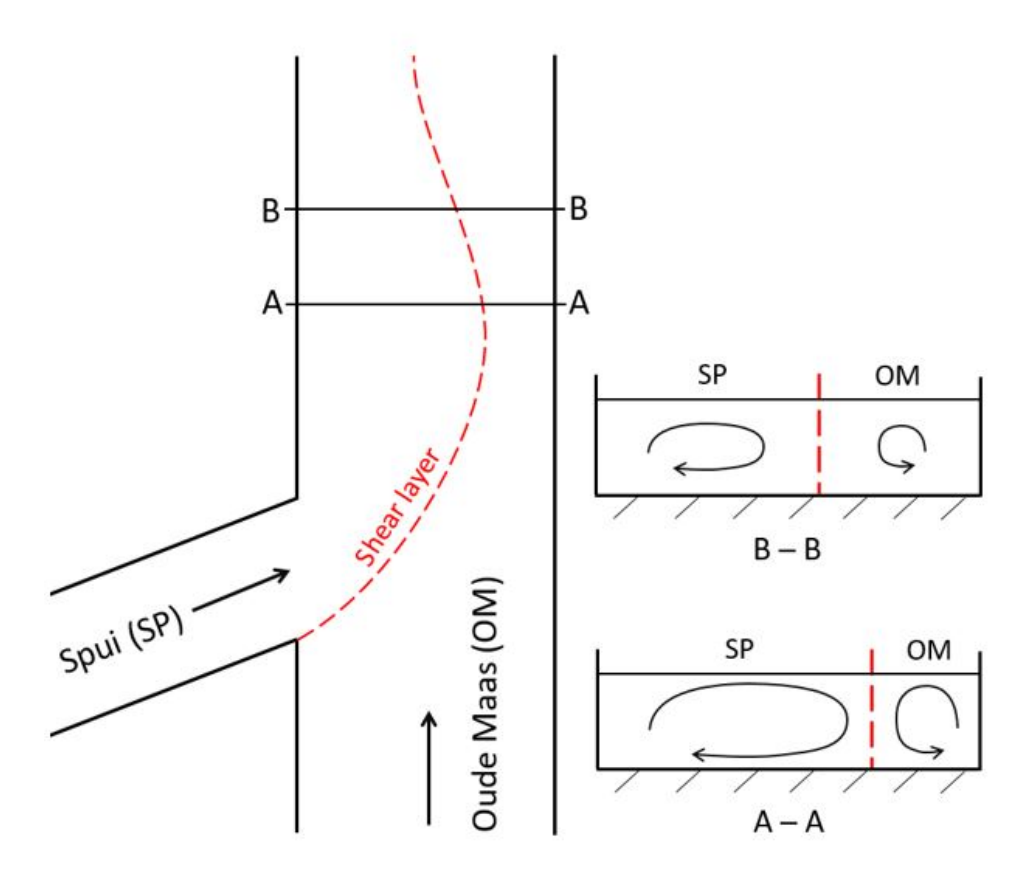


Figure 4.22: Expected secondary flow process if no scour hole is present.

The three characteristic patterns identified out of the Delft3D model results in appendix F are shaped completely different and show no resembles with this expectation. The main features of each of these three patterns is described in table 4.4. All patterns contain only one vertical recirculation cell that is located within the joined flow from the Spui. Dependent on the characteristic pattern, it can rotate clockwise or counter-clockwise. It is hypothesised that the slopes of the scour hole are responsible for the development of only one recirculating cell. According to literature, the secondary flow patterns starts developing in the deflecting flow of the Spui. If the clockwise recirculation hits the river bottom it follows the slope of the scour hole instead of hitting a flat bed (see figure 4.23). Hence only on recirculation cell forms. As a result it is expected that no shear layer exists downstream of the confluence, since there are no counter rotating flows. Despite, some shear is still expected at the confluence itself

where the two flows are mixing. Unfortunately, this hypothesis could not be confirmed since no model results with a flat river bed are available. It was not yet possible to construct a hypothesis that explains why the recirculating cell can migrate, rotate counter-clockwise or even grows in size. Potentially the field conditions give more insight in these phenomena. Therefore it was investigated when the three characteristic patterns are present.

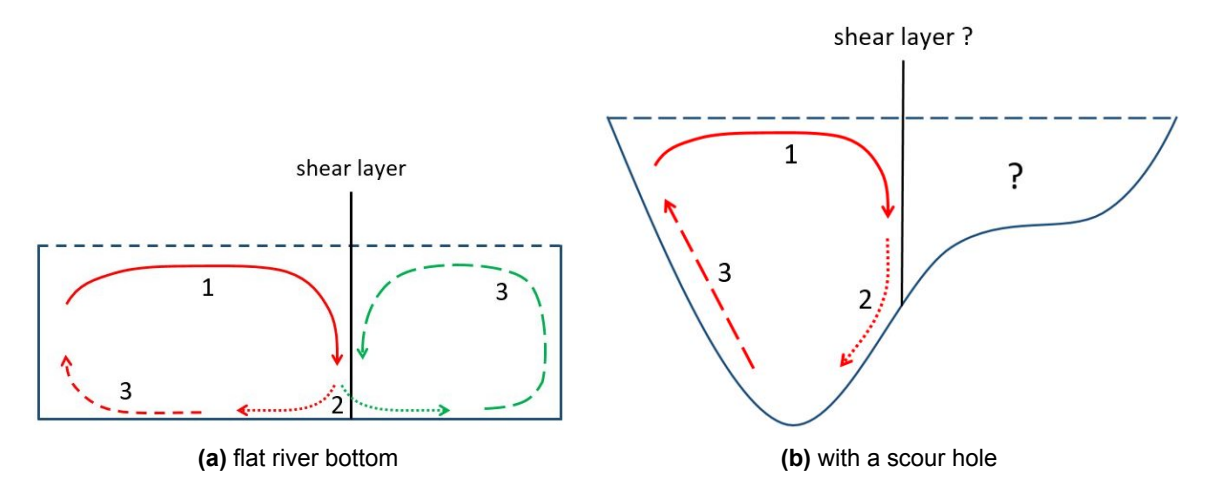


Figure 4.23: Schematization of the development of recirculation cells for a flat river bottom and one with a scour hole. The numbers represent the order in which the recirculation cell develops.

	amount of cells	location	rotation direction	development in streamwise direction
expectation literature	two	one in flow SP one in flow OM	clockwise counter-clockwise	shrinks shrinks
characteristic pattern 1	one	in flow SP	clockwise	shrinks fast
characteristic pattern 2	one	migrates in flow SP	clockwise	shrinks slowly
characteristic pattern 3	one	in flow SP	counter-clockwise	grows

Table 4.4: Features of the expected secondary flow patterns based on literature and the three characteristic shaped secondary flow patterns identified out of the Delft3D model.

In appendix F.2 the ebb flow of 50 tidal cycles within the Delft3D model is analyzed. Convincing evidence was found that the secondary flow during ebb flow, in all 50 tidal cycles, is shaped according to the following mechanism. It first takes the shape of characteristic pattern two and than reshapes to characteristic pattern one, all within the same tidal cycle. The characteristic pattern three was not encountered in the analysis. It was only observed once in the entire time frame of the model at time step 1198 (case 2 with the different field conditions). Unique for this time step were the high water levels. Appendix F.2 hypothesises that a water level threshold is present somewhere between 28.1 cm + NAP and 34.1 cm + NAP at Spijkenisse, which should be exceeded before the secondary flow takes

the shape of characteristic pattern three. Unfortunately, it remains uncertain if the secondary flow in the field behaves similarly since no kind of recirculation could be observed in the ADCP measurements.

Despite understanding when each of the characteristic patterns is present, no explanation could be found that shows why the secondary flow patterns can migrate, rotate counter-clockwise or even grow in size. The only difference encountered in the literature and the confluence/bifurcation Oude Maas and Spui, is the of presence the scour hole Beerenplaat. Therefore it is assumed that this is responsible for the unexpected behavior of the secondary flow patterns. One other possibility exists. The secondary flow patterns in the Delft3D model results can be affected by the chosen turbulence model and values for eddy viscosity, as was explained in section 4.1.1. Unfortunately it is not possible to verify this since no model output with different settings exists.

4.2.4. Conclusion on sub research question 2

The section 4.2 has focused on answering the question "How is the flow field at the confluence/bifurcation Oude Maas & Spui shaped during a tidal cycle?". This question has been answered by using the results of a Delft3D model and ADCP measurements. The model has been analyzed for two different cases. The base case had the most similar field conditions (water surface elevation and discharges) as found during the ADCP measurements. The second case had different forcing conditions to see how these influence the model results. On top of that, more investigation towards the secondary flow patterns during ebb flow was done. Below the characteristics of the flow field at the confluence/bifurcation Oude Maas and Spui are listed for peak ebb flow, peak flood flow and the moment the flow changes from flood to ebb or the other way around.

Peak ebb flow

- The system behaves as a confluence. The flow of both the Oude Maas and the Spui joins above and in the scour hole Beerenplaat.
- Four of the flow zones of a uni-directional confluence also occur at the bi-directional confluence
 Oude Maas and Spui. These are the stagnation zone, deflection zone, maximum velocity zone
 and the flow recovery zone. The horizontal flow recirculation zone is not seen. The presence
 of the shear layer is still questionable since no counteracting recirculating cells are observed.
 Despite, two flows with different velocities are running next to each other, which will lead to some
 shear.
- Secondary flow patterns develop downstream of the confluence Oude Maas and Spui. These
 patterns are present inside the scour hole and can take three characteristic shapes, that all contain only one vertical recirculation cell. These characteristic patterns differ quite a lot with what
 expectations based on literature. Most likely is caused by the presence of the scour hole. If
 these secondary flow patterns are similarly present in the field is still questionable since no flow
 recirculation was observed in the ADCP measurements.
- The flow is unequally distributed over the width of the tributaries, with larger velocities in the center and smaller velocities on the sides. However, this is dependent on the discharge. It was shown that a lower discharge leads to more uniform distributed flow velocities.
- The largest flow velocities occur downstream of the scour hole Beerenplaat, when the flow leaves the scour hole.
- Different forcing conditions will not lead to new flow features seen during peak ebb flow, it only affects the magnitude in which the current features appear.

Peak flood flow

- The system behaves as a bifurcation, meaning the flow is split over the Oude Maas and the Spui.
- The largest velocities are found on the same location as during peak ebb flow. In this scenario the flow enters the scour hole Beerenplaat here.

- The flow is unequally distributed over the width of the tributaries with also the largest velocities in the center and the smaller velocities on the sides. The larger flood discharges in the second case have not changed this.
- No large velocity zone is seen at the upstream edge of the scour hole Beerenplaat, in the direction of the Spui.
- Different forcing conditions will not lead to new flow features seen during peak flood flow, it only affects the magnitude in which the current features appear.

Flow changing from flood to ebb or the other way around

- The moment the flow direction switches is spatially varying at the confluence/bifurcation Oude Maas and Spui. As a result, flows with different direction and magnitude can easily form horizontal recirculation zones with low velocities. These zones disappear again if the system transitions towards peak ebb or flood flow.
- · No slack water conditions exist.
- The moment the flow direction has changed at the entire system is dependent on the tidal forcing
 and the river discharge. These both behave on different time scales, meaning the system never
 reaches a long term equilibrium. It is always varying and adapting to the new conditions. Consequently, the moment the flow direction changes during the tidal cycle is continuously changing.

4.3. 3D flow processes

This section focuses on answering the third sub research question: "Which of the 3D flow processes are present inside the scour hole Beerenplaat and what is the influence of the flow direction and intensity on them?". The expected 3D flow processes at a scour hole are a (curved) recirculation zone, flow contraction and a horseshoe vortex, as was explained in section 2.2.3.

It is intended to answer this question with both the Delft3D model and the ADCP measurements taken 11 February 2021, which were described in section 4.1. However, it is uncertain if both of these methods are suitable to show all 3D flow processes, due to their limitations. The Delft3D model can only simulate the larger turbulent scales and is not able to simulate the smaller scale turbulent fluctuations, which are paired with the horseshoe vortex and probably the recirculation zone. For the ADCP measurements an assumption is made that flow in between the four beams is homogeneous, which can filter out turbulent structures in the flow. On top of that, the ADCP device can not measure the flow velocities very close to the river bottom. Due to these limitations, the absence of 3D flow process in either method does not necessarily mean that they are not present in the field. This will be included during the analysis of the field presence. Table 4.5 shows a current overview of the 3D flow processes that can be present in each method and the capability of the methods to actually show them.

	Presence 3D processes		capability of method to show 3D processes	
	Delft3D model	ADCP measurements	Delft3D model	ADCP measurements
Flow contraction	?	?	capable	?
Recirculation zone	?	?	probably not suitable	?
Horseshoe vortex	X	?	not suitable	?

Table 4.5: Overview of 3D processes that can be present at scour hole Beerenplaat and the capability of the methods to show them.

4.3.1. Presence of 3D flow processes inside the scour hole Beerenplaat

To visualize the findings and keep this section brief, two model time step and two ADCP measurements are taken as representatives. For the Delft3D model these are time steps 359 (peak ebb flow) and 363 (peak flood flow), similar as the base case. For the ADCP measurements, the measurement 2 taken at 08:28 (peak ebb flow) and the measurement 7 taken at 15:57 (peak flood flow) will be used. For reference, figure 4.15 shows the locations of measurement two and seven. The presence of these 3D processes will be analyzed individually. First flow contraction will be addressed, after that the (curved) recirculation zone and finally the horseshoe vortex.

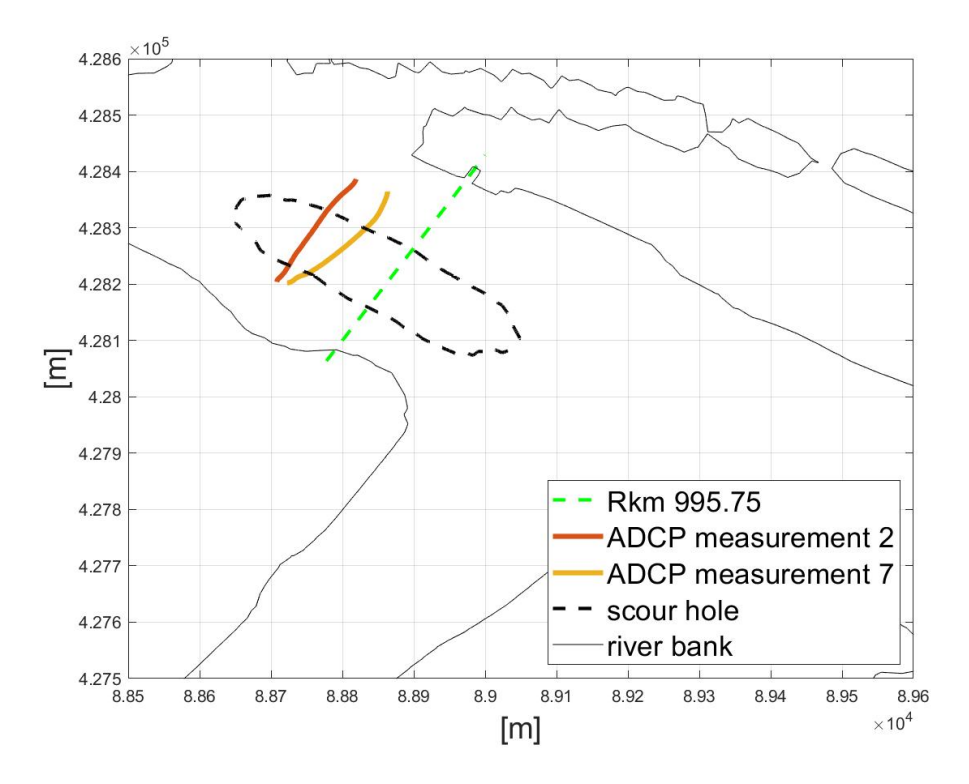
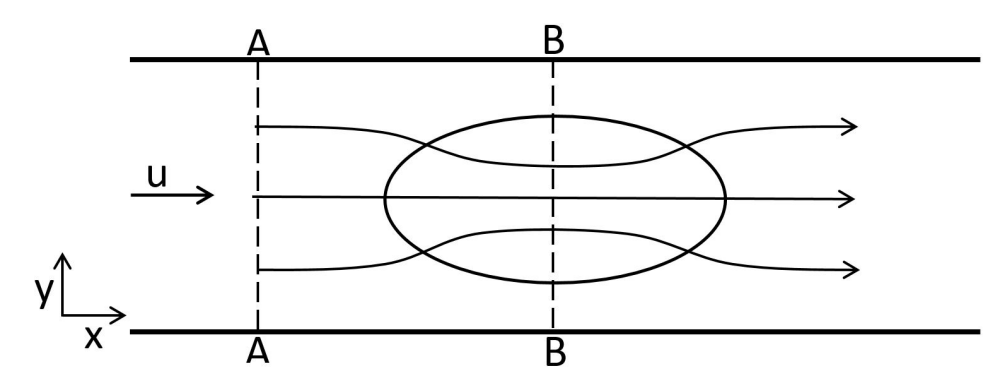


Figure 4.24: Location of ADCP measurements.

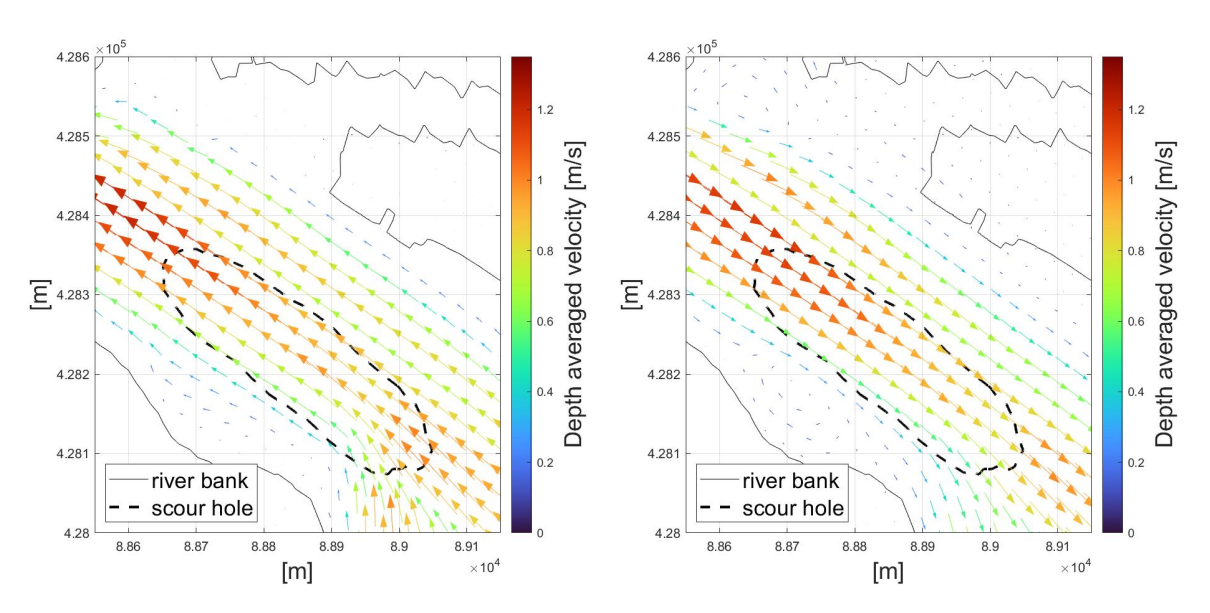
Flow contraction

Flow contraction contraction can be observed when the flow enters the scour hole, see figure 4.25a. It should be recognized by velocity vectors deflecting into the scour hole or by flow divergence if the flow leaves the scour hole again. Figure 4.25b and figure 4.25c show the flow velocity field during respectively peak ebb flow and peak flood flow, as was computed by the model. Looking at the depth averaged velocity vectors there can be seen that no flow contraction occurs. The vectors keep their direction while passing the scour hole. It appears as if some slight flow deflection is seen on the left side during peak ebb flow. However, the answering of the previous sub research question has shown that this is caused by the joining flow from the Spui. This can not be labeled as flow contraction since the flow on the right side of the scour hole shows no deflection inwards. In addition, no flow divergence is observed during either peak ebb flow or peak flood flow in the Delft3D model results. Identifying flow contraction in the ADCP measurements is a bit more difficult since they just show a single cross-section at the scour hole. However, it would be expected that flow contraction is seen in ADCP measurement 7 by flow entering the scour hole from the sides. Since ADCP measurement 2, taken during ebb flow, is located on the downstream slope, there is expected that flow divergence would occur here. Looking at figure 4.25d and figure 4.25e none of this can be observed. The ADCP measurements only show the presence of a very irregular cross-stream and vertical velocity field.

If this means that flow contraction does not occur inside the scour hole Beerenplaat or that the used methods are not capable to show it, is still uncertain. Based on the characteristics of the model explained in section 4.1.1 and appendix D.1, it is expected that the Delft3D model would be able to simulate this. Therefore the absence indicates that no flow contraction would occur in the field. Unfortunately, the ADCP measurement are not suitable to give any confirmation. The ADCP transects are just snapshot at one location and hence not the best method to capture any flow contraction. Despite, it is expected that the measurements would show some kind of a more regular pattern in the cross-stream direction, and not this irregular behavior. It suggest that either the flow was too turbulent for the ADCP device to capture it or that some acoustic interference was present. This makes the ADCP measurements not suitable for identifying flow contraction. Following the indications of the Delft3D model, it can be suggested that no flow contraction occurs at the scour hole Beerenplaat. An important remark to made is that both Bom (2017) and Stenfert (2017) concluded that flow contraction only occurs very subtle, questioning if this can even be observed in this analysis. Besides, it remains uncertain if and how the confluence/bifurcation affects this 3D flow processes. Therefore no conclusion on the presence of flow contraction at the scour hole Beerenplaat can be made.



(a) Schematization of flow contraction with streamlines, based on (Bom, 2017).



(b) Depth averaged flow velocities during peak ebb flow (model time step = 359).

(c) Depth averaged flow velocities during peak flood flow (model time step = 363).

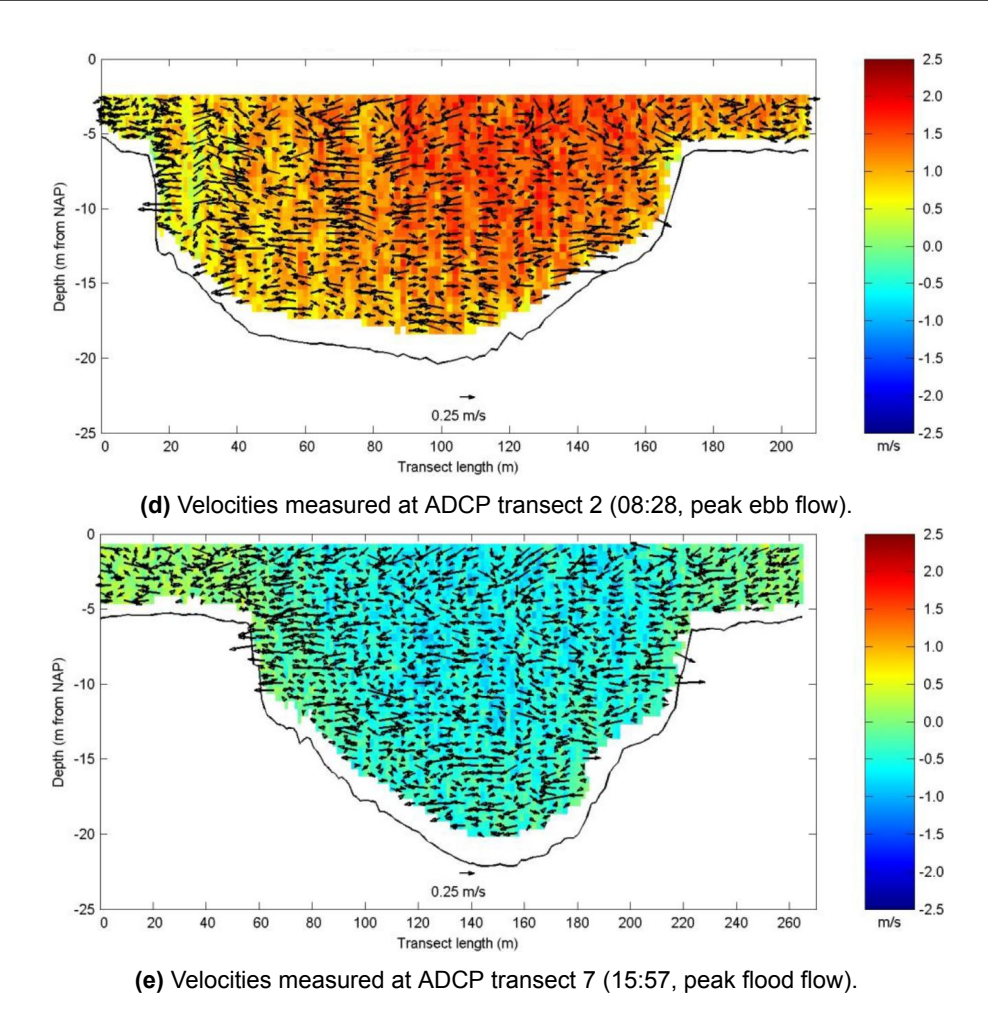
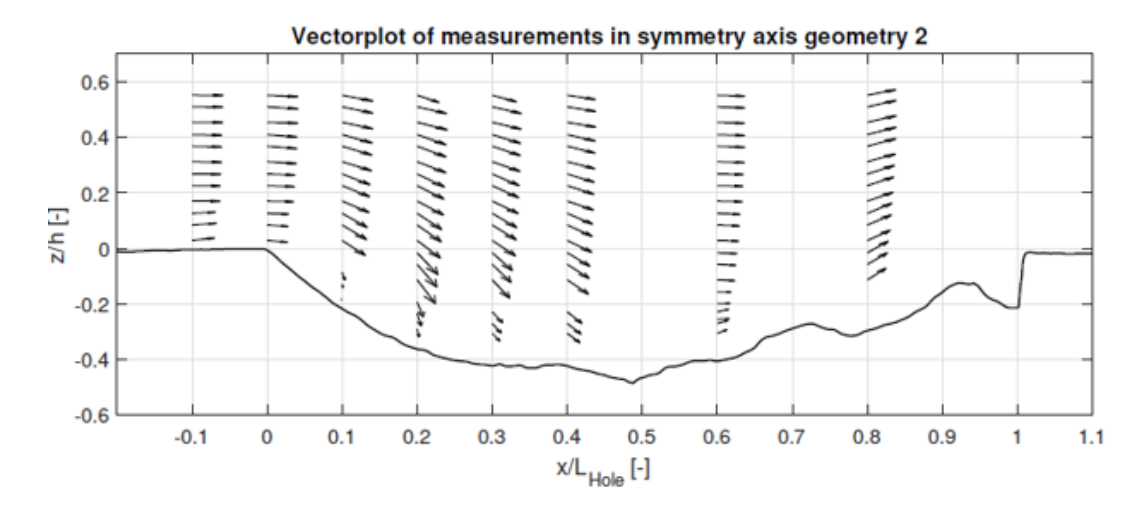


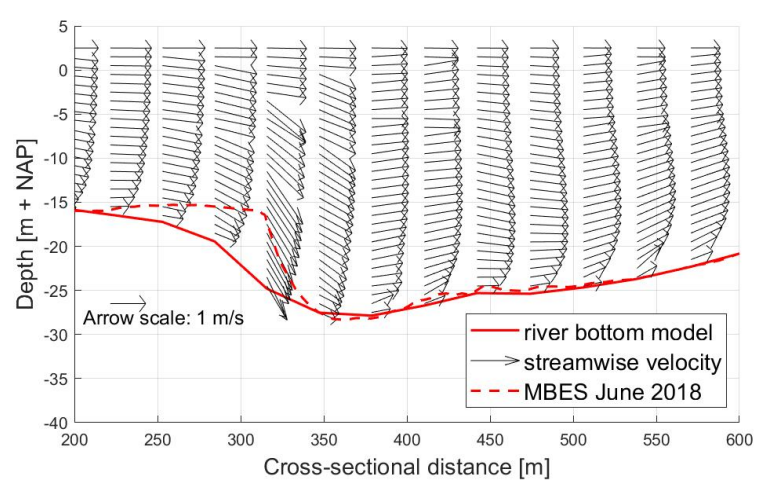
Figure 4.25: Velocities in both the model and the ADCP measurements, for identifying flow contraction.

Recirculation zone

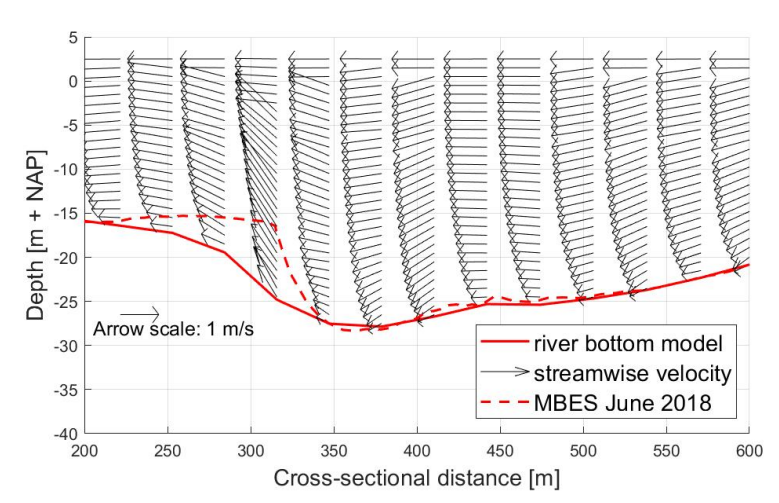
A three-dimensional recirculation zone should be observed inside the scour hole. As discussed in section 2.2.3, the recirculation zone can be found on the upstream slope of the scour hole and is curved due to the curvature of the upstream edge. Figure 4.26a shows an example of the streamwise velocities inside a scour hole when this recirculation zone is present. Similar kind of patterns could not be observed in the model results. Figure 4.26b and figure 4.26c show this for both the peak ebb and peak flood scenario. They suggest that the Delft3D model is not able to reproduce any recirculation zone in the streamwise direction. However, the relatively gentle slopes of the scour hole in this model would not even allow for the formation of a recirculation zone. The steepest slope is only 9.7°, which will not lead to the development of a recirculation zone as was described in section 2.2.3. Therefore it is not possible to comment on performance of the Delft3D model regarding the simulation of the recirculation zone. In reality the steepest slope of the scour hole is much steeper, around 25° in June 2018 (see section 3.1). As a result, it is expected that a recirculation zone will develop at the scour hole Beerenplaat, but only during ebb if the flow enters the scour hole on the steepest slope. This questions if the ADCP measurements confirm this. Looking at figure 4.24 it can be seen that the ADCP measurements are only taken on the very gentle slope. Section 3.1 has shown that this slope has an angle of 1.3° in February 2021, meaning that it would be impossible for the flow recirculating to develop here and hence being captured by the ADCP device. Therefore it can not be ruled out yet, if the limitations of the ADCP device make the method not suitable for capturing this 3D flow process.



(a) Streamwise velocities measured during laboratory experiment by Stenfert (2017).



(b) Streamwise velocities in the center of scour hole during peak ebb flow (model time step = 359).



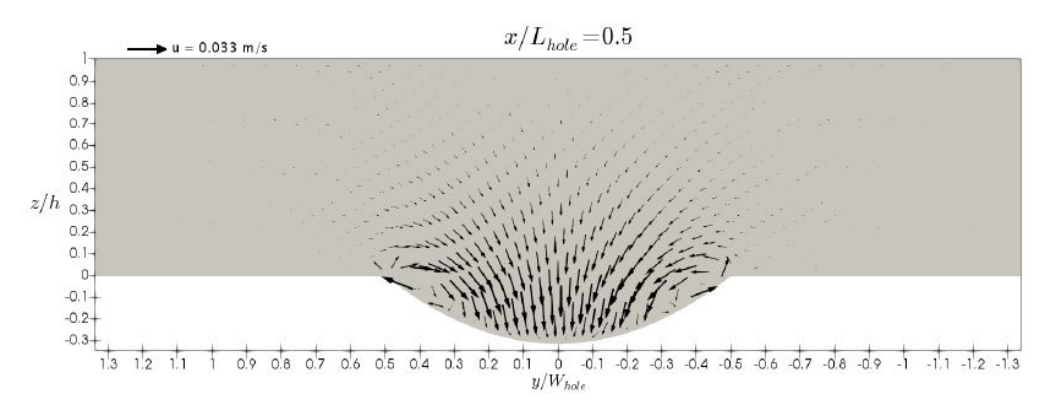
(c) Streamwise velocities in the center of the scour hole during peak flood flow (model time step = 363).

Figure 4.26: Velocities in the model, for identifying the recirculation zone. Cross-sectional distance 0 m is located at the confluence/bifurcation.

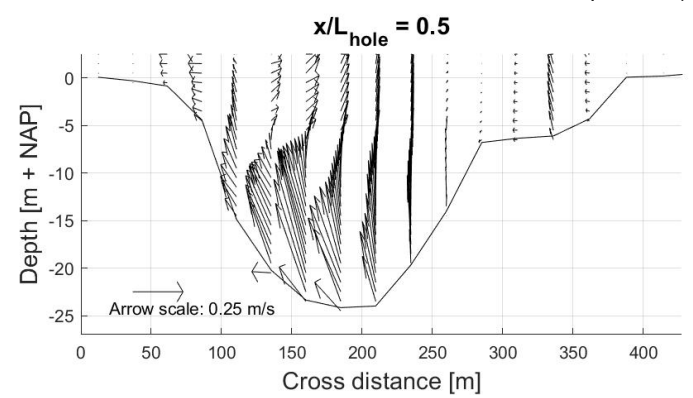
Horseshoe vortex

The horseshoe vortex develops when the flow enters the scour hole. It consists out of a recirculation zone until the reattachment point and after that reshapes into a less-structured wake. If present, the horseshoe vortex would be identified with lateral recirculation at the side slopes of the scour holes as is shown in figure 4.27a. As previously discussed in section 4.1.1, the Delft3D model will not be able to simulate the turbulent fluctuations paired with this. For confirmation, the figure 4.27b and figure 4.27c show the velocities at a cross-section during respectively peak ebb and peak flood flow. The horseshoe vortex is not seen in either scenario. As already shown, the cross-stream and vertical velocities measured by the ADCP device showed a very irregular velocity field, in which no patterns could be observed. This can be confirmed by looking at figure 4.27d and figure 4.27e. As was already discussed, this is most likely caused by either acoustic interference or a very turbulent flow. However, since the horseshoe vortex is shaped around the scour hole, it should be noticeable in the streamwise direction as well. Therefore an additional analysis of the measured streamwise velocities is done, which can be found in appendix G. It uses the idea that more turbulent fluctuations would present in the streamwise velocities if either the horseshoe vortex or the less structured wake is present. Despite this effort, only very irregular and sometimes contradictory patterns were found. It seems that the flow is to turbulent for the ADCP device to accurately capture it.

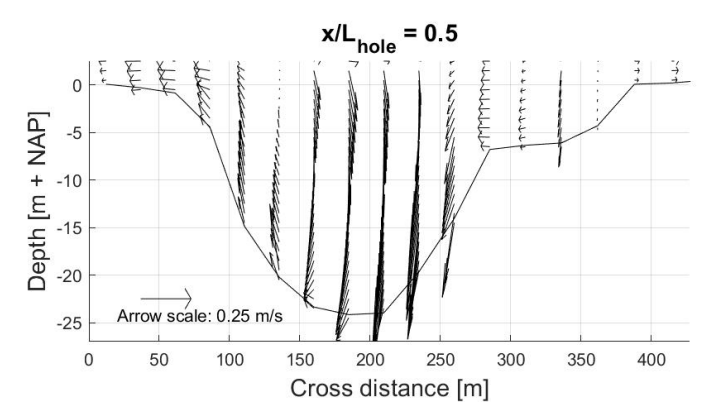
Since both methods are not suitable for identifying the horseshoe vortex no conclusion on the field presence of the horseshoe vortex can be made. Despite, one reasoning is constructed. Bom (2017) hypothesises that the formation of this horseshoe vortex requires three driving mechanisms, which are flow contraction, recirculation zone and curved upstream edge. A curved upstream edge is present for both the peak ebb and peak flood scenarios. The recirculation zone is only expected during peak ebb flow. No conclusion on the absence or presence of flow contraction could yet be made. Therefore it is hypothesised that the horseshoe vortex can only develop during ebb flow at the scour hole Beerenplaat, given that flow contraction is present and the hypothesis of Bom (2017) is correct.



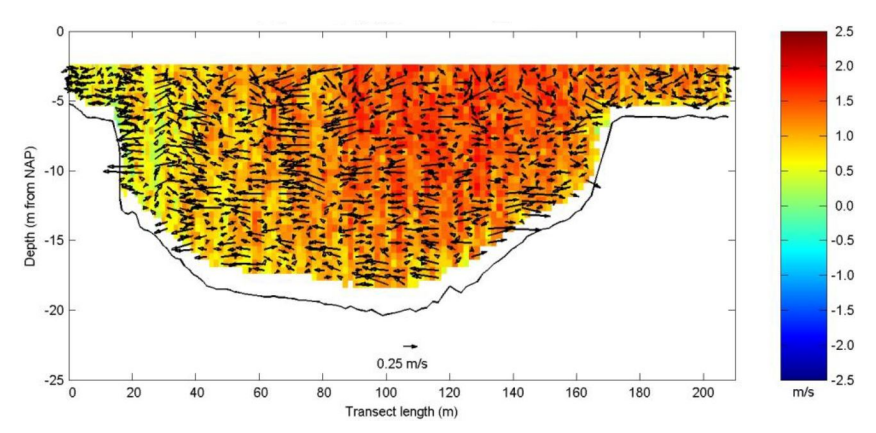
(a) Cross-stream and vertical velocities if lateral recirculation is present (Bom, 2017).



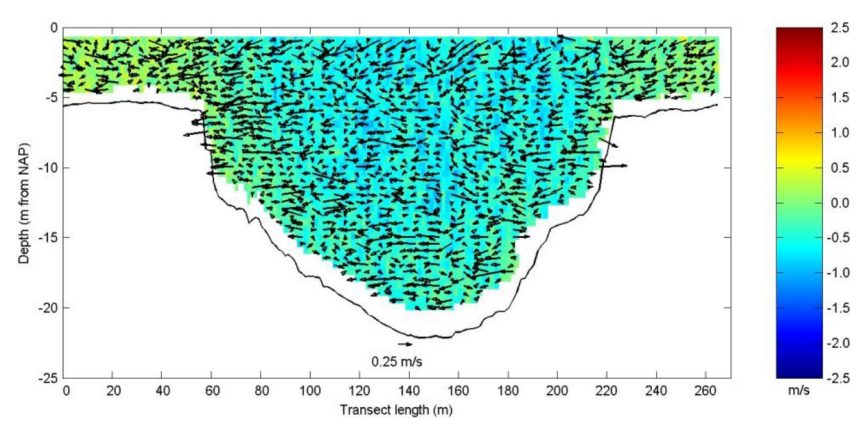
(b) Cross-stream and vertical velocities during peak ebb flow (model time step = 359).



(c) Cross-stream and vertical velocities during peak flood flow (model time step = 363).



(d) Velocities measured at ADCP transect 2 (08:28, peak ebb flow).



(e) Velocities measured at ADCP transect 7 (15:57, peak flood flow).

Figure 4.27: Velocities in the model and ADCP measurements, for identifying the horseshoe vortex. The location of the cross-section (x/L_{hole}) is at half the length of the scour hole.

4.3.2. Conclusion on sub research question 3

The goal of this section was to answer the third sub research question: "Which of the 3D flow processes are present at the scour hole Beerenplaat and what is the influence of the flow direction and intensity on them?". Analyzing both the Delft3D model results and the ADCP measurements have shown that none of the 3D flow processes are present in either method. This has been shown for both the representative model time steps and ADCP measurements. Important to mention is that this has been further investigated for more ADCP measurements and model time steps, which did not lead to any other observations. Despite, the absence of the 3D flow processes in both methods has been distorted by the functioning and limitations of both the model and the ADCP device. As a result, it did not necessarily mean that the 3D flow processes are not present in the field. On the 3D flow processes inside the scour hole Beerenplaat the following reasoning's were given.

- It is suggested that flow contraction would not occur at the scour hole Beerenplaat. However, it can be possible that this flow processes is to subtle to be observed. On top of that of that, it is uncertain if and potentially how the confluence/bifurcation flow affects this. Therefore no conclusion on the field presence can be given.
- Clear explanation has been given why no recirculation zone was observed in both the model and the ADCP measurements. However based on the actual profile of the scour hole Beerenplaat, it is expected that the (curved) recirculation zone is present during ebb flow. During flood, the flow enters the scour hole on its very gentle slope. This does not allow for the full development of a mixing layer and hence recirculation zone.
- It is hypothesised, that the horseshoe vortex only develops at the scour hole Beerenplaat during
 ebb flow, given the fact that flow contraction actually occurs and the hypothesis of Bom (2017) is
 correct. The horseshoe vortex can for sure not develop during flood flow, due to the influence of
 the geometry of the scour hole on the recirculation zone.

A first indication has been given on how the flow direction influences the presence of the recirculation zone and potentially the horseshoe vortex. This could not be done for flow contraction. Since none of the 3D flow processes were present in either the Delft3D model results or the ADCP measurements, it was not possible to investigate how they are influenced by the flow intensity.

	Presence 3D processes		capability of method to show 3D processes	
	Delft3D model results	ADCP measurements	Delft3D model results	ADCP measurements
Flow contraction	X	Х	plausible	not suitable
Recirculation zone	X	X	not suitable	not suitable
Horseshoe vortex	X	X	not suitable	not suitable

Table 4.6: Summary on the investigation of the 3D flow processes inside the scour hole Beerenplaat. A red cross means that the flow process was not observed.



Link between scour hole development and flow processes

This chapter will tackle the fourth sub research question: "To what extends do the flow processes at the scour hole Beerenplaat and their tidal response give an explanation of the morphological development?". The flow processes at the scour hole Beerenplaat are categorized into confluence/bifurcation flow (section 4.2) and the 3D flow processes inside the scour hole (section 4.3).

First a short recap of the morphological development of the scour hole Beerenplaat will be given, which was fully described section 3.1. After that, there will be looked at the erosive patterns caused by the hydraulic forcing of the confluence/bifurcation, followed by the contribution of the 3D flow processes. Finally the sub research question will be answered.

5.1. Recap morphological development

- The scour hole Beerenplaat expanded in both upstream and downstream direction (see figure 5.1).
 In the last ten years, the most scour has occurred on the upstream slope, which will most likely be the situation in the near future. During this upstream expansion, the angle of the upstream slope remained stable and the location with the largest scour depth migrated along.
- In February 2021 the depth of the scour hole Beerenplaat was approximately 12 meters. The
 field behavior and a first estimation with the Breusers equations have suggested that the scour
 hole has not yet reached its equilibrium depth. Hence scour is expected to occur inside the scour
 hole Beerenplaat.
- The most upstream part of the scour hole Beerenplaat appeared to grow into the Spui, suggesting
 that the hydraulic forcing of the confluence/bifurcation plays an important role. Therefore scour
 would be expected between the upstream edge of the scour hole Beerenplaat and the Spui.

5.2. Confluence/bifurcation flow

Scour only occurs if the hydraulic forcing is larger than the resistance of the sediment particles in the river bed. Unfortunately, exact information on sediment characteristics and soil composition at the scour hole Beerenplaat is lacking. Therefore it is not possible to compute sediment resistance and the accompanying erosion rates. Nevertheless, it is possible to identify the areas that are vulnerable to scour with the hydraulic forcing. By computing bed shear stresses, it can be visualized where the most attack of the bed by the flow occurs.

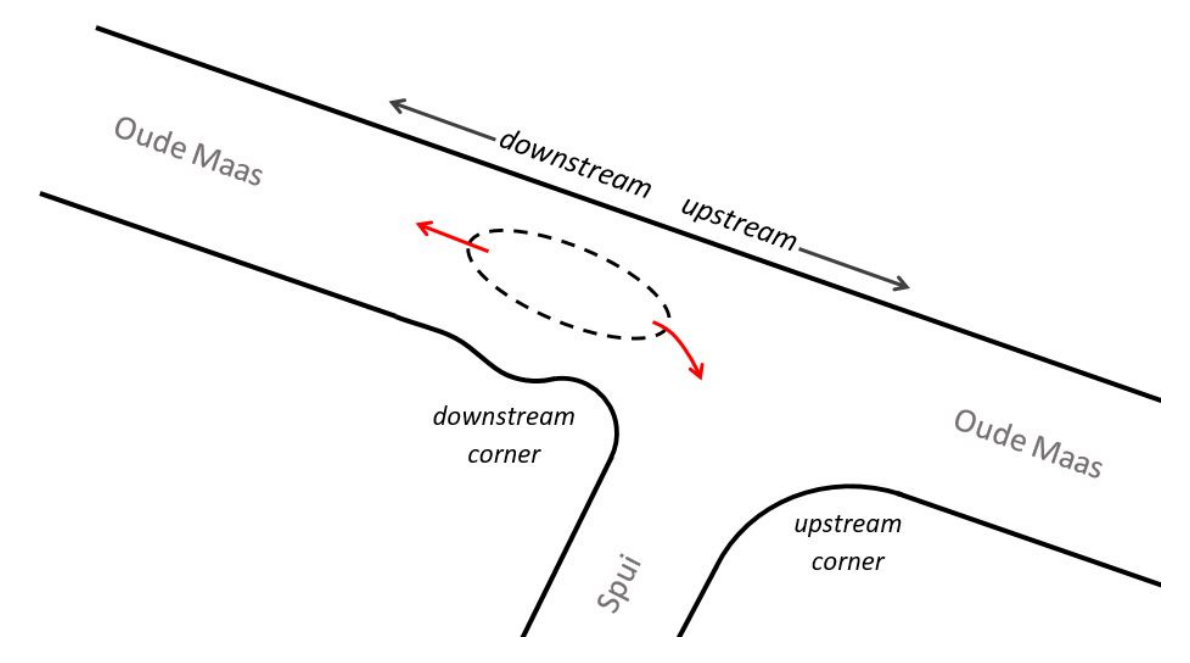


Figure 5.1: Schematization of the scour hole Beerenplaat. The red arrows represent the direction in which the scour is expanding.

Bed shear stresses are a measure of friction force of the flow exerted onto the river bed. If the bed shear stresses are larger than the sediment resistance, transport of sediment grains occurs. Hence, the areas with the largest bed shear stresses are the most vulnerable for scour. According to Xie et al. (2020), the bed shear stresses can be computed with equation (5.1). Important to mention is that the bed shear stress will be computed with the results of the Delft3D model. These did not contain any of the 3D flow processes inside the scour hole Beerenplaat. The presence of these 3D processes can influence the flow velocity, affecting therefore the bed shear stress. This section only covers the influence of the confluence/bifurcation flow.

The bed shear stresses are computed with equation (5.1). The depth averaged velocities and Chézy coefficient are computed at every cell in the model. The density of the water column is dependent on both temperature and salinity. The temperature of the system, during almost the entire run time of the model, is 9.1 °C. The salinity is varying quite a lot due to the continuous adaptation and mixing of the tide and the seasonal river discharge. Therefore a linear relation for salinity is included and the densities in the model are determine with with equation (5.2). Fresh water coming from the upstream part of the Rhine and the Meuse has a salinity of 0.5 ppt (parts per thousand). The average salinity of seawater is around 35 ppt which is forced into the delta by the tide. The densities of fresh water and sea water at a temperature of 9.1 °C are respectively 999.7 kg/m³ and 1027 kg/m³. The salinity is computed for every cell of the model and is depth averaged to compute the density per cell. With this information the bed shear stresses can be determined for different velocity fields.

$$\tau_b = \frac{\overline{u}^2 \cdot \rho_{wc} \cdot g}{C^2} \tag{5.1}$$

 au_b [N/m²] Bed shear stress C [m $^{0.5}$ /s] Chézy coefficient \overline{u} [m/s] Depth averaged flow velocity g [m/s²] Gravitational acceleration ho_{wc} [kg/m³] Density of water column

$$\rho_{wc} = \rho_w + (\frac{S}{34.5})(\rho_s - \rho_w) \tag{5.2}$$

 ho_{wc} [kg/m³] Density of water column ho_s [kg/m³] Density of sea water ho_w [kg/m³] Density of fresh water ho_s [ppt] Salinity

The section 4.2 has given an elaborate explanation of how the flow velocity field at the confluence/bifurcation Oude Maas and Spui is shaped during a tidal cycle. It was concluded that the velocity field during peak ebb flow and peak flood flow was similarly shaped at almost each tidal cycle within the model results. Only the intensity varied dependent on the hydraulic conditions. Since the flow velocity field is similarly shaped, it will not lead to completely different patterns of bed shear stresses for other tidal cycles. Therefore the bed shear stress will be analyzed only for the peak ebb flow and peak flood flow time steps of the base case, which are respectively time step 359 and 363. The bed shears stress patterns during these time steps are representative for what happens during each tidal cycle, only the intensity can be less or more. Figure 5.2 shows an overview of the bed shear stresses at the system during peak ebb flow and figure 5.3 during peak flood flow. Out of these figures the following remarks can be made.

For the direction and locations of terms such as downstream/upstream and Oude Maas/Spui, reference is made to figure 5.1.

- For both the ebb and flood scenario, higher bed shear stresses occur downstream of the scour hole than upstream. It suggest that the scour hole will expand faster towards sea than towards the confluence/bifurcation.
- It would be expected that some large bed shear stresses are present between the upstream edge of the scour hole and the Spui, which could explain why the scour hole expands in that direction. Only during ebb flow a slight indication of this is seen. Larger bed shear stresses are found at the downstream corner of the confluence which give a possible idea why the scour hole is being pulled in this direction. However this is a quite minuscule pattern which does not occur on the correct location. It would be expected on the most upstream edge of the scour hole, where the large growth towards the Spui was observed. Some slightly larger bed shear stresses are indeed present here but these are directed upstream towards the Oude Maas, not the Spui. During flood a similar pattern is observed. This all questions if the scour hole Beerenplaat will actually grow into the Spui. At least no area vulnerable to scour could be found that explains why the scour hole appears to grow into the Spui.
- The model results do not show any large bed shear stresses inside the scour hole, which suggest that there is not much attack of the bed by the flow here. However, the model does not include any of the 3D flow processes. As explained in section 2.2.3, these can be of large influence on the morphodynamics of scour holes. On top of that, it is known that the most attack of the bed occurs at the reattachment point, but at this location the bed shear stresses are almost zero. As a result, large bed attack would not even show up in figure 5.2 and figure 5.3. Due to this all, no comment can be given on any of the observations/developments occurring inside the scour hole, such as the equilibrium depth, migration of deepest location of the scour hole and the stable upstream slope angle. At least not with the bed shear stresses.
- For the two time steps of the base case it can be seen that the bed shear stresses within the ebb flow pattern are larger than that of the flood flow pattern. Important to point out is that this is not always the case. As mentioned, the intensity of the flow velocity field varies with the hydraulic conditions. If there are relatively high water levels in the system, it can be possible that the bed shear stresses pattern during peak flood flow is the most intense. Nevertheless, the pattern of the bed shear stresses shown for both peak ebb and peak flood flow of the base case, are representative patterns. The largest bed shear stresses are always encountered downstream of the scour hole.

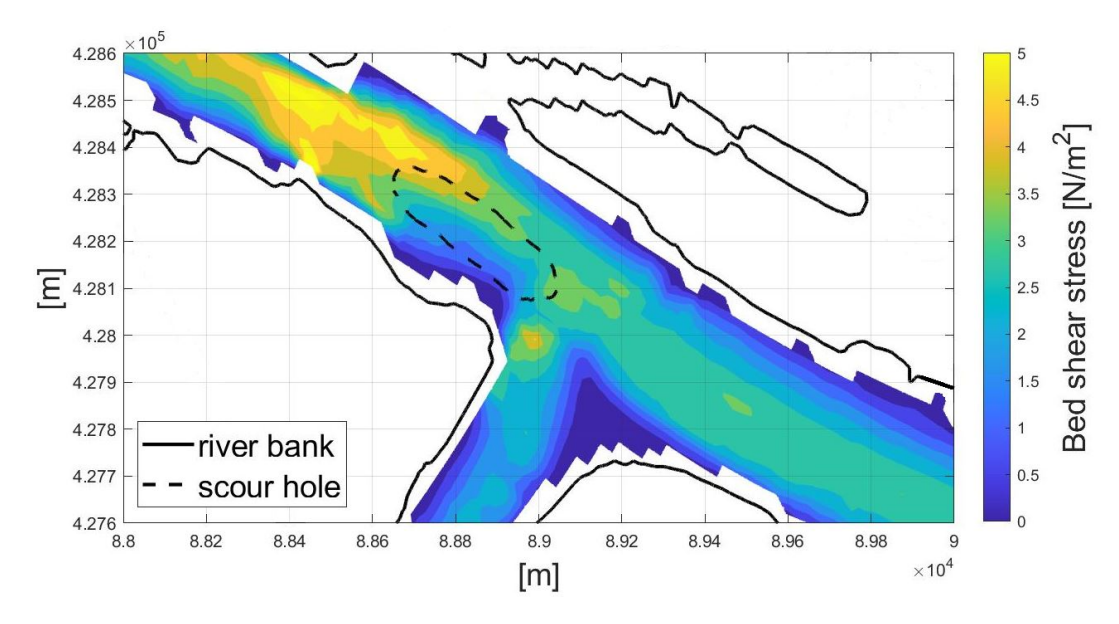


Figure 5.2: Bed shear stress at peak ebb flow during the base case (confluence, time step = 359).

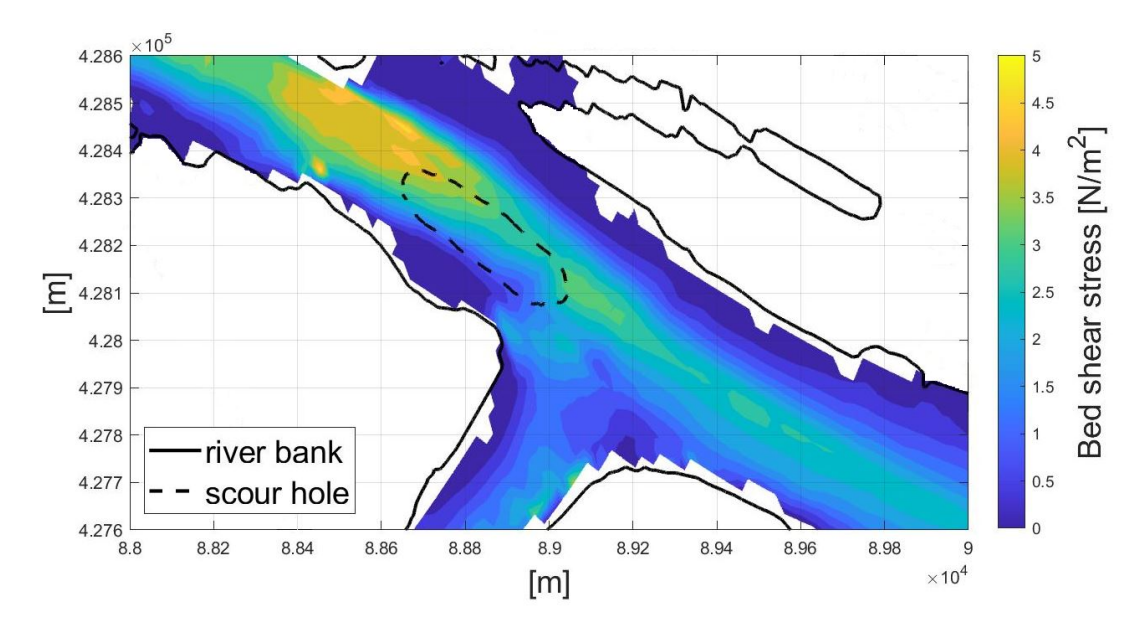


Figure 5.3: Bed shear stress at peak flood flow during the base case (bifurcation, time step = 363).

Discussion

As was shown during the investigation of the recirculation zone in section 4.3, the geometry of the scour hole in the model was not similar as what is encountered in the field. The slope located on the side of the confluence/bifurcation is in the model much more gentle than in reality. Due to this, the computed bed shear stresses show a twisted image during flood flow. Figure 5.4 illustrates the flow near the river bed for both the model and reality. During flood the flow enters the scour hole and follows the gentle slope of the river bottom ($\approx 1-2\,^\circ$), which is similar for both. However, when the flow leaves the scour hole it encounters a much steeper slope in reality than in the model, resulting in more flow acceleration. This will lead to larger bed shear stresses, meaning that more attack of the river bed is expected in the field than was shown in this section. How much more remains yet uncertain. Including this, the remarks made on the largest expansion direction and the growth towards the Spui during peak flood flow, are not appropriate for comparing with the morphological development of the scour hole Beerenplaat. It

is not expected that this incorrect geometry will lead to more deepening of the scour hole during flood since the hydraulic forcing reduces with the depth and no recirculation zone can develop.

Most likely the identified areas vulnerable for scour during ebb flow will not change due to this. Only the area vulnerable to scour will expand. The steeper slope will result in the formation of the 3D recirculation zone during ebb flow, as was reasoned in section 4.3. As discussed in section 2.2.3, this flow process is paired with more attack of the downstream slope, which is not yet included in the bed shear stresses. As a result the downstream area vulnerable to scour will expand and include the downstream slope of the scour hole Beerenplaat. Despite, this will still suggest that the scour hole develops faster downstream than upstream. How the 3D flow recirculation zone exactly affects the morphological development of the scour hole Beerenplaat will be discussed in the next section.

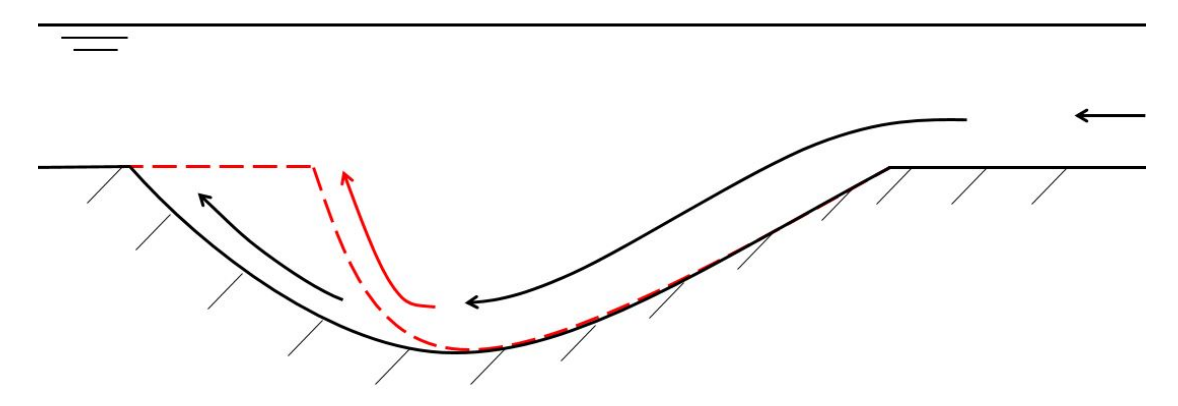


Figure 5.4: Influence of the geometry of the scour hole on the flow near the river bed during flood. The black lines represent the situation of the model and red lines the field scenario.

5.3. 3D flow processes inside the scour hole

In section 4.3, it was not possible to conclude which of the 3D flow processes are present at the scour hole Beerenplaat. Nevertheless, it is reasoned that the (curved) recirculation zone is expected during ebb flow. As described in section 2.2.3, the recirculation zone is responsible for a stable upstream slope. The morphological development showed a very dynamic upstream slope, but the angle of the slope was almost stable during the expansion. It is plausible that this has been caused by the recirculation zone present during ebb flow. On top of that, the recirculation zone indicates the presence of the reattachment point. This is the location where the most scour occurs. Therefore some attack of the river bed inside the scour hole Beerenplaat can be expected. However, if the scour hole becomes deeper is not certain. The flow velocities generally reduce with the depth and the transport of sediments out of a deeper hole requires more energy. As a result, the equilibrium depth exists at which the scour hole will not become much deeper. If the scour hole Beerenplaat is already at this stage can not be verified, but it is expected the recirculation zone has played a role in the deepening of the scour hole Beerenplaat. This also gives an explanation why the deepest point of the scour hole has migrated along with the upstream expansion. Since the scour hole expanded in upstream direction with a quite stable slope angle, the recirculation zone and reattachment point have moved along and hence the location where the scour hole is the deepest.

5.4. Conclusion on sub research question 4

This chapter has focused on finding an answer to the fourth sub research question "To what extends do the flow processes at the scour hole Beerenplaat and their tidal response give an explanation of the morphological development?". Table 5.1 shows a summary of the findings in this chapter. These exclude any contributions of the hydraulic forcing during flood, since the geometry of the scour hole in the model was not accurate.

There can be seen that the combination of flow processes at the scour hole partly explain the morphological development observed in the field. The most conflict is encountered in the fastest expansion direction and the indicated growth towards the Spui. This suggest that the attack of the bed during flood flow should for sure be included to potentially describe the morphological development. As a result, it was not possible to conclude if the scouring processes at the scour hole Beerenplaat can be approached without using information on the heterogeneous subsoil.

morphological development	confluence/bifurcation	3D flow processes recirculation zone (ebb flow)	
scour hole Beerenplaat	ebb flow		
faster upstream expansion than downstream expansion	slower upstream expansion than downstream expansion	no upstream expansion only downstream expansion	
scour hole becomes deeper, has not yet reached equilibrium depth	-	-	
upstream slope angle remains stable	-	suggests that upstream slope angle is constant	
deepest location scour hole moves upstream	-	suggests that deepest location migrates upstream	
scour hole grows into the Spui	no indication of growth towards Spui	-	

Table 5.1: Summary of morphological development observed in the field and the morphological development suggested by the hydraulic forcing of the confluence/bifurcation and 3D flow processes during ebb.



Discussion

Already a lot of discussion has been conducted within the answering of each sub research question. In section 3.1 explanations were given for why the scour hole Beerenplaat showed different development phases. During the investigation of the pilot nourishments at scour section 5 in section 3.2.2, hypothesis have been constructed that explain why estuarine sand waves developed after the nourishment. The limitations and validity of the Delft3D model were explained in section 4.1.1. The model results of the flow field at the confluence/bifurcation have been thoroughly compared to both field measurements and literature in section 4.2, to comprehend what is happening here. In section 4.2.3 it was discussed when each of the three characteristic secondary flow patterns develop and hypothesis has been given why only one recirculating cell developed at the scour hole Beerenplaat. During the investigation of the 3D flow process in section 4.3, it is extensively discussed how the results were affected by the functioning of both the Delft3D model and the ADCP device. In section 5.4 reasoning was given why the flow processes at the scour hole did not explain the morphological development. Despite this all, a few topics have been left untouched or should be emphasised more. These are divided under morphological development, hydraulic conditions, improvements and changes to the modelling approach and relevance for other scour holes in the Rhine-Meuse delta.

6.1. Morphological development

6.1.1. MBES measurements

Multiple MBES measurements have been used to describe the morphological development of the scour hole Beerenplaat and the pilot nourishment. The raw measurements of the MBES consisted out of X,Y,Z values, meaning that the depth has been measured at a grid. To achieve a full image of the river bottom, spline interpolation has been performed on the raw measurements. It estimates the values in between the grid points with a mathematical function that minimizes overall surface curvature. Due to this processing, some extra uncertainty is introduced on top of the error of the measuring device. This could have slightly affected some of the values estimated out of MBES measurements, such as the upstream and downstream expansion rates, slope angles and scour depth. This extra induced error is not similar for all MBES measurements. As was explained in section 2.3.2, the density of the grid, at which the device can measure, has significantly improved in recent years. This makes the estimates obtained out of the interpolated measurements from the last 10 years the most reliable. Since the size of the scour hole Beerenplaat is very large with respect to all MBES grids, it is not expected to be of significant influence on the results of this research.

6.1.2. Equilibrium scour depth

By analyzing the MBES measurements, it was suggested that the scour hole Beerenplaat will reach an equilibrium scour depth. The equilibrium scour depth was estimated with the Breusers equation. It suggested that the equilibrium depth of the scour hole Beerenplaat is within the range of 12-17.17 meters, dependent on the subsoil. The lower limit of 12 meters was based on the sand scenario and the upper limit of 17.17 meters on the clay scenario. However, using the Breusers equation for the clay scenario is beyond the range of applicability and therefore paired with uncertainty. It does, for example, not include lumps of clay being pulled off or the effect of consolidation. The proposed range of the equilibrium depth for the scour hole Beerenplaat could be narrower or wider. The lower limit of the sand scenario is still appropriate.

In addition, some assumptions were made to fit the Breusers equation for the scour hole Beerenplaat, which were not all discussed in section 3.1.1. Average soil parameters have been assumed for the clay scenario. For the soil properties of sand, an estimation out of the nourishment is obtained, which is not necessarily the sand that is present in the subsoil. The relative turbulence intensity r_0 has been estimated with an equation for scour holes after a sill with a bed protection, which is not the case here. For the contribution of the confluence a constant turbulence intensity value was assumed. Different r_0 values were computed for both peak ebb and peak flood flow, that were eventually averaged since the flow enters the scour hole from different sides. All with all, it shows that quite some assumptions and estimations were made. Therefore it can be questioned how accurate this range of the equilibrium depth is for the scour hole Beerenplaat. Despite, it illustrated possible behavior of the scour hole in the near future. To determine the actual equilibrium depth of the scour hole Beerenplaat, further research should be performed. Possibly, a combination of measurements on the composition of the subsoil and laboratory experiments could provide the solution.

One final remark should be made regarding the equilibrium scour depth. The MBES data showed that the scour hole is stabilizing, suggesting this equilibrium depth. It can be possible that the heterogeneous subsoil is responsible for this. If a poorly erodible clay layer is present, it would prevent the scour hole from becoming much deeper. Breaching of this layer could again allow for fast paced erosion. Taking measurements on the composition of the subsoil should be able to confirm this.

6.2. Hydraulic conditions

6.2.1. Comparison discharges model and ADCP measurements

During the comparison of the discharges computed by the model and the ADCP measurements in section 4.2.1 and appendix E, it was found that the model overestimates the average velocities during flood with 30%. Even if there is accounted for a delay of the peak flood flow. An explanation for this might lie within the operating of the Haringvliet sluices. Since January 2019, the Haringvliet sluices are regular left open during the tidal flood period, to promote the ecology in the Haringvliet. This shows that the operating of the sluices is not simulated within the Delft3D model, since the time frame is from 14 June 2018 until 17 November 2018. However, it could have affected the ADCP measurements taken on 11 February 2021.

There can be reasoned how the operating of the Haringvliet sluices affects the flow field at the confluence/bifurcation Oude Maas and Spui. It would allow for the tide to penetrate into the Haringvliet during flood and elevate the water levels in the estuary and most likely also the Spui. As a result, a different discharge distribution would occur at the bifurcation Oude Maas and Spui, with less flow being pushed into the Spui. This can also explain why lower flow velocities were encountered on the left side of the ADCP cross-sections, the side of the Spui. This is just a first hypothesis. For a complete understanding of how the operation of the Haringvliet sluices affects the flow field at the confluence/bifurcation, model runs should be performed that include this phenomena.

6.2.2. Flow field at confluence/bifurcation Oude Maas and Spui

During the analysis of the 3D flow processes in section 4.3 it was found that the geometry of the scour hole in the Delft3D model was quite different than the actual scour hole Beerenplaat. The slope of the scour hole on the side of the confluence/bifurcation is in reality much steeper. As a result, this affects the findings regarding the shaped flow field at the confluence/bifurcation Oude Maas and Spui section 4.2. It is expected that this mainly distorted the findings of the flow field during peak flood flow. Probably, much higher velocities are found at the upstream slope of the scour hole which could potentially explain the growth into the Spui. It will most likely not change the system behaving as a bifurcation during flood. Further analysis of a model with the correct geometry of the scour hole could confirm this.

6.2.3. Secondary flow process

During the analysis of the secondary flow process it was encountered that only one vertical recirculation cell developed while two were expected by literature. The scour hole was identified as a potential cause for this. However, what has been left out is the salinity. The tide pushes salt seawater into the river delta which eventually meets the fresh river water. Due to the lower density, the fresh water will flow on top of the saline water and develop a density driven current, as can be seen on figure 6.1. It can be possible that this occurs at the scour hole Beerenplaat and is responsible for the unexpected secondary flow patterns. Therefore the salinity differences in the model results are checked.

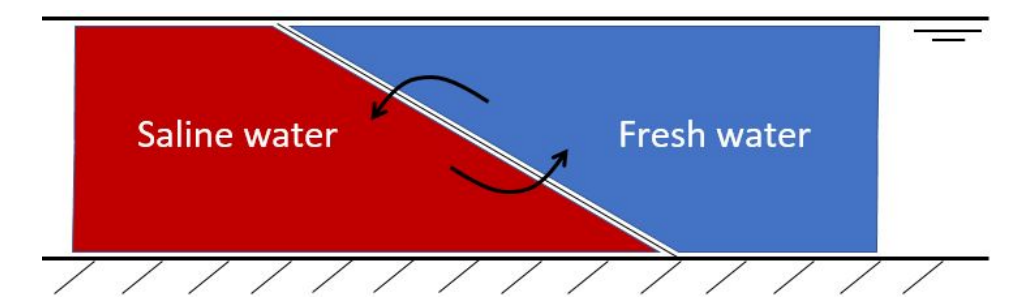


Figure 6.1: Density driven currents due to salinity differences.

The salinity in all representative time steps (358, 359, 657, 658, 1198, 1334), used for showing the three characteristic patterns, is investigated. If the flow took the shape of characteristic patterns one and two, with the clockwise recirculation, the flow consisted completely out of fresh water (see figure 6.2a). During the presence of characteristic pattern three, a different observation is done. Figure 6.2b shows the presence of salinity differences, with the most saline values found at the deepest point of the scour hole. As a result, density driven currents can form here. This seems to give an explanation why a characteristic pattern with unexpected behavior is observed during these conditions. In section 4.2.3, the scour hole was appointed as cause of the counter-clockwise rotation and growing recirculation cell. However, this section shows that the salinity is more likely the cause of it.

In section 4.2.3 it was hypothesised that a water level threshold should be exceeded before the secondary flow takes the shape of characteristic pattern three. In addition, these high water levels should be caused by influences from the sea since salinity differences appear to play a role. This was the case in the Delft3D model. Characteristic pattern three was only observed during time step 1198 of the model, which estimates the field conditions on 21 September 2018. In appendix D.2 a complete overview of the conditions during the time frame of the model can be found. It shows that there were relatively high wind speeds at Hoek van Holland, which are responsible for a large set-up. This allowed the influences of the sea to reach further into the delta and caused the salinity differences at the scour hole Beerenplaat.

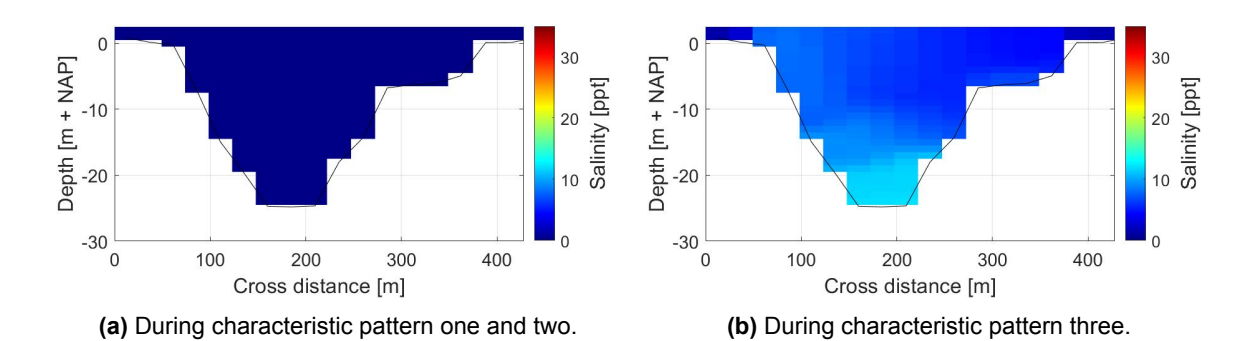


Figure 6.2: Salinity at the scour hole Beerenplaat during peak ebb flow. Fresh water has a salinity of 0.5 ppt and sea water has a salinity of 35 ppt.

6.3. Improvements and changes to the modelling approach

Within this research the output of a 3D Delft3D model has been used, to investigate the flow processes at the scour hole Beerenplaat. Unfortunately, it was not possible to fully succeed in this, since the bifurcation flow field during flood was distorted and the presence of the 3D flow processes could not be investigated. Key factors for this were the incorrect geometry of the scour hole and the limitation of the Delft3D model regarding turbulence. Therefore it will be discussed which improvements and changes can be made, to fully research the flow processes at the scour hole Beerenplaat.

To investigate the flow field at the scour hole during flood, the geometry of the scour hole Beerenplaat in the Delft3D model should be updated. During flood the flow enters the scour hole on a very gentle slope. Therefore it was hypothesised that no recirculation zone or horseshoe vortex will form. As a results, it is valuable to further investigate the flow field during flood with the output of a Delft3D model. Especially since future model runs will take place, due to the different purposes of the model. The MBES measurements of the Oude Maas, taken by Rijkswaterstaat, can be used to locally update the bathymetry in the model. With this improvement it is possible to confirm if there is significant attack of the upstream slope during flood flow. Furthermore, it would probably allow to commented on the growth of the scour hole into the Spui.

Despite improving the Delft3D model, it will still not allow for proper investigation of the 3D flow processes. The limitation of the model regarding turbulence would always hinder the simulation of these processes. Therefore a different type of Computational Fluid Dynamics (CFD) model should be developed to investigate this. One which is perfectly suitable to simulate the turbulent fluctuations paired with the 3D flow processes. Ideal would be to create a new model of the scour hole Beerenplaat that uses Direct Numerical Solving (DNS), meaning it solves for all turbulent scales. However, this is computationally very expensive and therefore less attractive. As a first alternative suggestion, Bom (2017) has shown that an OpenFOAM model with the Generalized k- ω turbulence model is able to produce these 3D flow characteristics. It is uncertain how computational efficient this model is for the actual dimensions of the scour hole Beerenplaat. Obviously, it is still important that the correct geometry of the scour hole is included in this new model. Based on the experiences of this research, two suggestions for the new model are made.

- The time step at which output is generated should not be too large. In the Delft3D model Δt_{output} was 2 hours, meaning that model results were only stored 6 times during an entire tidal cycle. This is not much for such a highly dynamic system. Within tens of minutes the system can already show different characteristics. To ensure that the 3D flow processes can be properly investigated during an entire tidal cycle, Δt_{output} should be lower.
- The horizontal grid of the new model should be finer than that of the Delft3D model. In the Delft3D model $\Delta x, \Delta y \approx$ 25 meters. It is expected that such a grid would be too coarse for accurately capturing the 3D flow processes.

Important to mention is that the influence of the Haringvliet sluices on the flow field at the scour hole Beerenplaat is not yet included. This can be done in the updated Delft3D model by extending the time frame beyond January 2019 and include the operating of the sluices in the initial and boundary conditions of the model.

6.4. Relevance for other scour holes in the Rhine-Meuse delta

This study has specifically focused on the scour hole Beerenplaat. However, much more scour holes are present in the Rhine-Meuse delta. As a result, it can be questioned how the findings of this research can be used for other scour holes. Unfortunately, it is hard to comment on this. The hydraulic conditions during an entire tidal cycle and the influence of the heterogeneous subsoil are not yet fully understood. Therefore it was not possible to link the morphological development of the scour hole Beerenplaat to for example the confluence/bifurcation. Nevertheless, one relation was identified which is also relevant for other scour holes. During the analysis of the morphological development of the scour hole Beerenplaat, it was found that the deepest point migrated upstream. In general, the deepest point of scour holes is the most critical since the steepest slopes are formed at this location. In chapter 5, this migration was linked to the hydraulic conditions inside the scour hole Beerenplaat, which were in turn affected by the profile of the scour hole. The profile contains a steep upstream slope and gentle downstream slope (see figure 6.3). It is expected that during flood, significant upstream expansion occurs due to flow accelerating over the steep upstream slope. As a result, the recirculation zone and reattachment point develop further upstream during the following ebb flow. This leads to migration of the deepest and most critical point of the scour hole Beerenplaat. Presumably this also occurs at other scour holes in the Rhine-Meuse delta, but only if they have the typical scour hole profile and flow reversal by the tide. The heterogeneous subsoil could still affect this.

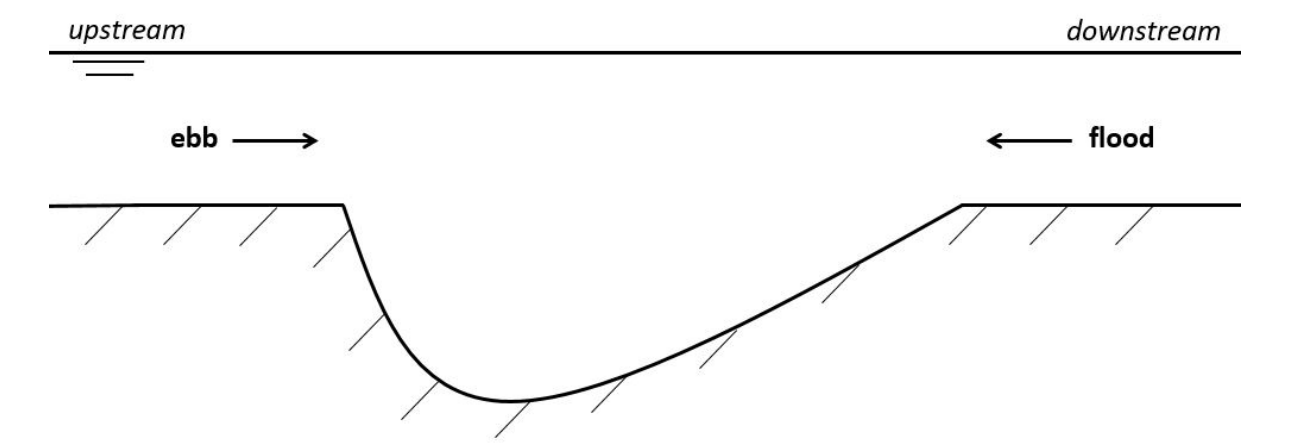


Figure 6.3: Illustration of tidal flow at a scour hole with a typical profile.

Conclusion

The conclusion on the main research question will be given based on evaluating the research objective and the answering of the sub research questions.

7.1. Research objective

As formulated in chapter 1, the objective of this research was:

Get a better understanding of how the hydrodynamic flow processes, that force the scour hole Beerenplaat, are influenced by the tide and establish a link between the behavior of the scour hole and these hydrodynamic processes.

The analysis of the taken ADCP measurement and the Delft3D model results have given quite good insight in how the confluence/bifurcation Oude Maas and Spui affects the flow field at the scour hole Beerenplaat during a tidal cycle. Unfortunately, they were not suitable for investigating any of the 3D flow processes or their tidal response. Despite, some hypothesis and expectations were given. An initial link between the flow process and morphological development of the scour hole Beerenplaat could not be established.

7.2. Sub research questions

- 1. What was the morphological development of the river bottom at the scour hole Beerenplaat and the location of the pilot nourishment in the Oude Maas?
 - The scour hole Beerenplaat has the typical scour hole profile with a steep upstream slope and quite gentle downstream slope. Though, it is a dynamic scour hole which has developed in three different phases. During these phases the scour hole expanded in both upstream and downstream direction, with different growth rates. Most likely these different phases are caused by either the heterogeneous subsoil, varying hydraulic conditions or anthropogenic influences. In the last ten years, larger upstream than downstream expansion rates were observed. During the upstream growth, the slope angle remained constant and the deepest point of the scour hole migrated along. On top of that, it was shown that the scour hole Beerenplaat appears to be growing into the Spui. It is expected that the scour hole will keep on expanding in the near future. Using the Breusers equations, it was suggested that the scour hole Beerenplaat has an equilibrium depth which has not yet been reached. Most likely the scour depth is close to, or in, the stabilization stage. Overall the scour hole Beerenplaat

- was, and probably still is, a dynamic scour hole. Presumably, it will pose more threat to the stability of banks and dikes in the near future.
- The part of the pilot nourishment constructed at scour section 6 has stabilized the river bed locally and prevented further deterioration of the river bottom. It will most likely function for a few more years since it has been eroded for only 10 25 % between June 2019 and February 2021. The other part of the pilot nourishment, constructed at the shallower scour section 5, is also still present in February 2021. Since the pilot nourishment, the river bottom at this section is characterized by estuarine sand waves, formed by both the seasonal river flow and the tide. It is hypothesised that due to the nourishment more suitable sediment (noncohesive or coarser) became available, which allowed for the growth of these bedforms.
- 2. How is the flow field at the confluence/bifurcation Oude Maas & Spui shaped during a tidal cycle?
 - The flow field at the scour hole Beerenplaat is continuously changing due to the tidal forcing
 and the river discharge. No stationary flow field exists. The tide is responsible for switching
 the flow direction in the system between ebb and flood. During ebb the flow is directed
 downstream towards sea but during flood the flow is moving upstream, land inwards.
 - At peak ebb flow the system behaves as a confluence with flow from both the Oude Maas and Spui joining at the scour hole Beerenplaat. The largest flow velocities are found when the flow leaves the scour hole. Four of the six flow zones, observed at a uni-directional confluence, are also seen here (stagnation zone, deflection zone, maximum velocity zone and a recovery zone). Horizontal flow recirculation was not observed and the presence of the shear layer was questionable since only one recirculation cell was seen in the secondary flow. Different hydraulic conditions during peak ebb flow will not lead to different features of the flow field. They only affects the magnitude in which the current features appear. The Delft3D model has shown that the secondary flow downstream of the confluence can take the shape of three characteristic patterns. While it would be expected that two counteracting recirculating cells are observed in the joining flows, all the characteristic patterns only contained one. This is most likely caused by the presence of the scour hole. It is reasoned that the secondary flow moves through two of the three patterns during ebb flow. The third pattern is only encountered if very high ebb water levels are present. These high ebb water level should be caused by a influences from sea and not by larger seasonal river discharges, since salinity is of influence. It is still uncertain if the secondary flow in the field behaves similar since it could not be identified out of the ADCP measurements.
 - During peak flood flow, the system behaves as a bifurcation, splitting the flow over both branches. The largest flow velocities are found on the same location but now the flow enters the scour hole here. No large flow velocities could be observed on the upstream slope or between the scour hole Beerenplaat and the Spui. However, this may be distorted by the incorrect geometry of the scour hole Beerenplaat in the model. A small horizontal flow recirculation zone was spotted at the downstream corner of the bifurcation. During flood, no secondary flow patterns were encountered at the scour hole Beerenplaat. Also for flood, different hydraulic conditions will not lead to different features of the flow field, it only affects the magnitude in which the current features appear.
 - When the flow changes direction, either from flood to ebb or the other way around, no slack
 water conditions are encountered. The moment the flow direction switches is not equal for
 the system, but is locally varying. As a result many horizontal recirculation zones form, but
 they are paired with only low velocities. The interaction of the tide and the seasonal river
 discharge determine the point in time at which the entire system has switched its direction.
- 3. Which of the 3D flow processes are present inside the scour hole Beerenplaat and what is the influence of the flow direction and intensity on them?
 - Unfortunately the limitations and functioning of both the ADCP device and the Delft3D model
 made them not suitable to investigate the 3D flow processes inside the scour hole Beerenplaat. Despite, some expectations and hypothesis have been given. A first indication is
 that flow contraction will not develop during either ebb or flood. However, this is still paired

with uncertainty due to the subtlety of the processes and potential influence of the confluence/bifurcation. It is expected that the (curved) recirculation zone will develop, but only during ebb if the flow enters the scour hole on its steepest side. Based on the hypothesis of Bom (2017), it is hypothesised the horseshoe vortex can form during ebb flow, given that flow contraction is actually present. The vortex will not develop during flood since the profile of the scour hole Beerenplaat does not allow the formation of a recirculation zone.

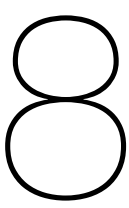
- Due to the absence of the 3D flow processes in the model results and the ADCP measurements, it was not possible to investigate the influence of the flow intensity on the 3D flow processes.
- 4. To what extend do the flow processes at the scour hole Beerenplaat and their tidal response give an explanation of the morphological development?
 - The confluence/bifurcation flow process could not be fully included since the Delft3D model results during flood flow were distorted. Due to an incorrect geometry of the scour hole in the model, there can not be accounted for the system behaving as a bifurcation. The hydraulic forcing of only the confluence does not explain any of the associated parts of the morphological development. The expected presence of the (curved) recirculation zone during ebb flow, has clarified why the upstream slope angle remained stable and why the location with the largest scour depth migrated upstream. Nevertheless, a large part of the morphological development of the scour hole Beerenplaat remains unexplained. Presumably, including the hydraulic forcing of the bifurcation would result in a much better explanation.

7.3. Main research question

How are the flow processes at the scour hole Beerenplaat influenced by the tide and in what way does this affect the morphological development?

- · If the tide would not be present, the (seasonal) river discharge would force the system, spanning the scour hole Beerenplaat and the junction of the Oude Maas and the Spui, on its own. In this situation the system would behave only as a confluence, characterized by the different flow zones and secondary flow. Most likely the system would reach stationary conditions over time. However, the presence of the tide interferes with this behavior. During ebb, the tide pushes no flow into the delta and the river discharge can maintain the upper hand. As a result, the system still behaves as a confluence with the similar characteristics. However, during flood the tide penetrates far into the delta, becoming dominant over the river discharge and changing the entire flow direction of the system. Now it behaves as a bifurcation, leading to a flow field with different characteristics. These different characteristics include flow direction, magnitude and secondary flow. Unfortunately, it remains yet uncertain how the flow field inside the scour hole Beerenplaat is exactly shaped during flood, due to the incorrect geometry of the scour hole in the Delft3D model. Despite, it is known that the system changes from a confluence to a bifurcation and the other way around during each tidal cycle. Since the tidal forcing and the seasonal river discharge each fluctuate with different time scales, the system will not reach stationary conditions. This shows how the flow field at confluence/bifurcation, which influences the scour hole Beerenplaat, is affected by the tide.
- The tide influences the 3D flow processes quite a bit. During ebb, the flow enters the scour hole on its steepest slope allowing for the development of a (curved) recirculation zone. During flood, it can not develop due to the very gentle slopes of the scour hole. It was not possible to conclude if flow contraction and the horseshoe vortex are present at the field. Despite, following the hypothesis of Bom (2017) it is possible to comment on the influence of the tide on the horseshoe vortex. If the horseshoe vortex is present at the scour hole Beerenplaat, it will not develop during flood flow since no recirculation zone can form.
- Due to the tide, the flow processes are differently shaped or present in between ebb and flood.
 As a result, different areas of the scour hole are attacked by the flow. During ebb flow, the hydraulic forcing intends to expand the scour hole in the downstream direction and make it deeper.

Contributors to this are the expected recirculation, attacking the deepest part of the scour hole at the reattachment point and impacting the downstream slope, and the system behaving as a confluence, implying attack of the downstream slope by the joined flow of the Oude Maas and Spui. During flood, it remains yet uncertain how the system behaving as a bifurcation affects the scour hole. However, it is expected that this part of the flow causes serious attack of the upstream slope. Significant deepening of the scour hole Beerenplaat during flood flow is not expected.



Recommendations

First, recommendations based on this research will be given. After that, recommendations on dealing with the dynamic scour hole Beerenplaat are given.

8.1. Recommendations based on this research

In order to fully understand the hydraulic conditions and the morphological development of the scour hole Beerenplaat, the following recommendations are given.

- Update the bathymetry in the Delft3D model and analyze the output of future model runs. In this way, there can be investigated how the system behaving as a bifurcation actually affects the scour hole Beerenplaat. It can confirm if there is indeed significant attack of the upstream slope during flood and could potentially explain the growth towards the Spui.
- Develop a new CFD model which is completely suitable to simulate and study the 3D flow processes inside the scour hole Beerenplaat. Based on Bom (2017), a first suggestion would be an OpenFOAM model with the Generalized k-ω turbulence model.
- Look into the influence of the operation of the Haringvliet sluices on the flow field. To achieve this, runs with the Delft3D model on a time frame after January 2019 can be done. The operating of the sluices must be included in the boundary and initial conditions.
- Investigate the composition of the heterogeneous subsoil at the scour hole Beerenplaat. This research expects that the heterogeneous subsoil played a role in the different morphological development phases and the equilibrium scour depth. Most likely, the composition of the subsoil should be included to understand the past and predict the future behavior of the scour hole Beerenplaat, even if the hydraulic conditions are fully understood.

8.2. Recommendations for the scour hole Beerenplaat

- Most likely the scour hole will not stop growing in the near future. Not in size or depth. Therefore it is recommended to monitor the scour hole and especially the steep slopes, since they pose the most threat to the stability of both banks and dikes. If intervention is required, a sand nourishment has been proven to be a viable option for stabilizing the river bottom at the Oude Maas.
- If more sand nourishments are constructed at the scour hole Beerenplaat, it is important to recognize that no slack water conditions exist. When the flow is changing direction, there is always some flow in transition around the scour hole. As a result, this can affect the construction of a

nourishment. Fine sediments dumped from the water surface can be transported by this flow, making the nourishment inefficient and waste available sediments. Therefore it is recommended to include this phenomena in the design of a new nourishments. If it appears to be a problem, coarser sediment should be used or the fine sediments should be dumped closer to the river bottom.

- The ADCP measurements have given insight in the hydraulic conditions at the scour hole Beerenplaat. However, they are only a snapshot of what is occurring during an entire tidal cycle. The Delft3D model has shown that the flow field is very dynamic and continuously changing. On top of that, the flow in the cross-stream direction appeared to turbulent for the ADCP device to accurately capture. Therefore no additional value is seen in taking more of these ADCP measurements at the scour hole Beerenplaat.
- Contrary, the MBES measurements were found very valuable for understanding the scour hole Beerenplaat and are a good tool for monitoring its behavior. It is recommended to continue with taking and evaluating these measurements.
- If it is intended to construct more shallow nourishments in the Rhine-Meuse delta, there is recommended to further investigate the development of estuarine sand waves at them. The rather large bed form height can pose a threat for the navigability of vessels, especially in shallower parts of the delta. It is yet uncertain if the formation of such bedforms at the pilot site was a coincidence or that the two should be linked in the Rhine-Meuse delta.

- 1. Alhaddad, S. M. S. (2021). *Breaching Flow Slides and the Associated Turbidity Currents* (Doctoral Thesis). Technical University Delft.
- 2. Allen, J. R. L. (1968). The nature and origin of bed-form hierarchies. Sedimentology, 10, 161–182.
- 3. Allen, J. R. L. (1980). Sand waves: A model of origin and internal structure. *Sedimentary geology*, 281–328.
- 4. Ashmore, P. E., Ferguson, R. I., Prestegaard, K. L., Ashworth, P. J., & Paola, C. (1992). Secondary flow in anabranching confluences of a braided, gravel-bed stream. *Earth Surface Processes and Landforms*, *17*, 299–311.
- 5. Babakaiff, C. S. (1993). Flow Hydraulics, Bedforms and Macroturbulence of Squamish River Estuary (MSc Thesis). Simon Fraser University.
- 6. Beltaos, S., Carter, T., & Prowse, T. (2011). Morphology and genesis of deep scour holes in the mackenzie delta. *Canadian Journal of Civil Engineering*, 38(6), 638–649.
- 7. Best, J. L. (1986). The morphology of river channel confluences. *Progress in Physical Geography: Earth and Environment*, *10*(2), 157–174.
- 8. Best, J. L., & Bridge, J. S. (1992). The morphology and amplitude of low amplitude bedwaves upon upper-stage plane beds and the preservation of planar laminae. *Sedimentology*, *39*, 737–752.
- 9. Bilal, A., Xie, Q., & Zhai, Y. (2020). Flow, Sediment, and Morpho-Dynamics of River Confluence in Tidal and Non-Tidal Environments. *Marine Science and Engineering*, *8*(591).
- 10. Biron, P., Best, J. L., & André, G. R. (1996). Effects of bed discordance on flow dynamics at open channel confluences. *Journal of Hydraulic Engineering*, *122*, 676–682.
- 11. Biron, P., Roy, A., Best, J., & Boyer, C. (1993). Bed morphology and sedimentology at the confluence of unequal depth channels. *Geomorphology*, *8*, 115–129.
- 12. Bom, S. (2017). Scour holes in heterogeneous subsoil: A numerical study on hydrodynamic processes in the development of the scour holes (Master Thesis). Technical University Delft.
- 13. Boyer, C., Roy, A. G., & Best, J. L. (2006). Dynamics of river channel confluence with discordant beds: Flow turbulence, bed load sediment transport, and bed morphology. *Journal of Geophysical Reserach: Earth Surface*, *111*, 1–22.
- 14. Breusers, H. N. C. (1966). *Conformity and time scale in two-dimensional local scour* (Publication 40). Delft Hydraulics.
- 15. Breusers, H. N. C., & Raudkivi, A. J. (1991). Scouring (1st ed.). Balkema.
- 16. Buschman, F., Forzoni, A., van den Ham, G., & Hijma, M. (2015). *Opvullen en afdekken ontgrondingskuilen in de Oude Maas* (Technical Report 1220038-015-ZWS-0002). Deltares.
- 17. Chiew, Y. M., & Parker, G. (1994). Incipient sediment motion on non-horizontal slopes. *Journal of Hydraulic Research*, *32*(15), 649–660.
- 18. Colbo, K., Ross, T., Brown, C., & Weber, T. (2014). A review of oceanographic applications of water column data from multibeam echosounders. *Estuarine, Coastal and Shelf Science*, *145*, 41–56.
- 19. Dai, w., Bilal, A., Xie, Q., Ahmad, I., & Joshi, I. (2020). Numerical modeling for hydrodynamics and near-surface flow patterns of a tidal confluence. *Journal of Coastal Research*, *36*, 295–312.
- 20. Delft Hydraulics. (1970). Begin van Beweging (report M 1048).
- 21. Deltares. (2021). D-Flow Flexible Mesh (User Manual).
- 22. Dietz, J., & Wittke, W. (1969). *Kolkbildung in feinen oder leichten Sohlmaterialien bei strömendem Abfluß* (Phd thesis). Universität Fridericiana Karlsruhe.

23. Ghobadian, R., & Shafai Bajestan, M. (2007). Investigation of Sediment Patterns at River Confluence. *Journal of Applied Sciences*, 7(10), 1372–1380.

- 24. Ginsberg, S. S., & Perillo, G. M. E. (1999). Deep-scour holes at tidal channel junctions, bahia blanca estuary, Argentina. *Marine Geology*, *160*(1).
- 25. Hoffmans, G. J. C. M. (1990). *Concentration and flow velocity measurements in a local scour hole* (report 4-90). Faculty of Civil Engineering, Hydraulic and Geotechnical Engineering Division, Delft University of Technology, Delft.
- 26. Hoffmans, G. J. C. M. (1992). *Two-dimensional mathematical modelling of local-scour holes* (Doctoral Thesis). Technical University Delft.
- 27. Hoffmans, G. J. C. M., & Booij, R. (1993). The influence of upstream turbulence on local scour holes. *Proc. 25th IAHR-congress, Tokyo*.
- 28. Hoffmans, G. J. C. M., & Verheij, H. J. (1997). Scour manual. A.A. Balkema.
- 29. Huismans, Y., Koopmans, H., Wiersma, A., de Haas, T., Berends, K., Sloff, K., & Stouthamer, E. (2021). Lithological control on scour hole formation in the rhine-meuse estuary. *Geomorphology*, *385*.
- 30. Huismans, Y., & van Duin, O. (2016). *Advies beheer rivierbodem van de Rijn-Maasmonding* (Technical Report 1208925-000-ZWS-0040). Deltares.
- 31. Hulscher, S. J. M. H. (1996). Tidal-induced large-scale regular bed form patterns in a three-dimensional shallow water model. *Journal of Geophysical Research*, 20, 727–20, 744.
- 32. Hulscher, S. J. M. H., & Dohmen-Janssen, C. M. (2005). Introduction to special section on marine sand wave and river dune dynamics. *Journal of Geophysical Research*.
- 33. Izbash, S. V. (1932). Construction of Dams by dumping of Stone in running Water. Moscow-Leningrad.
- 34. Jansen, P. P., van Bendegom, L., van den Berg, J., de Vries, M., & Zanen, A. (1979). *Principles of river engineering: The non-tidal alluvial river*. Delftse Uitgevers Maatschappij.
- 35. Julien, P., Klaassen, G., Ten Brinke, W., & Wilbers, A. (2002). Case study: Bed resistance of rhine river during 1998 flood. *Journal of Hydraulic Engineering*, *128*(12), 1042–1050.
- 36. Khosravinia, P., Malekpour, A., Nikpour, M. R., & Dalir, A. H. (2020). Scour depth in confluences considering tributary flow, bank slope, and post-confluence conditions. *Water supply*, *20*(6), 2389–2399.
- 37. Kleinhans, M. G., Leuven, J. R. F. W., Braat, L., & Baar, A. (2017). Scour holes and ripples occur below the hydraulic smooth to rough transition of movable beds. *Sedimentology*, *64*, 1381–1401.
- 38. Koopmans, H. (2017). Scour holes in tidal rivers with heterogeneous subsoil under anthropogenic influence (Master Thesis). Technical University Delft.
- 39. Kostaschuk, R., & Best, J. (2005). Response of sand dunes to variations in tidal flow: Fraser estuary, canada. *Journal of Geophysical Research*, *10*(04).
- 40. Kostaschuk, R., Best, J., Villard, P., Peakall, J., & Franklin, M. (2005). Measuring flow velocity and sediment transport with an acoustic Doppler current profiler. *Geomorphology*, *68*(1-2), 25–37.
- 41. Lesser, G. R., Roelvink, J. A., van Kester, J. A. T. M., & Stelling, G. S. (2004). Development and validation of a three-dimensional morphological model. *Coastal Engineering*, *51*, 883–915.
- 42. McGovern, D. J., Ilic, S., Folkard, A. M., McLelland, S. J., & Murphy, B. J. (2014). Time development of scour around a cylinder in simulated tidal current. *Journal of Hydraulic Engineering*, 140(6).
- 43. Nakagawa, H., & Nezu, I. (1987). Experimental investigation on turbulent structure of backward-facing step flow in an open channel. *Journal of Hydraulic Research*, *25*(1), 67–88.
- 44. Paarlberg, A. J., Dohmen-Janssen, C. M., Hulscher, S. J. M. H., Termes, P., & Schielen, R. (2010). Modelling the effect of time-dependent river dune evolution on bed roughness and stage. *Earth Surfaces Processes and Landforms*.
- 45. Parker, G. (1983). Confluence Scour in Coarse Braided Streams. *Water Resourche Research*, 19, 392–402.
- 46. Parker, G., & Garcia, M. (1991). Entrainment of bed sediment into suspension. *Journal of Hydraulic Engineering*, 117(4), 414–435.

47. Porter, K. E., & Simons, R. R. (2014). Laboratory investigation of scour development through a spring-neap tidal cycle. *Journal of Hydraulic Engineering*.

- 48. Raudkivi, A. J. (1997). Ripples on Stream bed. Journal of Hydraulic Engineering, 123.
- 49. Reesink, A. J. H., Parson, D. R., Ashworth, P. J., Best, J. L., Hardy, R. J., Murphy, B. J., McLelland, S. J., & Unsworth, C. (2018). The adaptation of dunes to changes in river flow. *Earth Science Reviews*, *185*, 1065–1087.
- 50. Rijkswaterstaat. (2019). Het verhaal van de Rijn-Maasmonding.
- 51. Rijkswaterstaat Zuid-Holland. (2012). *Stroomwijzer Rijn-Maasmonding watersysteemdeel de Oude Maas.* van Spijk, A. & Broekhuizen, A.
- 52. Rodi, W. (1984). Turbulence models and their application in hydraulics, state-of-the-art paper article sur l'etat de connaissance. *IAHR Paper presented by the IAHR-Section on Fundamentals of Division II: Experimental and Mathematical Fluid Dynamics*.
- 53. Schiereck, J. G., & Verhagen, H. J. (2019). *Introduction to bed, bank and shore protection* (2nd ed.). VSSD.
- 54. Shadeed, R., Mohammadian, A., & Gildeh, H. K. (2019). A comparison of standard k–ε and realizable k–ε turbulence models in curved and confluent channels. *Environmental Fluid Mechanics*, 19, 543–568.
- 55. Shadeed, R., Yan, X., & Mohammadian, A. (2021). Review and comparison of numerical simulations of secondary flow in river confluences. *Water*, *13*(14).
- 56. Shakibania, A., Majdzade Tabatabai, M. R., & Zarrati, A. R. (2010). Three-dimensional numerical study of flow structure in channel confluences. *Canadian Journal of Civil Engineering*, 37, 772–781.
- 57. Shields, A. (1936). *Anwendung der Aenlichtkeitsmechanik und der Turbulenzforschung auf die Geschiebebewegung* (Preußischen Verscuhsansalt für Wasserbouw).
- 58. Simpson, M. R. (2002). *Discharge measurements using a broadband acoustic Doppler current profiler*. U.S. Geological Survey Open-File Report 01–01.
- 59. Sloff, C. J. (2020). *Morfologische ontwikkeling suppletiepilot Oude Maas* (Conceptual report 11205234-015). Deltares.
- 60. Sloff, C. J., van Spijk, A., Stouthamer, E., & Sieben, A. (2013). Understanding and managing the morphology of branches incising into sand-clay deposits in the Dutch Rhine Delta. *International Journal of Sediment Research*, 28, 127–138.
- 61. Smith, J., & Mclean, S. (1984). A model for flow in meandering streams. *Water Resources Research WATER RESOUR RES*, 20.
- 62. Song, C. G., Seo, I. W., & Kim Do, Y. (2012). Analysis of secondary current effect in the modeling of shallow flow in open channels. *Advances in Water Resources*, *41*, 29–48.
- 63. Stenfert, J. G. (2017). Scour holes in heterogeneous subsoil: An experimental study to improve knowledge of the development of scour holes in heterogeneous subsoil (Master Thesis). Technical University Delft.
- 64. Sterlini, F., Hulscher, S. J. M. H., & Hanes, D. M. (2009). Simulating and understanding sand wave variation:a case study of the golden gate sand waves. *Journal of Geophysical Research*.
- 65. Struiksma, N., Olesen, K. W., Flokstra, C., & de Vriend, H. (1985). Bed deformation in curved alluvial channels. *Journal of Hydraulic Research*, 23, 57–79.
- 66. Uijttewaal, W., Huismans, Y., & Koopmans, H. (2016). *A scaled experimental pilot-study on deep scour holes in riverbeds of heterogeneous composition* (Technical Report). TU delft, Deltares.
- 67. Unde, M. G., & Dhakal, S. (2009). Sediment characteristics at river confluences: A case study of the mula-kas confluence, maharashtra, india. *Progress in Physical Geography: Earth and Environment*, 33, 208–223.
- 68. van der Meulen, T., & Vinje, J. J. (1975). *Three-dimensional local scour in noncohesive sediments* (Proc. 16th IAHR-congress). Sao Paulo.
- 69. van der Sande, W. M., Roos, P., & Hulscher, S. J. M. H. (2019). Investigating idealized modelling of estuarine sand waves. *Marine and River Dune Dynamics*.

70. Van Velzen, G., Raaijmakers, T. C., & Hoffmans, G. J. C. M. (2015). Scour development around the eastern scheldt storm surge barrier-field measurements and model prediction. *Scour and Erosion - Cheng, Draper and An*.

- 71. van Balen, W. (2010). *Curved open-channel flows a numerical study* (Doctoral Thesis). Technical University Delft.
- 72. van Gerwen, W. (2016). *Modelling the equilibrium height of offshore sand waves* (Master thesis). University of Twente.
- 73. van Rijn, L. C. (1984a). Sediment transport, Part 1: Bed load transport. *Journal of Hydraulic Engineering*, *110*(10), 1431–1456.
- 74. van Rijn, L. C. (1984b). Sediment transport, Part 2: Suspended load transport. *Journal of Hydraulic Engineering*, 110(10), 1613–1631.
- 75. van Rijn, L. C. (1984c). Sediment transport, Part 3: Bed forms and alluvial roughness. *Journal of Hydraulic Engineering*, *110*(12), 1733–1755.
- 76. van Rijn, L. C. (1993). *Principles of sediment transport in rivers, estuaries and coastal seas*. Aqua Publications.
- 77. Ven Te Chow. (1959). Open channel hydraulics. McGraw-Hill.
- 78. Vermeulen, B., Hoitink, A. J. F., Hidayat, H., & van Berkum, S. W. (2014). Sharp bends associated with deep scours in a tropical river: The river mahakam (east kalimantan, indonesia). *Journal of Geophysical Research: Earth Surface*, 119(7), 1441–1454.
- 79. Vermeulen, B., Sassi, M. G., & Hoitink, A. J. F. (2014). Improved flow velocity estimates from moving-boat ADCP measurements. *Water Resource Research*, *50*, 4186–4196.
- 80. Weber, L. J., D., S. E., & Mawer, N. (2001). Experiments of flow at a 90 °open-channel junction. *Journal of Hydraulic Engineering*, 127(5), 340–350.
- 81. Wilkerson, G., Sharma, S., & Sapkota, D. (2019). Length for Uniform Flow Development in a Rough Laboratory Flume. *Journal of Hydraulic Engineering*, 145.
- 82. Xie, Q., Yang, S., J.and Lundström, & Dai, W. (2020). Understanding Morphodynamic Changes of a Tidal River Confluence through Field Measurements and Numerical Modeling. *Journal of Coastal Research*, 36, 295–312.
- 83. Yuan, S., Tang, H., Xiao, Y., Qiu, X., & Xia, Y. (2018). Water flow and sediment transport at open-channel confluences: An experimental study. *Journal of Hydraulic Research*, *56*, 333–350.
- 84. Zanke, U. (1978). Zusammenhänge zwischen Strömung und Sedimenttransport, Teil 2: Berechnung des Sedimenttransportes hinter befestigten Sohlenstrecken-Sonderfall zweidimensionaler Kolk (Phd thesis). TU Hanover.
- 85. Zarillo, G. A. (1982). Stability of bedforms in a tidal environment. *Marine Geology*, 337–351.
- 86. Zuylen, J. A. (2015). *Development of scour in non-cohesive sediment under a poorly erodible top layer* (Master Thesis). Technical University Delft.



Additional literature

A.1. Initiation of motion

To grasp how scour holes become larger it is important to understand when soil particles start to move. This initiation of motion is different for non-cohesive sediments like sand and for cohesive sediments like clay.

Non-cohesive sediments

According to Schiereck and Verhagen (2019), probably the best known formula to describe initiation of motion of non-cohesive sediments is Shields (1936). This equation considers the forces proposed on a horizontal river bed during uniform flow. The load forces on the bed are represented by the critical shear stress that the flow exerts on the bed. The resistance is represented by the weight of the soil particles at the bottom. If the loading exceeds the strength there will be movement of sediment particles. The shield mobility parameter can be computed with equation (A.1). Shield was able to construct a graph (figure A.1) based on experimental data, which shows the critical mobility parameter versus the sedimentological parameter for different stages or particle movement. The sedimentological parameter has been defined by van Rijn (1984a) and can be described by equation (A.2). The Shields graph can be used to determine if erosion takes place for certain flow conditions. An important remark to make, turbulent oscillations and pressure fluctuations can entrain particles which in turn can be picked up by larger turbulent features. The Shields equations does not account for that.

$$\psi_c = \frac{load}{strength} = \frac{\tau_c}{(\rho_s - \rho_w)gd} = \frac{u*_c^2}{\Delta gd} = \frac{\overline{u}_c^2}{C^2 \Delta d}$$
 (A.1)

Where: ψ_c [-] critical mobility parameter d[m] grain size $[N/m^2]$ critical shear stress relative density Δ [-] [kg/m³] density of the soil $u*_c$ [m/s] critical flow velocity depth averaged critical flow velocity density of water \overline{u}_c [m/s] [kg/m³] ρ_w gravitational acceleration $[m^{0.5}/s]$ $[m/s^2]$ Chézy coefficient

$$D* = d\left(\frac{\Delta g}{\nu}\right)^{1/3}$$

$$\nu = \frac{40 \cdot 10^{-6}}{20 + \theta}$$
(A.2)

A.1. Initiation of motion 88

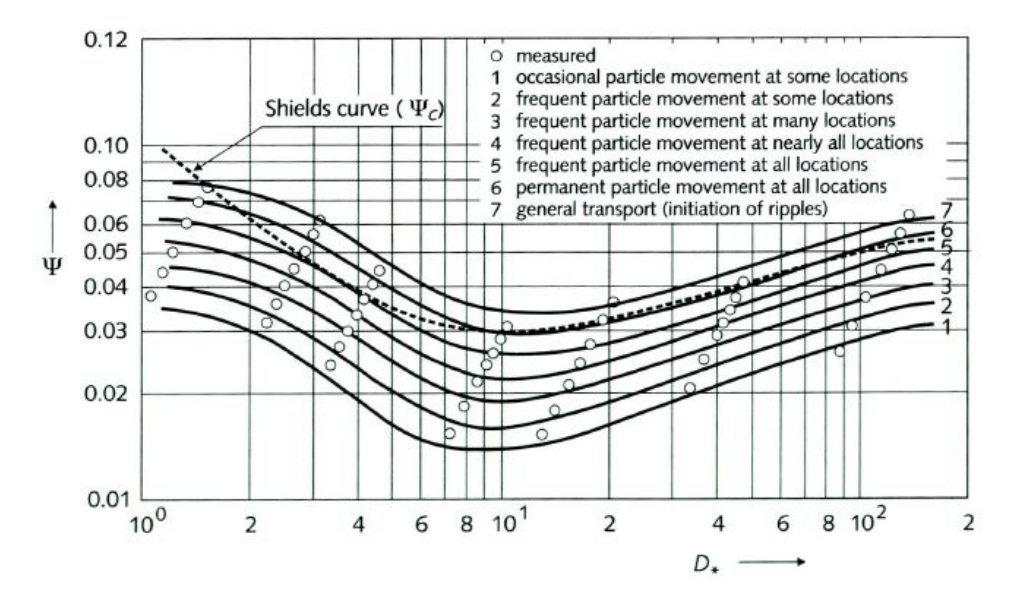


Figure A.1: Critical Shield parameter versus the sedimentological parameter (Hoffmans & Verheij, 1997).

Where: D* [-] sedimentological parameter θ [°C] temperature

 ν [m²/s] kinematic viscosity

Cohesive sediments

In general there are no applicable equations for the initiation of motion of cohesive sediments in relation to scour hole development. Most equations are related to one or two particular parameters influencing the erosion or a specific sediment. Furthermore, the erosion of cohesive sediment is a complex process due to the cohesive bonds between particles (Hoffmans & Verheij, 1997). However, there are significant cohesive clay layers present at the Rhine-Meuse delta, that play a role in the behaviour and development of scour holes. Therefore a short explanation of the erosion mechanisms of clay and initiation of motion is given. Sloff et al. (2013) assumed two possible mechanisms for the erosion of a cohesive clay layer. The first mechanisms is abrasive erosion, during which grains are slowly peeled of the clay layer, if the exerted shear stresses are higher than the critical shear stress of the material (Hoffmans & Verheij, 1997). The second mechanism is the pulling-off of fragments of clay by the flow. For a first estimate of the initiation of motion, the results of Ven Te Chow (1959) in table A.1 can be used to indicate a critical flow velocity at which this occurs.

	Porosity		
	20%	40%	60%
Critical velocity [m/s]	1.5 - 1.8	1.0 - 1.2	0.1 - 0.4

Table A.1: Critical velocity of clay (Ven Te Chow, 1959).

A.1.1. Adaptation Shields equation

The Shields equation only holds for uniform flow over a horizontal bed, which is not encountered often in nature. To allow for a practical application of the Shields equation, Schiereck and Verhagen (2019) derived a slope factor K_s that reduces the strength and a turbulence factor K_v that increases load, to account for non-uniform flow. These factors allow the adapted Shields equation (equation (A.3)) to be used in more situations. However, the turbulence factor K_v can only be used for a first approach since it has been determined with curve-fitting through data sets and does not necessarily describe complete influence of turbulence on erosion. Contrary, the factor K_s can be used throughout since the results of

laboratory experiments (Chiew & Parker, 1994; Delft Hydraulics, 1970) showed similar behaviour.

$$\psi_c = \frac{load}{strength} = \frac{K_v^2 \ \overline{u}_c^2}{K_s \ C^2 \Delta d} \tag{A.3}$$

A.1.2. Izbash

An alternative approach is to determine initiation of motion with Izbash. This approach considers the forces on an individual grain and tries to determine the balance between these forces. If the active forces (flow, turbulence, etc.) are larger than the passive forces (gravity and friction between grains) sediment grains will starts to move. The balance of forces could be reduced until equation (A.4). Izbash (1932) found experimentally the value for the constant K reducing equation (A.4) into equation (A.5).

A drawback of this approach is that Izbash did not give a clear description of the location of the velocity and the diameter. According to Schiereck and Verhagen (2019), this approach can be used best in the case of shallow water and big stones since this is less critical. Furthermore, it is a suitable approach in cases of non-uniform flow or in conditions where the velocity does not depend on an equilibrium between flow force and bed friction force (e.g. water jets) (Schiereck & Verhagen, 2019).

$$u_c^2 = K\Delta gd \tag{A.4}$$

$$u_c = 1.2\sqrt{2\Delta g d} \tag{A.5}$$

Where: g [m/s 2] gravitational acceleration d [m] diameter Δ [-] relative density K [-] constant u_c^2 [m/s] critical flow velocity at which grains start to move

A.2. Sediment transport

Flowing water is able to transport sediment grains from the river bottom. The transport of sediment can be subdivided into two main mechanisms. First there is bed load transport which represents the transport of sediment over the bottom via rolling and sliding. The second mechanism is the suspended load transport which transports sediments that are suspended in the fluid. The bed load mechanism only transports bed material but the suspended load mechanism transports both bed material and wash load. Wash load is defined as the transport of material finer than bed material and has no relation to the transporting capacity of the stream (Jansen et al., 1979).

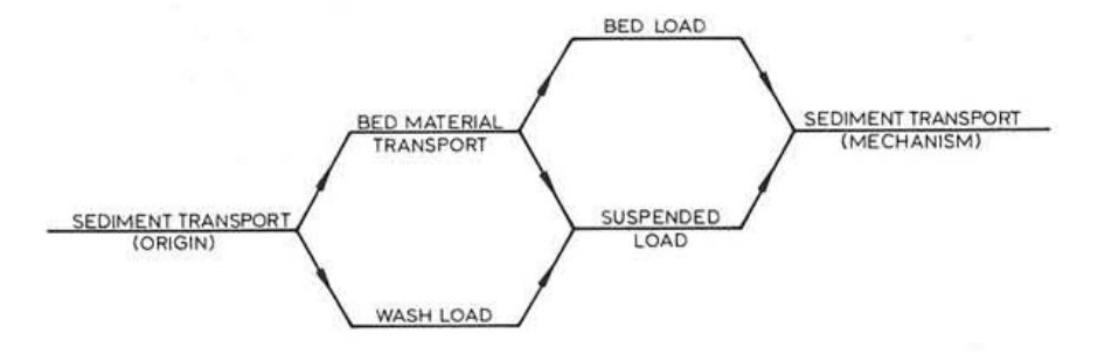


Figure A.2: Sediment transport (Jansen et al., 1979).

The amount of sediment transported by the flow is dependent on how erosion or sedimentation affects a certain river stretch. Exner was able to derive equation (A.6) that describes the exchange of sediments between the flow and the bed. The equation is based on the principle of mass conservation in a control volume (figure A.3). If either the bed erodes or sedimentates there will respectively be a positive or negative gradient in the sediment transport by the flow.

$$\frac{\partial z_b}{\partial t} + \frac{\partial q_s}{\partial x} = 0 \tag{A.6}$$

Where: z_b [m] bed level

t [s] time

 $q_s \quad [\mathrm{m}^2/\mathrm{s}] \quad \text{total sediment transport per unit width}$

x [m] length

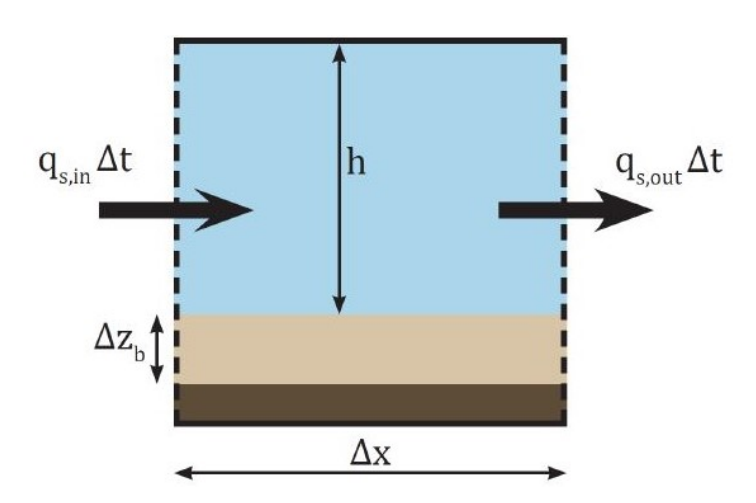


Figure A.3: Control volume for the derivation of the Exner equation, obtained from Bom (2017).

To describe the total sediment transport per unit width (q_s) , a sediment transport equation is required. Such sediment transport equation is often a function of the flow velocity and sediment properties. Many different empirical relations have been derived which try to describe the transport as accurate as possible. These are divided into relations that describe the bed load transport or the suspended load transport. Within this research, only the well known transport equations will be mentioned. A detailed description of these transport relations is at this stage out of the scope.

Bed load transport equations

Well known bed load transport equations are derived by Meyer-Peter-Müller and Engelund-Hansen. The Meyer-Peter-Müller equation can be used to compute the bed load transport with uniform size grains. The Engelund-Hansen equation can be used to compute the total bed-material transport. This includes a part of the suspended load but does not capture the wash load transport.

Suspended load transport equation

Parker and Garcia (1991) performed a study during which they investigated seven different equations that predict the suspended load transport and tested them against standard set of data. They were able to conclude that van Rijn (1984a) and Smith and Mclean (1984) predict the data the best. Based on these two relations Parker and Garcia (1991) also derived a suspended load transport equation with better predictive capabilities. However this equation was not tested on a broad range of different data sets and therefore the accuracy of the predictive capability can be questioned.

A.3. Scour holes 91

A.3. Scour holes

A.3.1. Types of scour

Scour can most easily be explained by looking at the simplified control volume in figure A.4. In this figure S_1 and S_2 represent respectively the incoming and outgoing total sediment transport per unit width. Scour of the bed occurs if there is a positive transport gradient in the downstream direction. In other words if $S_2 > S_1$. This can happen due to differences in either velocity or turbulence or in both (Schiereck & Verhagen, 2019).

Scour of the bed can be sub-classified into two groups, clear-water scour and live-bed scour. Clear-water scour occurs when there is no sediment transported into the control volume from upstream. In that case $S_2>S_1=0$. On the opposite, live-bed scour occurs when there is a supply of sediment into the control volume, $S_2>S_1>0$. According to Hoffmans (1992), these bed scour types influence the development of scour holes.

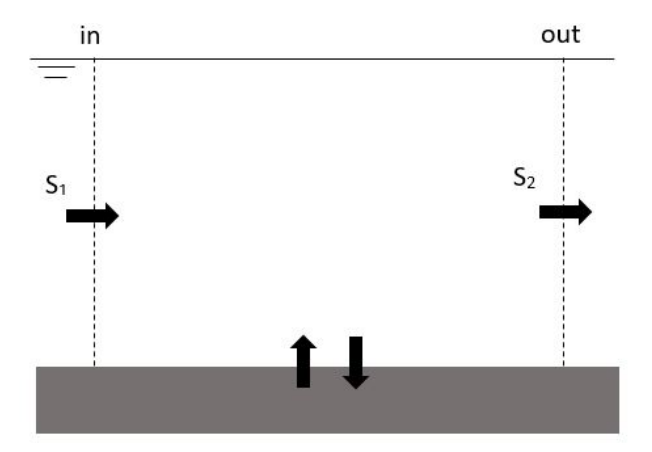


Figure A.4: Control volume for clear-water and live-bed scour, based on Schiereck and Verhagen (2019).

A.3.2. Empirical equation for equilibrium depth

Much research has be done to the Breusers method which describes scour hole development behind non erodible bed protections. According to Hoffmans and Verheij (1997) the Breusers method can be used to predict scour due to 3-dimensional flow, if the method is combined with computational results of horizontal models or with measurements obtained from scale models. Koopmans (2017) and Stenfert (2017) have focused on using the empirical Breusers equation to describe scour holes in the Rhine-Meuse delta that are characterized by the heterogeneous subsoil. First the empirical method of Breusers will be explained and after that there will be looked at the applicability of the Breusers method for scour holes in heterogeneous subsoil.

The Breusers method, equation (A.7), has been derived for clear-water scour holes behind a non erodible bed protection. This equation can be used to compute the (equilibrium) depth of the scour hole. It is an empirical equation to which much research has been done that fitted the exponent γ to different experimental data sets with different flow conditions (Breusers, 1966; Dietz & Wittke, 1969; van der Meulen & Vinje, 1975). According to this method scour holes behind a non erodible bed protection will eventually reach an equilibrium depth. Due to the sudden depth increase the flow conditions become less intense and are not able to erode more sediments from the bottom of the scour hole. This equation, and hence reaching an equilibrium depth, does not indicate that the other dimensions of the scour hole have also reached an equilibrium. According to Hoffmans and Verheij (1997), equation (A.8) can be used as a first estimate for the characteristic time t_1 under non steady flow conditions. The relation of U_d has been proposed by Hoffmans (1992) and the equation for α by Hoffmans and Booij (1993).

A.3. Scour holes

The critical velocity u_c of non-cohesive sediments can be determined with the equations of Shields or Izbash, as were described in appendix A.1.

$$\frac{y_m}{y_{m,e}} = 1 - e^{\ln\left(1 - \frac{\lambda}{y_{m,e}}\right)\left(\frac{t}{t_1}\right)^{\gamma}} \tag{A.7}$$

Where: y_m [m] maximum scour depth at t [s] time

 $y_{m,e}$ [m] equilibrium scour depth t_1 [s] characteristic time at which $y_m=\lambda$

 λ [m] characteristic length scale γ [-] coefficient

$$t_{1} = \frac{K \cdot h_{0}^{2} \cdot \Delta^{1.7}}{(\alpha \cdot U_{d} - u_{c})^{4.3}}$$

$$U_{d} = \eta \cdot U_{m,t}$$

$$\alpha = 1.5 + 4.4 \cdot r_{0} \cdot f_{c}$$
(A.8)

[hours \cdot m^{2.3}/s^{4.3}] coefficient, K = 330Where: Kinitial water depth h_0 [m] Δ [-] relative density coefficient for flow velocity and turbulence intensity [-] characteristic mean velocity U_d [m/s] [m/s]critical mean velocity u_c $U_{m,t}$ [m/s] maximum velocity during a tide coefficient, $\eta = 0.75 - 0.85$ [-] [-] relative turbulence intensity, see part below r_0 roughness function, $f_c = C/C_0$ or $f_c = 1$ if $C < C_0$ f_c [-] C $[m^{0.5}/s]$ Chézy coefficient $[m^{0.5}/s]$ C_0 Reference Chézy coefficient, C_0 = 40

Important to mention is that the Breusers equation can only be used if the scour depth is larger than the water depth. Despite, scour holes can develop that have a smaller equilibrium depth than the water depth. Therefore Van Velzen et al. (2015) has adapted Breusers formulation towards equation (A.9).

$$\frac{y_m}{y_{m,e}} = 1 - e^{-\left(\frac{t}{t_1}\right)^{\gamma}} \tag{A.9}$$

Relative turbulence intensity

A statement for the relative turbulence intensity at a sill with a bed protection has been derived by Hoffmans and Booij (1993) (see equation (A.10)). The relative turbulence intensity is described at the transition of the non erodible bed protection and the erodible river bottom.

$$r_0 = \sqrt{0.0255 \left(1 - \frac{D}{h_0}\right)^{-2} \left(\frac{L_p - 6D}{6.67h_0} + 1\right)^{-1.08} + 1.45 \frac{g}{C^2}} \quad \text{for } L_p > 6D$$
 (A.10)

Where: h_0 [m] initial water depth L_p [m] length of the bed protection

D [m] sill height C [m $^{0.5}$ /s] Chézy coefficient at the bed protection

A.3. Scour holes

Bom (2017) reasons that this can be reduced towards equation (A.11) for scour holes in Rhine-Meuse delta. No sill is present at these scour holes and therefore the sill height D is set to 0 meter. The bed protection length L_p is assumed to be infinitely long since the highly erodible sand layers in the delta are protected by the poorly erodible sand layers in almost the entire delta. These poorly erodible clay layers are seen as a bed protection. This reduces equation (A.10) to equation (A.11). It is assumed that the Chézy value at the clay layer upstream of the scour hole should be used.

$$r_0 = 1.2\sqrt{\frac{g}{C^2}}$$
 (A.11)

A.3.3. Undermining of scour holes in heterogeneous subsoil

There is often referred to undermining if erosion below a bed protection occurs. However, this type of erosion can also occur in a heterogeneous subsoil without a bed protection. In that case the poorly erodible clay and peat layers on top of the highly erodible sand layers can be seen as a bed protection. The flow in a scour hole will erode the poorly erodible layers on top much slower than the highly erodible layers below. Stenfert (2017) performed small scale laboratory experiments to show how undermining would influence the flow inside the scour hole. During these laboratory experiments the poorly erodible layer was made out of concrete and would therefore not fail. The experiments showed that eventually the flow underneath the poorly erodible layer would re-feed the scour hole, as can be seen in 3c of figure A.5. It is expected that this will not happen in the Rhine-Meuse delta since the poorly erodible top layer consist out of clay and peat that will fail and collapse. Zuylen (2015) tried to simulate this type of failure due to undermining in laboratory experiments. These experiments showed that the poorly erodible top layer behaved as a falling apron, which showed that undermining was reduced but did not influence the depth development of the scour hole. To what extend undermining, failure of the top layer and behaviour of a falling apron happens in the field is uncertain. However it could be of significant influence on the behaviour and development of scour holes in the delta.

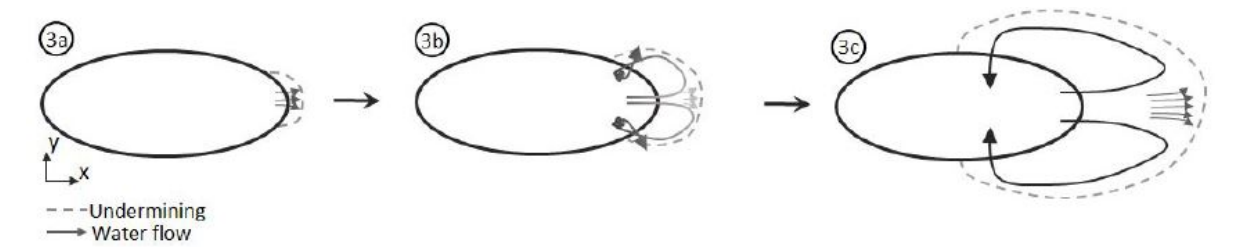


Figure A.5: Top view of the undermining process in a scour hole (Stenfert, 2017).

A.3.4. Effect of tide on scouring process

As already indicated, tidal effects play an important role for scour holes in the Rhine-Meuse delta. During the tidal cycle flow velocities fluctuate and even the flow direction can change. This makes the tidal influence on scour holes a complicated situation, since scour is dependent on these changing flow velocities. Studies on generation and development of scour holes in tidal environments without direct cause are rarely found (Ginsberg & Perillo, 1999). However some research has been done to scour holes with tidal conditions around hydraulic structures. Main conclusion of some of these studies are listed below. McGovern et al. (2014) was able to conclude that changing the flow direction will reshape the scour hole and make it more symmetric. Erosion will now take place on the former gentle downstream slope and sedimentation will take place on the former steep slope. Eventually the original shape of the scour hole will be mirrored if the new flow direction persists, as can be seen on figure 2.13b. However, a tide is (semi)diurnal and therefore the new flow direction will not persist long enough to develop a mirrored profile. The final profile is expected to be more symmetrical and therefore in between the two extremes. Porter and Simons (2014) focused on the influence of the tide on the time

scale of scour. The study was able to conclude that the time scales of scour in the spring-neap cycle are significantly different than for unidirectional flow conditions. Furthermore it could be concluded that the tidal asymmetry has a strong impact on the scour depth development.

Zuylen (2015) included the aspect of tidal conditions on scour holes formed in heterogeneous subsoil. A 2D clear-water scour laboratory experiment was created in which flow was reversed over a scour hole formed under unidirectional conditions (figure 2.13a). Out of the experiment it could be concluded that the transport of sedimentation of the former steep slope is mainly done by a migrating sand bar from the former gentle downstream slope. Much uncertainty on how tidal effects influence the scour hole development is still present.

A.4. Flow and sediment transport in a river bend

Flow

The flow in a bend is characterized by two components, the streamwise component and the transverse component as can be seen on figure A.6.

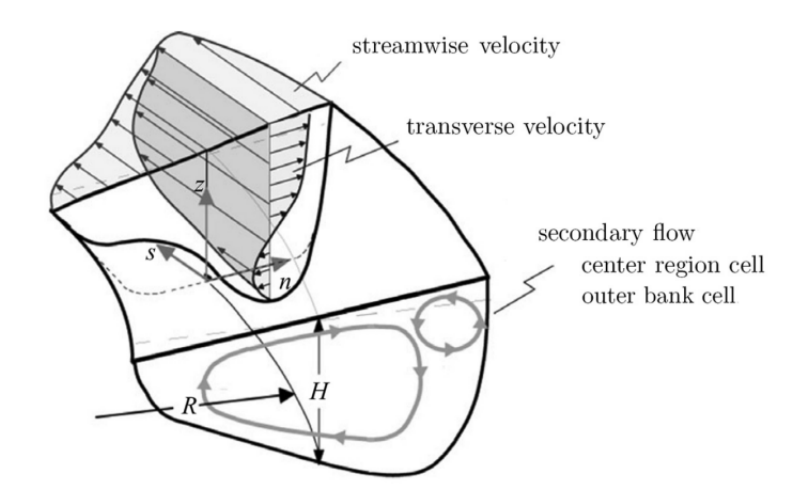


Figure A.6: Illustration of flow in a river bend (van Balen, 2010).

The streamwise component can be best explained by looking at uniform flow. The slope continuously transforms potential energy, via kinetic energy in the main flow and in the turbulent eddies, into heat (Schiereck & Verhagen, 2019). Eventually, an equilibrium will be reached between the bottom shear stress and the pressure component of the flow. If uniform conditions (stationary flow and a constant cross-section) persist long enough, the flow will be fully developed as can be seen on figure A.7 and a logarithmic velocity profile is created (Wilkerson et al., 2019). In reality the streamwise component will not be the idealized logarithmic profile since uniform flow conditions are not present. However, the flow will always tend to develop towards this equilibrium between the bottom shear stress and the pressure component causing this idealized profile.

The transverse component is also often referred to as secondary flow. In the river bend a balance between a centrifugal force and a pressure gradient is the cause of this secondary flow. The centrifugal force increases the water level in the outer bend and decreases the water level at the inner bend resulting into a pressure gradient. The centrifugal force is smaller at the river bottom since it is dependent on flow velocity. The flow velocity at the bottom is lower due to bottom friction and hence the centrifugal force is not evenly distributed over the depth, as can be seen on figure A.8a. The balance between this centrifugal force and pressure gradient results into the secondary flow pattern. This secondary flow causes the streamwise velocities to be the highest in the outer half of the bend, which has important consequences for the morphology in river bends (van Balen, 2010). The combination of the streamwise and transverse component causes a spiral flow profile as can be seen on figure A.6.

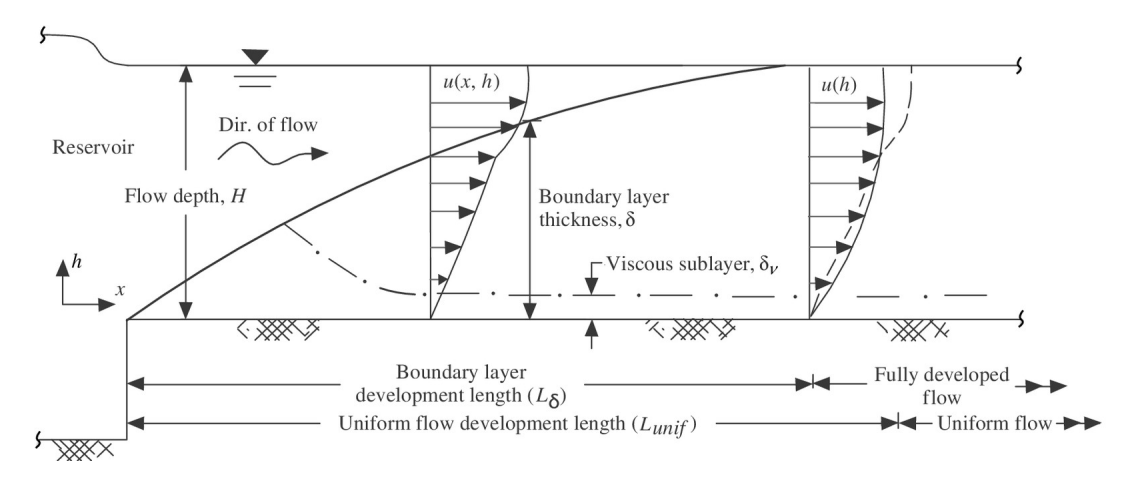
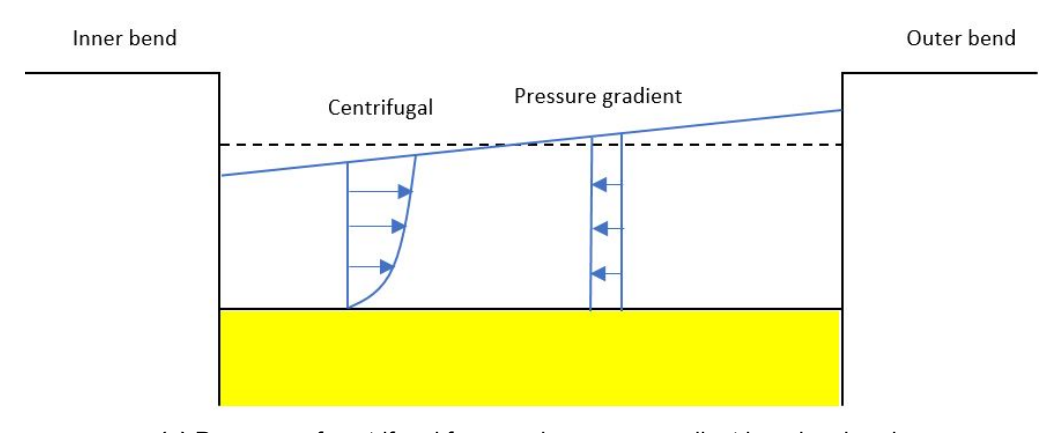


Figure A.7: Development of uniform flow (Wilkerson et al., 2019).



(a) Presence of centrifugal force and pressure gradient in a river bend.

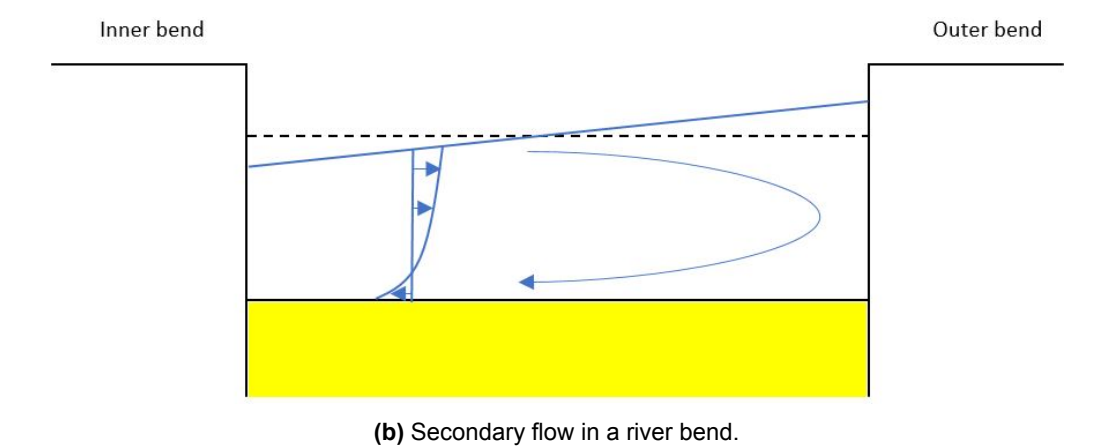


Figure A.8: The transverse component in bend flow.

Sediment transport

As already indicated, the largest flow velocities occur in the outer bend. These flow velocities create a scour pool in the outer bend that reacts with an overshoot phenomenon (Struiksma et al., 1985). This scour hole has an equilibrium depth $y_{m,e}$ represented by the asymptote in figure A.9. In the upstream part of the scour pool overdeepening takes place, due to this overshoot phenomenon. After that, the

river bed dampens until the equilibrium depth in the downstream direction. At the inner bend a point bar is being formed. Due to the lower flow velocities and the spiral flow moving along the bottom from the outer bend to the inner bend, sediment is being deposited here. These scour and sedimentation processes will eventually create the meandering pattern that characterizes the lower reaches of rivers.

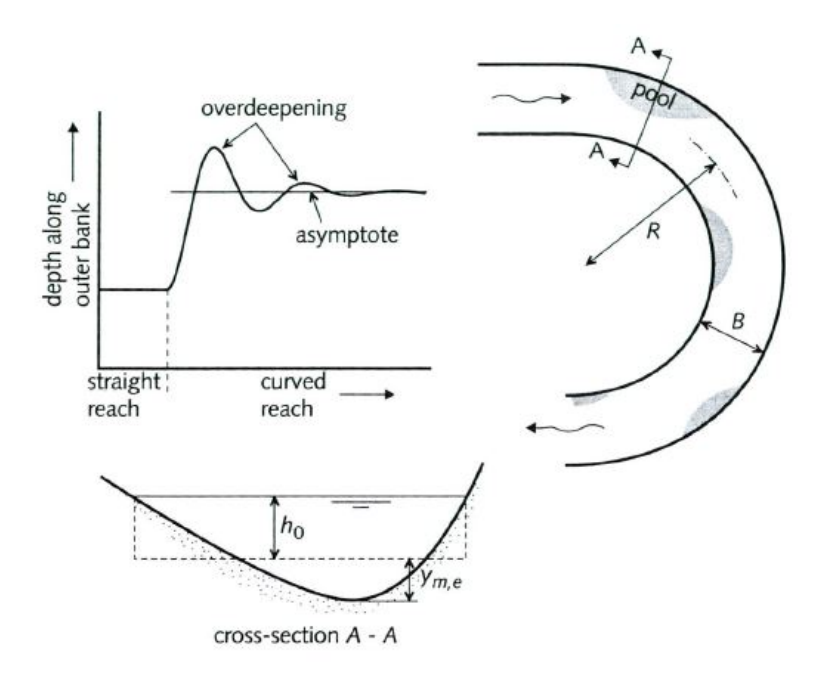


Figure A.9: Scour in a river bend (Hoffmans & Verheij, 1997).

A.5. Bed forms

A.5.1. Classification

As previously indicated, it was observed that during a 2D laboratory experiment sediments were transported by a bar Zuylen (2015). Supported by the 3D small scale laboratory experiments of Koopmans (2017) and Stenfert (2017), that also showed the presence of ripples and dunes, it can be said that bed forms are an important aspect of scour hole development. These bed forms are also observed in the field. Figure A.10 shows the development of the scour hole Beerenplaat. In figure A.10a there can clearly be seen that there is presence of ripples/dunes on the bottom of the scour hole. Looking at figure A.10b it can be seen that the bed features have migrated and changed in shape within eight months. Since bed features can be observed in experimental scour holes and in the field, a brief explanation of typical bed forms is given.

Bed forms and thus the hydraulic roughness of the bottom are complicated to predict since they depend on flow conditions and sediment transport rates that in turn are dependent on the channel bed configuration and thus the hydraulic roughness (van Rijn, 1984c). Those bed forms are able to increase drag and so affect flow and sediment transport. The timescales at which bed forms move throughout the river system is much smaller than the timescale of the flow velocity (Raudkivi, 1997).

Four main stability fields of bed forms on a sand bed are identified by many researches, as can be seen in figure A.11. The first field is no motion during which the forcing does not exceed the resistance of the grains and no movement of sediments will occur. The other extreme is the upper-stage plane bed field, during which the bed is almost plane and characterized by a series of very-low relief bed waves (J. L. Best & Bridge, 1992). In between there are more characterizing bed forms. In the medium coarse to coarse sand, dunes can form, of which the dune height is strongly dependent on the flow depth (van Rijn, 1984c). Dunes are characterized by their asymmetrical profile and the presence of

eddies as can be seen on figure A.12b. The bed feature that forms in the fine to medium coarse sand is called a ripple. The height of ripples is much smaller with respect to dunes and is independent of the flow depth (Raudkivi, 1997). Finally, one other bed form should be mentioned that is not present in figure A.11. This is the anti-dune that can develop in super critical flow conditions where the bed waves and water surface are in phase (Raudkivi, 1997). Anti-dunes migrate in the opposite direction as the water surface.

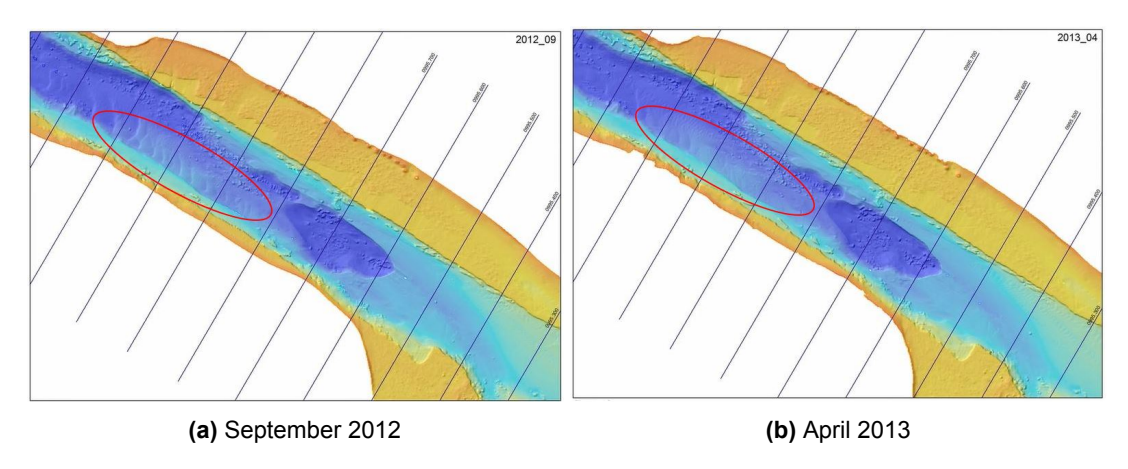


Figure A.10: GIS maps of the scour hole Beerenplaat and the Oude Maas (Rijkswaterstaat WNZ).

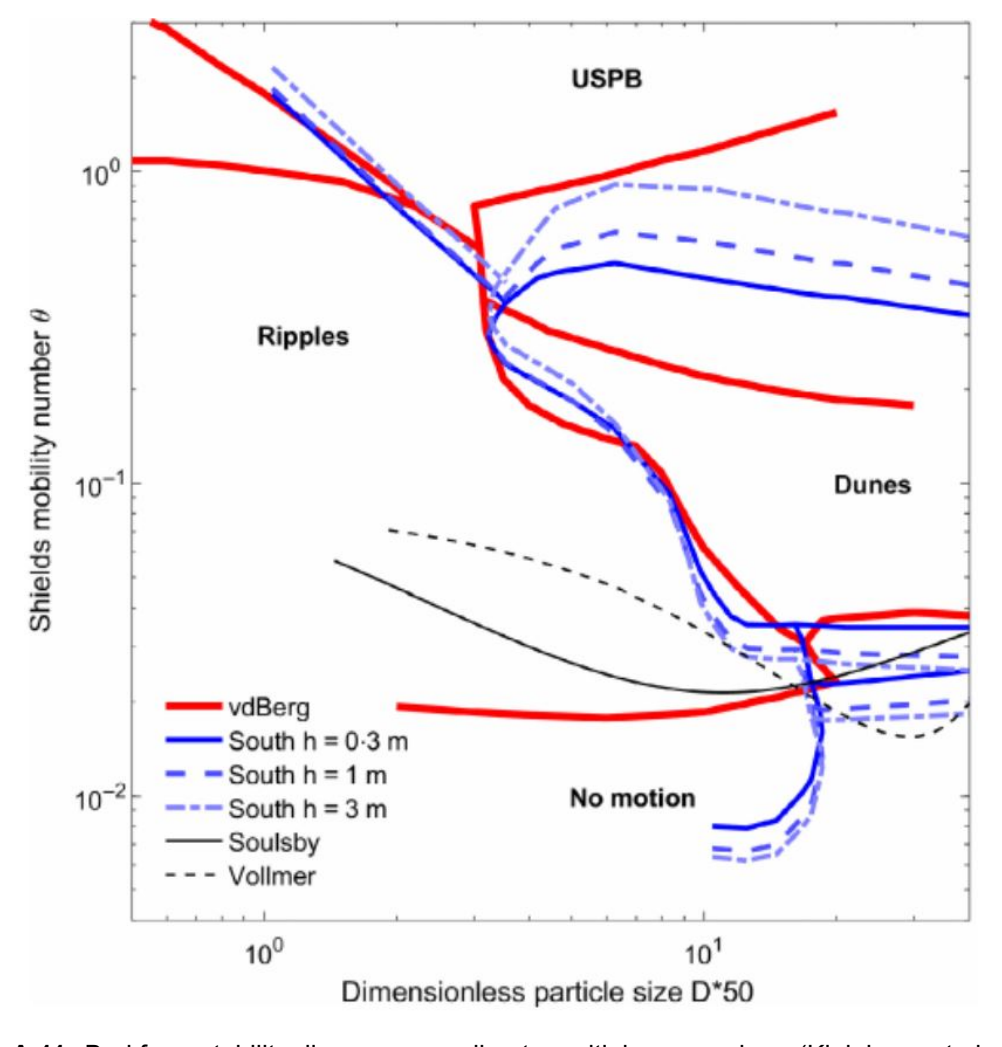


Figure A.11: Bed form stability diagram according to multiple researchers (Kleinhans et al., 2017).

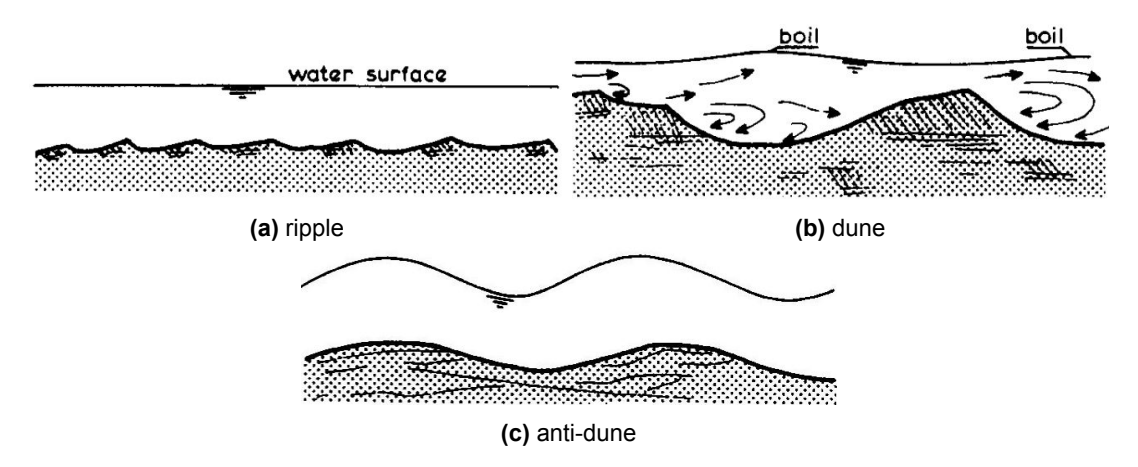


Figure A.12: Illustration of different bed forms (van Rijn, 1993).

A.5.2. Response of river dunes on changing river flow

Reesink et al. (2018) have focused on the behaviour of dunes in changing river flow. The formation of bed forms including dunes is a complex process. Bedforms determine the hydraulic roughness of the river, which in turn affect the flow depth and discharge that are again of influence on sediment transport conditions and hence the formation of bedforms. Despite this complex relation, Reesink et al. (2018) were able to conclude the following dune behaviour based on flume experiments with bedforms in non-cohesive soil.

- Flattening of crests in the case of a decreasing water depth or increasing flow velocity.
- · Increasing trough scour due to the increased flow velocity.
- Formation of trains of superimposed bedforms (figure A.13) due to the increased flow depth and decreased flow velocity.



Figure A.13: Superimposition of bed forms (Reesink et al., 2018).

A.5.3. Behaviour of marine sand waves

Hulscher (1996) defines the formation of marine sand waves as follows. Small perturbations are present in the river bottom that cause flow alternations. As a result flow is accelerated on the stoss side and decelerated after the crest. During a symmetrical tidal cycle this occurs on both sides of the perturbation forming residual circulation cells as can be seen on figure 2.18a. As a result, sediment grains are transport from the troughs towards the crest. If the height of the sand wave is large enough, flow separation occurs resulting into even steeper slopes (Allen, 1980).

Since temporal changes in tidal conditions are occurring on a much larger scale than that of rivers, the sand waves can reach an equilibrium in the case of a symmetrical tide. In literature (e.g. Hulscher (1996), Sterlini et al. (2009), and van Gerwen (2016)) this equilibrium can be described by a combination of linear and non-linear models. The linear models assume that the interaction between the flow, the sea bed and the sand wave growth is linear and describe the initial formation of the sand wave quite well. The later stages are described with non-linear models since the growth of the sand wave should be slowed down. In these non-linear models, the suspended load transport and tidal asymmetry are important factors for reaching a realistic equilibrium sand wave height.

A.5.4. Tidal response of estuarine sand waves

Kostaschuk and Best (2005) researched the response of large dunes on a semi-diurnal tide in the Fraser estuary in Canada. Contrary to other researches they focused on the response during a single tidal cycle. In figure A.14 a schematized tidal cycle can be found. During this tidal cycle, Kostaschuk and Best (2005) identified three different responses of the river dunes. The first response occurs early during the tidal fall. Flow velocities start to increase which causes scour in the dune troughs resulting into an increase of the dune height. The second response of the dunes is caused by the peak velocities during the low tide. The high velocities are able to cause scour of the dune crests reducing the dune height. During the third response there is slack tide with almost no flow velocities. Therefore sediments are able to fall out of suspension, resulting into a further reduction of the dune height. Eventually, the dune height will be in equilibrium with the strongest flow velocities occurring during low tide. According to Kostaschuk and Best (2005), the dune length is not influenced by the tidal cycle. Just as for the river flow, the response of the dunes lags behind the tidal cycle but the lag is much smaller than that of the river flow (Babakaiff, 1993).

Zarillo (1982) investigated the stability of bedforms in the estuary near the Sapelo island in Georgia, United States of America. The study encountered multiple sand dune fields in the estuary that are ebb orientated, which is a result of the large pressure gradients and related bed-shear values that develop during ebb. On top of that, the research verifies the conclusion that the bedform height is in equilibrium with the strongest flows occurring during ebb flow. The equilibrium height can be computed with theoretical based models like van Rijn (1984a, 1984b, 1984c) or with empirical relations derived form flume and field test. In both Kostaschuk and Best (2005) and Zarillo (1982) the empirical relation of Allen (1968) is used for computation of this equilibrium height of the bedforms.

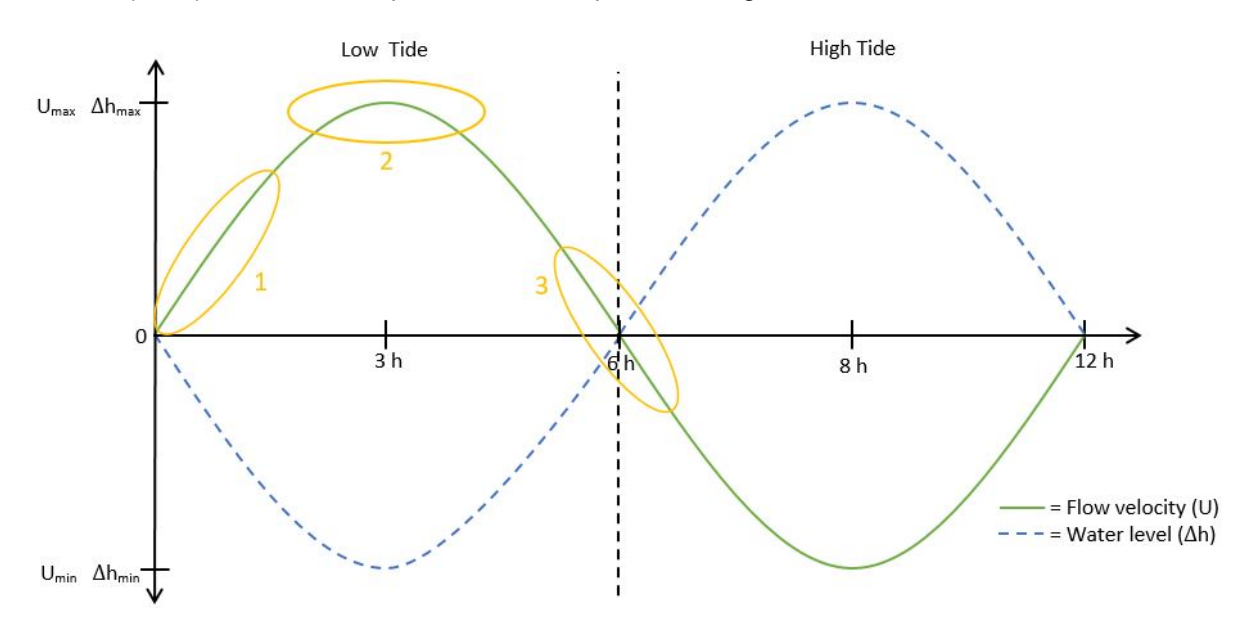
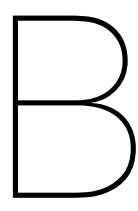


Figure A.14: Response of river dunes on a semi-diurnal tide, based on Kostaschuk and Best (2005).

$$H = 0.086 \cdot d^{1.19} \tag{A.12}$$

H [m] Height estuarine sand wave

d [m] River depth



Characteristic time scour hole Beerenplaat

This appendix computes the characteristic time t_1 for the scour hole Beerenplaat which is used to understand the scour depth development with the Breusers equation in section 3.1.1. This characteristic time scale is the period required for the scour depth to become equal to the initial water depth h_0 and is fully described in appendix A.3.2. For non-steady flow conditions, as found at this tidal influenced scour hole, equation (B.1) can be used as a first estimate for the characteristic time (Hoffmans & Verheij, 1997). It is chosen to compute the critical velocity of sand $u_{c,sand}$ with the Shields equation (see appendix A.1) since the water depth at the pilot site is quite large and the sediment diameter quite small. The characteristic time scale is computed for two cases, a scour hole in a clay bottom and a scour hole in sand bottom. The Rhine-Meuse delta has a heterogeneous subsoil which mostly consist of alternating sand and clay layers. Therefore it is chosen to work out these two extreme cases of homogeneous river bottoms. It is expected that the scour hole Beerenplaat behaves somewhere in between the scenarios. First, remarks will be given which explain the data sources used for some of the parameters and motivate the decisions and assumptions that have been made. After that, each of the parameters will be computed and the time scale t_1 is determined for both the homogeneous sand and clay subsoil.

$$t_1 = \frac{330 \cdot h_0^2 \cdot \Delta^{1.7}}{\left(\alpha \cdot U_d - u_c\right)^{4.3}} \tag{B.1}$$

- The average water surface elevation η has been determined with data from the measurements of Rijkswaterstaat located at Spijkenisse (see waterinfo.rws.nl).
- For the density it is assumed that the water at the scour hole Beerenplaat is sea water. The
 densities of the subsoil have been obtained out of NEN9997 (table 2b) by assuming average soil
 properties.
- The median sand diameter d_{50} has been determined based on 10 soil samples of the sediment that is nourished at the pilot site. Figure B.1 shows the sieve curves of the samples. No characteristics of the non-cohesive sediments at the scour hole Beerenplaat prior to the pilot nourishments are available.
- The maximum velocity during a tide $U_{m,t}$ has been determined out of the ADCP measurements. The largest velocities are found during the second measurements at 08:28 during ebb. The velocity is averaged over the entire measured cross-section at the scour hole.
- For the critical Shields parameters there is chosen to work with transport stage 7. For a scour
 hole to develop, real transport of grains is required. An initiation of motion is not sufficient. Hence
 the choice for transport stage 7.

- The Chézy value C is obtained out of the results of the Delft3D model used to answer the subquestion 2 and 3 in chapter 4. A full explanation of the model (e.g. time frame, grid, conditions, etc.) can be found in section 4.1.1.
- The relative turbulence intensity r_0 has been determined with the reduced equation of Hoffmans and Booij (1993), equation (B.2), as was described in appendix A.3.2. The Chézy value upstream of the scour hole, at the poorly erodible clay layers should be used. Since the flow changes direction between ebb and flood the relative turbulence intensity r_0 is computed for both cases with the corresponding Chézy values. After that, they will be averaged to obtain a representative value of r_0 at the scour hole Beerenplaat. Equation (B.2) does not consider the turbulence caused by the mixing of flows at the confluence during ebb flow. Schiereck and Verhagen (2019) suggest that $r_{0,max}\approx 0.2-0.3$ for free turbulence. Looking at the size of the channel, it is expected that the a full mixing layer can develop here. Since neither of the flow is stagnant a value of $r_0=0.2$ is is assumed to account for the additional turbulence caused by the confluence. Such a principle should not be included in the flood scenario since the splitting and deceleration of the flow happens after the flow has left the scour hole.

$$r_0 = 1.2\sqrt{\frac{g}{C^2}}$$
 (B.2)

```
h_0 = \eta - d [m] d = -15.85 [m + NAP] location river bottom out of MBES \eta = 0.226 [m + NAP] average water surface elevation at Spijkenisse (Rijkswaterstaat)
```

 $h_0 = 15.85 + 0.226 = 16.08$

```
\begin{split} &\Delta = \left(\rho_{sediment} - \rho_{water}\right)/\rho_{water} \text{ [-]} \\ &\rho_{sand} = 2038.7 \quad \text{[kg/m}^3\text{]} \qquad \text{density of a saturated medium packed sand (NEN9997, table 2b)} \\ &\rho_{clay} = 1732.9 \quad \text{[kg/m}^3\text{]} \qquad \text{density of a saturated medium dense clay (NEN9997, table 2b)} \\ &\rho_{water} = 1025 \quad \text{[kg/m}^3\text{]} \qquad \text{density of sea water} \end{split}
```

$$\Delta_{sand} = (2038.7 - 1025)/1025 = 0.99$$

 $\Delta_{clay} = (1732.9 - 1025)/1025 = 0.69$

$$\begin{array}{ll} U_d = \eta \cdot U_{m,t} & \text{[m/s]} \\ \eta = 0.8 & \text{[-]} & \text{coefficient = 0.75 - 0.85 (Hoffmans, 1992)} \\ U_{m,t} = 1.19 & \text{[m/s]} & \text{max. velocity during tide (ADCP measurement 2, average of cross-section)} \end{array}$$

 $U_d = 0.8 \cdot 1.19 = 0.952$

$$\begin{split} u_{c,sand} &= C \; \sqrt{\psi \; \Delta \; d_{50}} \quad \text{[m/s]} \\ C &= 56 \qquad \qquad \text{[m}^{0.5}\text{/s]} \\ d_{50} &= 0.0004 \qquad \qquad \text{[m]} \\ \psi &= 0.04 \qquad \qquad \text{[-]} \\ \Delta_{sand} &= 0.99 \qquad \text{[-]} \end{split}$$

Chézy value at the scour hole (out of Delft3D model) based on sediment samples, see remarks above based on d_{50} and Shields curve with transport stage 7

$$u_{c,sand} = 56 \sqrt{0.04 \cdot 0.99 \cdot 0.0004} = 0.22$$

$$u_{c,clay} = 1.3$$
 [m/s]

for a medium dense clay (Ven Te Chow (1959), see appendix A.1)

$$\begin{split} r_{0,ebb} &= \sqrt{\left(1.2\sqrt{\frac{g}{C_{ebb}^2}}\right)^2 + 0.2^2} \quad \text{[-]} \\ C_{ebb} &= 53.57 \quad \text{[m}^{0.5}\text{/s]} \\ g &= 9.81 \quad \text{[m/s}^2\text{]} \end{split}$$

averaged value over the time frame of the Delft3D model upstream of the scour hole

$$r_{0,ebb} = \sqrt{\left(1.2\sqrt{\frac{9.81}{53.57^2}}\right)^2 + 0.2^2} = 0.21$$

$$\begin{split} r_{0,flood} &= 1.2 \sqrt{\frac{g}{C_{flood}^2}} \quad \text{[-]} \\ C_{flood} &= 56.36 \quad \text{[m}^{0.5}\text{/s]} \\ g &= 9.81 \quad \text{[m/s}^2\text{]} \end{split}$$

averaged value over the time frame of the Delft3D model downstream of the scour hole

$$r_{0,flood} = 1.2\sqrt{\frac{9.81}{56.36^2}} = 0.07$$

$$r_0 = 0.5 (r_{0,ebb} + r_{0,flood}) = 0.5 (0.21 + 0.07) = 0.14$$

$$\alpha = 1.5 + 4.4 \cdot r_0 \cdot (C/C_0) \text{ [-]}$$

$$C = 56 \qquad \qquad \text{[m}^{0.5}/\text{s]}$$

$$C_0 = 40 \qquad \qquad \text{[m}^{0.5}/\text{s]}$$

$$r_0 = 0.14 \qquad \qquad \text{[-]}$$

Chézy value at the scour hole (out of Delft3D model) reference Chézy coefficient

$$\alpha = 1.5 + 4.4 \cdot 0.14 \cdot (56/40) = 2.362$$

$$t_{1,sand} = \frac{330 \cdot h_0^2 \cdot \Delta_{sand}^{1.7}}{\left(\alpha \cdot U_d - u_{c,sand}\right)^{4.3}} = \frac{330 \cdot 16.08^2 \cdot 0.99^{1.7}}{\left(2.362 \cdot 0.952 - 0.22\right)^{4.3}} = 5.51 \; months$$

$$t_{1,clay} = \frac{330 \cdot h_0^2 \cdot \Delta_{clay}^{1.7}}{\left(\alpha \cdot U_d - u_{c,clay}\right)^{4.3}} = \frac{330 \cdot 16.08^2 \cdot 0.69^{1.7}}{\left(2.362 \cdot 0.952 - 1.3\right)^{4.3}} = 77.86 \; months$$

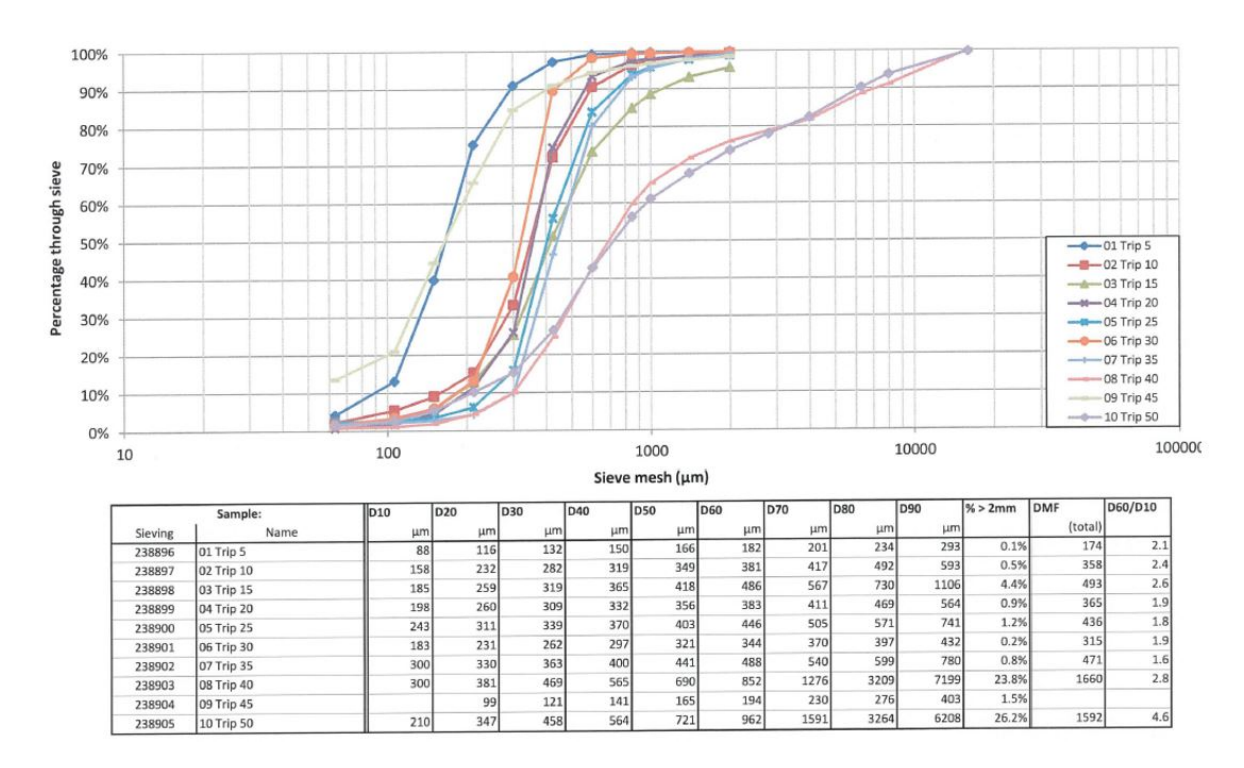
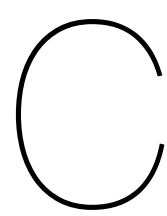


Figure B.1: Sieve data of 10 soil samples from the nourished sediments at the pilot site in the Oude Maas (Rijkswaterstaat WNZ).



Estuarine sand waves

This appendix analyzes the presence of the estuarine sand waves at scour section 5, which were identified in section 3.2.2. No literature is available on how estuarine sand waves are formed. According to Hulscher and Dohmen-Janssen (2005) and van der Sande et al. (2019), the best course of action is to separately look at the influence of seasonal river flow (forming the river dunes) and the tide. First the dimensions of the estuarine sand waves are given, then the influence of the seasonal river flow and the tide are separately discussed. Finally it is hypothesised why the estuarine sand waves developed only after the pilot nourishment.

C.1. Dimensions

	February	2021	
Sand	Crest	Trough	Height
Wave	[m + NAP]	[m + NAP]	[m]
1	-0.3818	-0.8868	0.505
2	0.2398	-0.7383	0.9781
3	0.4525	-0.9978	1.4503
4	0.6783	-1.2766	1.9549
5	0.345	-1.3224	1.6674
6	0.6138	-1.2256	1.8394
7	0.7145	-0.9328	1.6473
8	0.6948	-1.4042	2.099
9	0.9497	-0.9197	1.8694
10	0.525	-0.6855	1.2105
11	0.8226	-0.8676	1.6902
12	0.1943	-0.94	1.1343
13	1.0541	0.295	0.7591
14	1.9387	1.0808	0.8579
		Average:	1.404

Table C.1: Height of estuarine sand waves in February 2021.

C.1. Dimensions

	June	2020			December	2020	
Sand	Crest	Trough	Height	Sand	Crest	Trough	Height
Wave	[m + NAP]	[m + NAP]	[m]	Wave	[m + NAP]	[m + NAP]	[m]
1	0.4486	-1.4484	1.897	1	0.4802	-1.1114	1.5916
2	1.1305	-1.3039	2.4344	2	1.1858	-1.2764	2.4622
3	0.8316	-1.1865	2.0181	3	0.8474	-1.269	2.1164
4	0.8336	-1.1952	2.0288	4	0.6144	-1.2732	1.8876
5	0.8675	-1.2087	2.0762	5	0.8263	-1.1245	1.9508
6	1.3822	-1.3845	2.7667	6	0.9663	-1.3931	2.3594
7	0.908	-1.5143	2.4223	7	1.0406	-1.3212	2.3618
8	0.6361	-0.7918	1.4279	8	1.1262	-0.8282	1.9544
9	0.5321	-0.8629	1.395	9	0.6934	-0.702	1.3954
10	1.3431	-1.5173	2.8604	10	1.624	-1.2383	2.8623
11	1.0341	-1.0168	2.0509	11	1.3328	-1.0404	2.3732
12	0.4238	-1.2781	1.7019	12	-0.2912	-0.9786	0.6874
13	0.8237	-0.7764	1.6001	13	0.6844	-0.868	1.5524
14	1.94	1.0618	0.8782	14	1.5436	-0.4316	1.9752
15	1.996	0.3621	1.6339	15	2.5261	1.0069	1.5192
				16	2.0801	0.526	1.5541
		Average:	1.946			Average:	1.913

Table C.2: Height of estuarine sand waves in June and December 2020.

	June	2019			December	2019	
Sand	Crest	Trough	Height	Sand	Crest	Trough	Height
Wave	[m + NAP]	[m + NAP]	[m]	Wave	[m + NAP]	[m + NAP]	[m]
1	0.1186	-1.0421	1.1607	1	-0.242	-1.2001	0.9581
2	0.4601	-0.6231	1.0832	2	0.466	-0.9778	1.4438
3	0.8807	-0.5105	1.3912	3	0.6594	-0.754	1.4134
4	0.9247	-0.7212	1.6459	4	0.8259	-0.8084	1.6343
5	-0.1402	-0.7557	0.6155	5	0.7664	-0.9589	1.7253
6	0.2403	-0.2728	0.5131	6	0.2528	-0.8549	1.1077
7	0.6776	-1.1936	1.8712	7	0.5184	-0.2613	0.7797
8	0.3644	-1.5832	1.9476	8	0.3592	-0.5196	0.8788
9	0.217	-0.2997	0.5167	9	-0.0327	-1.4337	1.401
10	0.6933	-1.3885	2.0818	10	0.5802	-0.8066	1.3868
11	0.3994	-0.6085	1.0079	11	0.7706	-0.5377	1.3083
12	0.1953	-0.4802	0.6755	12	0.4117	-0.985	1.3967
13	0.9217	0.1657	0.756	13	0.4493	-0.9781	1.4274
14	2.2938	0.2752	2.0186	14	0.5659	-0.235	0.8009
				15	1.3747	0.7236	0.6511
				16	1.726	0.1246	1.6014
		Average:	1.235			Average:	1.245

Table C.3: Height of estuarine sand waves in June and December 2019.

C.1. Dimensions

	June	2018			December	2018	
Sand	Crest	Trough	Height	Sand	Crest	Trough	Height
Wave	[m + NAP]	[m + NAP]	[m]	Wave	[m + NAP]	[m + NAP]	[m]
1	-15.8442	-16.6609	0.8167	1	-15.4365	-16.4473	1.0108
2	-15.8365	-16.2172	0.3807	2	-15.2171	-16.2038	0.9867
3	-15.815	-16.4837	0.6687	3	-14.4035	-14.8899	0.4864
4	-15.6319	-16.4274	0.7955	4	-14.2	-14.7929	0.5929
5	-15.5526	-16.0809	0.5283	5	-13.784	-14.5567	0.7727
6	-14.6774	-15.0547	0.3773	6	-13.2436	-14.231	0.9874
7	-14.0373	-14.4785	0.4412	7	-13.6366	-14.4152	0.7786
8	-13.3303	-14.1887	0.8584	8	-13.7227	-14.679	0.9563
9	-13.4854	-13.9265	0.4411	9	-14.2445	-14.7839	0.5394
10	-13.7071	-14.0987	0.3916	10	-13.8344	-14.819	0.9846
11	-13.9301	-14.4457	0.5156	11	-13.728	-14.8278	1.0998
12	-14.233	-14.7182	0.4852	12	-14.015	-15.2984	1.2834
13	-13.8563	-14.6929	0.8366	13	-13.778	-15.0881	1.3101
14	-13.713	-14.6926	0.9796	14	-14.0563	-14.9313	0.875
15	-14.3535	-15.329	0.9755	15	-14.0683	-14.3581	0.2898
16	-13.8086	-15.3525	1.5439	16	-13.8273	-14.413	0.5857
17	-14.2885	-14.9782	0.6897	17	-13.7848	-14.0933	0.3085
18	-14.0903	-14.503	0.4127	18	-13.7577	-14.9809	1.2232
19	-14.0254	-14.8384	0.813	19	-13.1113	-14.8561	1.7448
20	-13.6129	-14.4544	0.8415	20	-13.9407	-14.6934	0.7527
21	-13.6357	-14.043	0.4073	21	-12.7878	-13.6787	0.8909
22	-12.2471	-13.2184	0.9713	22	-12.7833	-13.4074	0.6241
		Average:	0.690			Average:	0.867

Table C.4: Height of estuarine sand waves in June and December 2018.

C.2. Seasonal river flow and river dunes

The presence of river dunes, formed by the seasonal river flow, is dependent on the flow velocities, which induce bed load transport, and water levels in a river. The water levels form the upper limit of the dune height. However due to the sea, the daily averaged water levels are almost fixed at scour section 5. Therefore it is tried to approach the problem with the flow velocities and literature findings. No measurement station is present at the pilot site that continuously measures the flow velocities. Therefore an alternative approach is taken that uses hydraulic data which is available. Equation (C.1) shows that the change in flow velocities between two measurements can be determined with the discharge Q, water surface elevation η and water depth d. It is assumed that the flow width B_c remains constant. This change of flow velocities, in combination with literature regarding behaviour of river dunes, can be used to check if river dunes would develop and grow. In turn this could explain the presence of the estuarine sand waves.

The discharge is estimated with discharge graphs from Rijkswaterstaat Zuid-Holland (2012). These graphs estimate the discharge at the pilot site based on the discharge at Lobith, considering the operation of the Haringvliet sluices. They have been constructed with SOBEK computations. There is chosen to work with monthly averaged values since the goal is to investigate what caused the development of the estuarine dunes, not to perform accurate computations. The monthly averaged water surface elevation η can be found in figure C.2b and has been measured by Rijkswaterstaat upstream of the pilot site at Goidschlaxoord and downstream at Spijkenisse. It is chosen to estimate the water surface elevation at the pilot site by averaging the measurement of the two stations. The water depth at scour section 5 has been determined with averaging of the MBES measurements and can be found in table C.5. The factor α has been computed monthly for the period of June 2018 until February 2021 and can be found in table C.6.

$$u = \frac{Q}{A_c} = \frac{Q}{h \cdot B_c} = \frac{Q}{(\eta + d) \cdot B_c}$$

$$\alpha = \frac{u_1}{u_2} = \frac{\frac{Q_1}{(\eta_1 + d_1) \cdot B_{c_1}}}{\frac{Q_2}{(\eta_2 + d_2) \cdot B_{c_2}}} = \frac{(\eta_2 + d_2) \cdot Q_1}{(\eta_1 + d_1) \cdot Q_2}$$
(C.1)

u	[m/s]	flow velocity	h	[m]	water height
A_c	$[m^2]$	cross-sectional flow area	η	[m]	water surface elevation
B_c	[m]	flow width	d	[m]	water depth

Date	Average water depth [m]
June 2018	-14.17
December 2018	-14.23
June 2019	-14.32
December 2019	-14.40
June 2020	-14.50
December 2020	-14.57
February 2021	-14.53

Table C.5: Average water depth in scour section 5.

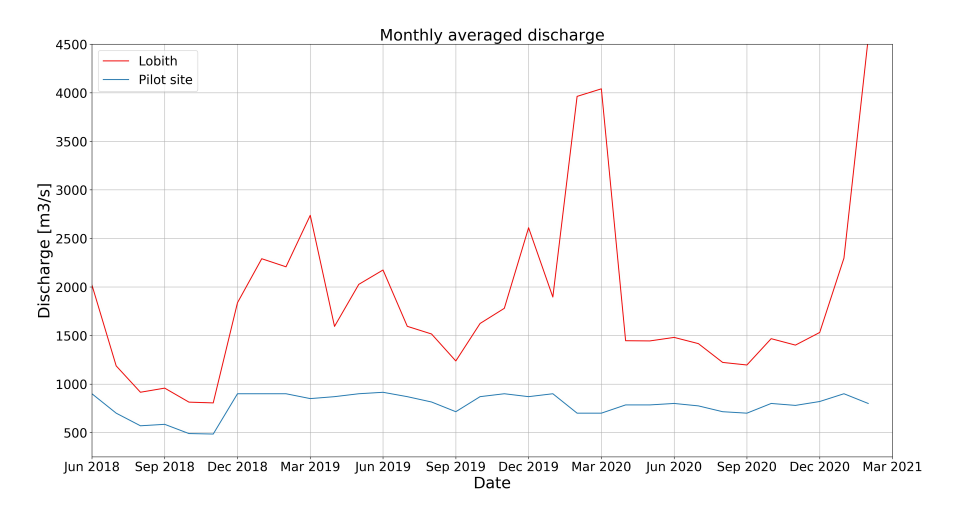
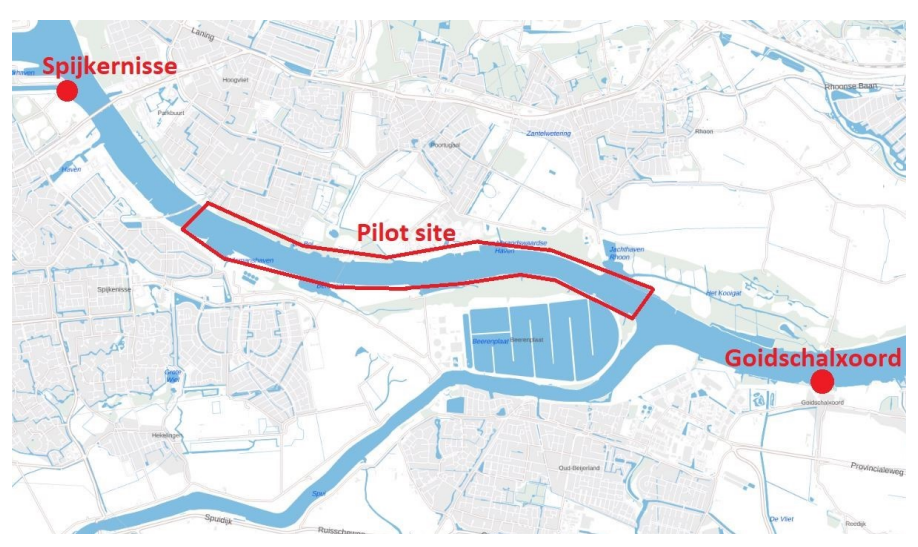


Figure C.1: Discharge at Lobith and estimated at the pilot site.



(a) Location of measurement stations.

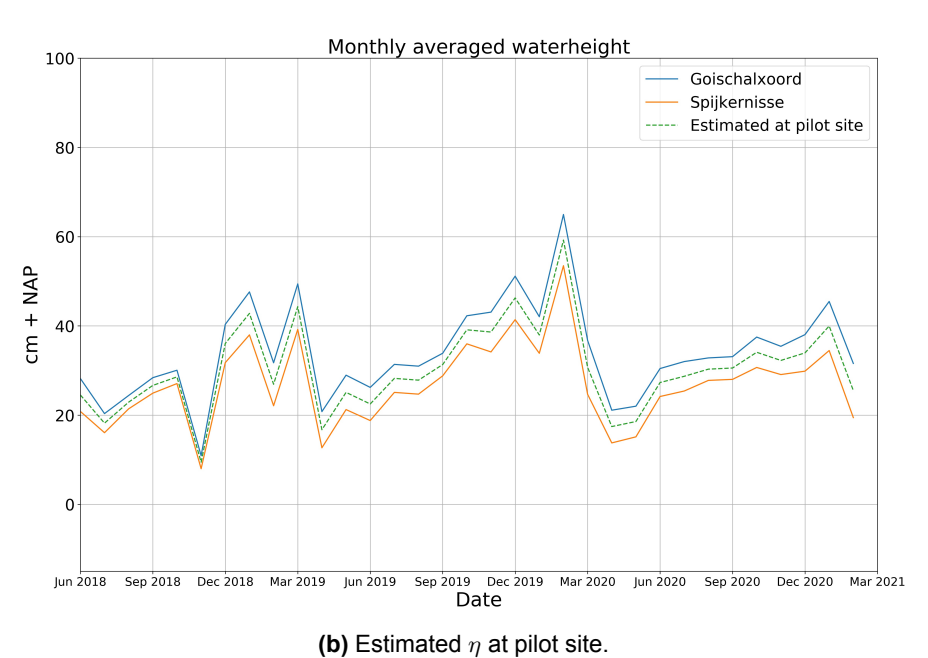


Figure C.2: Water surface elevation (η) at scour section 5.

		average sand			average sand
$U_{\cdots} =$	$\alpha \cdot U_{Jun\ 2018}$	wave height	$U_{\cdots} =$	$\alpha \cdot U_{Dec\ 2019}$	wave height
$U_{Jun\ 2018} =$	1.0 $\cdot U_{Jun\ 2018}$	0.69 m	$U_{Dec\ 2019} \ =$	1.0 \cdot $U_{Dec\ 2019}$	1.25 m
$U_{Jul\ 2018}\ =$	1.29 \cdot $U_{Jun~2018}$		$U_{Jan\ 2020}\ =$	$0.97 \cdot U_{Dec\ 2019}$	
$U_{Aug\ 2018}\ =$	1.58 \cdot $U_{Jun~2018}$		$U_{Feb\ 2020}\ =$	1.23 \cdot $U_{Dec\ 2019}$	
$U_{Sep\ 2018}\ =$	1.54 \cdot $U_{Jun~2018}$		$U_{Mar\ 2020}\ =$	1.26 \cdot $U_{Dec\ 2019}$	
$U_{Oct\ 2018}\ =$	1.83 \cdot $U_{Jun~2018}$		$U_{Apr\ 2020}\ =$	1.14 \cdot $U_{Dec\ 2019}$	
$U_{Nov\ 2018}\ =$	1.88 \cdot $U_{Jun~2018}$		$U_{May\ 2020}\ =$	1.14 \cdot $U_{Dec\ 2019}$	
$U_{Dec\ 2018}\ =$	1.0 $\cdot U_{Jun\ 2018}$	0.87 m	$U_{Jun\ 2020}\ =$	1.11 \cdot $U_{Dec\ 2019}$	1.95 m
		average sand			average sand
$U_{\cdots} =$	$\alpha \cdot U_{Dec\ 2018}$	wave height	$U_{\cdots} =$	$\alpha \cdot U_{Jun\ 2020}$	wave height
$U_{Dec\ 2018} =$	1.0 \cdot $U_{Dec\ 2018}$	0.87 m	$U_{Jun\ 2020}\ =$	1.0 \cdot $U_{Jun~2020}$	1.95 m
$U_{Jan\ 2019}\ =$	1.0 \cdot $U_{Dec\ 2018}$		$U_{Jul\ 2020}\ =$	1.03 \cdot $U_{Jun~2020}$	
$U_{Feb\ 2019}\ =$	1.0 \cdot $U_{Dec\ 2018}$		$U_{Aug\ 2020}\ =$	1.12 \cdot $U_{Jun\ 2020}$	
$U_{Mar\ 2019}\ =$	1.06 \cdot $U_{Dec\ 2018}$		$U_{Sep\ 2020}\ =$	1.14 \cdot $U_{Jun~2020}$	
$U_{Apr\ 2019}\ =$	1.05 \cdot $U_{Dec\ 2018}$		$U_{Oct\ 2020}\ =$	1.0 $\cdot U_{Jun\ 2020}$	
$U_{May\ 2019}\ =$	1.01 \cdot $U_{Dec\ 2018}$		$U_{Nov\ 2020}\ =$	1.02 \cdot $U_{Jun~2020}$	
$U_{Jun\ 2019}\ =$	1.0 \cdot $U_{Dec\ 2018}$	1.24 m	$U_{Dec\ 2020}\ =$	$0.98 \cdot U_{Jun~2020}$	1.91 m
		average sand			average sand
$U_{\cdots} =$	$\alpha \cdot U_{Jun\ 2019}$	wave height	$U_{\cdots} =$	$\alpha \cdot U_{Dec\ 2020}$	wave height
$U_{Jun\ 2019}\ =$	1.0 \cdot $U_{Jun~2019}$	1.24 m	$U_{Dec\ 2020}\ =$	1.0 \cdot $U_{Dec\ 2020}$	1.91 m
$U_{Jul\ 2019}\ =$	1.05 \cdot $U_{Jun~2019}$		$U_{Jan\ 2021}\ =$	$0.90 \cdot U_{Dec\ 2020}$	
$U_{Aug\ 2019}\ =$	1.12 \cdot $U_{Jun~2019}$		$U_{Feb\ 2021}\ =$	1.02 \cdot $U_{Dec\ 2020}$	1.40 m
$U_{Sep\ 2019}\ =$	1.28 \cdot $U_{Jun~2019}$				
$U_{Oct\ 2019}\ =$	1.04 \cdot $U_{Jun~2019}$				
$U_{Nov\ 2019}\ =$	1.01 \cdot $U_{Jun~2019}$				
$U_{Dec\ 2019}\ =$	1.04 \cdot $U_{Jun~2019}$	1.25 m			

Table C.6: Change of flow velocities at scour section 5.

The change in flow velocities can again be used to describe the response of river dunes based on literature and be compared with the field behaviour of the estuarine sand waves (see table C.7). It shows that often the change in flow velocity and the corresponding response of the river dunes correctly explains the growth of dune height. However, from December 2018 - June 2019 the dune height increases a lot while there are not much changes in hydraulic data. Similar is the case of June 2020 - December 2020, where there is an increase in flow velocity that according to literature would cause additional trough scour and flattening of the dune crest. This is not seen back in the taken MBES measurements. On top of that, river dunes are only prominent part of the time while the bedforms seen in the MBES measurement are quite systematic and continuously present during all measurements. This suggest that the seasonal river flow plays a role in the development and behaviour of an estuarine sand waves but that another mechanism should be included to describe it.

		Change	Expected response	Field behaviour	Explains height
Date	Netto α	Height	river dunes	estuarine sand wave	change?
Jun 2018		0.69 m	Trough scour	Trough scour	
↓ ↓	$\alpha > 1.0$	\downarrow	Flattening dune crest	Flattening dune crest	Yes
Dec 2018		0.87 m			
Dec 2018		0.87 m		Trough scour	
↓ ↓	$\alpha\approx 1.0$	\downarrow	No significant growth	Bedform growth	No
Jun 2019		1.24 m			
Jun 2019		1.24 m	Trough scour	Trough scour	
+	$\alpha > 1.0$	\downarrow	Flattening dune crest	Flattening dune crest	Yes
Dec 2019		1.25 m			
Dec 2019		1.25 m	Trough scour	Trough scour	
↓	$\alpha > 1.0$	\downarrow	Flattening dune crest	Flattening dune crest	Yes
Jun 2020		1.95 m			
Jun 2020		1.95 m	Trough scour	Trough scour	
↓ ↓	$\alpha > 1.0$	\downarrow	Flattening dune crest	Flattening dune crest	No
Dec 2020		1.91 m			
Dec 2020		1.91 m			
\	$\alpha < 1.0$	\downarrow	Sedimentation troughs	Sedimentation troughs	Yes
Feb 2021		1.40 m			

Table C.7: Hydraulic changes and response of river dunes. The expected behavior of the river dunes has been obtained out of the literature described in appendix A.5.

C.3. Tidal conditions and response estuarine sand waves

Research has be done to the response of estuarine sand waves on the tide, as was explained in appendix A.5.4. Zarillo (1982) investigated the stability of bedforms in the estuary near Sapelo island in Georgia, United States of America and Kostaschuk and Best (2005) researched the response of bedforms on variations in tidal flow at the Fraser estuary in Canada. Just as marine sand waves the estuarine sand waves initially start growing fast. Over time this growth slows down until eventually an equilibrium is reached. Both researches concluded that this equilibrium height is reached with the strongest flow velocities occurring during low tide.

Tidal data is investigated to see if any significant changes have occurred during since the pilot nourishment. There is looked at the low tide values since these determine the eventually equilibrium height of the estuarine sand waves. The low tide values oscillate yearly with an amplitude of approximately 15 centimeters as can be seen in figure C.3. Therefore it is expected that the estuarine sand waves grow fast until an equilibrium is reached and after that will show an oscillatory response to the tide.

When there is looked at the height of the estuarine sand waves since the pilot nourishment in table C.7, there can be seen that it grows quite fast. Most likely this is a contribution of the tide. Noticeable are the two stabilization plateaus occurring from June 2019 - December 2019 and from June 2020 - December 2020. These stabilization plateaus question if the equilibrium height is already reached. The equilibrium height of bedforms created by the tide, can be computed with either theoretical based models or estimated with empirical relations, as was described in appendix A.5.3. At this stage it is not possible to use the theoretical based models due to the lack of sufficient measurements on flow velocities and grains sizes. Therefore the empirical relation of Allen (1968) is used as a first estimate of the equilibrium height of the estuarine sand waves (see table C.8). This indicates that the equilibrium height has probably been reached at the second stabilization plateau from June 2020 - December 2020. It is uncertain what caused the first stabilization plateau from June 2019 - December 2019. As shown

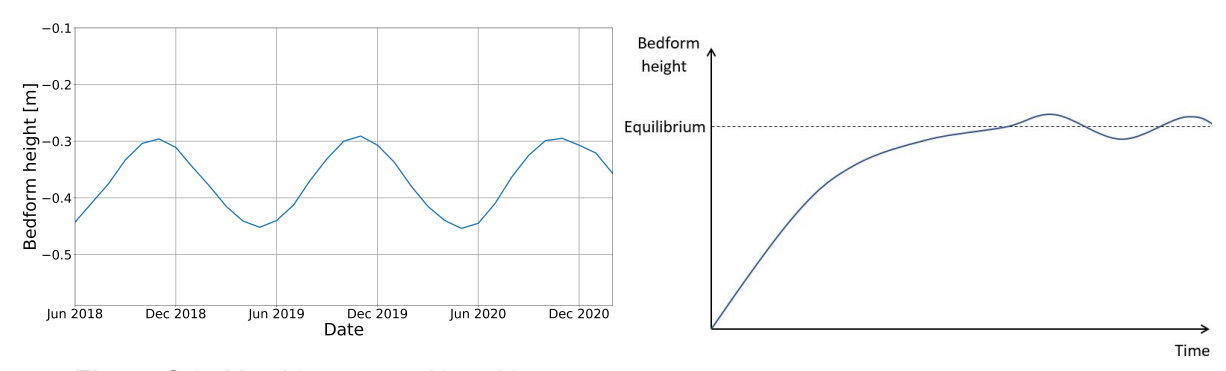


Figure C.3: Monthly averaged low tide at Spijkenisse.

Figure C.4: Expected bedform height by the tide.

in table C.7 the growth or stabilization of the estuarine sand waves could not be explained only by the seasonal river flow from December 2018 - June 2019 and from June 2020 - December 2020. The tidal forcing can explain this behaviour. From December 2018 - June 2019 the bedform height has not yet reached the equilibrium and therefore the tidal forcing will still create a larger bed form. From June 2020 - December 2020 the bedform tends to stabilize, most likely since the equilibrium height is almost reached.

Besides the two highlighted contributions of the tide, the tide was always present and contributing to the development of the bedforms. Together with the varying seasonal river flow this resulted in the presence of these large bedforms. It is expected that the tide is responsible for the development of the systematic pattern, since this is often seen by marine bedforms. On top of that, the tide causes the continuous presence of the estuarine sand waves. Seasonal river flow develops river dunes that are only prominent part of the time. This is not seen back in estuarine sand waves at the pilot site. Most probably the tide overrules this principle since its ongoing presence always forces the bedforms in the Rhine-Meuse delta.

Date	Average water depth [m]	Average dune height [m]	Equilibrium bedform height [m]
June 2018	-14.17	0.69	2.02
December 2018	-14.23	0.87	2.03
June 2019	-14.32	1.24	2.04
December 2019	-14.40	1.25	2.06
June 2020	-14.50	1.95	2.07
December 2020	-14.57	1.91	2.08
February 2021	-14.53	1.40	2.08

Table C.8: First estimation of equilibrium bedform height with empirical relation of Allen (1968).

C.4. Change in conditions since pilot nourishment

The analysis above has shown that the tidal forcing and the river discharge together can explain why these bedforms have grown in the last years. However not yet answered is why the estuarine sand waves only formed after the nourishment. This suggest that some conditions have changed. Below, a list of hypothesis is given on the conditions that could have changed and triggered the formation of the estuarine sand waves after the pilot nourishment.

If possible, the hypothesis is rejected or confirmed.

- The first condition that could have changed since the nourishment is the sediment type at the river bottom. The Rhine-Meuse delta has a very heterogeneous subsoil, which includes many cohesive sediments like clay and peat. Potentially, not enough non-cohesive sediment was present before the pilot nourishment to allow for the formation of the fully developed estuarine sand waves. The nourishment itself consisted out of 150,000 m³ of non-cohesive sand, dredged from the Nieuwe Waterweg. This change could have allowed the hydraulic conditions to form the estuarine sand waves. Prior to the nourishment only a few irregular bedforms were present at the scour section. Most likely these were transported from upstream and moved over the poorly erodible clay and/or peat layers. Unfortunately, no kind of soil samples or borings from scour section 5 are available to confirm or reject this hypothesis.
- The other sediment conditions that influences the size and presence of bedforms is the grain size. Very fine sediments have a much lower critical suspension threshold, meaning that relatively gentle hydraulic conditions can already pick up and suspend the grains. Therefore only very small bedforms can develop on the river bottom since the critical suspension threshold is easily exceeded and sediments are transported out of the pilot site. Coarser sediments have a much higher critical suspension threshold and hence much larger bedforms can develop. It could be possible that scour section 5 contained too fine sediments which limited the formation of any significant bedforms. If the nourishment introduced coarser sand than the original material at the river bottom, it could have allowed for the formation of the large estuarine sand waves. As explained in the first hypothesis, there are no soil samples or borings of scour section 5 available. Therefore this hypothesis can not be confirmed or rejected. However, many bedforms are present both upstream and downstream of the scour hole which do suggest that the material in the Oude Maas is coarse enough to create bedforms.
- The third possibility is that the pilot nourishment has introduced more and larger perturbations than before the nourishment. A requirement for the development of any bedforms by the tide is that enough flow alternations should be present such that the tide can develop its circulation cells (Hulscher & Dohmen-Janssen, 2005; van Gerwen, 2016). These flow alternations are caused by perturbations in the river bottom. If the nourishment introduced more, larger or more closely packed perturbations, it could explain the development of the estuarine sand waves. The tide will then start developing the systematic sinusoidal bedforms towards an equilibrium. Eventually the height of these bedforms becomes large enough to allow for flow separation, allowing for even faster development and more influence of the seasonal river flow.

Out of the MBES measurements there is checked if the amount, average height or average distance between the perturbations has changed since the pilot nourishment. As can be seen in table C.9 there are no changes in the amount of perturbations. On top of that, the average height of these perturbations has decreased and only a small difference in distance between perturbations is present. Therefore the hypothesis that the estuarine sand waves developed due to the introduction of more and larger perturbations by the pilot nourishment, can be rejected.

	Amount of perturbations	Average perturbation height [m]	Average distance between crest perturbations [m]
December 2017	19	0.91	61.16
June 2018	19	0.69	65.72

Table C.9: Change in perturbations since the pilot nourishment.

It could also be possible that there were no changes in conditions at scour section 5 but that the
estuarine sand wave developed elsewhere and fully migrated into the pilot site. Therefore there
is looked at the river bottom upstream of scour section 5 in figure C.5. Scour section 5 is located
from Rkm 999.8 - 1001 and the pilot nourishment has been performed in the spring of 2018 at
the left side of the scour section. The red arrows represent the distance along the channel where
the estuarine sand waves are found.

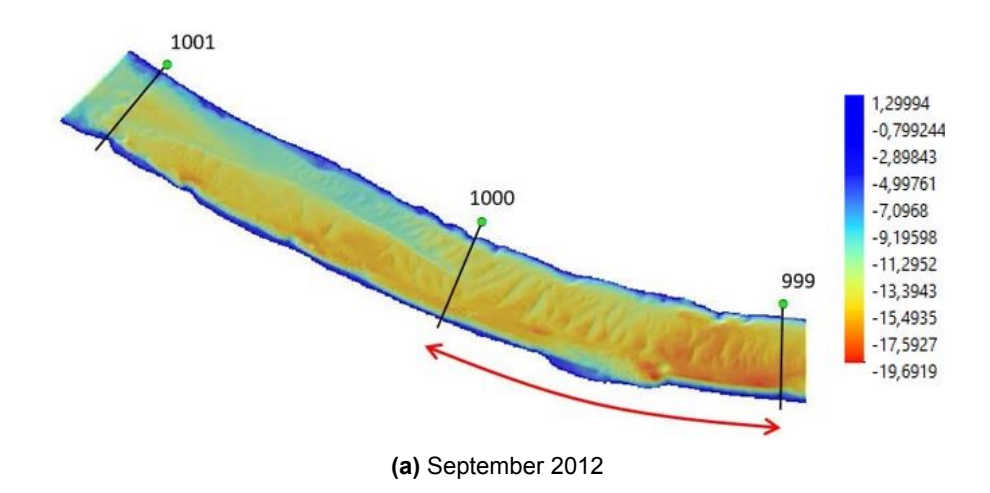
It can be seen that that before the nourishment in 2012, a sand wave is present at Rkm 999 - 1000. Five years later in June 2017 this sand wave is still present at the same location. Some

smaller and irregular bedforms have entered scour section 5 but the large sand wave has not fully migrated in. It seems to be bound to the area of Rkm 999 - 1000 during a period of 5 years. After the pilot nourishment in June 2018, the estuarine sand waves are also encountered at scour section 5. This suggests that the bedforms grow out of the nourished sediments and not that they migrated entirely into the section. Otherwise this would have already happened before the pilot nourishment. However looking at figure C.5b and figure C.5c, it is suggested that the bedforms are growing not entirely simultaneously in scour section 5. It appears earlier on the upstream side of the nourishment. Therefore any influence of upstream bedforms is not yet ruled out.

The unverified and rejected individual hypothesis have shown more insight into what could have caused the development of the bedform at scour section 5. It seems most plausible that a combination of these causes are underlying to the development of the estuarine sand waves at scour section 5. Due to the nourishment more suitable sediment (non-cohesive) for the creation of bedforms has been deposited at the river bottom. The flow alternations, caused by the already present sand waves upstream of scour section 5, could have contributed to the development of the estuarine sand waves in the nourished sediments. Before the nourishment this could not happen since the sediment conditions where not sufficient.

Recommendations

Further analysis on the above stated hypothesis is recommended. This is required to conclude if the development of the estuarine sand waves at the pilot site is a one time occurring phenomena or that the development of these bedforms is coupled to shallow nourishments in the Rhine-Meuse delta. Especially since they can pose a danger to the navigability of vessels in shallower parts of the delta. A more general but valuable recommendation is to further investigate the behaviour of the estuarine sand waves on a theoretical basis. It would be beneficial to understand how the estuarine sand waves responses to seasonal river flow and the tide combined, not separately as done in this research. In this way more accurate and quantitative predictions can be done of the occurrence, size and shape of estuarine sand waves. Finally, it would be wise to analyse future MBES measurements of the pilot site and monitor the development of these bedforms. It could help in understanding the behavior and formation of these sand waves.



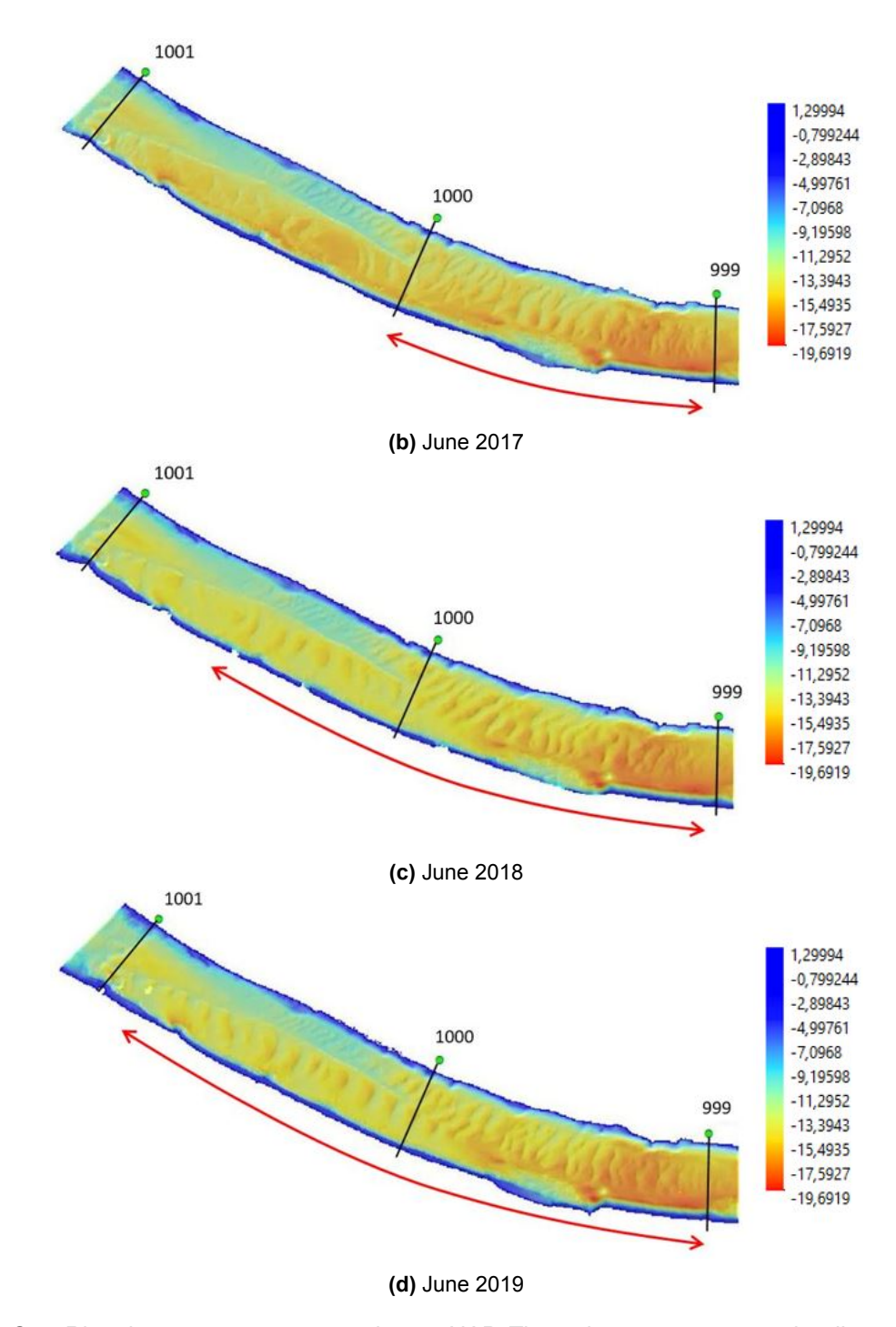


Figure C.5: River bottom measurements in m + NAP. The red arrows represent the distance along the channel where the estuarine sand waves are found.



Characteristics Delft3D model and field conditions

D.1. Characteristics Delft3D model

The output of a Delft3D model that simulates the entire Rhine-Meuse delta is used for answering of the sub research questions two (section 4.2), three (section 4.3) and four (chapter 5). Only the results of a partition of this model will be used within this research. This partition spans the area of the confluence/bifurcation Oude Maas and Spui, equal to the area of interest in figure D.1. The most important settings of the model of the Rhine-Meuse delta can be found in table D.1. Remarks regarding the bathymetry, initial conditions, boundary conditions and validation of the model are made below the table.

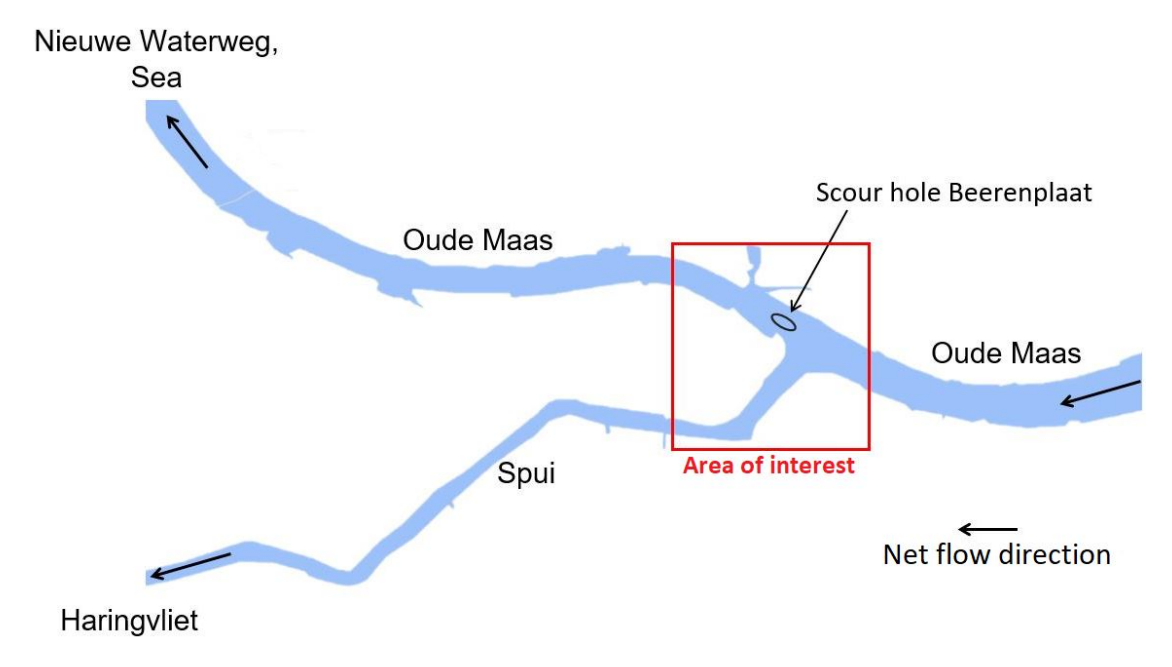


Figure D.1: Location of the scour hole Beerenplaat.

Parameter	Value	Remark
$\Delta x \approx$	25 m	at partition 93, varies slightly per cell
$\Delta y pprox$	$25~\mathrm{m}$	at partition 93, varies slightly per cell
max. Courant number	0.7	
time frame	14-06-2018 uı	ntil 17-11-2018
$\Delta t_{max} =$	30 s	
$\Delta t_{output} =$	2 hours	time step at which output is saved
Turbulence model	$k - \epsilon$	
Uniform horizontal eddy viscosity	$0.1 \; m^2/s$	
Uniform horizontal eddy diffusity	$0.1 \; m^2/s$	
Uniform vertical eddy viscosity	$5\cdot 10^{-5}~\mathrm{m}^2/\mathrm{s}$	
Uniform vertical eddy diffusity	$5\cdot 10^{-5}~\mathrm{m}^2/\mathrm{s}$	
Salinity	on	

Table D.1: Main settings of the Delft3D model.

- The bathymetry used within the model has been measured in 2018 by both Rijkswaterstaat and Havenbedrijf Rotterdam. It shows similar characteristics as the recent measured bathymetries that were described in chapter 3. It is however robuster than the MBES measurements, since the MBES measured on a much finer grid than at which the model output is generated. The bathymetry of partition 93 can be seen in figure D.2.
- The model only covers the hydrodynamical simulations. Sediment transport is not enabled within the settings. The bathymetry during the entire time frame of the model is similar as on 14 June 2018 in figure D.2.
- For the initial conditions, models runs were performed for both water levels and salinity. The water levels have been obtained with a two week Delft3D simulation. The salinity has been determined from with an 2D Delft3D model of the entire Rhine-Meuse delta, which is precursor of this model.
- · To account for spin up time, the model results of the first few weeks should not be used.
- For the discharge boundary conditions, discharges of the Lek, Waal and Maas have been used, which were measured by Rijkswaterstaat. The boundary conditions for salinity and water level at sea have been obtained from 3D simulations of the entire North Sea. The boundary conditions for the pumping stations, have been obtained from various "waterschappen".
- Due to the long time development of the model, it has already been validated. This has been done
 based on different measurements taken by both Rijkswaterstaat and Havenbedrijf Rotterdam on
 both salinity and water levels. Besides validating this also allowed for improvement of the model.
- The bathymetry in figure D.2 shows that the confluence/bifurcation is actually discordant, meaning that the meeting branches have different bed levels. As explained in section 2.2.5 a discordant confluence can have essential effect on the flow regime, sediment motion and the resulting morphology at a confluence.

D.2. Field conditions

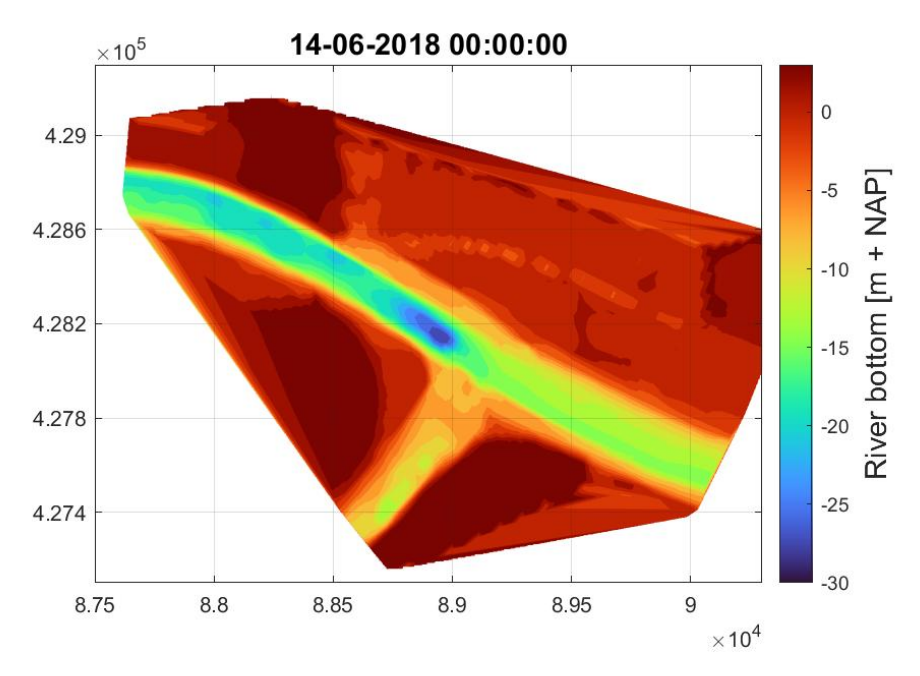
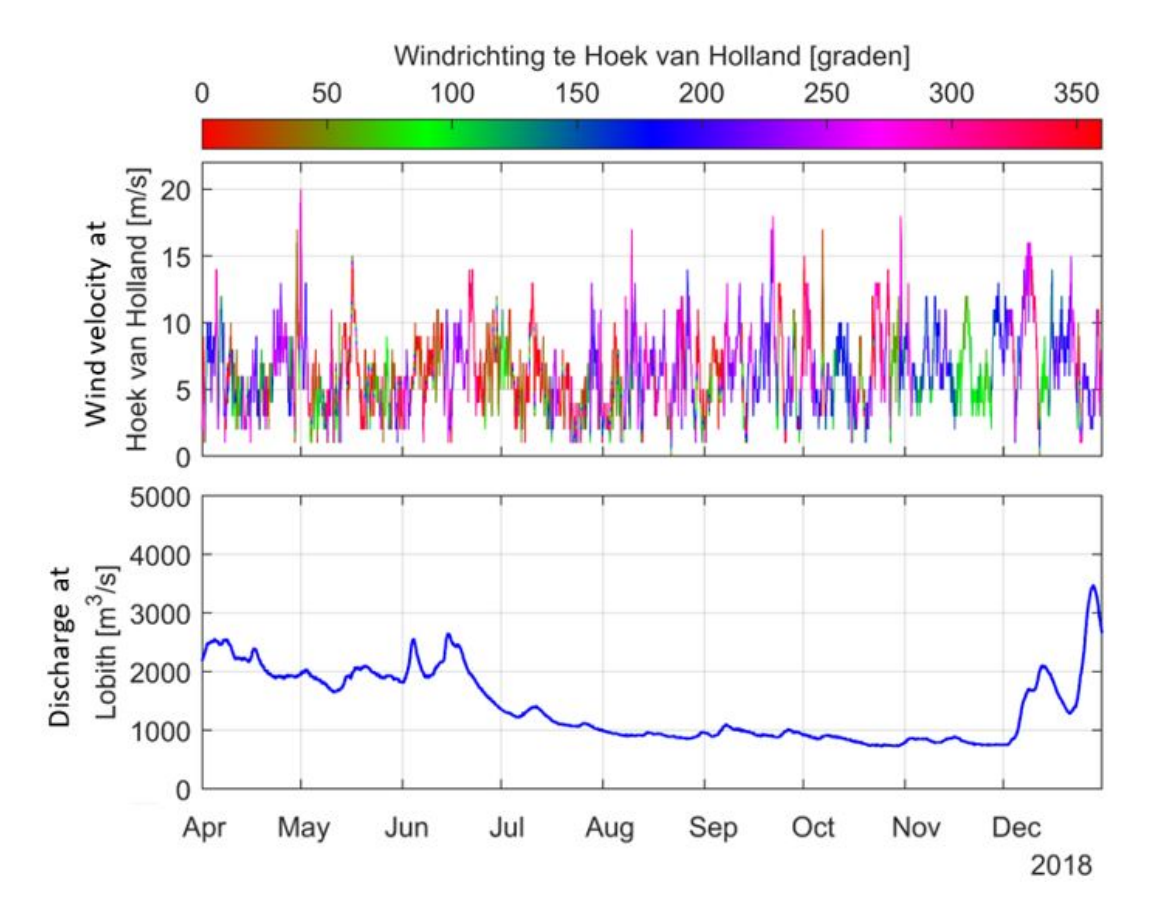


Figure D.2: Bathymetry at partition 93 on 14 June 2018.

D.2. Field conditions

Below an overview of the field conditions during the time frame of the Delft3D model can be seen.



D.2. Field conditions

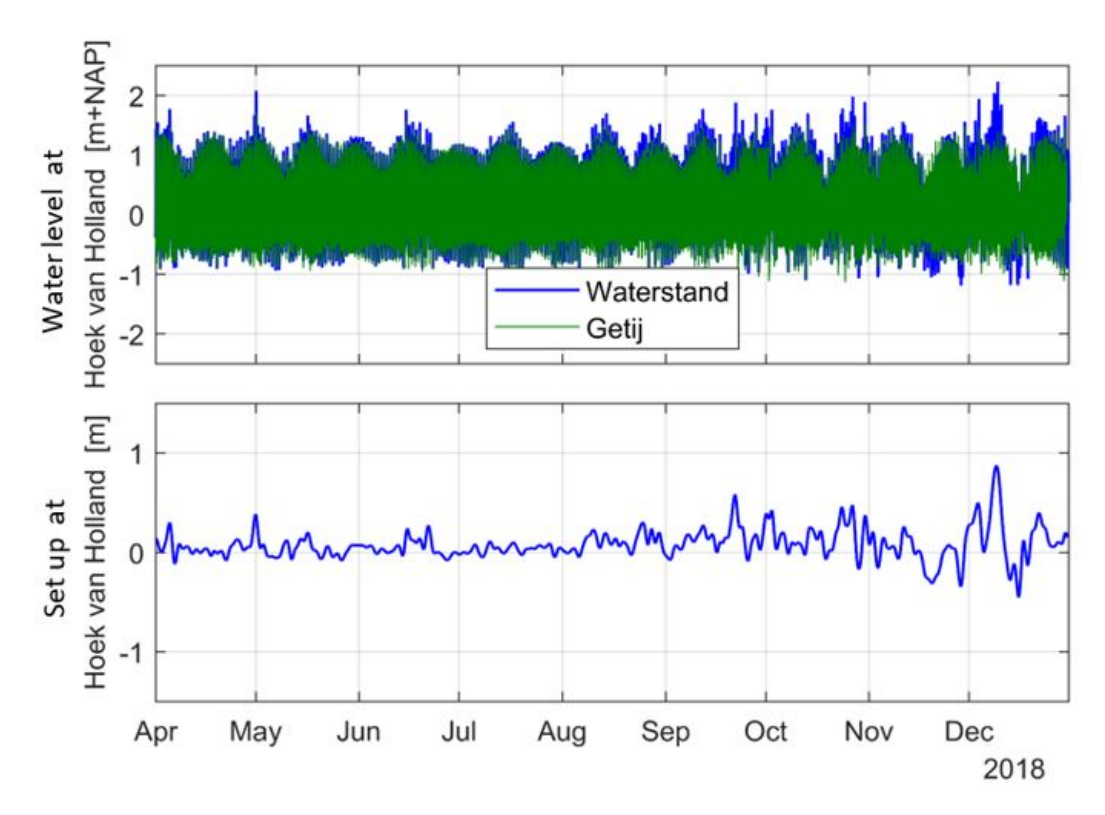
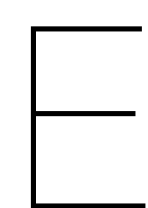


Figure D.3: Field conditions during the time frame of the model, investigated by V. Chavarrias (Deltares).



Comparison model results and ADCP measurements

Within the answering of sub research question 2 in section 4.2, the flow field at the confluence/bifurcation Oude Maas and Spui is investigated for the base case. During this base case, a period of the model is selected which has similar field conditions as on 11 February 2021, when the ADCP measurements were taken. This period is from 13 July 12:30 until 14 July 12:30, contains two tidal cycles and has almost equal water levels at Spijkenisse (see figure E.1). Not yet investigated is the accuracy of this new period in the model, to estimate the discharges and flow velocities measured by the ADCP device. This will be addressed within this appendix.

First, there will be looked at the match of the discharges and flow velocities for peak ebb flow and after that for peak flood flow. Figure E.1 and figure E.2 show which of the model output time steps of the new period can be compared with which ADCP measurements.

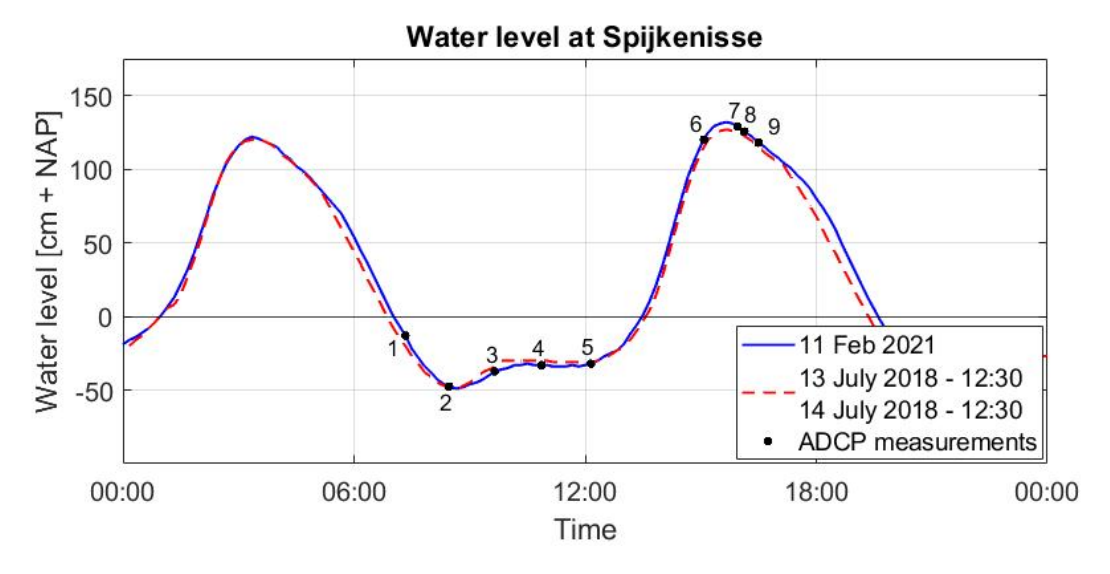


Figure E.1: Comparison of water levels at Spijkenisse (measured by Rijkswaterstaat).

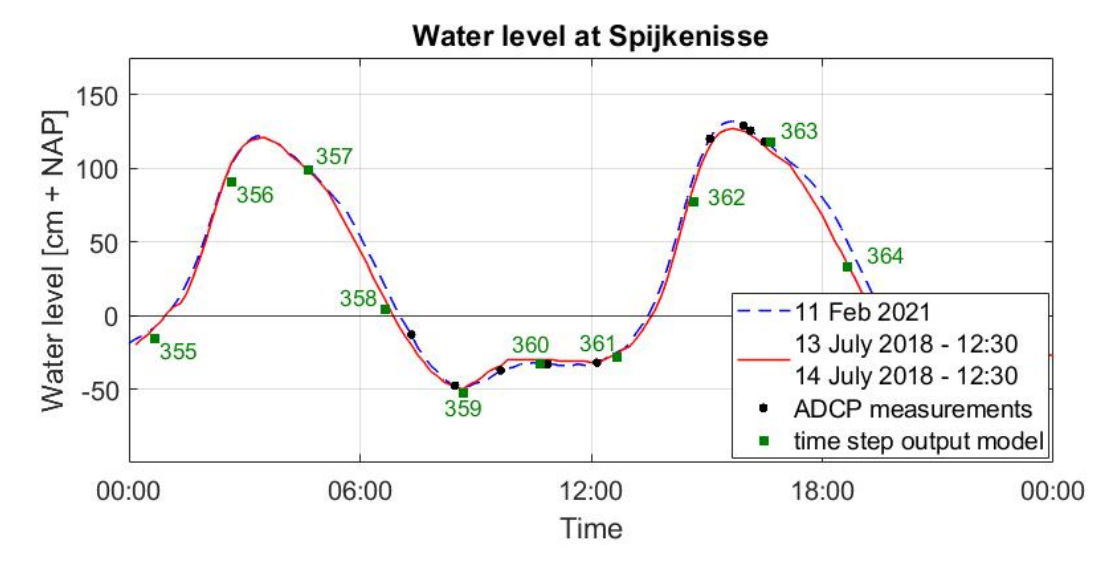


Figure E.2: Water levels at Spijkenisse measured in the field by Rijkswaterstaat and computed in the model.

Peak ebb flow

Table E.1 compares the discharges of two ADCP measurements with the model results of cross-sections on the corresponding locations during ebb flow. It shows that the discharges computed by the model are larger but are paired with a larger flow area. Therefore the average velocity has been computed to relate the differences. The average velocity in both ADCP measurements is around 10 % larger than computed by the model around same moment. This questions how the velocity is distributed over the cross-section. Figure E.3 shows the depth averaged ebb velocities at Rkm 995.8 of both the model and the ADCP measurement 2. This figures shows that the peak of the depth averaged velocities measured by the ADCP device is not captured in the model results. Closer to the edges of the scour hole, the ADCP measurements and the model results match better. Also noticeable, is that a smaller scour hole is measured by the ADCP device than computed by the model, which is caused by the grid of the model. The ADCP device measures the velocities every 1 - 1.5 meters within the cross-section while the model computes it at a 25 meter interval, making it much more robust.

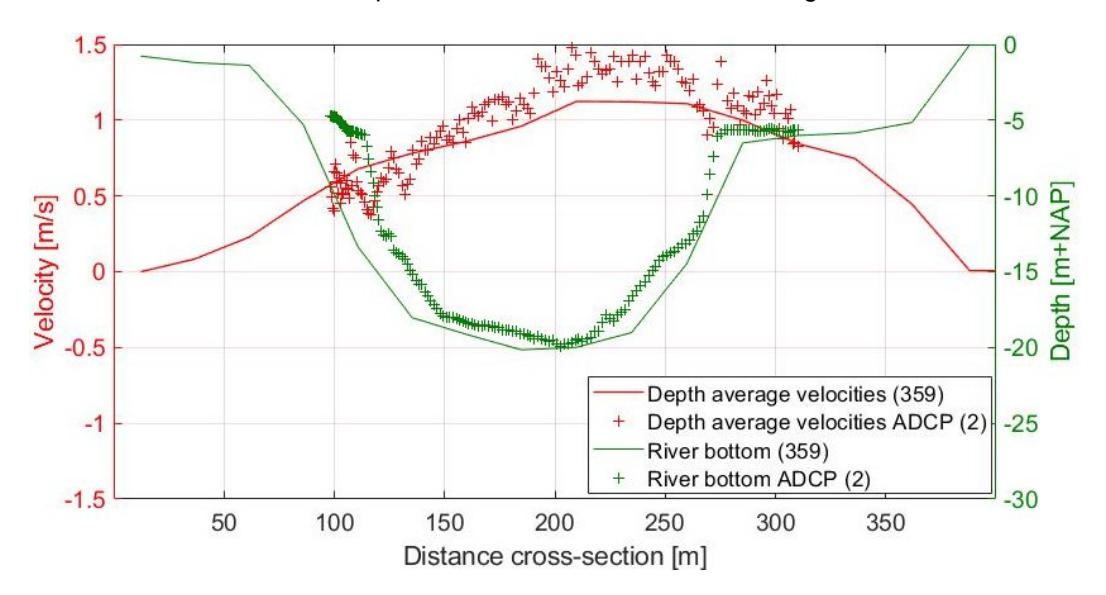


Figure E.3: Streamwise velocities and river bottom at time step 359 and ADCP measurement 2.

		Ebb cros	s-section 1	Ebb cros	s-section 2
		Model time step 359	ADCP measurement 2	Model time step 360	ADCP Measurement 4
Discharge	[m ³ /s]	3846.8	3031	3309.9	2694
Flow area	$[m^2]$	3966.3	2886	4080.9	3078
Average velocity	[m/s]	0.97	1.05	0.81	0.88

Table E.1: Comparison of discharges in the model and the ADCP measurements during peak ebb flow.

Peak flood flow

The same discharge and velocity comparison is done with the time step 363 and ADCP measurement 9 for peak flood flow. Table E.2 shows that the model overestimates the discharges that are measured in the field. This questions how the velocity field is distributed over the cross-section. In figure E.4 can be seen that the velocities computed by the model during peak flood flow are much larger. The model results have an average velocity that is around 4 times higher. An explanation for this could lie within a mismatch of the moment that peak flow velocities occur. During ADCP measurement 9, relatively small depth averaged velocities are found that indicate the peak flood has either passed or still should come. Therefore the discharge out of time step 363 is compared with all earlier taken ADCP measurements during flood (6, 7 and 8) in table E.2. What can be seen is that the flood peak has already passed and that actually none of the ADCP measurements at this cross-section have similar discharges or average velocities, during flood flow. The most resembles is found with ADCP measurements 6. The model computes average velocities in this section that are around 30 % larger than measured in the field. In figure E.5 can be seen that the depth averaged velocities at this ADCP measurement 6 are much closer than in measurement 9. They follow the trend of the velocity distribution at the cross-section but still show some mismatch around the left edge of the scour hole (75-150 m). At this section the velocities are still positive (seawards directed), while in the rest of the cross-section the water column is moving land inwards. Therefore there is also looked at the velocity distribution over the depth. In figure E.6 can be seen that the velocities in the field at 15:05 (ADCP measurement 6) show the same behavior as computed in the model at 16:40 (time step 363). The largest land inwards velocities are found on the center right side of the scour hole. The model shows, that outside the scour hole the streamwise velocities are close to zero. The ADCP measurements indicates that the same occurs on the left edge of the scour hole with even positive velocities. The robustness of the model can be responsible for showing slightly different results. The delay of the model at this flood period is around 1 hours and 35 minutes. A similar type of delay was not observed during peak ebb flow.

		Flood cross-s	section 1			
		Model	ADCP 9	ADCP 6	ADCP 7	ADCP 8
		time step 363	(16:30)	(15:05)	(15:57)	(16:08)
Discharge	[m ³ /s]	-3522.1	-717	-2356	-1472	-1191
Flow area	$[m^2]$	3988.5	3416	3570	3482	3448
Average velocity	[m/s]	-0.88	-0.21	-0.66	-0.42	-0.35

Table E.2: Comparison of discharges in the model and the ADCP measurements during flood.

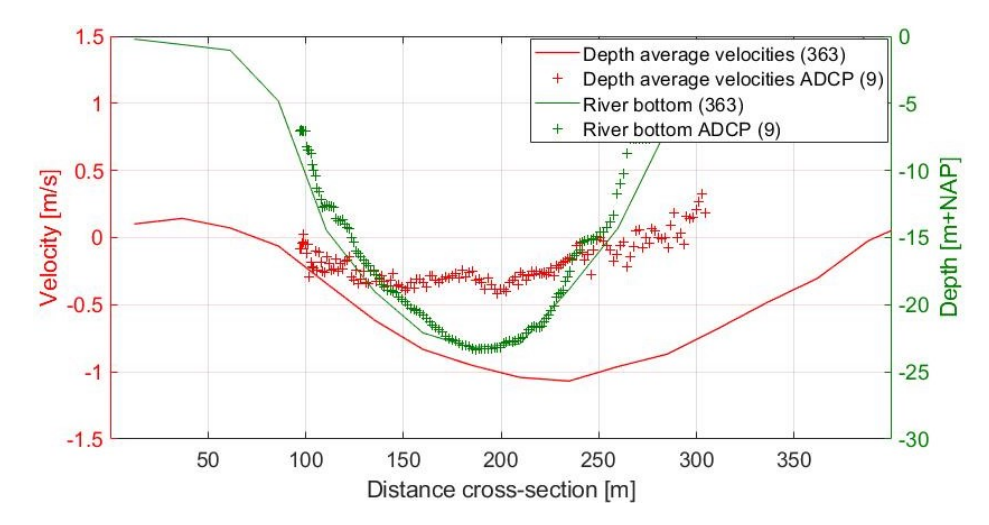


Figure E.4: Streamwise velocities and river bottom at time step 363 and ADCP measurement 9.

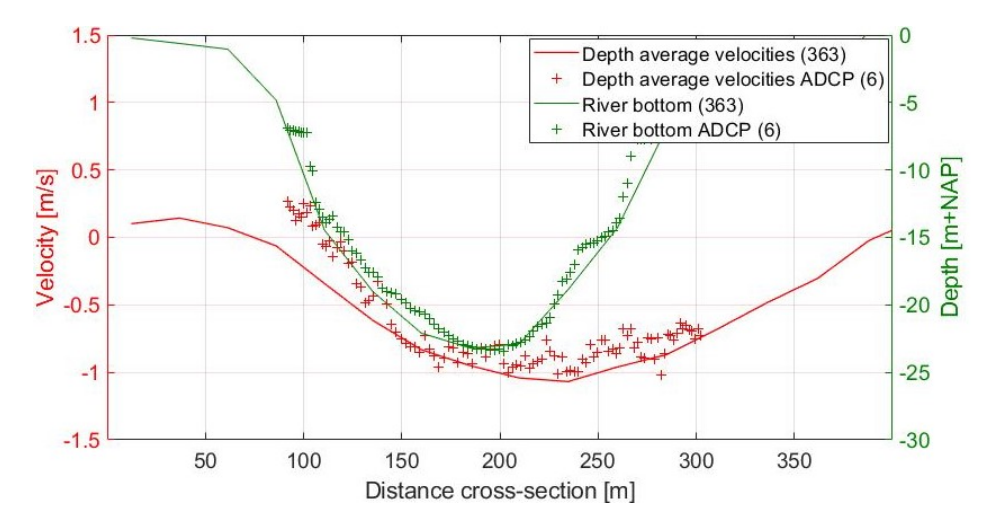
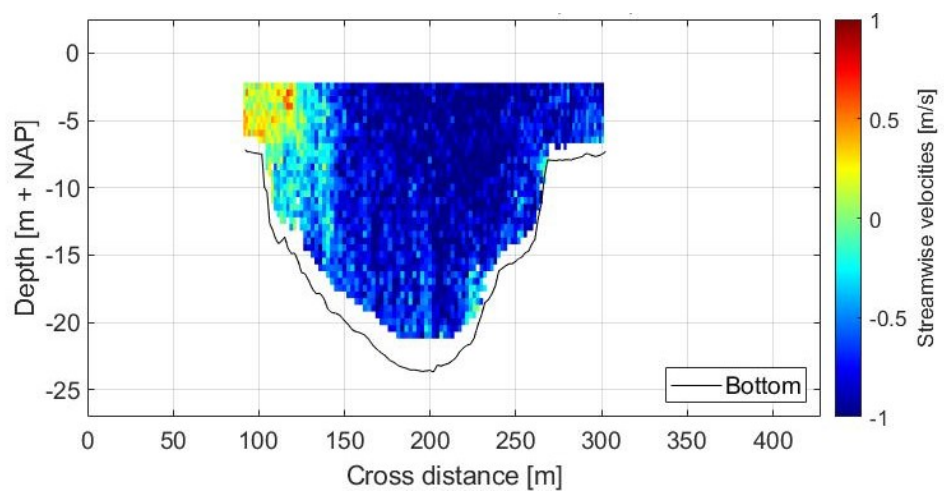
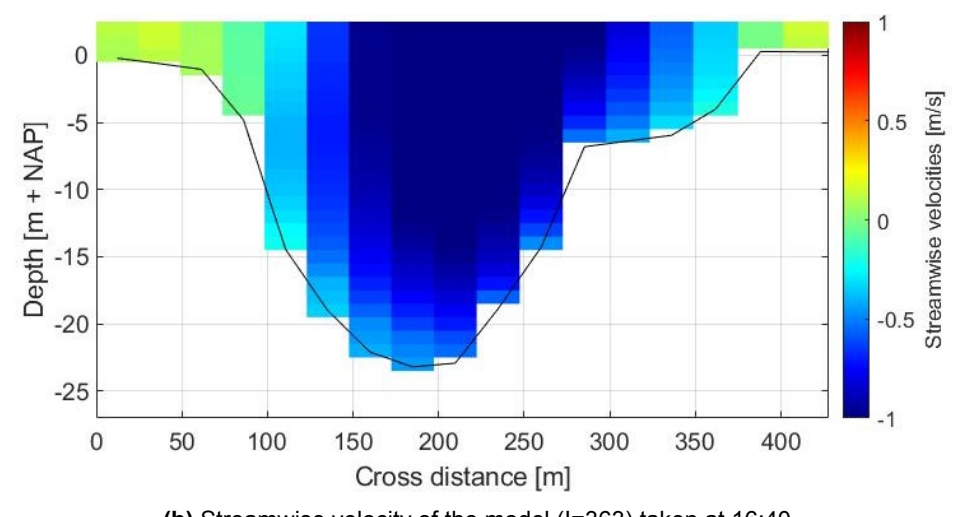


Figure E.5: Streamwise velocities and river bottom at time step 363 and ADCP measurement 6.



(a) Streamwise velocity during ADCP measurement 6 taken at 15:05.



(b) Streamwise velocity of the model (I=363) taken at 16:40.

Figure E.6: Velocities in both the ADCP measurement and model at Rkm 995.8.

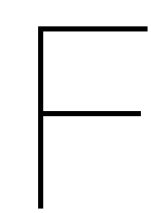
Conclusion

On the match between the field ADCP measurements and the model results during peak ebb flow and peak flood flow, the following observations were made.

- The flow direction in the system switches between the ebb and flood flow, in both the field measurements and the Delft3D model results.
- The model results follow the field behavior during ebb quite well but have a slight underestimation of the average streamwise velocities with 10 %.
- The model produces similar velocities during flood as were observed in the ADCP measurements, but only if there is accounted for a time delay of 1 hour and 35 minutes. This time delay could suggest that the model struggles with simulating the moment flow direction changes in the system. The average streamwise velocities in the field are overestimated with 30 %.
- The under and overestimation of the streamwise velocities in the model can be explained by the robustness of the model in both time and space. The model has an output time step of Δt_{output} = 2 hours, while table E.2 shows that the discharge can be 300 m³/s less in only 11 minutes (between ADCP 7 & 8). The results of the Delft3D model are computed and stored on a grid with $\Delta x, y \approx$ 25 m and Δz = 1 m. The grid on which the ADCP measurements are performed has Δx = 0.1 m, Δy = 0.4 m and Δz = 0.5 m. This makes the model robust with respect to the ADCP measurements in both time and space. As a result it can not capture the same detailed and time specific behavior as is seen in the ADCP measurements.

Overall it can be concluded that the model results show a similar behavior during peak ebb and peak flood flow but have respectively an underestimation or overestimation of the average flow velocities. Most likely this also affects the moment at which the flow direction changes in the system, causing a time delay. Despite, the model results show similar flow characteristics in the streamwise direction, as were found in the ADCP measurements.

One final remark should be made. During this analysis there is not accounted for the measurement error of the ADCP device. This should be included to determine the actual accuracy of the model to simulate the field conditions on 11 February 2021.



Secondary flow patterns

This appendix analyzes the secondary flow patterns at the scour hole Beerenplaat, These were observed in section 4.2 during peak ebb flow in both the base case and the second case with different conditions. Vertical flow recirculation cells were observed downstream of the confluence/bifurcation Oude Maas and Spui. However, the amount of cells in a cross-section and their behavior does not match with expectations based on literature. As described in section 2.2.5, two counteracting recirculation cells should be present in a single cross-section downstream of the confluence. However, only one recirculation cell was observed in the model results and the rotation direction and location even varied. Therefore this appendix will investigate the secondary flow patterns in the model more extensively in both time and space and will discuss how these affect the presence of the shear layer.

F.1. Characteristic patterns

It was shown that the secondary flow patterns developed during peak ebb flow, when the system behaved as a confluence and the flow of both the Oude Maas and the Spui were joining inside the scour hole. However, these observations were done by only looking at one cross-section in the Oude Maas for both cases. To better understand how the secondary flow is formed, the model results will be analyzed at four new cross-sections that are shown in figure F.1. These cross-sections are only located at the scour hole since the model results show that the the secondary flow patterns are bound to this area. Upstream of the scour hole, closer to the confluence/bifurcation, the flow from the Spui has not yet deflected enough to cause any recirculation. Figure figure F.2a shows an example of this. Downstream of the scour hole, the recirculation has already disappeared as is showed in figure F.2b. Therefore the four cross-sections are located only at the scour hole. To include the time differentiation, the secondary flow patterns has been analyzed at every time step with peak ebb flow. When moving trough these time steps, it was encountered that the secondary flow can be shaped in three different characteristic patterns over the four cross-sections. First, it will be shown what the three characteristic patterns are and afterwards it will be explained how these differ with the expected secondary flow according to literature.

In figure F.3, figure F.4 and figure F.5 schematizations of the three characteristic patterns can be seen. Important to mention is that these are purely visualizations and no exact representation of the model results. The velocity magnitudes and directions in the model output can vary with the three schematizations. On top of that, the figures only show the cross-stream and vertical velocities. The streamwise velocities are intentionally left out for better visualization of the recirculating behavior. Finally, it is important to state that the schematizations do not include the profile of the scour hole. In reality it would become shallower in the streamwise direction.

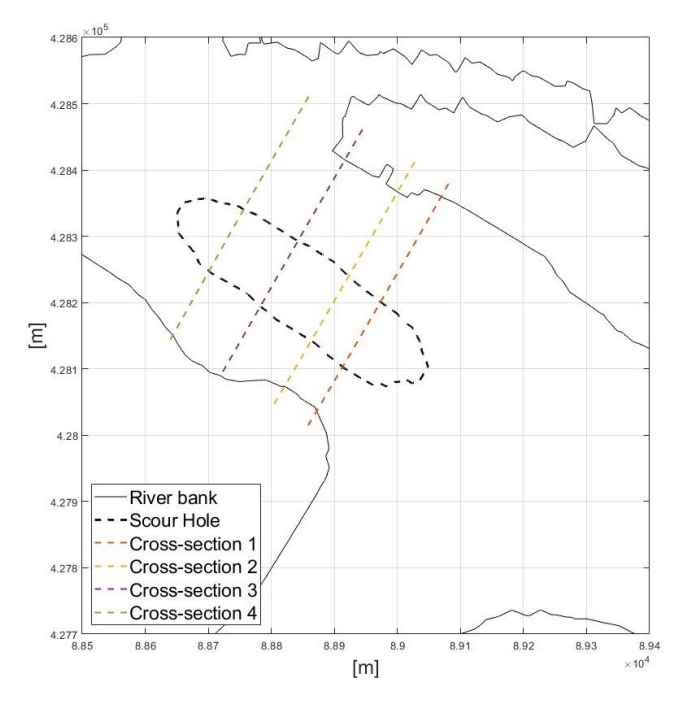
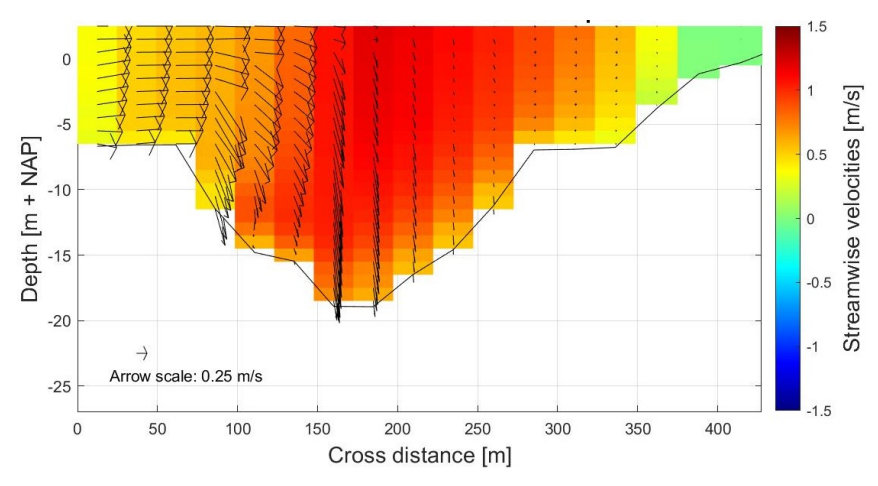
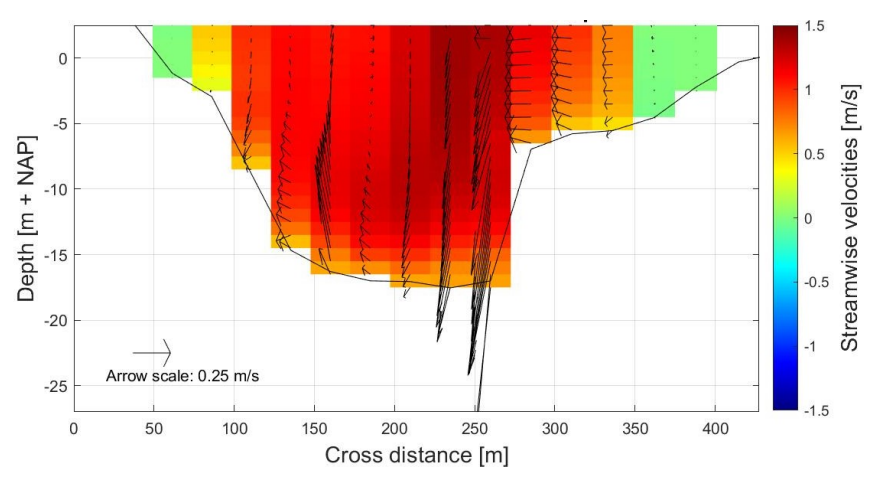


Figure F.1: Four cross-sections at which the secondary flow patterns are analyzed.



(a) When the flow enters the scour hole at time step = 359 (peak ebb flow).



(b) When the flow leaves the scour hole at time step = 359 (peak ebb flow).

Figure F.2: Cross sections showing the velocities at the scour hole Beerenplaat. Velocity vectors represent the cross-stream and vertical velocities.

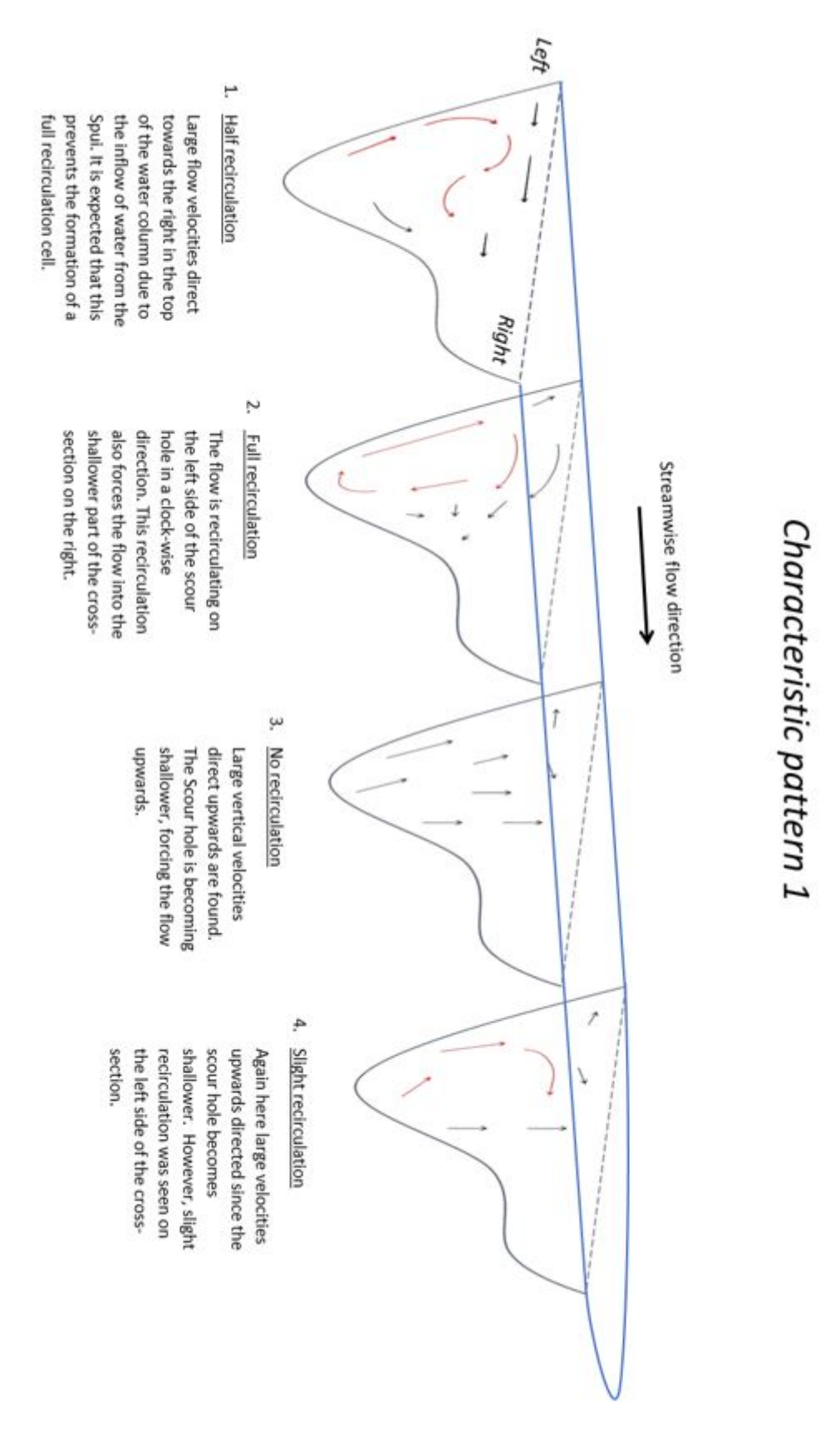


Figure F.3: Characteristic pattern 1 of the secondary flow downstream of the confluence Oude Maas and Spui.

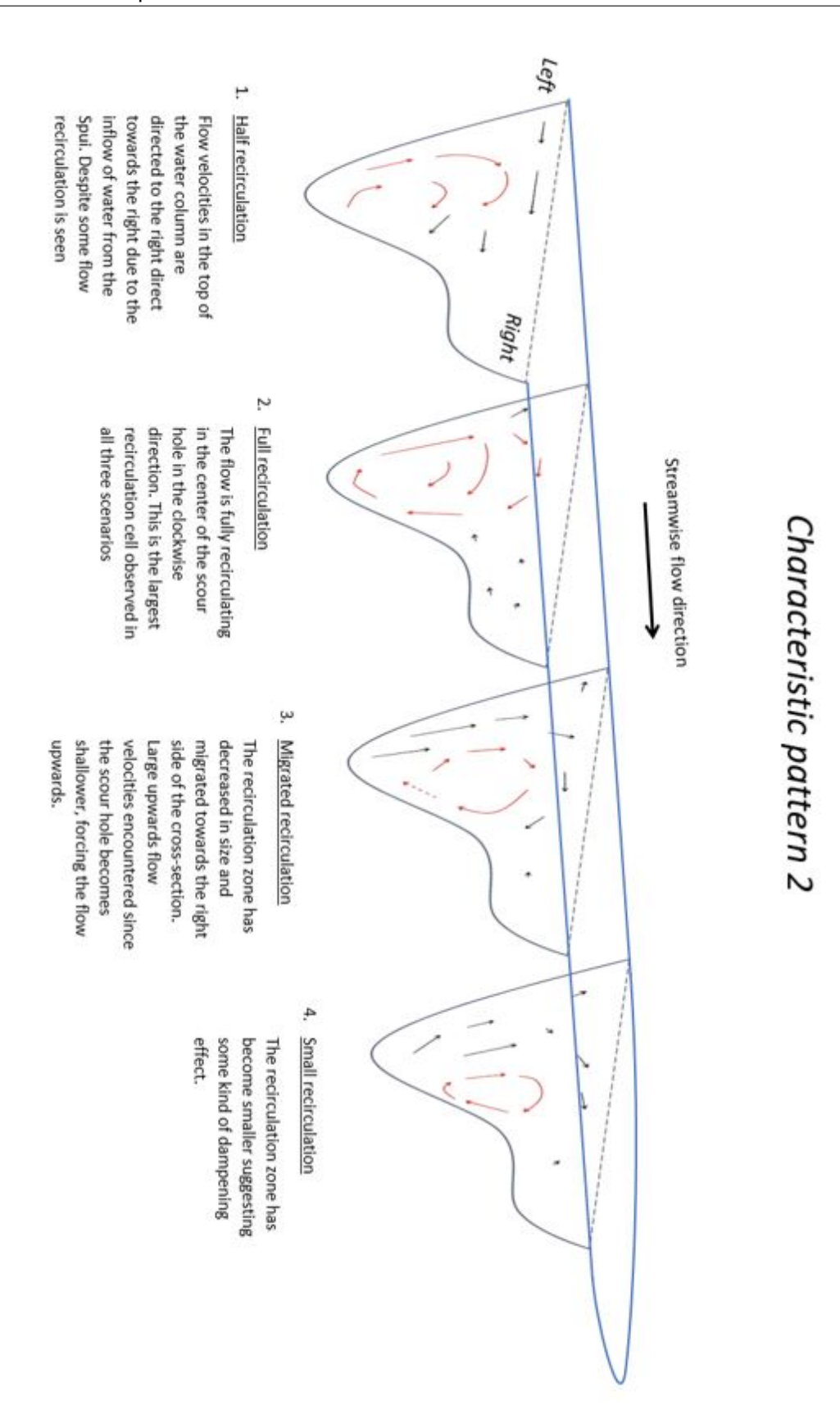


Figure F.4: Characteristic pattern 2 of the secondary flow downstream of the confluence Oude Maas and Spui.

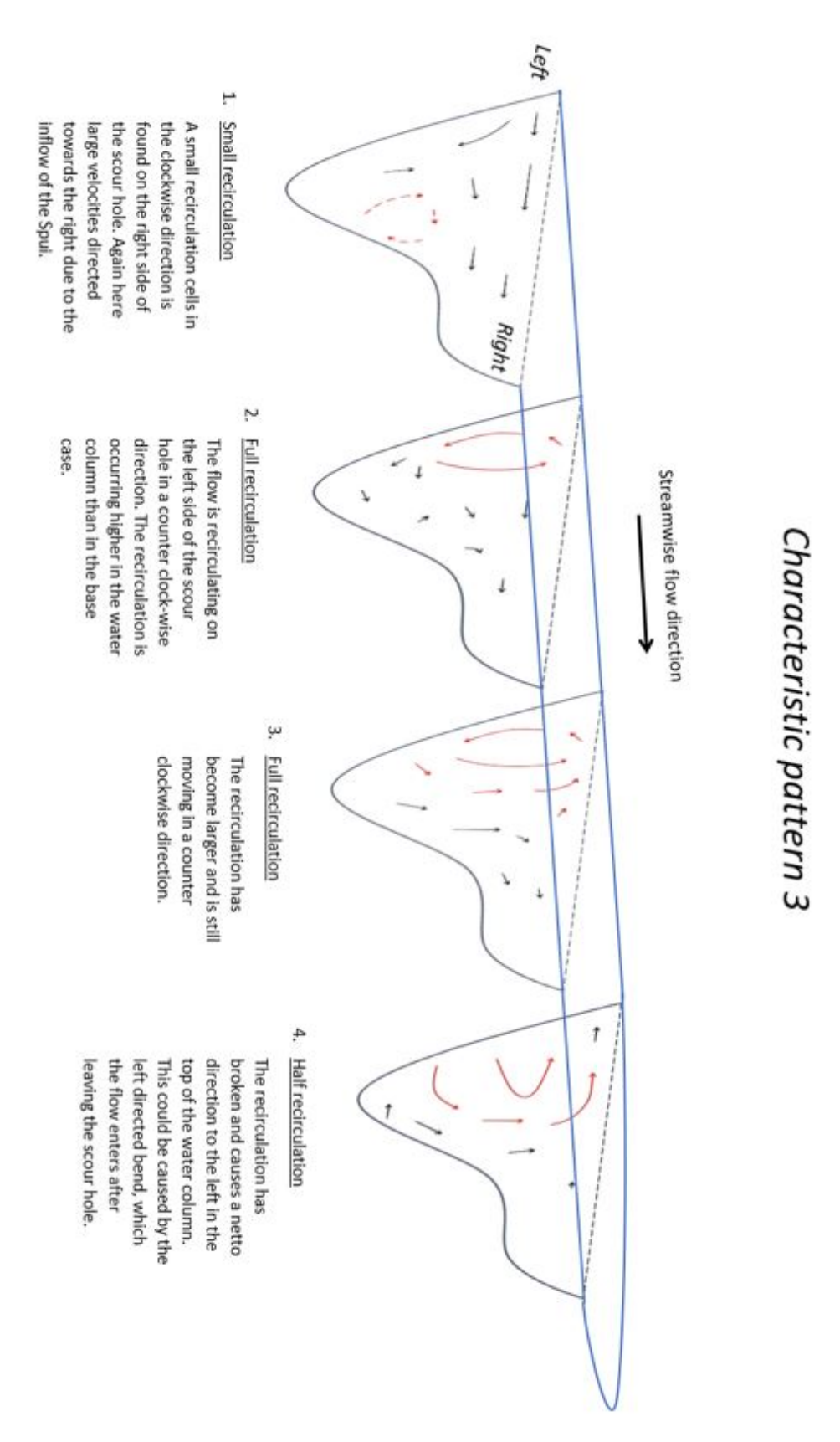
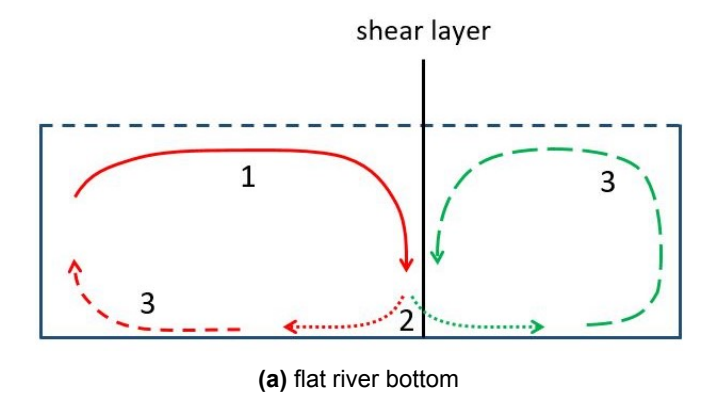


Figure F.5: Characteristic pattern 3 of the secondary flow downstream of the confluence Oude Maas and Spui.

In all three characteristic patterns the secondary flow is characterized by the presence of vertical recirculation cells. In characteristic pattern 1 the full recirculation cell is only present in cross-section two with some formation already in the cross-section one. The cell is located on the left side of the scour hole and rotates in the clockwise direction. At the third cross-section it has completely disappeared. Characteristic pattern two behaves initially quite similar. The vertical recirculation cell is forming in the clockwise direction at the first cross-section and grows towards full recirculation in the entire scour hole at cross-section two. After that it becomes smaller and migrates towards the right side of the scour hole. The vertical recirculation cell in pattern two is present in all cross-section and rotates in a clockwise direction. The third characteristic patterns is completely different than the first two. It starts with a very small recirculating cell on the right side of the scour hole which rotates in the clockwise direction. After that it changes towards a counter-clockwise larger recirculation on the left side of the scour hole. The recirculation cell keeps on growing between the second and third cross-section and eventually breaks in the fourth, resulting in large velocities directed to the left.

These three characteristic patterns significantly differ with what is expected downstream of a confluence according to the literature. As described in section 2.2.5, the literature predicts that two recirculation cells are present downstream of the confluence which rotate in opposite directions. The largest rotating cell was expected at the left side of the channel in the flow from the Spui and should rotate in a clockwise direction. On the right side, in the flow from the Oude Maas, a smaller recirculation cell moving in a counter-clockwise direction was expected. Both these recirculating cells should decrease in the streamwise direction. The three characteristic secondary flow patterns behave differently. At maximum, only one vertical recirculation cell is present. In pattern one, the clockwise recirculation occurs on the correct location, which is the left side of the channel. However, looking at the second characteristic, which also rotates clockwise, the recirculation cell first occurs in the entire scour hole but than migrates to the unexpected right side. Surprisingly, the third characteristic pattern consists out of counter-clockwise recirculation on the left side, which should be expected on the opposite right side. More deviating behavior is seen, when there is looked at the size of the cells. The recirculation cells should, after they have formed, decrease in size in the streamwise direction. It appears that characteristic one and two follow this behavior, but characteristic pattern three does not. The third pattern even shows a recirculation cell that grows instead of shrinks, which is again not what is expected.

Most likely the scour hole plays an important role for this deviating behavior. A first hypothesis regarding the difference in amount of cells is given below. The findings in literature were mainly obtained from flume test with a flat river bottom. The recirculation cells start developing on the left side with a clockwise motion, due incoming and deflecting flow from the Spui. If the river bottom is flat, the downwards moving flow will be pushed in two opposite directions at the bottom (see figure F.6a). As a result, two counteracting recirculation cells and a shear layer can develop. If a scour hole is present, it is hypothesised that the downward flow gradually follows the slope and only one recirculating cell forms (see figure F.6b). Unfortunately, this hypothesis can not be confirmed or rejected since no model runs were performed without the scour hole. On top of that, this hypothesis does not explain why the recirculation cell can rotate counter-clockwise or why the size increases in the streamwise direction, as was wall found for characteristic shape three. It could be possible that an explanation for this lies within the forcing conditions. Therefore it will be investigated when each of the characteristic patterns is present.



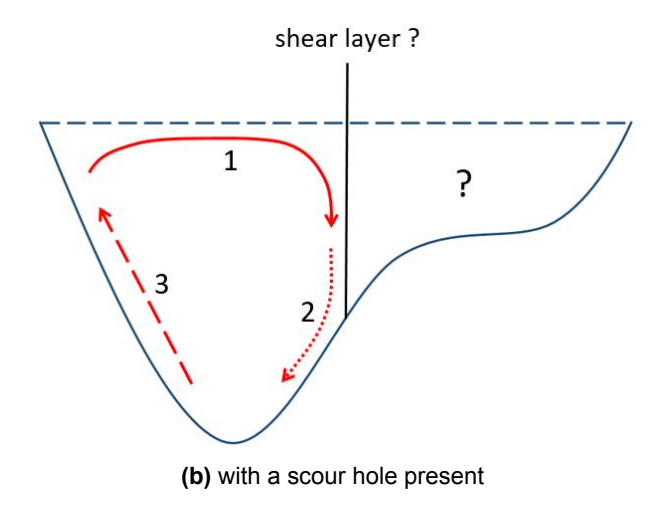


Figure F.6: Schematization of the development of recirculation cells for a flat river bottom and one with a scour hole. The numbers represent the order in which the recirculation cell develops.

F.2. Conditions for development characteristic patterns

50 individual tidal cycles within a period of the model are analyzed to determine when each of the characteristic patterns develops. The complete results of this analysis can be found in appendix F.5. A summary of the characteristic patterns encountered in these 50 tidal cycles can be seen in figure F.7. Together with six representative time steps in table F.1, it will be explained under which conditions each of these patterns develops.

In this section only one cross-section of each representative time step is used for the visualization of the secondary flow. The model results at all four cross-section of these time steps can be found in appendix F.4.

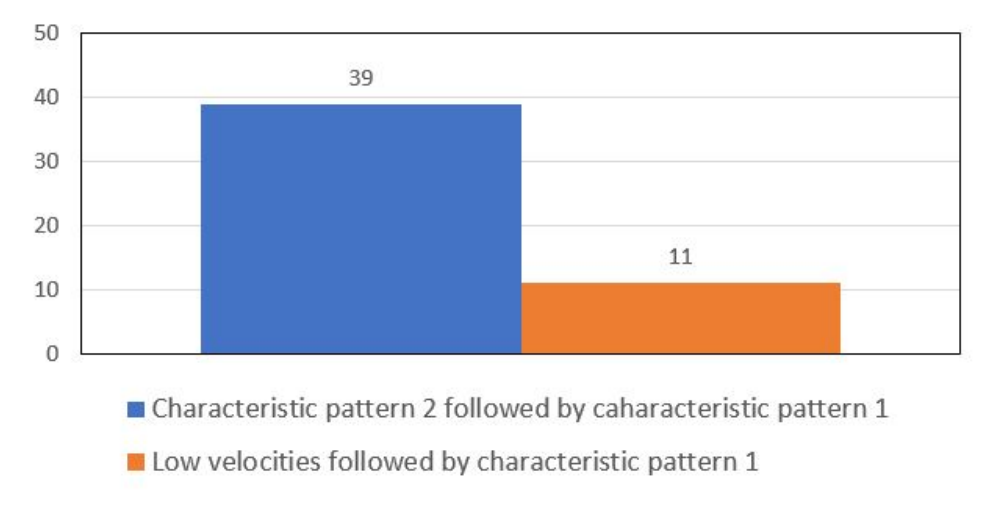


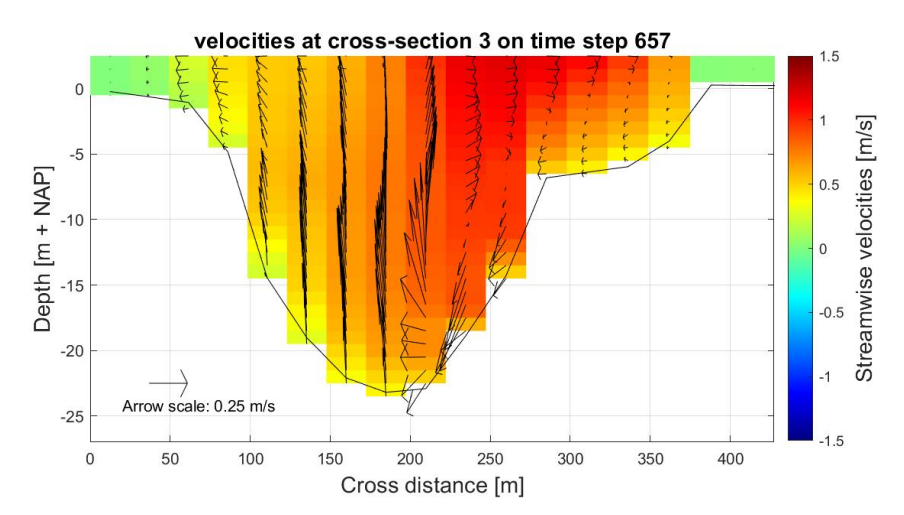
Figure F.7: Secondary flow patterns observed during ebb in 50 tidal cycles of the model. The tidal cycles are located between time step 599 - 915.

Representative time steps	Real time	Remark	Characteristic pattern	Water level [cm + NAP]
358	13 Jul 2018 20:00	-	X	4.5
359	13 Jul 2018 22:00	base case	1	- 52.5
657	7 Aug 2018 18:00	-	2	- 25.3
658	7 Aug 2018 20:00	-	1	- 24.5
1198	21 Sep 2018 20:00	case 2	3	34.1
1334	6 Oct 2018 04:00	-	mix of 2 and 3	28.1

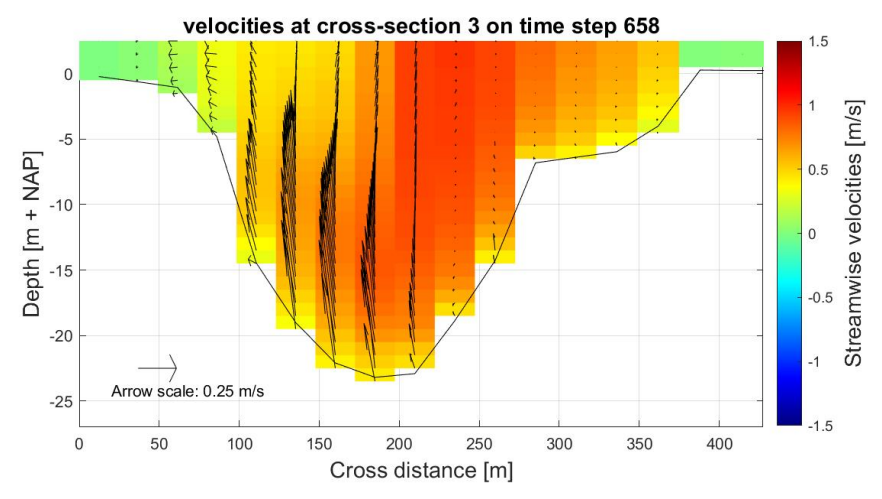
Table F.1: Overview of the characteristic secondary flow pattern per representative time step.

Figure F.7 shows that in 39 of the 50 tidal cycles, the secondary flow first takes the shape of characteristic pattern two and has the shape of characteristic pattern one in the consecutive time step. This observation is made during the ebb flow of the same tidal cycle. For visualization of this mechanism, a closer look is taken at time steps 657 and 658. Figure F.8 compares the third cross-section of both time steps. It shows that the secondary flow first takes the shape of characteristic pattern two in time step 657, with a recirculation zone on the right side of the scour hole. In the next time step, the shape of characteristic pattern one can be seen, with no recirculation zone present in cross-section three.

In the remaining 11 cases out of figure F.7, only characteristic pattern one was observed. However, if one time step earlier is investigated, very low flow velocities are encountered meaning that the system did not yet behave as a confluence. For visualization there can be looked at time step 358. As seen in table F.1, time step 359 has secondary flow shaped with characteristic pattern one. This suggests that time step 358 would be shaped with characteristic pattern two. However as can be seen on figure F.9, the flow is still in transition from flood to ebb and has very small flow velocities. Despite, it is still expected that the characteristic pattern two is present during this tidal cycle. Most likely the model results do not always capture this. This is caused by the rather large output time step (2 hours), which paired with the tidal cycle in the North Sea (12 hours and 25 minutes) will not compute results during the same moments of each tidal cycle. It can be possible that the secondary flow behaves as characteristic pattern two somewhere between time step 358 and 359, but that it is not captured in the model results. Despite this limitation, the analysis of the 50 tidal cycles has shown convincing evidence that the secondary flow patterns first take the shape of characteristic pattern two and reshape towards characteristic pattern one, during the ebb flow of the same tidal cycle.



(a) Velocities at cross-section 3 on time step 657 with a recirculation cell on the right side (characteristic shape two).



(b) Velocities at cross-section 3 on time step 658 with no recirculation cell (characteristic shape one).

Figure F.8: Comparison of cross-section three in model time step 657 and 658.

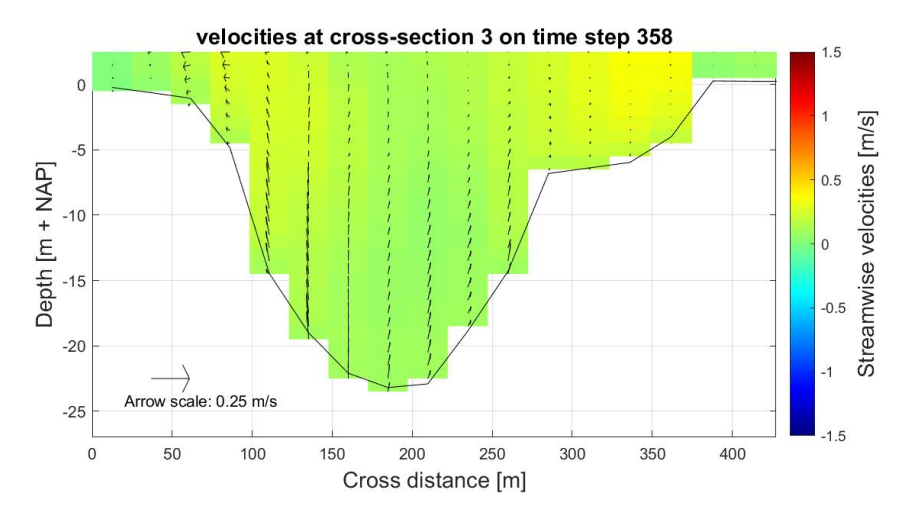


Figure F.9: Velocities at cross-section 3 on time step 358.

Out of the 50 analyzed tidal cycles, none showed the presence of secondary flow with the fully developed characteristic pattern three. This can be explained since pattern three was only encountered once during the analysis of all tidal cycles (at time step 1198). This indicates that some conditions are special for this time step. Looking at figure F.10, it can be seen that the ebb water levels at Spijkenisse were the highest during time step 1198. It appears that this determines if the secondary flow takes the shape of characteristic pattern three. This suspicion is more plausible when a closer look is taken at the velocities of time step 1334, which also contains quite high ebb water levels at Spijkenisse. Figure F.11 and figure F.12 show the velocities at respectively cross-section three and four during this time step. It can be concluded that this time step is a mix of the characteristic patterns two and three, since cross-section three contains a clockwise rotating cell on the right side and cross section four a half counter-clockwise recirculating cell on the left side. This gives the idea that the high water levels force the secondary flow to behave as characteristic pattern three. As a result, it can be hypothesised that a water level threshold is present somewhere between 28.1 cm + NAP (time step 1334) and 34.1 cm + NAP (time step 1198) at Spijkenisse. If this is exceeded, the secondary flow takes the shape of characteristic pattern three. Below this threshold some kind of transition zone is present before it again takes the shape of characteristic pattern two followed by characteristic pattern one. Unfortunately no tidal cycles with similar high ebb water levels as time steps 1198 and 1334 were present in the model and therefore this hypothesis can not be confirmed or rejected.

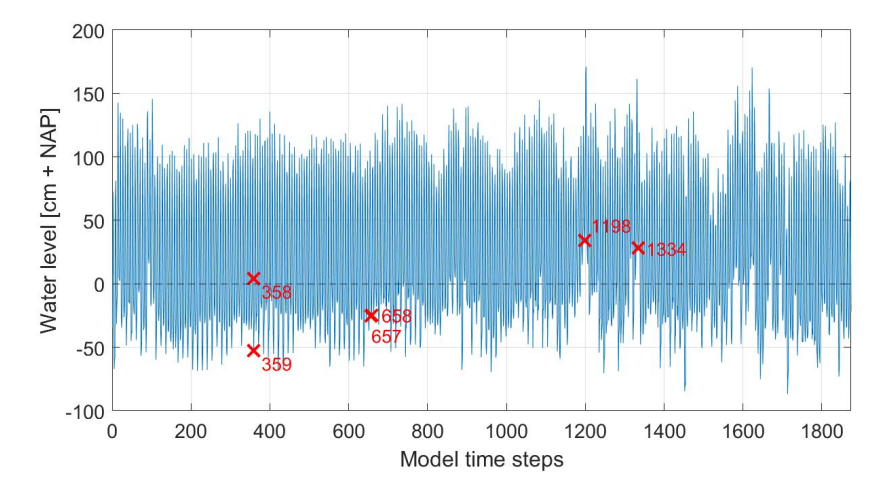


Figure F.10: Water levels at Spijkenisse according to the model and representative time steps at which the model output is analyzed for the three characteristic situations.

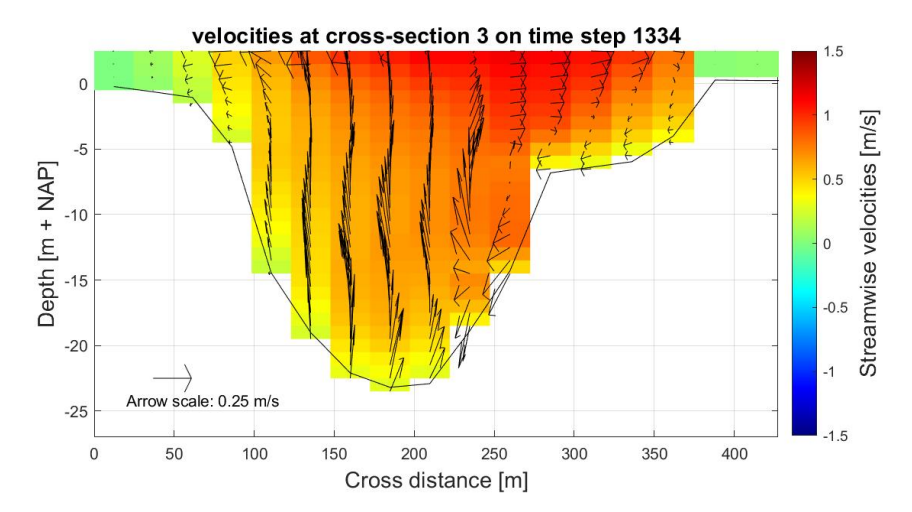


Figure F.11: Velocities at cross-section 3 on time step 1334.

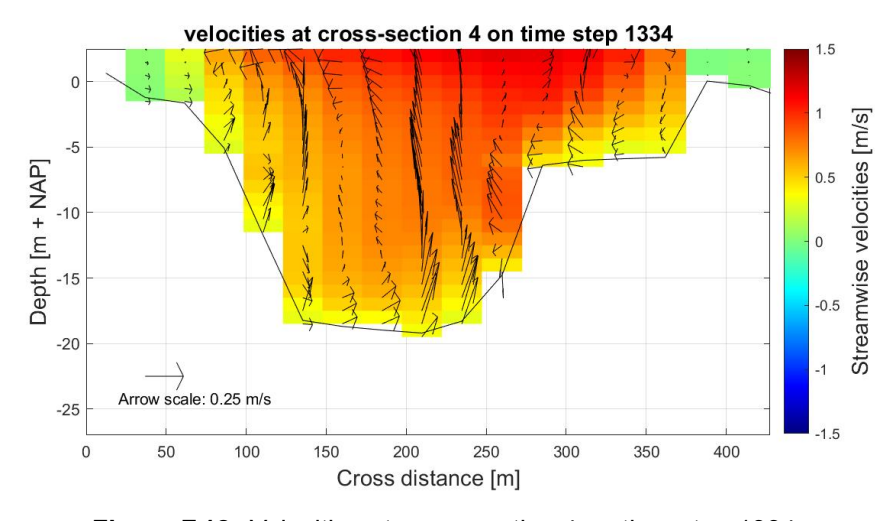


Figure F.12: Velocities at cross-section 4 on time step 1334.

F.3. Summary 134

Now that it is known when each of the three patterns develops, the unexpected behavior of characteristic pattern three can be addressed. It has an counter-clockwise rotation cell was found on the left side of the scour hole that also grew in size in the streamwise direction. Since it is known that the fully developed characteristic pattern three is only present at time step 1198, a closer look is taken at the velocity field with figure F.13. No deviating behavior in the velocity magnitude or deflection is seen with respect to the literature. The flow from the Spui deflects in the same direction and even a horizontal recirculation zone is present downstream of the confluence. The only difference observed is the scour hole. Therefore it is assumed that the unexpected behavior is caused by the presence of the scour hole Beerenplaat. Maybe the profile of the scour hole, which becomes shallower in the streamwise direction, plays a role. If for example the river bottom becomes more shallower on the left side than on the right side, it can lead to larger upwards directed velocities and potentially force these recirculation cells. However, a confirmation or a more detailed and elaborate explanation why and how this unexpected secondary flow pattern is formed here, could not be found within the model results.

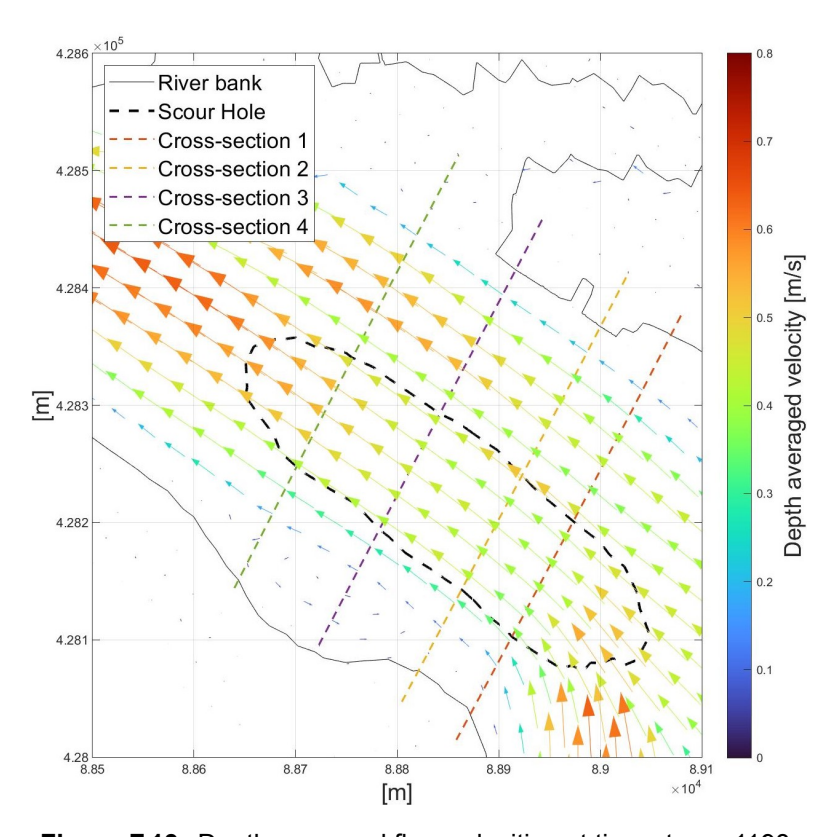


Figure F.13: Depth averaged flow velocities at time step = 1198.

F.3. Summary

So concluding, out of the Delft3D model output the following behavior regarding the secondary flow during ebb flow, when system behaves as a confluence, was found. Whether or not these secondary flow patterns behave similar in the field is yet uncertain since no recirculating cells were observed in the ADCP field measurements.

The secondary flow can take the shape of three characteristic patterns. Characteristic shape
one has one relatively small recirculation cell in the clockwise direction, which is not present in
the entire scour hole. The second characteristic contains a much larger recirculation cell, which
spans the length of almost the entire scour hole. It rotates in the clockwise direction, migrates
from the left side to the right side and dampens out in the streamwise direction. The third characteristic pattern is completely different. It mainly recirculates in the counter-clockwise direction

and becomes initially larger in the streamwise direction and then breaks inside the scour hole. These three characteristics are the representative shapes of the secondary flow. In the model no other defining shapes were found.

- During the ebb flow of a single tidal cycle, the secondary flow first takes the shape of characteristic pattern two and than changes towards characteristic pattern one. Most likely this principle occurs during almost every tidal cycle.
- If significantly high ebb water levels are present, the secondary flow will take the shape of characteristic pattern three. Most likely the water levels should exceed a threshold water level that is located somewhere between 28.1 cm + NAP and 34.1 cm + NAP at Spijkenisse.
- These three characteristic patterns for the secondary flow do not always match with what is expected according to literature. For all three patterns the amount of recirculation cells observed did not match. Plausible reasoning has been given that the scour hole limits the secondary flow to form only one recirculation cell, instead of the two that should be present. On top of that, the rotation direction and the growth in downstream direction of the recirculation cell in characteristic pattern three, differs a lot with the literature findings. It is assumed that this is caused by the scour hole but no reasoning could be find why or how this occurs.
- It is expected that no shear layer will develop downstream of the confluence, since there are no
 counteracting recirculating cells present in either characteristic pattern. However, some shear is
 expected if the flow of both the Spui and Oude Maas are running alongside each other with a
 velocity difference. Therefore it is assumed that the shear layer only develops at the confluence
 and is not present downstream of it, as would be expected by the literature.
- The characteristic patterns of the secondary flow described in this section are the extreme situations. The model conditions (e.g. tidal influence and seasonal river discharge) can cause the secondary flow to be less developed than either of these characteristic patterns or maybe lead to a mix of them.

F.4. Velocities at four cross-sections for representative time steps

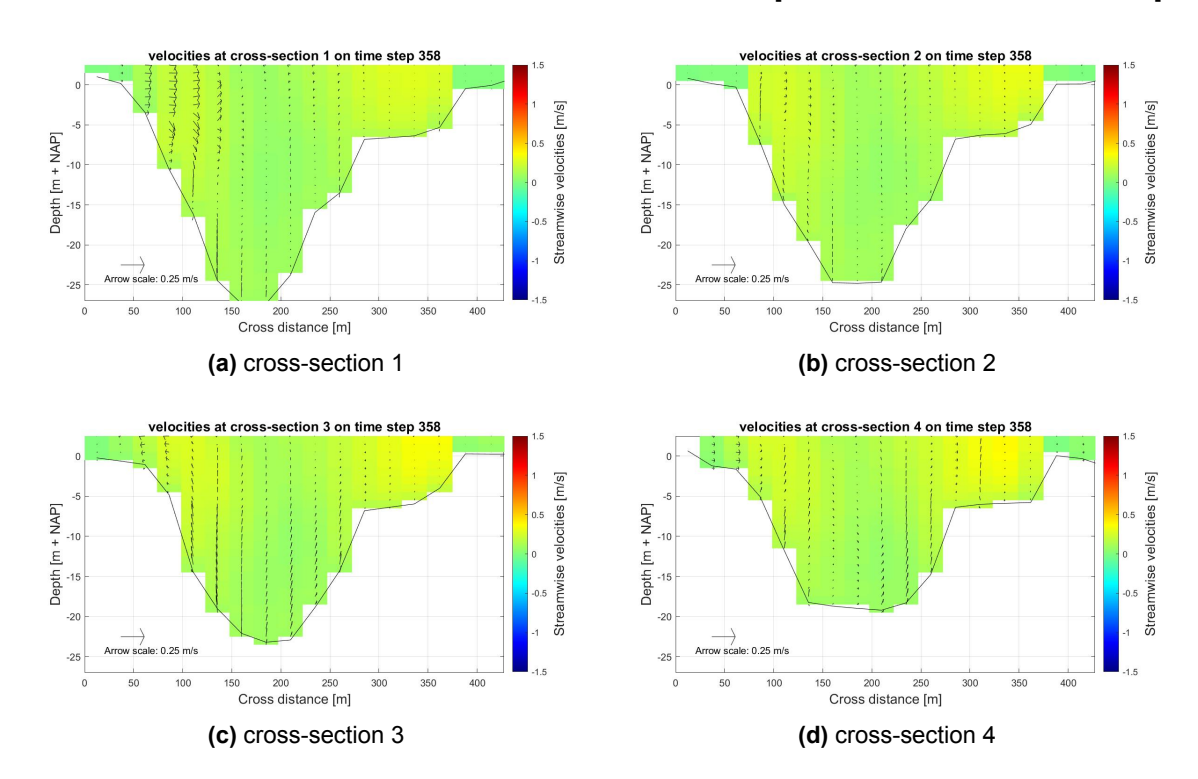


Figure F.14: Delft3D model output at time step 358 (= 13 Jul 2018 20:00).

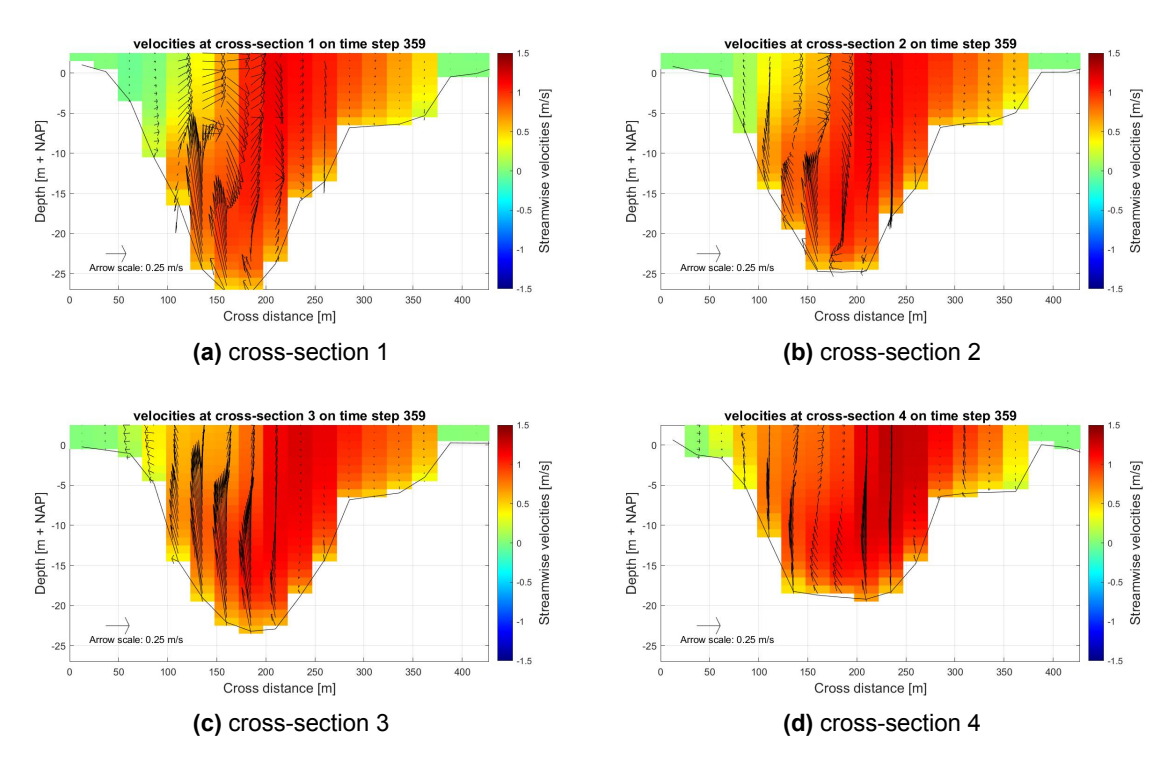


Figure F.15: Delft3D model output at time step 359 (= 13 Jul 2018 22:00).

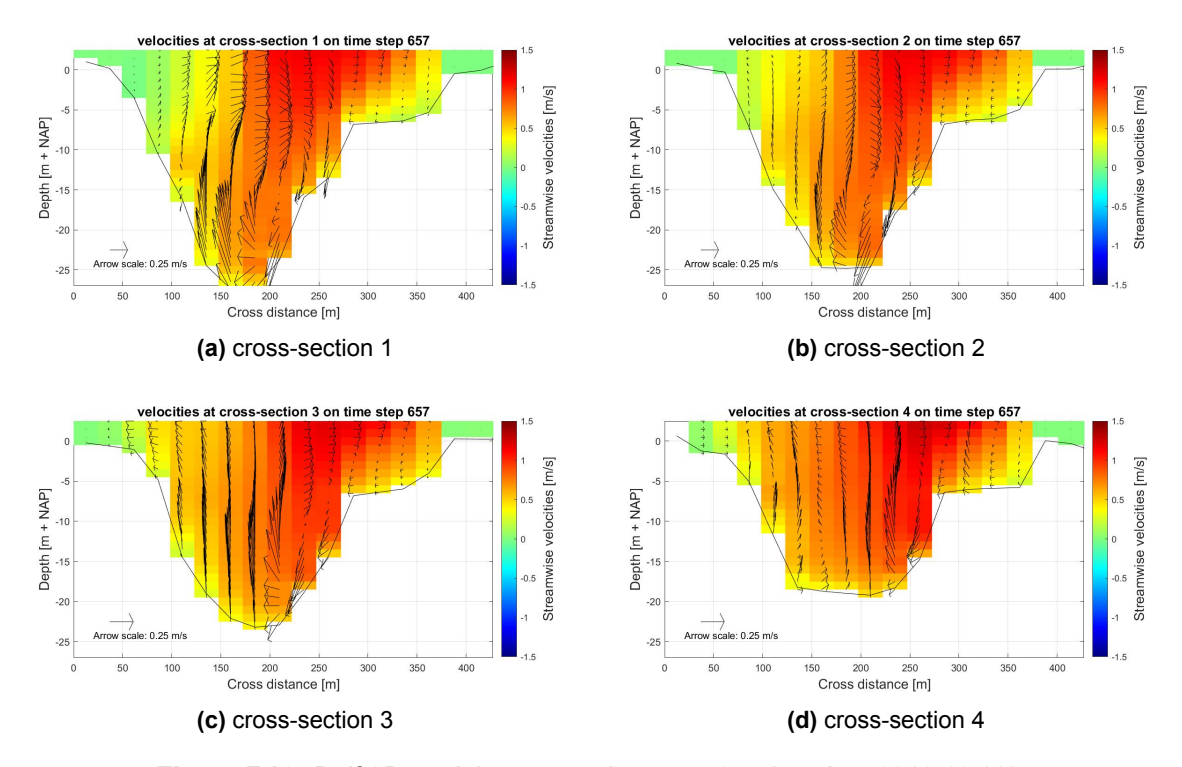


Figure F.16: Delft3D model output at time step 657 (= 7 Aug 2018 18:00).

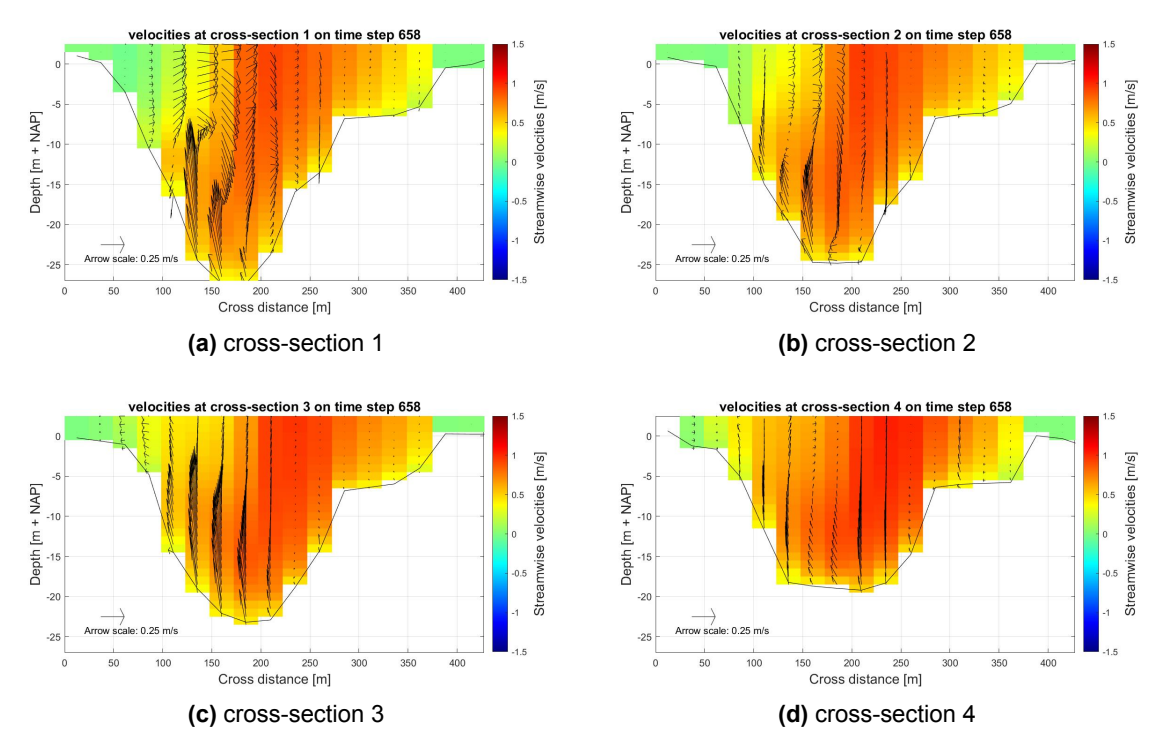


Figure F.17: Delft3D model output at time step 658 (= 7 Aug 2018 20:00).

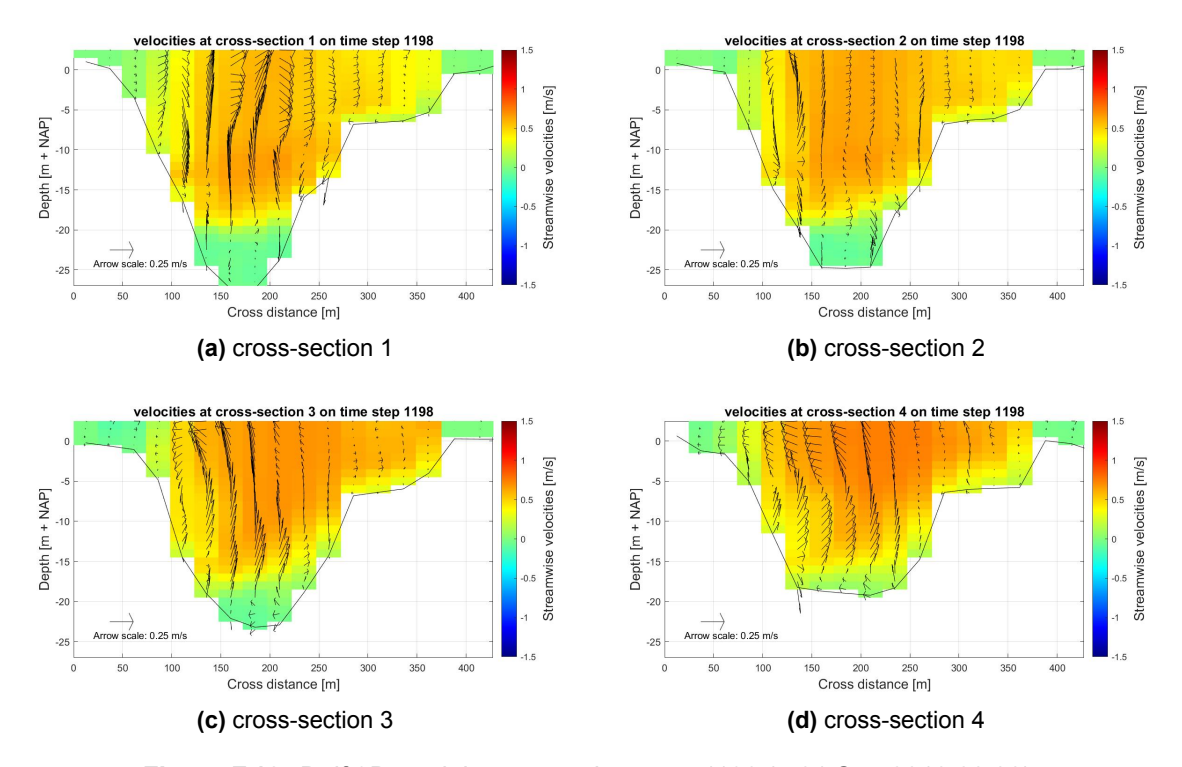


Figure F.18: Delft3D model output at time step 1198 (= 21 Sep 2018 20:00).

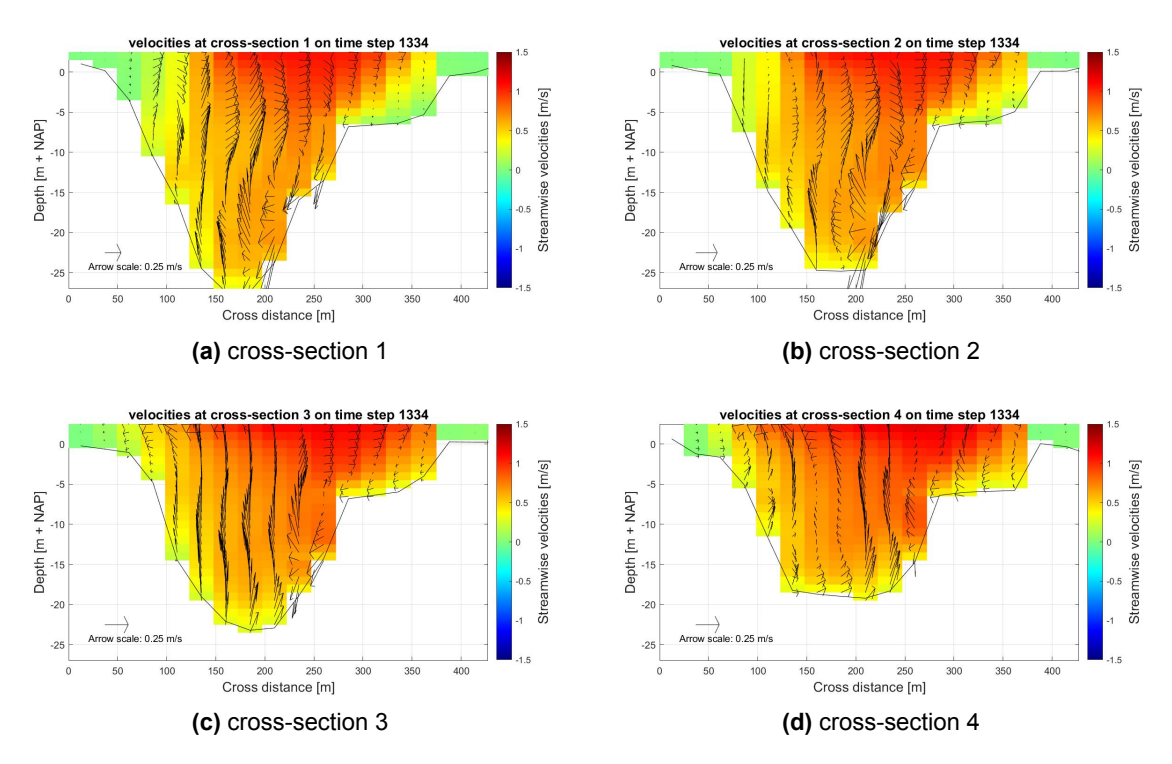


Figure F.19: Delft3D model output at time step 1334 (= 6 Oct 2018 04:00).

F.5. Secondary flow patterns in model results

The secondary flow patterns during ebb flow of 50 tidal cycles will be investigated. The tidal cycles are located between model output time step 599 and 915. The period was chosen randomly, not based on any conditions. Table F.2 shows two consecutive time steps in the ebb part of each of these tidal cycles. At both these time steps, the presence of secondary flow patterns has been evaluated. Figure F.20 shows the water levels during these 50 tidal cycles.

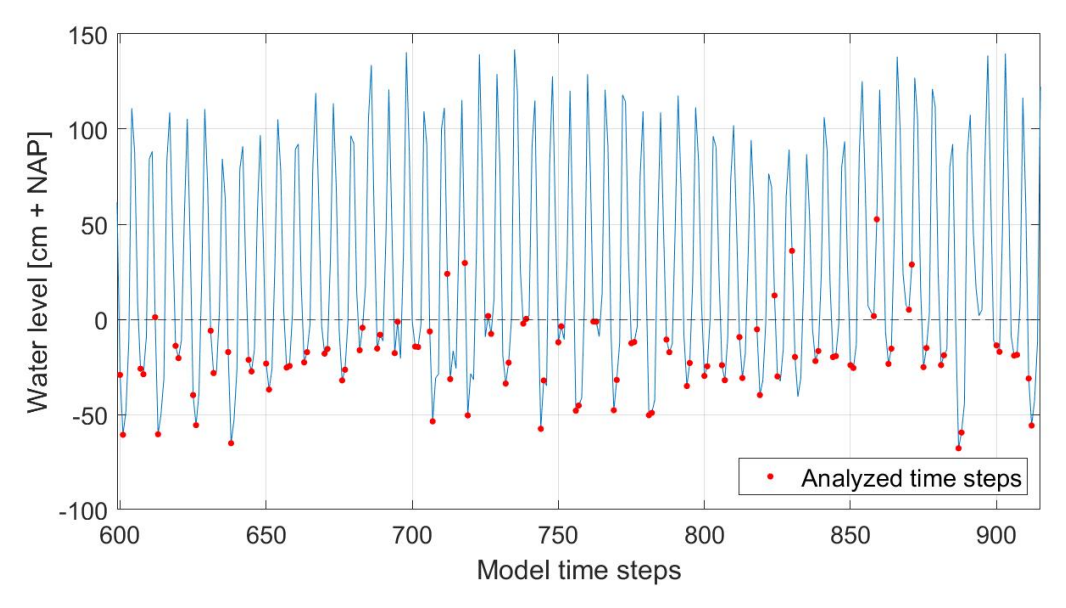


Figure F.20: Water levels for all analyzed time steps in table F.2.

Tidal cycle	first ebb	characteristic	second ebb	characteristic	
	time step	pattern	time step	pattern	
1	600	2	601	1	
2	607	2	608	1	
3	612	-	613	1	
4	619	2	620	1	
5	625	2	626	1	
6	631	-	632	1	
7	637	-	638	1	
8	644	2	645	1	
9	650	2	651	1	
10	657	-	658	1	
11	663	2	664	1	
12	670	2	671	1	
13	676	2	677	1	
14	682	2	683	1	
15	688	2	689	1	
16	694	2	695	1	
17	701	2	702	1	
18	706	-	707	1	
19	712	-	713	1	
20	718	-	719	1	
21	726	2	727	1	
22	732	2	733	1	
23	738	2	739	1	
24	744	2	745	1	
25	750	2	751	1	
26	756	2	757	1	
27	762	-	763	1	
28	769	2	770	1	
29	775	2	776	1	
30	781	2	782	1	
31	787	2	788	1	
32	794	2	795	1	
33	800	2	801	1	
34	806	2	807	1	
35	812	2	813	1	
36	818	-	819	1	
37	824	-	825	1	
38	830	2	831	1	
39	838	2	839	1	
40	844	2	845	1	
41	850	2	851	1	
42	858	2	859	1	
43	863	2	864	1	
44	870	2	871	1	

45	875	2	876	1
46	881	2	882	1
47	887	-	888	1
48	900	2	901	1
49	906	2	907	1
50	911	2	912	1

Table F.2: Secondary flow patterns present at two consecutive time steps of the ebb flow for 50 tidal cycles. The dash means that the velocities were very low and the system did not yet behave as a confluence with secondary flow patterns.



Analysis horseshoe vortex ADCP measurements

This appendix contains an analysis of the ADCP measurements, focused on identifying the horseshoe vortex out of the streamwise velocities. It uses the idea that the streamwise velocity can be split into an averaged flow velocity component \overline{u} and a fluctuating component \widetilde{u} (see equation (G.1)). This fluctuating component represent the turbulence. It can be expected that at the horseshoe vortex, more turbulence is encountered. It is realized that more factors can lead to turbulent fluctuations within the ADCP measurements, such as the confluence/bifurcation or any of the other 3D flow processes. These can not be filtered out and therefore can influence the results within this analysis. Despite, this approach is still used since the cross-stream velocity vectors were not sufficient to comment on the presence of the horseshoe vortex. The results of this analysis will be seen as a first estimate and therefore interpreted with some caution. The following steps are performed for eight of the ADCP measurements to identify the presence of the horseshoe vortex out of the streamwise velocities.

1. The ADCP measurements are depth averaged, getting a representative velocity for each column of bins. Figure G.1 shows the depth averaged velocities in the streamwise direction measured at ADCP transect two.

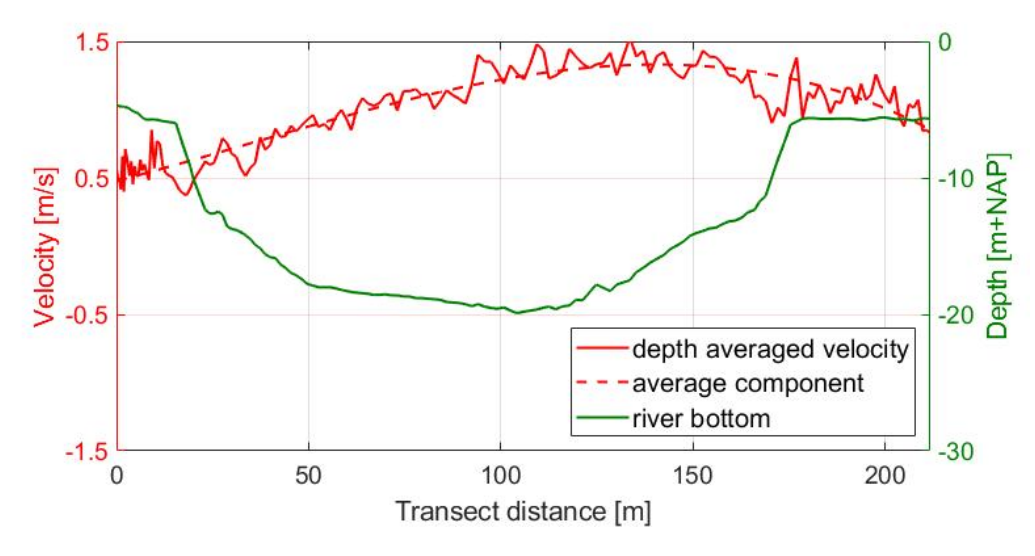


Figure G.1: Velocities measured at ADCP transect 2 (08:28).

2. The depth averaged velocities are split according to equation (G.1) in an averaged component \overline{u} and a fluctuating component \widetilde{u} . The average component for each of the transects has been obtained with polynomial curve fitting (third degree, least squares). In figure G.1 the average component of ADCP transect two can be seen.

$$u = \overline{u} + \widetilde{u} \tag{G.1}$$

u [m/s] Depth averaged flow velocity

 \overline{u} [m/s] Averaged flow velocity component

 \widetilde{u} [m/s] Turbulence component

3. The fluctuating component \widetilde{u} is the absolute difference between the average component and the measured depth averaged velocities. Figure G.2 shows as example the fluctuating component of ADCP transect two. This fluctuating component represent the turbulence measured within the flow.

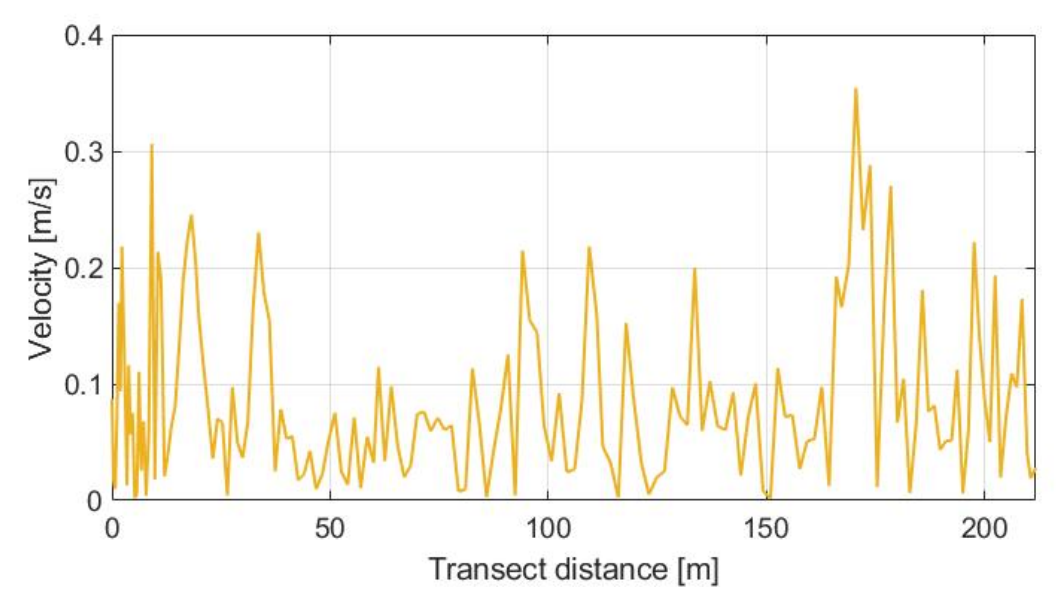


Figure G.2: Fluctuating turbulence component \tilde{u} of ADCP transect 2 (08:28).

4. It is expected that the presence of the horseshoe vortex would lead to much higher fluctuating components than in areas were it is not present. This questions what part of the transect should be investigated. Since it is possible that the ADCP transect has been taken downstream of the reattachment point, the presence of both the horseshoe vortex and the less structured wake should be addressed. Based on the numerical simulations of Bom (2017), the convergence angle of the wake and the transects of the ADCP measurements, four areas of interest are established. It is assumed that the horseshoe vortex occurs in the area between the edge of the scour hole and 25 meters towards the center. The wake develops within the area of the edge of the scour hole and 10 meters to the outside. Figure G.3 shows these four areas. For each of them, the average turbulent fluctuations within this area is computed.

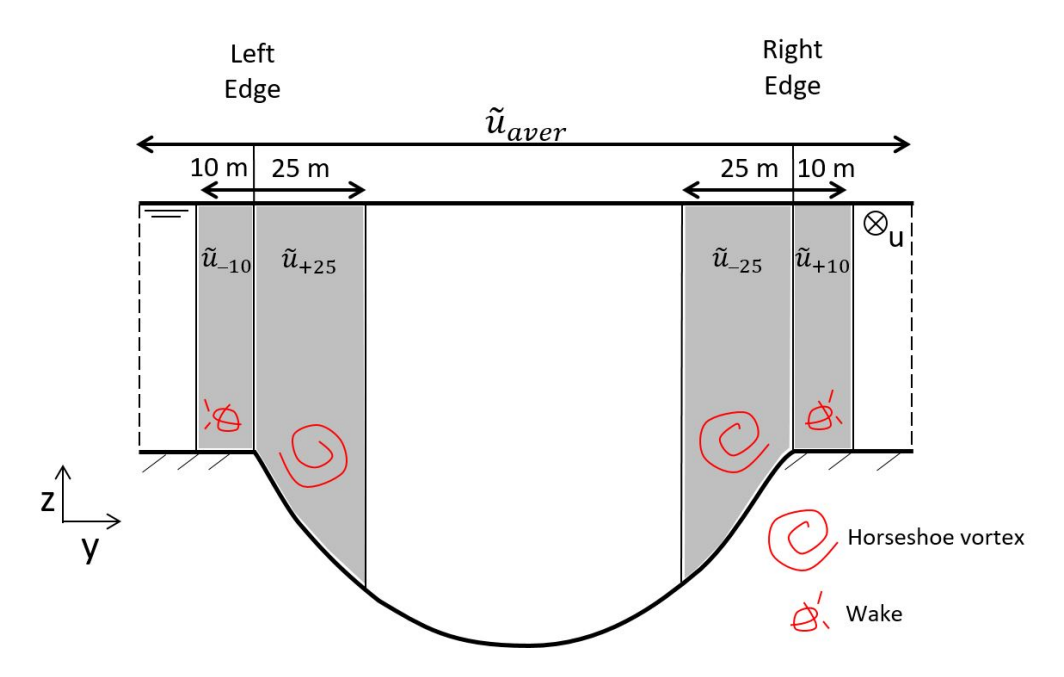


Figure G.3: Location of turbulent fluctuation values of table G.1.

5. The horseshoe vortex or wake can be identified by having significantly higher turbulent fluctuations. Therefore the fluctuations at the four areas are compared with an average value of the entire transect called \widetilde{u}_{aver} .

These steps have been done for eight ADCP measurements. In appendix G.1 and appendix G.2 the turbulent fluctuations at the four areas of each of the eight transects are shown. Table G.1 shows a summary of the turbulent fluctuations in all areas. The bold values mean that the turbulent fluctuations at that area are 20 % larger than the average turbulent fluctuations of the entire transect (\tilde{u}_{aver}), indicating they are significantly larger. The dash means that this area was not fully present within the transect and therefore no values could be obtained. Out of table G.1 no decisive conclusion regarding the presence of the horseshoe vortex can be made. Only a part of the areas within the measurements have significantly larger turbulent fluctuations (20 %). Contrary, there are also areas that have much lower or almost similar turbulent fluctuations than the average of the entire transect. No significantly larger and consistent pattern can be found that shows any indication of the horseshoe vortex or the less-structured wake.

Tidal situation	Measurement	Time	\widetilde{u}_{aver}	Left Edge		Right Edge	
				$\widetilde{u}_{-10\ m}$	$\widetilde{u}_{+25\ m}$	$\widetilde{u}_{-25\ m}$	$\widetilde{u}_{+10\ m}$
Flow direction towards sea	1	07:20	0.109	-	-	0.146	0.094
	2	08:28	0.085	0.095	0.116	0.142	0.106
	3	09:39	0.076	0.076	0.074	0.102	0.050
	4	10:52	0.074	0.052	0.060	0.078	0.086
	5	12:09	0.060	-	0.044	0.073	0.073
Flow direction inland	6	15:05	0.068	0.082	0.071	0.057	0.063
	8	16:08	0.055	-	0.078	0.058	0.051
	9	16:30	0.050	-	0.055	0.067	0.056

Table G.1: Averaged turbulence values in the streamwise direction. Bold values are 20 % larger than \widetilde{u}_{aver} .

These findings have been obtained by averaging the streamwise velocities over the depth. However, it can be possible that this averaging filtered out some of the turbulent characteristics. Therefore the turbulent fluctuations over the depth are also investigated. This has been done for all eight ADCP measurement on multiple locations for both the horseshoe vortex and the less structured wake. As an example there will be looked at the velocities on four locations of ADCP measurement two taken at 08:28. Figure G.4 shows the river bottom measured at ADCP transect two. It would be expected that the the horseshoe vortex is present in between the areas with the black dashed lines. Therefore at locations one and four much more turbulent fluctuations should be observed than in the locations two and three. Figure G.5 shows the streamwise velocities at each of the four locations. Again here, an average component is constructed with polynomial curve fitting (third degree, least squares). If the horseshoe vortex is present the deviations from this average component should be much larger at locations one and four than at two and three. This is not observed. The difference between the streamwise velocities and the average component is quite similar for all locations and over the water depth. It does not show any presence of the horseshoe vortex. This comparison has also been made within all other ADCP measurements including the presence of the less structured wake. Neither of them showed any decisive evidence of the horseshoe vortex. Therefore it is concluded that the horseshoe vortex is not present within the streamwise velocities of the ADCP measurements.

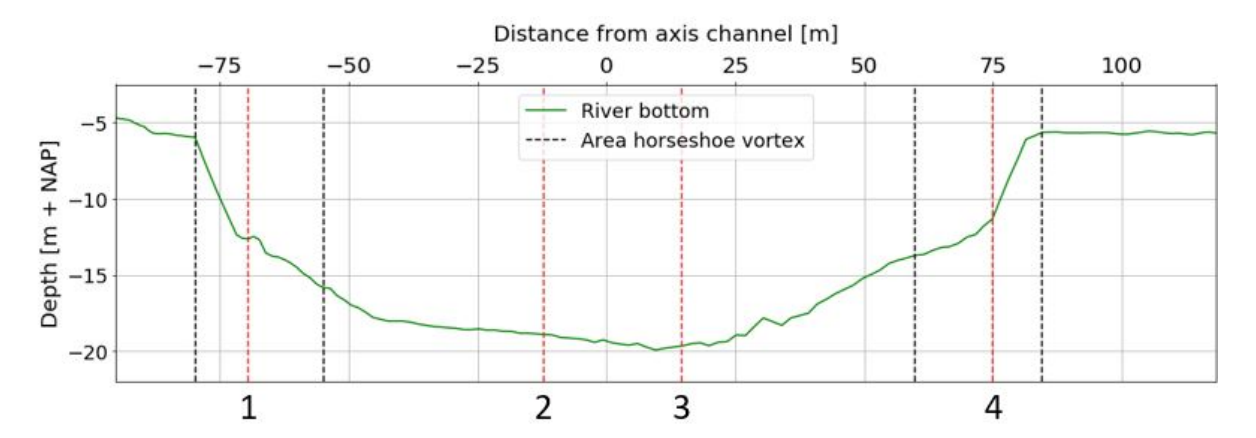
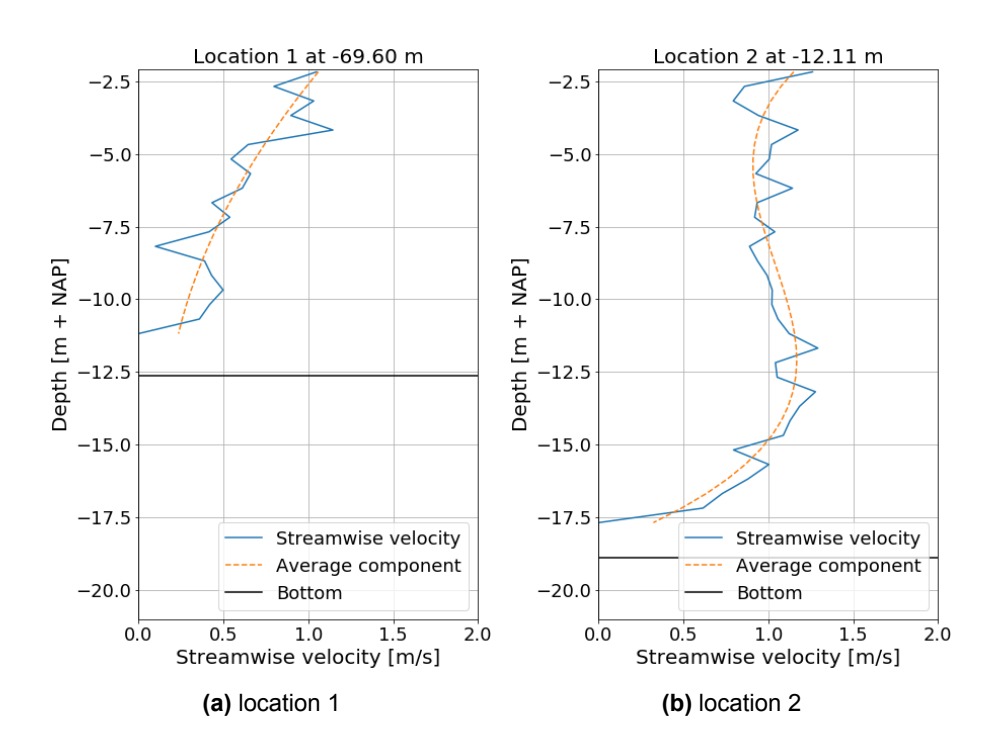


Figure G.4: Locations where velocities are analyzed for identifying the horseshoe vortex.



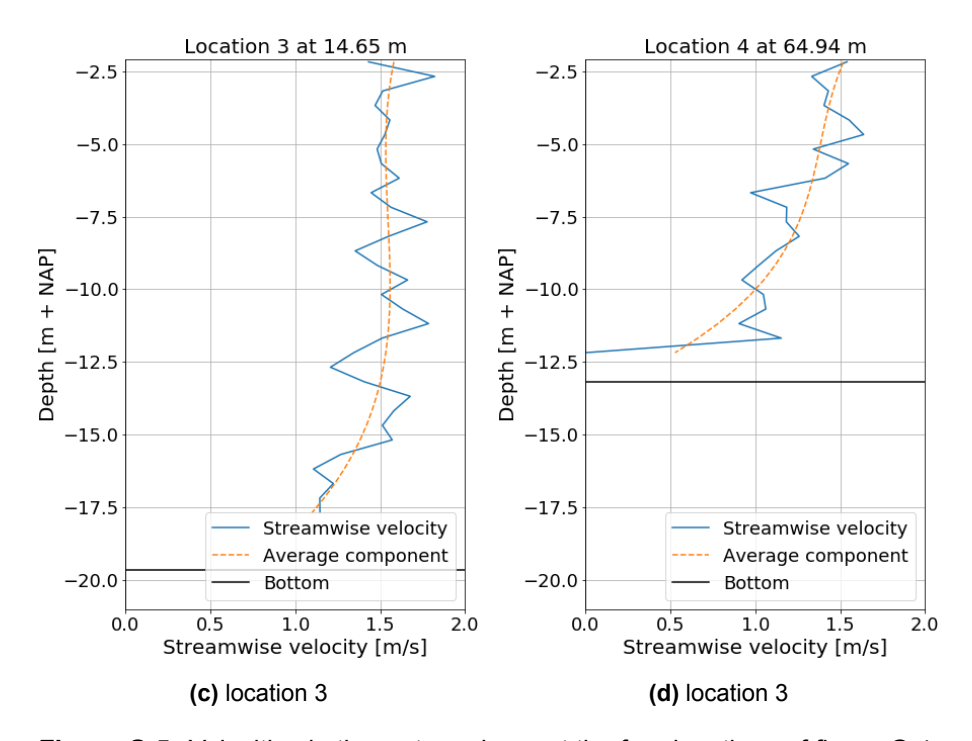


Figure G.5: Velocities in the water column at the four locations of figure G.4.

G.1. Identification of horseshoe vortex

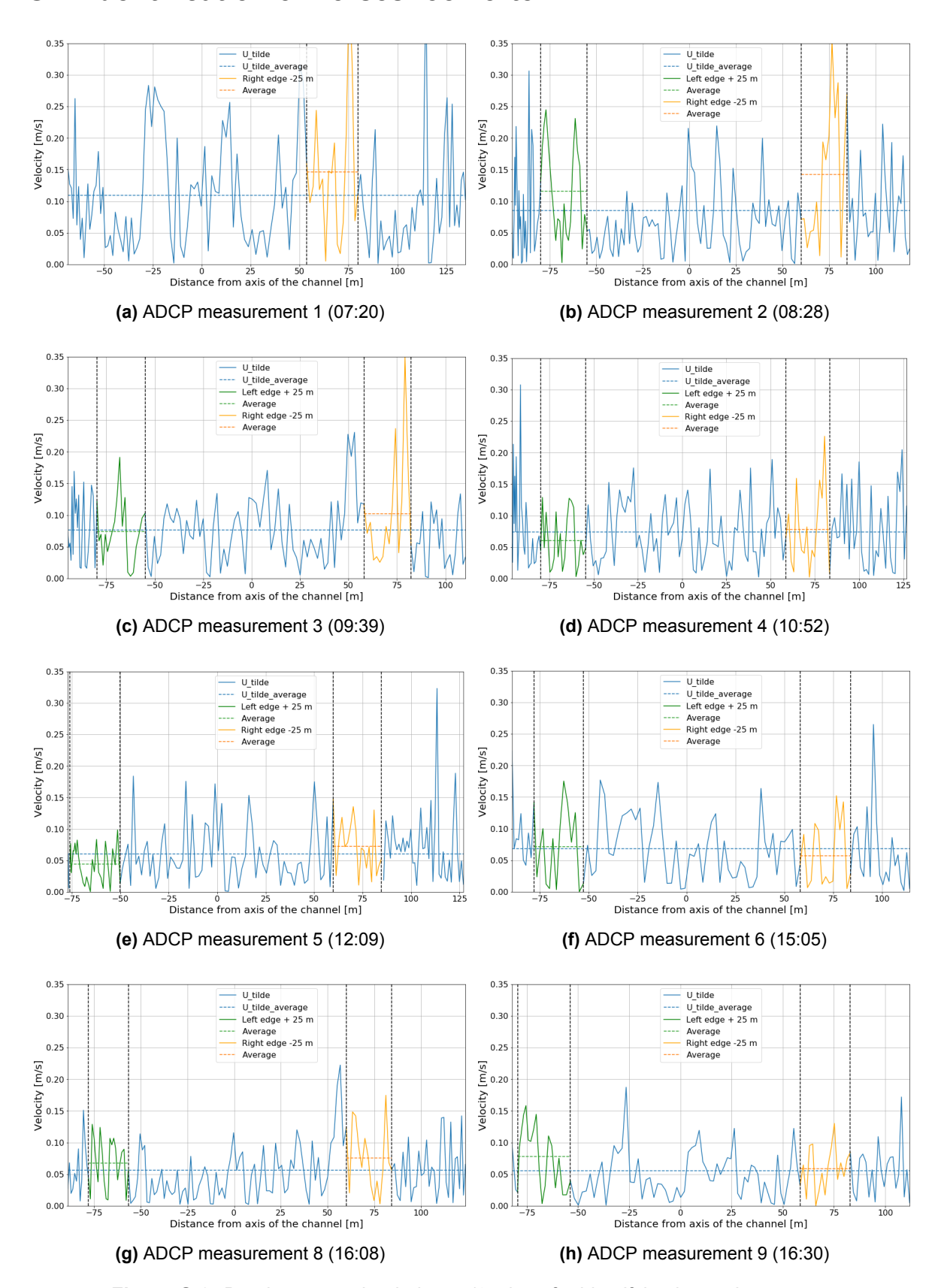


Figure G.6: Depth averaged turbulence \tilde{u} values for identifying horseshoe vortex.

G.2. Identification of wake

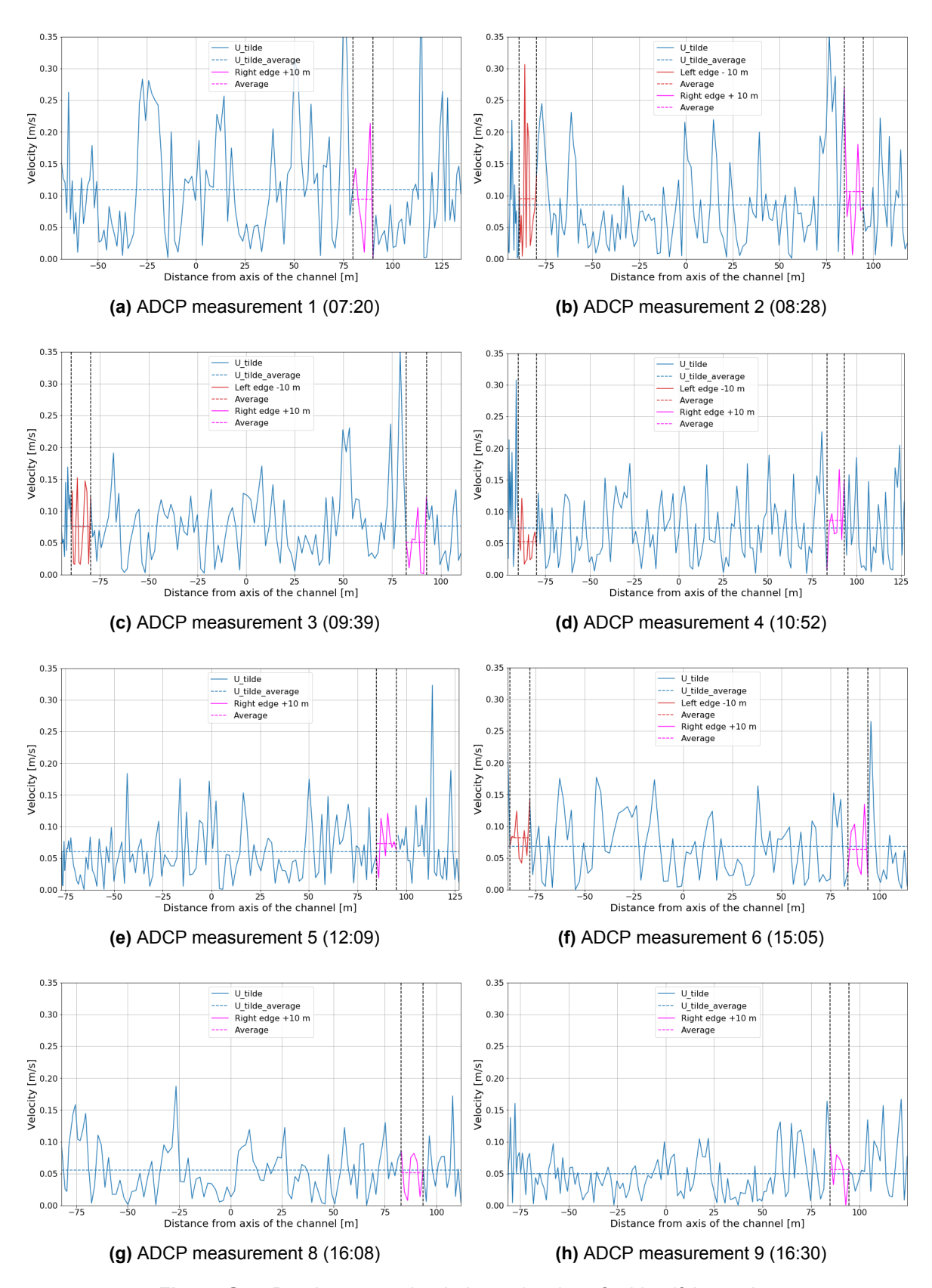


Figure G.7: Depth averaged turbulence \tilde{u} values for identifying wake.